GEOTHERMAL INVESTIGATIONS OF THE U.S. GEOLOGICAL SURVEY IN LONG VALLEY, CALIFORNIA, 1972-73

Reprinted from the Journal of Geophysical Research,
Volume 81, p. 721-860 and 1527-1532.

CONTENTS

Geothermal Investigations of the U.S. Geological Survey in Long Valley, California, 1972–1973

L. J. P. MUFFLER

U.S. Geological Survey, Menlo Park, California 94025

D. L. WILLIAMS

U.S. Geological Survey, Denver, Colorado 80225

During 1972 and 1973 the U.S. Geological Survey (U.S.G.S.) conducted detailed geological, geophysical, hydrological, and geochemical investigations in Long Valley, California, as part of a new geothermal research program. The goal of these investigations was to understand a typical hot water geothermal system, thus providing a basis for extrapolation to other hot water areas and for regional exploration and assessment of geothermal resources. Although the U.S.G.S. investigations have thoroughly characterized the surface expression and geophysical signatures of the Long Valley geothermal system, our understanding of the geothermal system at depth is incomplete. The available data allow us to make only a crude estimate of 350–700 MW cent. for the electric power generation potential. Refinement of this estimate must await exploration of the area by deep drill holes.

U.S. Geological Survey Geothermal Research Program

The geothermal research program of the U.S. Geological Survey (U.S.G.S.) is a multidisciplinary earth science investigation whose goal is the understanding of the factors that control the nature and distribution of geothermal resources. A corollary objective is to provide the resource data needed to evaluate the extent to which geothermal energy can help meet the energy demands of the United States.

The U.S.G.S. has conducted modest geological and geochemical investigations of hot spring phenomena since 1945, primarily at Steamboat Springs, Nevada [*White et al.*, 1964; *White*, 1968*b*], Imperial Valley, California [*White*, 1968*a*; *Muffler and White*, 1969], and Yellowstone National Park, Wyoming [*White et al.*, 1975]. In addition, U.S.G.S. work in heat flow [*Sass et al.*, 1971], volcanology [*Smith and Bailey*, 1968], and experimental geochemistry [*Fournier and Rowe*, 1966] proved to have significance in geothermal exploration. It was not until November 1971, however, that a formal program of geothermal investigations was authorized by Congress, thus allowing a significant expansion of U.S.G.S. geothermal research [*Muffler*, 1972].

It was recognized clearly during this expansion of the geothermal research program that it was impossible to understand the distribution of geothermal resources in large regions or to make meaningful resource estimates without a detailed understanding of representative geothermal systems. Accordingly, the U.S.G.S. selected two geothermal areas in the United States for detailed study by all feasible geological, geophysical, geochemical, and hydrological methods. The first area selected was the region southwest of Clear Lake in northern California, chosen because it contains The Geysers (Figure 1), the world's largest known vapor-dominated (dry steam) geothermal system, currently producing electricity at 502 MW. The second area selected was Long Valley, California, known from shallow drilling and chemical analysis of hot spring waters to be a hot water geothermal system. The U.S.G.S. goal is to gain an understanding of the nature and extent of the geothermal resources in each of these two type areas, thus providing a basis for extrapolation and assessment of geothermal resources.

Long Valley was chosen as the type area for hot water geothermal systems because of the following factors: (1) hot spring chemistry indicating that any geothermal reservoir present would contain hot water, not steam, and would be at least 180°C; (2) a geologic setting characterized by young volcanism (<0.7 m.y.), reasonable potential of adequate reservoir rock (caldera fill), and small enough target size (the caldera is 15 km × 30 km) to be studied reasonably quickly; (3) our judgment that although Long Valley was clearly a favorable geothermal target, no systematic investigation was available to the public; (4) the prospect of extensive deep drilling by the geothermal industry in the near future (The U.S.G.S. hoped to develop cooperation with industry patterned after the situation in the Salton Sea geothermal field in the early 1960's); and (5) good accessibility and logistic feasibility.

Long Valley was not chosen as a type area because it appeared to have a greater commercial potential than other hot water geothermal areas in the United States. Indeed, data available in 1971 indicated that reservoir temperatures were perhaps only marginal for power generation under the economic conditions then prevailing.

Pertinent Information Available in 1971

Volcanology. It has been recognized since the work of *Gilbert* [1938] that the Bishop Tuff, of Pleistocene age, was most likely erupted from vents in Long Valley. *Gilbert* [1938, p. 1860] further suggested that young faults in Long Valley and perhaps even the depression itself were related to extrusion of magma from beneath the valley. The extent and depth of this volcanic depression were outlined by *Pakiser* [1961] and by *Pakiser et al.* [1964], who concluded from gravity data that an elliptical block 15 km × 30 km had subsided as much as 5.5 km. Further data on this depression were provided by *Dalrymple et al.* [1965], who used potassium-argon dating to show that the Bishop Tuff was erupted during a single igneous event about 0.7 m.y. ago.

Using these data and the geologic maps of *Rinehart and Ross*

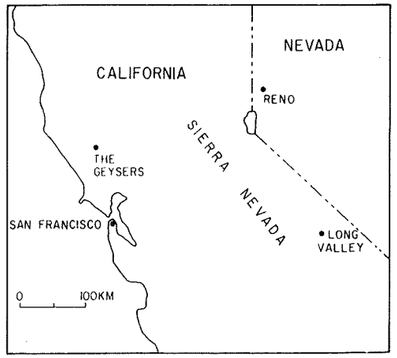

Fig. 1. Map showing location of Long Valley and The Geysers, California.

[1957, 1964] and *Huber and Rinehart* [1965], *Smith and Bailey* [1968, pp. 629–630] concluded that Long Valley was very likely a resurgent caldera and suggested that much of the volcanic rock exposed within the caldera is younger than the extrusion of the Bishop Tuff and formation of the caldera. It appeared that Long Valley had been an active volcano during the past few hundred thousand years and might still be underlain by magma or intrusive rock at temperatures approaching magmatic.

Hot springs and geothermal wells. The hot springs of Long Valley have been known since the last century [*Whiting,* 1888, p. 356]. The springs are described by *Waring* [1915, pp. 146–148, 384] and shown on Plate 1 and Figure 39 of *Rinehart and Ross* [1964]. Areas of hydrothermal alteration are also shown on Plate 1 of *Rinehart and Ross* [1964] and are discussed by *Cleveland* [1962].

Between 1959 and 1964, nine geothermal wells were drilled at Casa Diablo hot springs by Magma Power Company, and a tenth well was drilled about 4.8 km east [*McNitt,* 1963, p. 29; *California Division of Oil and Gas,* 1972]. The deepest well reached 324 m, and the maximum recorded temperature was about 180°C [*McNitt,* 1963, pp. 25–29; *California Department of Water Resources,* 1967].

Chemical analyses of waters from hot springs and geothermal wells indicated that the geothermal system was of the hot water type [*White et al.,* 1971, pp. 77–80]. Silica and Na/K geothermometry using the methods of *Fournier and Rowe* [1966] and *Ellis* [1970] suggested minimum reservoir temperatures of 180°C. *White* [1965, table 1] calculated a convective heat flow of 7×10^7 cal s^{-1} from the hydrothermal system of Long Valley by using data on total boron and the relation of boron to heat content of waters discharged from the geothermal wells at Casa Diablo hot springs.

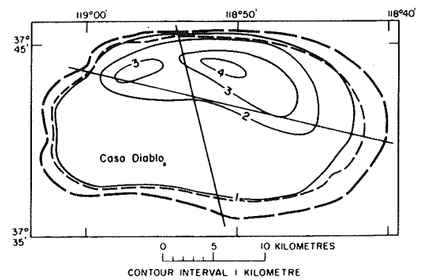

Fig. 2. Map showing depth (in kilometers) of fill in Long Valley caldera. The outer heavy dashed line marks the topographic boundary of the valley floor. The inner dashed line is the approximate location of the caldera ring fracture. The two crossing solid lines show the approximate location of seismic refraction profiles from *Hill* [1976].

U.S.G.S. Investigations in Long Valley, 1972–1973

The papers following in this issue of *Journal of Geophysical Research* present the data and basic interpretations derived from U.S.G.S. geothermal investigations in Long Valley during 1972 and 1973. The data accompanied by preliminary interpretations were presented at the Fall Annual Meeting of the American Geophysical Union in 1973 (*Eos Trans. AGU,* vol. 54, pp. 1211–1213, 1973) and in part amplified in U.S.G.S. open file reports [*Anderson and Johnson,* 1974; *Bailey,* 1974; *Dalrymple and Lanphere,* 1974; *Hoover et al.,* 1974; *Lewis,* 1974; *Sass et al.,* 1974; *Stanley et al.,* 1973; *Willey et al.,* 1974]. (U.S.G.S. open file reports serve to make unpublished information available to the public quickly. When a report or map is open-filed, a copy is placed in one or more depositories, and its availability is announced in the monthly periodical *New Publications of the Geological Survey* (available free from the U.S.G.S., National Center, Stop 329, Reston, Virginia 22092). This announcement lists all the depositories (U.S.G.S. offices, plus selected state agencies) and notes the location of reproducible copy if such exists. Open file reports released prior to May 1974 are listed in various U.S.G.S. circulars (1974, no. 706; 1973, no. 696; 1972, no. 668)).

A number of U.S.G.S. geothermal investigations in Long Valley are still in progress, including geologic mapping and petrology, heat flow, hydrology (supplemented by shallow drilling), magnetic, telluric, and magnetotelluric soundings, system modeling, water and gas chemistry, teleseismic analysis, and thermal infrared studies. Accordingly, the papers presented in this issue of the *Journal of Geophysical Research* should be viewed collectively as a progress report.

Geothermal Energy Potential

Bailey et al. [1976] suggest that Long Valley has been an active geothermal area for the past several hundred thousand years. The papers by *Lachenbruch et al.* [1976], *Sorey and Lewis* [1976], *Mariner and Willey* [1976], *Stanley et al.* [1976], *Kane et al.* [1976], and *Steeples and Iyer* [1976] reaffirm this and earlier interpretations that Long Valley is an active hot water geothermal area with high conductive and convective heat flows and is underlain at depth by a hot intrusive mass that may still contain some residual magma.

By using the results of several of these investigations it is possible to make a preliminary estimate of the geothermal energy potential of Long Valley. To do so, we must make estimates of size, temperature, and porosity of the high-temperature reservoir or reservoirs and of the efficiency of converting this high-temperature water to useful energy.

From the seismic refraction results of *Hill* [1976], the gravity interpretation of *Kane et al.* [1976], and the geologic structure of *Bailey et al.* [1976], we have constructed a model of the low-density rocks under Long Valley (Figure 2) and estimate their volume V to be 810 km^3. We interpret these low-density rocks to be primarily caldera fill (ie., the Bishop Tuff and overlying sedimentary and volcanic rocks) plus that part of the rhyolites of Glass Mountain downdropped into the caldera [*Bailey et al.,* 1976].

The bulk density ρ_b of the caldera fill can be calculated from the formula $\rho_b = (\rho_0 V - M_D)/V$, where ρ_0 is the bulk density of rocks surrounding the caldera (2.67 g/cm^3) and M_D is the mass calculated by Gauss' theorem from the integrated gravity anomaly (3.33×10^{17} g) [*Kane et al.,* 1976]. The resulting bulk density of fill ρ_b is 2.26 g/cm^3, yielding a density difference of 0.41 g/cm^3, similar to the 0.45 g/cm^3 assumed by *Kane et al.* [1976].

If we assume that all the voids and pores in the fill are full of fluid, then the porosity of the fill ϕ is $(\rho_g - \rho_b)/(\rho_g - \rho_f)$, where ρ_f is the average water or fluid density and ρ_g is the average grain density of the rocks making up the caldera fill. For ρ_g we have used the average density of 2.60 g/cm^3 from two different, carefully investigated, densely welded, and devitrified rhyolite ash flow tuffs from the Creede caldera, Colorado [*Ratté and Steven,* 1967]. This should be a reasonable estimate for the intracalcera Bishop Tuff (R. A. Bailey, personal communication, 1975), and since most of the rest of the fill is also derived from rhyolite volcanics, we used this value for the grain density of the entire caldera fill. The resulting bulk porosity of the Long Valley caldera fill is 0.19. If grain density of the fill were 2.50 g/cm^3, the porosity would be only 0.15.

Mariner and Willey [1976] and *Sorey and Lewis* [1976], using various geochemical thermometers, estimate that the temperature of the geothermal reservoir is at least 200°–210°C. *McKenzie and Truesdell* [1975], using a sulfate isotope geothermometer, calculate a reservoir temperature of 240°–250°C.

The caldera fill above the Bishop Tuff consists of a variety of rhyolitic flows and tuffs, rhyodacite flows, basalt flows, and (in the eastern half) lake, marsh, and periglacial sediments [*Bailey et al.,* 1976]. Although some of this near-surface rock is hydrothermally altered, it appears to be relatively impermeable except along faults and does not appear to contain a high-temperature geothermal reservoir [*Stanley et al.,* 1976]. Thus any significant geothermal resource in the Long Valley caldera would have to be in the Bishop Tuff and the rhyolites of Glass Mountain.

Three pieces of evidence lead us to believe that such a reservoir does exist. First, all of the hot springs appear to occur along active faults [*Stanley et al.,* 1976; *Bailey et al.,* 1976], suggesting that they are acting as conduits for hot water from some deeper zone. Second, the springs all yield approximately the same geochemically derived temperature and have almost identical chloride-boron ratios implying that they are tapping a single, well-mixed reservoir [*Sorey and Lewis,* 1976]. Finally, the Bishop Tuff extends throughout the lower part of the caldera fill and, based on the gravity data of *Kane et al.* [1976], appears to have significant porosity (> 0.15). Inclusions of Bishop Tuff found in postcaldera rhyolite tuffs exposed in the central part of the caldera are densely welded [*Bailey et al.,* 1976]. Accordingly, we infer that the porosity indicated by the gravity data is due to fractures or to local accumulations of high-porosity pumiceous material [*Kane et al.,* 1976].

Seismic data of *Hill* [1976], deep electrical data of *Stanley et al.* [1976], and shallow drilling results of *Lachenbruch et al.* [1976] allow us to construct a model showing the depth to the top of the Bishop Tuff (Figure 3). The difference in volumes calculated from Figures 2 and 3 is interpreted as the volume of Bishop Tuff and downdropped rhyolites of Glass Mountain within the caldera. This figure of 450 km^3 compares with 375 km^3 estimated for the intracaldera volume of Bishop Tuff alone [*Bailey et al.,* 1976]. What proportion of these rocks constitutes a reservoir is unknown. The reservoir could be substantially larger, including rocks outside the caldera, or a significant high-temperature reservoir may not exist at all.

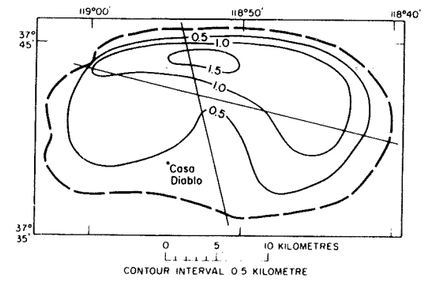

Fig. 3. Map showing depth (in kilometers) to top of Bishop Tuff in Long Valley caldera. The caldera boundary and seismic profiles are shown as in Figure 2.

Assuming that the reservoir has a volume of 450 km^3 and a porosity of 0.15, we have calculated the total heat above 0°C contained in the rock and water of the reservoir (Table 1). The geothermal resource, however, is commonly considered to be only the part of the heat that can be recovered and used under foreseeable economic conditions [*Muffler,* 1973, p. 255]. The extractable energy from Long Valley is shown in Table 1 under two assumptions [*Muffler,* 1973, p. 257]: (1) that the temperature of the reservoir will fall with time to 180°C, below which extraction will become uneconomic, and (2) that only 50% of the available energy between the reservoir temperature and 180°C will ever be extracted, owing to impermeable rock, insufficient number of drill holes, and nonoptimum drill hole spacing, etc.

Implicit in our discussion is the use of Long Valley geothermal energy for the generation of electricity. Accordingly, in Table 1 we have calculated the amount of electricity that could be generated by using conventional flashed steam techniques. We consider only the flashed steam, assume that the separation temperature is 145°C and that the thermodynamic efficiency is 14.3% (as at The Geysers [*Bruce,* 1971]), and use as a reservoir temperature the average of the initial and final conditions.

Of the many factors that affect the geothermal resource estimates for Long Valley, four are of paramount significance: (1) reservoir volume, which could range from a very small size to perhaps 1000 km^3, (2) recoverability, which could range from 0% for a completely impermeable 'reservoir' to perhaps greater than 100% for a reservoir with significant heat and fluid recharge, (3) temperature (a small change in estimated initial reservoir temperature can have a substantial effect on extractable energy estimates (e.g., Table 1)), (4) technology and economics of use (we have assumed conventional flash steam electrical generation; advanced technology or use for heating purposes obviously would increase the resource estimates of Table 1, the limiting factors being technologic, economic, and social, not geologic).

Much of the information required to refine these estimates can be obtained only in deep drill holes, but the expected deep exploration of the caldera by private industry has not yet taken

TABLE 1. Geothermal Resources of Long Valley

Reservoir Temperature, °C	Heat Above 0°C in Reservoir, J	Extractable Energy, J	Electrical Energy, MW cent.
220	24×10^{19}	2.1×10^{19}	350
250	27×10^{19}	3.6×10^{19}	700

place for a variety of reasons including the delay in leasing of federal lands. Full understanding of the Long Valley geothermal system and an accurate determination of its geothermal resource potential must await a series of deep wells coupled with a properly designed program to acquire pertinent drill hole data both during and after drilling.

REFERENCES

Anderson, L. A., and G. R. Johnson, A self-potential survey of Long Valley caldera, Mono County, California, open file report, U.S. Geol. Surv., Washington, D. C., 1974.

Bailey, R. A., Preliminary geologic map and cross section of the Casa Diablo geothermal area, Long Valley caldera, Mono County, California, open file report, U.S. Geol. Surv., Washington, D. C., 1974.

Bailey, R. A., G. B. Dalrymple, and M. A. Lanphere, Geology and geochronology of Long Valley caldera, Mono County, California, *J. Geophys. Res., 81,* this issue, 1976.

Bruce, A. W., Geothermal power—On line, Proceedings of First Northwest Conference on Geothermal Power, Olympia, Washington, Wash. Dep. of Natur. Resour., Olympia, Wash., 1971.

California Department of Water Resources, Investigation of geothermal waters in the Long Valley area, Mono County, 141 pp., Sacramento, Calif., 1967.

California Division of Oil and Gas., Geothermal map G 5-1, Casa Diablo, 1 inch:2000 feet, Sacramento, Calif., 1972.

Cleveland G. B., Geology of the Little Antelope Valley clay deposits, Mono County, California, *Calif. Div. Mines Geol. Spec. Rep., 72,* 28, 1962.

Dalrymple, G. B., and M. A. Lanphere, Preliminary potassium-argon age data on volcanic rocks from Long Valley caldera and vicinity, Mono County, California as of 22 February, 1974, open file report U.S. Geol. Surv., Washington, D. C., 1974.

Dalrymple, G. B., A. Cox, and R. R. Doell, Potassium-argon age and paleomagnetism of the Bishop Tuff, California, *Geol. Soc. Amer. Bull., 76,* 665–674, 1965.

Ellis, A. J., Quantitative interpretation of chemical characteristics of hydrothermal systems, in *Geothermics, Spec. Issue 2,* vol. 2, part 1, pp. 516–528, International Institute for Geothermal Research, Pisa. Italy, 1970.

Fournier, R. O., and J. J. Rowe, Estimation of underground temperatures from the silica content of water from hot springs and wet-steam wells, *Amer. J. Sci., 264,* 685–697, 1966.

Gilbert, C. M., Welded tuff in eastern California, *Geol. Soc. Amer. Bull., 49,* 1829–1862, 1938.

Hill, D. P., Structure of Long Valley caldera from seismic refraction experiments, *J. Geophys. Res., 81,* this issue, 1976.

Hoover, D. B., F. C. Frischknecht, and C. L. Tippens, Evaluation of audiomagnetotelluric techniques as a reconnaissance exploration tool in Long Valley, Mono and Inyo counties, California, open file report, U.S. Geol. Surv., Washington, D. C., 1974.

Huber, N. K., and C. D. Rinehart, Geologic map of the devils postpile quadrangle, Sierra Nevada, California, *Geol. Quadrangle Map GQ-437,* U.S. Geol. Surv., Washington, D. C., 1965.

Kane, M. F., R. L. Brace, and D. R. Mabey, Gravity and magnetic anomalies in Long Valley, California, *J. Geophys. Res., 81,* this issue, 1976.

Lachenbruch, A. H., J. H. Sass, R. J. Munroe, M. L. Sorey, and R. E. Lewis, Surficial thermal regime inside Long Valley caldera, *J. Geophys. Res., 81,* this issue, 1976.

Lewis, R. E., Data on wells, springs, and thermal springs in Long Valley, Mono County, California, open file report, 52 pp., U.S. Geol. Surv., Washington, D. C., 1974.

Mariner, R. H., and L. M. Willey, Geochemistry of thermal waters in Long Valley, California, *J. Geophys. Res. 81,* this issue, 1976.

McKenzie, W. F., and A. H. Truesdell, Geothermal reservoir temperatures estimated from oxygen isotope composition of dissolved sulfate and water from hot springs, in *Abstracts, Second U.N. Symposium on the Development and Use of Geothermal Resources,* Lawrence Berkeley Laboratory, University of California, Berkeley, Calif., 1975.

McNitt, J. R., Exploration and development of geothermal power in California, *Calif. Div. Mines Geol. Spec. Rep., 75,* 45 pp., 1963.

Muffler, L. J. P., U.S. Geological Survey research in geothermal resources, in *Compendium of First Day Papers, First Conference of the Geothermal Resources Council, El Centro, California,* edited by D. N. Anderson and L. H. Axtell, pp. 11–18, Geothermal Resources Council, Davis, Calif., 1972.

Muffler, L. J. P., Geothermal resources, United States Mineral Resources, *U.S. Geol. Surv. Prof. Pap. 820,* 251–261, 1973.

Muffler, L. J. P., and D. E. White, Active metamorphism of upper Cenozoic sediments in the Salton Sea geothermal field and the Salton Trough, southeastern California, *Geol. Soc. Amer. Bull., 80,* 157–182, 1969.

Pakiser, L. C., Gravity and volcanism and crustal deformation in Long Valley, California, *U.S. Geol. Surv. Prof. Pap. 424-B,* 250–253, 1961.

Pakiser, L. C., M. F. Kane, and W. H. Jackson, Structural geology and volcanism of Owens Valley region, California—A geophysical study, *U.S. Geol. Surv. Prof. Pap. 438,* 68 pp., 1964.

Ratté, J. C., and T. A. Steven, Ash flows and related volcanic rocks associated with the Creede Caldera, San Juan Mountains, Colorado, *U.S. Geol. Surv. Prof. Pap. 524-H,* 58 pp., 1967.

Rinehart, C. D., and D. C. Ross, Geology of the Casa Diablo Mountain quadrangle, California, *Geol. Quadrangle Map GQ-99,* U.S. Geol. Surv., Washington, D. C., 1957.

Rinehart, C. D., and D. C. Ross, Geology and mineral deposits of the Mount Morrison quadrangle, Sierra Nevada, California, *U.S. Geol. Surv. Prof. Pap. 385,* 106 pp., 1964.

Sass, J. H., A. H. Lachenbruch, R. J. Munroe, G. W. Greene, and T. H. Moses, Jr., Heat flow in the western United States, *J. Geophys. Res., 76,* 6376–6413, 1971.

Sass, J. H., A. H. Lachenbruch, and R. J. Munroe, Thermal data from heat-flow test wells near Long Valley, California, open file report, 43 pp., U.S. Geol. Surv., Washington, D. C., 1974.

Smith, R. S., and R. A. Bailey, Resurgent cauldrons, Studies in Volcanology, *Geol. Soc. Amer. Mem., 116,* 613–662, 1968.

Sorey, M. L., and R. E. Lewis, Discharge of hot spring systems in Long Valley caldera, *J. Geophys. Res., 81,* this issue, 1976.

Stanley W. D., D. B., Jackson, and A. A. R. Zohdy, Preliminary results of deep electrical studies in the Long Valley caldera, Mono and Inyo counties, California, open file report, 62 pp., U.S. Geol. Surv., Washington, D. C., 1973.

Stanley, W. D., D. B. Jackson, and A. A. R. Zohdy, Deep electrical investigations in the Long Valley geothermal area, California, *J. Geophys. Res., 81,* this issue, 1976.

Steeples, D. W., and H. M. Iyer, Low-velocity zone under Long Valley as determined from teleseismic events, *J. Geophys. Res., 81,* this issue, 1976.

Waring, G. A., Springs of California, *U.S. Geol. Surv. Water Supply Pap. 338,* 410 pp., 1915.

White, D. E., Geothermal energy, *U.S. Geol. Surv. Circ., 519,* 1–17, 1965.

White, D. E., Environments of generation of some base-metal ore deposits, *Econ. Geol., 63*(4), 301–335, 1968*a*.

White D. E., Hydrology, activity, and heat flow of the Steamboat springs thermal systems, Washoe County, Nevada, *U.S. Geol. Surv. Prof. Pap. 458-C,* 109 pp., 1968*b*.

White, D. E., G. A. Thompson, and C. H. Sandberg, Rocks, structure, and geologic history of Steamboat Springs thermal area, Washoe County, Nebraska, *U.S. Geol. Surv. Prof. Pap. 458B,* 63 pp., 1964.

White, D. E., L. J. P. Muffler, and A. H. Truesdell, Vapor-dominated hydrothermal systems compared with hot-water systems, *Econ. Geol., 66,* 75–97, 1971.

White, D. E., R. O. Fournier, L. J. P. Muffler, and A. H. Truesdell, Physical results of research drilling in thermal areas of Yellowstone National Park, Wyoming, *U.S. Geol. Surv. Prof. Pap. 892,* 70 pp., 1975.

Whiting, H. A., Mono County, *Annu. Rep. 8,* pp. 352–401, Calif. Mining Bur., Sacramento, Calif., 1888.

Willey, L. M., J. R. O'Neil, and J. B. Rapp, Chemistry of thermal waters in Long Valley, Mono County, California, open file report, 19 pp., U.S. Geol. Surv., Washington, D. C., 1974.

(Received January 15, 1975;
revised July 24, 1975;
accepted July 28, 1975.)

Volcanism, Structure, and Geochronology of Long Valley Caldera, Mono County, California

ROY A. BAILEY

U.S. Geological Survey, Reston, Virginia 22092

G. BRENT DALRYMPLE AND MARVIN A. LANPHERE

U.S. Geological Survey, Menlo Park, California 94025

Long Valley caldera, a 17- by 32-km elliptical depression on the east front of the Sierra Nevada, formed 0.7 m.y. ago during eruption of the Bishop tuff. Subsequent intracaldera volcanism included eruption of (1) aphyric rhyolite 0.68–0.64 m.y. ago during resurgent doming of the caldera floor, (2) porphyritic hornblende-biotite rhyolite from centers peripheral to the resurgent dome at 0.5, 0.3, and 0.1 m.y. ago, and (3) porphyritic hornblende-biotite rhyodacite from outer ring fractures 0.2 m.y. ago to 50,000 yr ago, a sequence that apparently records progressive crystallization of a subjacent chemically zoned magma chamber. Holocene rhyolitic and phreatic eruptions suggest that residual magma was present in the chamber as recently as 450 yr ago. Intracaldera hydrothermal activity began at least 0.3 m.y. ago and was widespread in the caldera moat; it has since declined due to self-sealing of near-surface caldera sediments by zeolitization, argillization, and silicification and has become localized on recently reactivated northwest-trending Sierra Nevada frontal faults that tap hot water at depth.

INTRODUCTION

In the western United States, only three calderas are known to be large enough and young enough to possibly still contain residual magma in their chambers: the Valles caldera (~1.1 m.y. old) in north central New Mexico; the Long Valley caldera (~0.7 m.y. old) in central eastern California, and the Yellowstone caldera (~0.6 m.y. old) in northwestern Wyoming. Detailed mapping of the Valles caldera [*Smith et al.*, 1961, 1970] and the Yellowstone caldera [*Christiansen and Blank,* 1969; *U.S. Geological Survey,* 1972; *Keefer,* 1972] has contributed much to the understanding of caldera evolution and mechanisms. Long Valley caldera (Figures 1 and 2) heretofore has not been mapped in detail, although a number of excellent studies of the general geology of the region have been made, notably by *Gilbert* [1938, 1941], *Gilbert et al.* [1968], *Kistler* [1966*a*, *b*], *Rinehart and Ross* [1957, 1964], and *Huber and Rinehart* [1967]. Inclusion of Long Valley as one of the target areas of the U.S. Geological Survey Geothermal Research Program has provided an opportunity to apply a wide range of geologic, geochemical, and geophysical techniques to the study of a large, active geothermal system; it also has provided the first opportunity to synthesize the volcanic history of this fascinating area. This paper is a preliminary report of the geologic and chronological studies based on mapping and sampling carried on during the summers of 1972 and 1973. Geologic mapping and petrologic studies are continuing. The petrologic model presented in the summary is based primarily on field studies, supplemented by preliminary petrography and limited preexisting petrochemical data, and should be considered tentative.

K-AR DATING TECHNIQUE

Samples for age measurement were collected from outcrops at locations shown on Figure 3. When it was possible, biotite or sanidine in the size range of 149–420 μm was separated by using standard magnetic and heavy liquid techniques. Sanidine concentrates were treated with a dilute HF solution to remove small bits of attached glass and fragments of other mineral grains. Obsidian used for dating was totally unhydrated and not devitrified. Small blocks sawed from many of the hand specimens were used for dating. For samples that contained phenocrysts the obsidian was crushed to between 2 and 4 mm, and pure glass fragments were handpicked for analysis. Basalt and andesite were examined in thin sections to be sure that they met the usual criteria for whole-rock K-Ar dating [*Mankinen and Dalrymple,* 1972].

Argon was measured by isotope dilution mass spectrometry using an ^{38}Ar tracer and extraction techniques, mass analysis, and data reduction procedures described by *Dalrymple and Lanphere* [1969]. Potassium was determined by using the lithium metaborate fusion technique and flame photometry [*Suhr and Ingamells,* 1966; *Ingamells,* 1970]. Errors given in Table 1 and in the text are standard deviations of analytical precision, estimated by using the method of *Cox and Dalrymple* [1967].

The analytical data and calculated K-Ar ages are given in Table 1 and discussed in the appropriate sections along with the stratigraphy, petrology, and structure. A summary of the age data, showing stratigraphic relations and relevant statistical data, is presented in Figure 4.

GEOLOGIC SETTING

Long Valley caldera is at the east base of the Sierra Nevada, 50 km northwest of the town of Bishop and 30 km south of Mono Lake (Figure 1). The caldera is an elliptical depression about 32 km from east to west by 17 km from north to south; it has an area of about 450 km² (Figure 2). The eastern half of the caldera, Long Valley proper, is a broad, crescentic grass- and sage-covered valley of low relief, at an elevation near 2070 m (6800 ft). The western half of the caldera is a forested area of higher relief at an average elevation of 2440 m (8000 ft); it forms the 'Mammoth embayment,' a prominent reentrant in the Sierra Nevada range front near the town of Mammoth Lakes. In the west central part of the caldera a group of faulted and dissected hills rises to 2590-m (8500 ft) elevation. Between

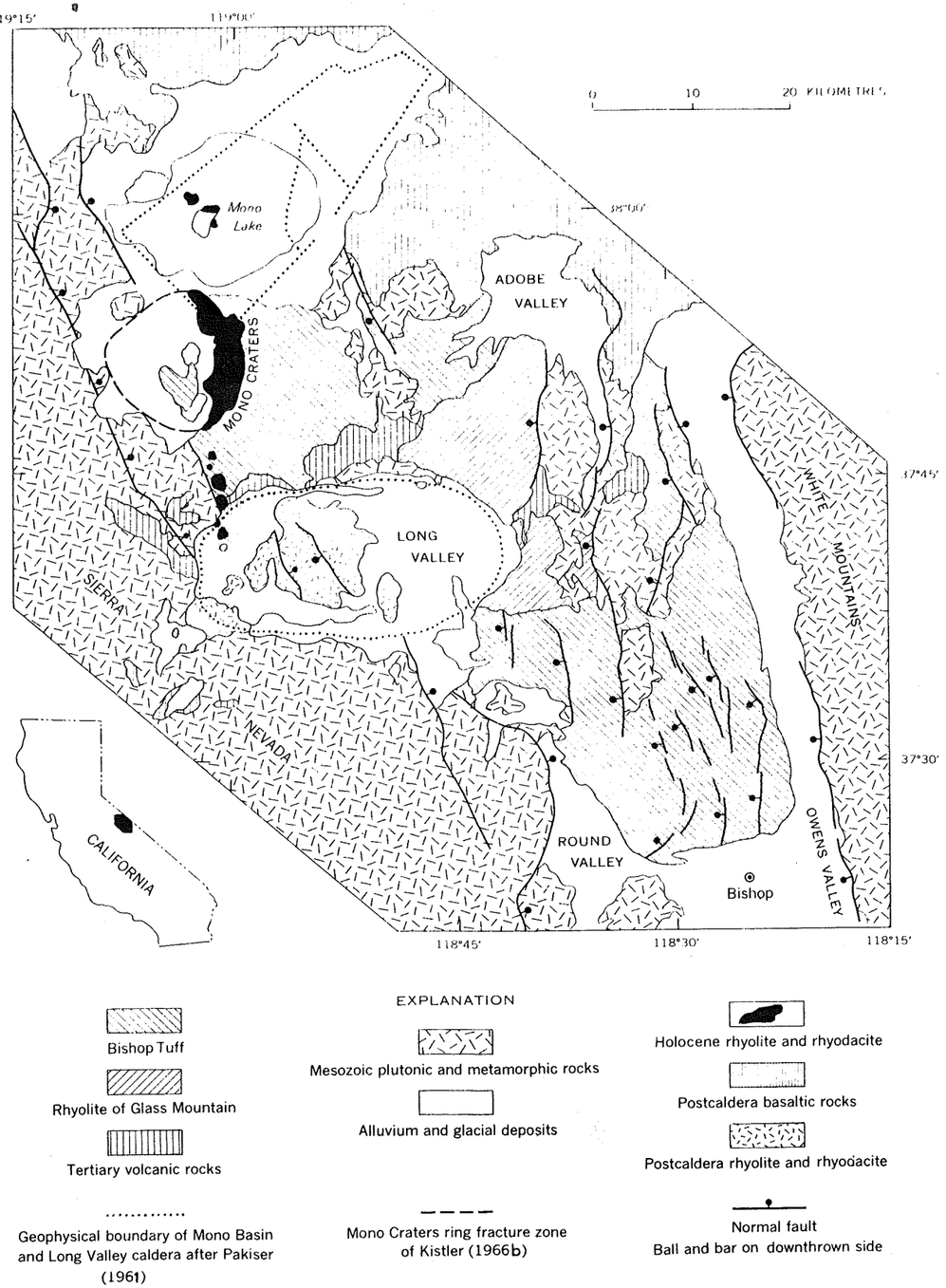

Fig. 1. Index map and generalized geologic map of the Long Valley–Mono basin area.

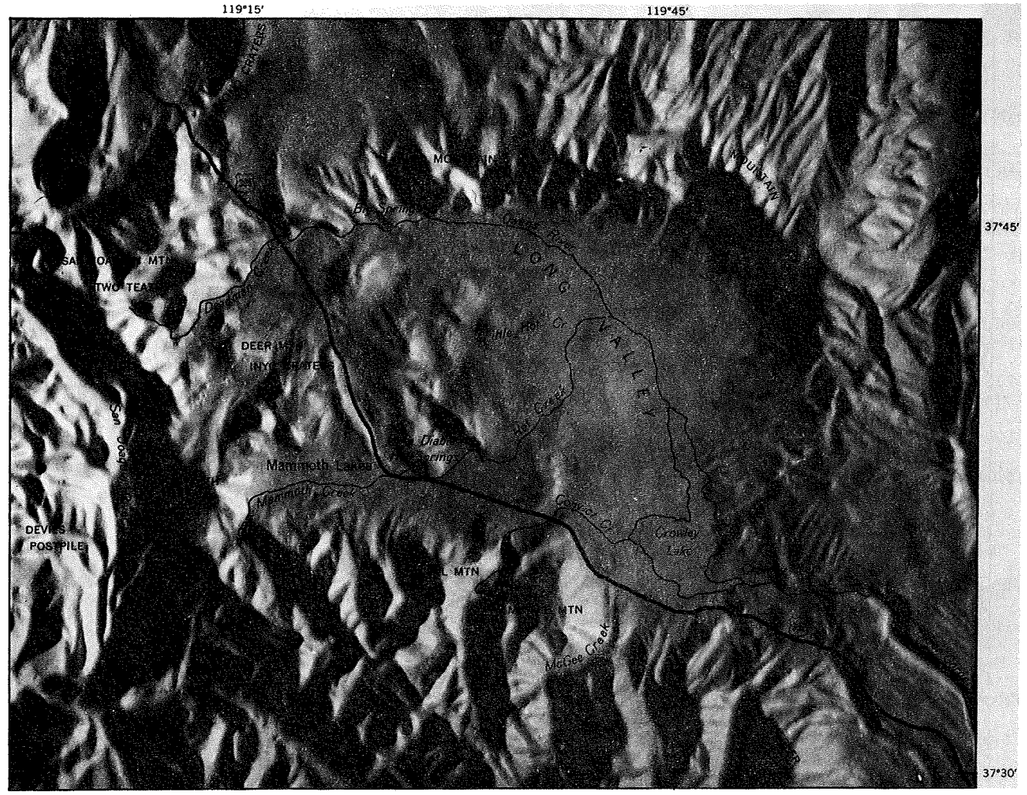

Fig. 2. Shaded relief map of Long Valley caldera.

these central hills and the caldera walls is an annular moat, which is drained on the north by Deadman Creek and the upper Owens River and on the south by Mammoth Creek and Hot Creek. The walls of the caldera are well defined and rise steeply on all sides except the southeast. On the south the wall rises precipitously 1000 m to remnants of a late Tertiary erosion surface [*Rinehart and Ross*, 1964, Plate 1; *Curry*, 1971] at an elevation of 3050 m (10,000 ft) on the shoulders of McGee and Laurel mountains. In the west the wall rises 500 m to the eastern slopes of San Joaquin Mountain and Two Teats. On the north and northeast the wall is formed by the steep south face of Bald Mountain and of Glass Mountain, which rises 1200 m to an elevation of about 3350 m (11,000 ft). The east wall, in contrast, is a low terraced escarpment with a maximum relief of only 250 m, and the southeast wall is little more than an arch that merges with the surface of the Volcanic Tableland, which slopes gently southeast toward Bishop.

The pre-Tertiary basement rocks in the immediate vicinity of Long Valley caldera are Jurassic and Cretaceous granodiorites and granites of the Sierra Nevada batholith and Paleozoic and Mesozoic metamorphic rocks of the Mount Morrison and Ritter range roof pendants [*Bateman et al.*, 1963; *Rinehart and Ross*, 1964] (Figure 3). Overlying the basement rocks on an erosion surface of moderate relief are late Tertiary volcanic rocks, mainly basalt, andesite, and rhyodacite.

Basalt and andesite flows with a cumulative thickness of 200–250 m crop out in the west wall of the caldera, as well as along part of the north wall. Thinner, less extensive sequences of flows from small local centers occur also on the east rim south of Glass Mountain and on the south rim on McGee Mountain. Rhyodacites overlie the basaltic rocks on the west rim and form the main mass of San Joaquin Mountain and Two Teats, the dissected remnants of a large Pliocene volcano northwest of the caldera. Three additional masses of rhyodacite, the largest of which is Bald Mountain, occur on the north rim.

Abundant basaltic inclusions found in postsubsidence intracaldera rhyolites suggest that the thick sequences of basaltic rocks on the west and north walls extend well into the caldera area. In contrast, rhyodacite inclusions are rare in the postcaldera rhyolites, suggesting that no comparable thickness of rhyodacite occurs within the caldera. The available evidence indicates that no great accumulation or edifice of precaldera volcanic rocks existed within the caldera area, as is true of many other resurgent cauldrons [*Smith and Bailey*, 1968; *Smith et al.*, 1970]. The wide and sporadic distribution of precaldera volcanic centers suggests that these Tertiary rocks are not directly related to the Long Valley magma chamber, although they may represent an early part of the volcanic cycle that culminated with the voluminous rhyolites of Long Valley.

These Tertiary volcanic rocks range in age from 3.2 to 2.6 m.y. old. Units in the vicinity of Long Valley that have been dated by the K-Ar method include (1) the basalt at Old Mam-

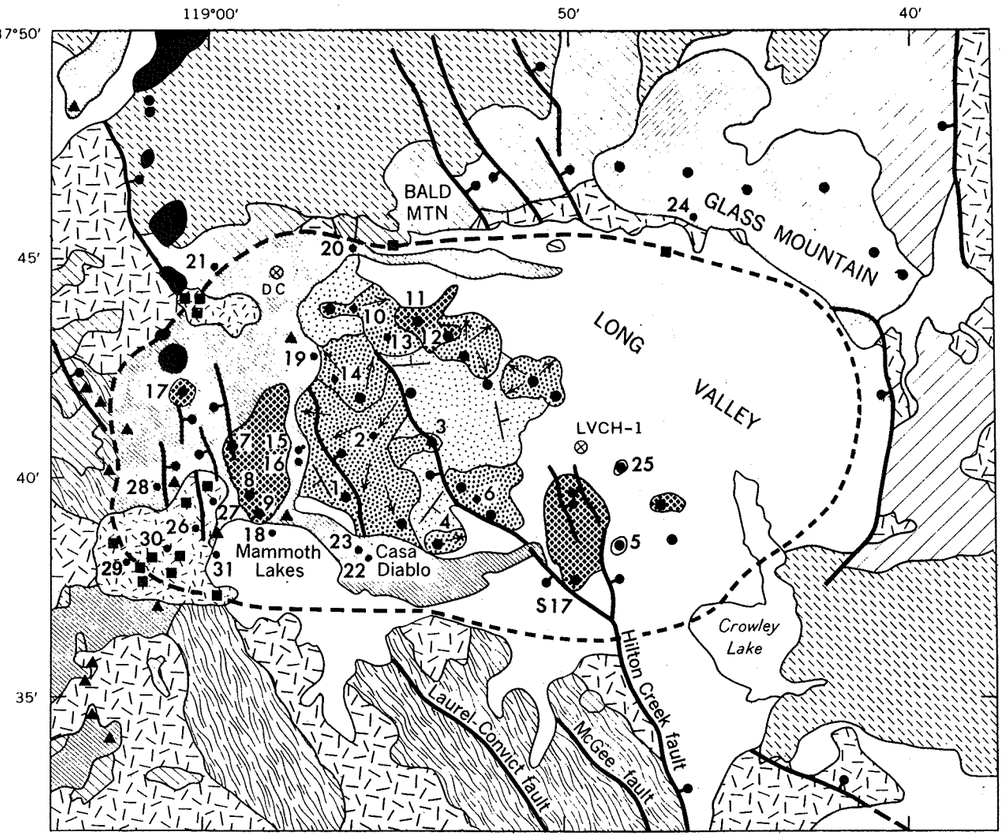

Fig. 3. Generalized geologic map of Long Valley caldera.

TABLE 1. K-Ar Age Data on Volcanic Rocks From Long Valley Caldera, California

Sample No.	Map No. (Figure 3)	Rock Type	Material Dated	K_2O*, wt %	Argon: Weight, g	Argon: $^{40}Ar_{rad}$, 10^{-12}mol/g	Argon: $100\ ^{40}Ar_{rad}/^{40}Ar_{total}$	Calculated Age,† 10^6 yr
72G001	1	Aphyric rhyolite	Obsidian	5.10 (2)	3.470	5.189	43.5	0.675 ± 0.016
					3.461	4.948	29.1	
72G002	2	Biotite rhyolite	Obsidian	5.24 (2)	4.228	5.125	53.4	0.660 ± 0.027
					4.188	5.070	16.5	
72G003	3	Pyroxene rhyolite	Obsidian	5.25 ± 0.06 (4)	3.870	5.199	16.7	0.664 ± 0.029
					4.075	5.131	34.6	
72G004	4	Pyroxene rhyolite	Obsidian	5.22 (2)	4.426	5.312	34.7	0.670 ± 0.014
					4.442	5.057	57.0	
72G005	5	Hornblende-biotite rhyolite	Sanidine	10.96 (2)	5.828	5.263	48.2	0.324 ± 0.010
72G006	6	Pyroxene rhyolite	Obsidian	5.02 (2)	4.089	5.583	46.4	0.73 ± 0.016
					4.197	5.280	45.3	
72G007	7	Hornblende-biotite rhyolite	Sanidine	10.88 (2)	12.182	1.724	64.4	0.106 ± 0.003
72G008	8	Hornblende-biotite rhyolite	Sanidine	11.24 (2)	5.080	1.330	9.1	0.094 ± 0.006
					5.872	1.590	33.5	
72G009	9	Hornblende-biotite rhyolite	Sanidine	11.32 (2)	6.755	1.735	38.8	0.103 ± 0.002
					6.112	1.744	34.2	
72G010	10	Aphyric rhyolite	Obsidian	5.07 (2)	3.430	5.145	43.9	0.673 ± 0.014
					4.458	4.967	53.0	
72G011	11	Hornblende-biotite rhyolite	Sanidine	10.64 (2)	6.544	7.293	40.4	0.468 ± 0.010
					7.160	7.440	40.7	
72G012	12	Hornblende-biotite rhyolite	Sanidine	10.45 (2)	5.799	8.023	62.3	0.509 ± 0.011
					5.158	7.730	76.0	
72G013	13	Aphyric rhyolite	Obsidian	5.14 (2)	4.932	4.992	54.5	0.658 ± 0.014
					5.384	5.036	41.6	
72G014	14	Pyroxene rhyolite	Obsidian	5.15 (2)	3.955	4.958	57.4	0.634 ± 0.013
					3.908	4.725	34.5	
72G015	15	Basalt	Whole-rock	1.654 (2)	10.578	0.367	3.1	0.149 ± 0.070
72G016	16	Basalt	Whole-rock	1.663 (2)	11.078	0.372	8.8	0.151 ± 0.027
72G017	17	Hornblende-biotite rhyolite	Sanidine	10.63 (2)	4.347	1.890	24.8	0.113 ± 0.004
					12.901	1.728	32.2	
73G001	18	Andesite	Whole-rock	2.13 ± 0.01 (4)	9.102	0.700	2.8	0.222 ± 0.080
73G008	19	Basalt	Whole-rock	2.00 ± 0.00 (4)	8.379	0.428	8.8	0.145 ± 0.015
73G009	20	Basalt	Whole-rock	1.63 ± 0.05 (8)	12.256	0.271	13.3	0.104 ± 0.011
					14.187	0.201	4.3	
73G010	21	Andesite	Whole-rock	3.01 ± 0.01 (4)	14.401	12.787	70.2	2.87 ± 0.09
73G012	22	Basalt	Whole-rock	2.26 ± 0.06 (4)	5.837	0.482	5.5	0.126 ± 0.025
					7.784	0.372	4.7	
73G014	23	Basalt	Whole-rock	1.82 ± 0.01 (4)	12.806	0.148	4.3	0.062 ± 0.013
					11.736	0.194	3.5	
73G016	24	Biotite rhyolite	Sanidine	9.75 ± 0.26 (4)	1.053	27.749	61.6	1.92 ± 0.05
73G017	25	Hornblende-biotite rhyolite	Sanidine	11.34 ± 0.03 (4)	4.084	6.029	55.5	0.349 ± 0.006
					3.433	5.812	58.2	
			Biotite	8.93 ± 0.06 (4)	1.337	6.645	4.7	0.503 ± 0.105
73G018	26	Rhyodacite	Biotite	8.60 (2)	1.688	2.212	4.1	0.145 ± 0.029
					1.995	1.422	2.8	
73G019	27	Rhyodacite	Biotite	7.12 (2)	1.897	1.460	2.6	0.138 ± 0.079
73G021	28	Basalt	Whole-rock	1.57 ± 0.01 (4)	11.928	0.211	5.7	0.093 ± 0.012
					10.930	0.225	4.8	
73G023	29	Rhyodacite	Sanidine	7.76 (2)	2.251	0.582	9.2	0.050 ± 0.010
73G024	30	Rhyodacite	Biotite	8.22 (2)	1.841	1.436	2.4	0.118 ± 0.048
73G025	31	Andesite	Whole-rock	2.63 ± 0.01 (4)	7.543	0.366	7.1	0.083 ± 0.010
					9.418	0.320	14.8	

*Mean and, where more than two measurements were made, standard deviation. Number of measurements is in parentheses.

†$\lambda_\epsilon = 0.585 \times 10^{-10}\ yr^{-1}$, $\lambda_\beta = 4.72 \times 10^{-10}\ yr^{-1}$, $^{40}K/K = 1.19 \times 10^{-4}$ mol/mol. Where more than one measurement was made on a sample, the age given is the weighted mean; weighting was by the inverse of the variance. Errors given are estimates of the standard deviation of analytical precision [*Cox and Dalrymple*, 1967].

moth Mine and (2) andesite from San Joaquin ridge, both 3.1 ± 0.1 m.y. old [*Dalrymple*, 1964*a*]; (3) basalts in the Benton range that erupted from a cone on the northeast rim of the caldera 3.2 ± 0.1 m.y. ago [*Dalrymple*, 1964*a*]; (4) basalt in the Owens River gorge, 3.2 ± 0.1 m.y. old [*Dalrymple*, 1963]; (5) andesite in the northwest wall, 2.87 ± 0.09 m.y. old (location 21; location numbers refer to map locations in Figure 3 and Table 1); (6) basalt on McGee Mountain, 2.6 ± 0.1 m.y. old [*Dalrymple*, 1963]; and (7) quartz latites from Two Teats, 3.0 ± 0.1 m.y. old [*Dalrymple*, 1964*a*] and 2.7 ± 0.1 m.y. old [*Curry*, 1966].

RHYOLITES OF GLASS MOUNTAIN

The earliest volcanic rocks that can be related to the Long Valley magma chamber are the rhyolites of Glass Mountain (Figure 3). Glass Mountain is a thick accumulation (>1000 m) of domes, flows, and shallow intrusions flanked by extensive fans of pyroclastic deposits that consist of pumice and ash

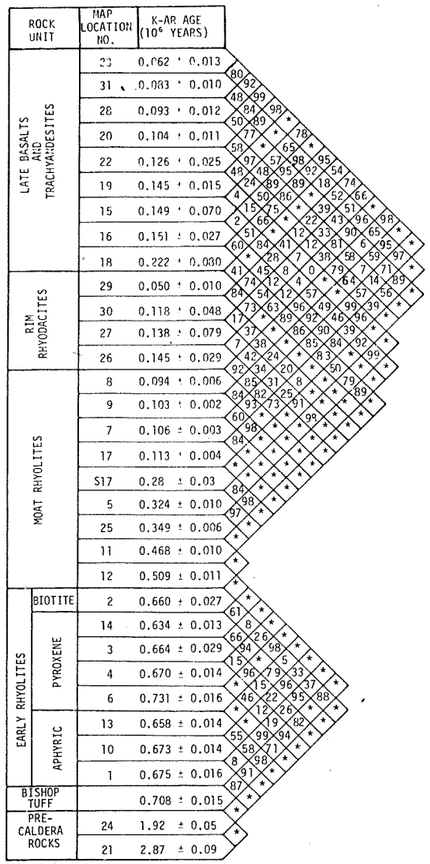

Fig. 4. Maximum probability, in percent, that the calculated ages of any two volcanic units are truly different and not the result of random errors in the analytical procedure. A probability of more than 99% is indicated by an asterisk.

falls, small ash flows, blocky Pelean avalanche deposits, and epiclastic conglomeratic sediments [*Gilbert*, 1941; *Rinehart and Ross*, 1957]. Dissected remnants of the flanking fans extend northeast into Adobe Valley and south along the east side of the caldera. Similar fans probably extended southwest from Glass Mountain, but the southwest half of the mountain has been downfaulted along the caldera boundary faults and is now buried beneath the sedimentary and volcanic fill of Long Valley. The vents and intrusive centers of Glass Mountain are well exposed in its south face. They are arranged in an arc approximately parallel to the northeast wall of Long Valley caldera, which suggests that their location was controlled by an incipient caldera ring fracture and that they represent early leakage from the Long Valley magma chamber.

The rhyolites of Glass Mountain are aphyric to sparsely porphyritic, and, according to *Noble et al.* [1972], are highly differentiated, peraluminous, and high in silica (containing about 77%). Two K-Ar ages, one of 0.90 ± 0.10 m.y. obtained on sanidine from obsidian near the top of Glass Mountain [*Gilbert et al.*, 1968, p. 302] and another of 1.92 ± 0.05 m.y. on sanidine from a biotite rhyolite low on the southwest side (location 24), indicate that Glass Mountain was built by eruptions that extended over a period of at least 1 m.y.

Bishop Tuff

The Bishop tuff, a voluminous rhyolite ash flow sheet, erupted about 0.7 m.y. ago [*Dalrymple et al.*, 1965] from vents now buried within Long Valley caldera [*Gilbert*, 1938, pp. 1859–1860]. From these vents, ash flows spread radially southeast through the low area now occupied by the Owens River, north over the west shoulder of Glass Mountain into Adobe Valley, northwest over Deadman Summit into Mono basin, and west over the low pass now occupied by Mammoth Mountain into the valley of the Middle Fork of the San Joaquin River (Figure 1). The most extensive exposure of Bishop tuff is on the Volcanic Tableland southeast of the caldera [*Gilbert*, 1938; *Sheridan*, 1965]. Lesser exposures occur in the southeastern part of the Adobe Valley and in the southern part of the Mono basin [*Gilbert*, 1938], where the sheet is extensively covered by pumice from the Mono craters. Small erosional remnants also cling to the walls of the Middle Fork of the San Joaquin near Reds Meadow [*Huber and Rinehart*, 1967].

The Bishop tuff is a crystal-rich rhyolite tuff that contains up to 30% phenocrysts of quartz, sanidine, plagioclase, biotite, and Fe-Ti oxides [*Gilbert*, 1938; *Sheridan*, 1965]. Available chemical data [*Bateman*, 1965, Table 21; *Sheridan*, 1965, Table 5] indicate that the Bishop tuff differs only slightly in composition from top to bottom and is not a strongly differentiated sheet. According to *Sheridan* [1968] the tuff exposed in the lower Owens River gorge is a double cooling unit, which indicates that it was emplaced during two eruptive pulses.

Gilbert [1938, p. 1833] estimated that the Bishop tuff covers an area of 1040–1150 km² and has a volume of about 140 km³. His estimate, however, did not include the large volume of tuff buried within the caldera. Although Bishop tuff is not exposed anywhere within the caldera, blocks of the tuff occur as accidental inclusions in early postcaldera rhyolite tuffs exposed in the central part of the caldera, clearly indicating that Bishop tuff underlies the tuffs at depth [*Bailey*, 1973]. Most of the inclusions are of densely welded tuff, suggesting that the intracaldera Bishop tuff is probably quite thick. By analogy with intracaldera welded tuffs exposed in older, more deeply dissected resurgent cauldrons [*Ratté and Steven*, 1967; *Byers et al.*, 1968; *Lipman and Steven*, 1970; *Lipman et al.*, 1973; R. L. Smith and R. A. Bailey, unpublished data, 1970], the intracaldera Bishop tuff is probably of the order of 1000 m thick. Seismic refraction studies of the caldera [*Hill*, 1976] suggest a thickness of 1000–1500 m. By using a thickness of 1000 m and the area of the subsided cauldron block (350 km² as defined by the inferred position of the main boundary faults in the caldera moat), the volume of intracaldera Bishop tuff is estimated to be about 350 km³. Thus the total volume of Bishop ash flows is of the order of 500 km³, two-thirds of which accumulated within the subsiding caldera.

The volume of Bishop ash that was carried away by winds and thinly dispersed over much of the western United States is difficult to estimate on the basis of presently available data. However, using (1) the distribution of Bishop ash indicated by *Izett et al.* [1970] and (2) one-half the maximum thickness (3 m) of Bishop pumice fall in the vicinity of the caldera and (3) assuming logarithmic thinning of the ash downwind, we calculate a volume of 300 km³. Although this estimate seems surprisingly large, we believe our method of calculation yields a conservative figure. Furthermore, the relative proportion of ash fall to ash flows (3:5) does not seem unreasonable when it is compared with the ratio (1:1) of the Mazama ash to its associated Crater Lake ash flows [*Williams and Goles*, 1968], especially when one takes into account the likelihood that the Crater Lake eruption had a stronger vertical component.

The foregoing volumes of ash and tuff, when they are reduced by appropriate factors for their porosity, indicate that the total volume of magma ejected during eruption of the Bishop tuff was of the order of 600 km³.

Hildreth and Spera [1974] report on the basis of mineralogical and geochemical studies that the initial ash falls of the Bishop tuff erupted at temperatures of 745°C under a pressure of less than 2 kbar and that the ash flows erupted at 800°C under pressures of greater than 3 kbar. These data suggest that the roof of the chamber was at a depth of about 6 km at the time of initial outburst and that the last ash flows came from a depth of about 10 km. These data are in fair agreement with evidence to be discussed below, i.e., that the maximum amount of caldera collapse associated with the eruption of the Bishop tuff was about 3 km.

K-Ar ages on samples from three exposures of the Bishop tuff range from about 0.68 to 0.74 m.y. [*Dalrymple et al.*, 1965], but none of the individual measurements are significantly different from the weighted mean age of 0.708 ± 0.015 m.y. at the 95% level of confidence. Both the K-Ar ages and the paleomagnetic data, from welded parts of the Bishop tuff, are consistent with the interpretation that this ash flow sheet was emplaced within a time span of no more than a few centuries [*Dalrymple et al.*, 1965].

Caldera Subsidence

As a result of eruption of the Bishop tuff the Long Valley magma chamber was partially emptied, and its roof consequently collapsed. Collapse probably took place along arcuate ring faults, although few of these are now exposed. One outer ring fault, with a maximum displacement of 250 m, can be traced for a distance of 12 km along the east wall of the caldera (Figure 3), but the gravity gradient on the eastern margin of the caldera [*Pakiser*, 1961; *Pakiser et al.*, 1964; *Kane et al.*, 1976] requires much greater displacement, and the main boundary fault must be buried in the caldera fill to the west. The main boundary fault probably lies well within the caldera moat, and the present diameter of the caldera undoubtedly has been enlarged by slumping of the initially unstable walls and by subsequent erosion.

Although *Gilbert* [1938, 1941] recognized Long Valley as the source of the Bishop tuff and suggested that most of the recent faulting in the depression was a result of extrusion of a large volume of magma from beneath it, the caldera origin of Long Valley has been questioned by some investigators, probably because the boundary faults are largely covered and actual displacement on them cannot be measured. The gravity studies of *Pakiser* [1961] and *Pakiser et al.* [1964] lent support to the caldera origin by more clearly defining its oval shape and establishing that it contained a great thickness of low-density fill. Pakiser (in the work by *Rinehart and Ross* [1964]) elaborated on the mechanism of eruption and collapse, but because he overestimated the volume of fill [*Kane et al.*, 1976], he concluded that volcanism alone could not account for the amount of subsidence, and consequently he considered Long Valley a volcano-tectonic depression. Recognition of a resurgent dome within the depression [*Smith and Bailey*, 1968] provided indirect evidence for caldera origin, but perhaps the most convincing evidence is that provided by the inclusions of Bishop tuff in the early rhyolites in the depression and by the timing of subsidence established by K-Ar dating. Bishop tuff inclusions in the early postcaldera rhyolite tuffs, which are at least 500 m thick, indicate that Bishop tuff has definitely subsided to a considerable depth within the depression (a minimum of 800 m below the general level of Bishop tuff on the north caldera rim). K-Ar dating (Figure 4) of the Bishop tuff (0.71 m.y.) and the earliest intracaldera rhyolites (0.73–0.68 m.y.) indicates that this subsidence occurred within a very short time following eruption of the Bishop tuff. Thus subsidence can clearly be associated with eruption of the Bishop tuff and is not the result of tectonic movements, which have been continuously active in the general area over a much longer time at much slower rates.

The minimum amount of subsidence of the cauldron block is about 1000 m, indicated by the topographic relief between the floor of Long Valley and the shoulders of Glass Mountain and remnants of the Tertiary erosion surface on the south rim of the caldera. The average thickness of low-density materials in the eastern half of the caldera beneath Long Valley, indicated by the gravity model of *Kane et al.* [1976, Figure 5] and by the seismic refraction study of *Hill* [1976], is about 3000 m. Of this thickness, 500–1000 m is probably downfaulted precaldera rhyolite of Glass Mountain. The caldera fill, including the Bishop tuff, in Long Valley is therefore about 2000–2500 m thick, so the maximum subsidence in the eastern part of the caldera is of the order of 3000 m.

The topographic relief on the walls in the west half of the caldera, about 300–600 m, is considerably less than in the east. Part of this difference may be accounted for by the infill of young basaltic lavas in the western moat, but they probably do not greatly exceed 200 m in thickness. The average thickness of low-density rocks in the western part of the caldera, indicated by *Kane et al.* [1976, Figure 5] and *Hill* [1976], is about 1700 m, of which about 200 m probably is precaldera volcanic rocks, judging from exposures in the west and north walls of the caldera. Thus the caldera fill, including Bishop tuff, in the west probably is about 1500 m, and the total subsidence is of the order of 2000 m. Subsidence in the west therefore is about 1000 m less than in the east.

This difference in subsidence in the east and west is especially evident in the gravity maps of *Kane et al.* [1976, Figures 2, 3], a conspicuous feature of which is a northwest-trending gradient transecting the middle of the caldera. This gradient coincides with the northward projection of the Hilton Creek fault, a major active Sierra Nevada frontal fault, and is thought to reflect either precaldera displacement of the basement (down to the east) on the intracaldera segment of the fault or, as suggested by *Hill* [1976], differential displacement on the fault during caldera collapse. It is also evident from the gravity and seismic refraction studies that the caldera fill thickens markedly to the north, suggesting that the floor tilted in that direction during subsidence.

The total volume of caldera subsidence can be estimated from the gravity model and the present topography. The volume of the present topographic depression, based on reconstruction of the precaldera topography, is about 200 km³. The volume of the subsurface depression calculated from the gravity model [*Kane et al.*, 1976, Figure 3] is about 800 km³ [*Muffler and Williams*, 1976]. Probably about one quarter of this volume is subsided precaldera volcanic rocks; hence the subsurface volume occupied by the Bishop tuff and younger rhyolite tuffs and lavas is about 600 km³, and the total combined subsurface and topographic subsidence is of the order of 800 km³. About 75% of this volume can be accounted for by the

estimated 600 km³ of magma ejected during eruption of the Bishop tuff, and possibly an additional 5–10% can be accounted for by minor subsidence accompanying eruption of postcaldera tuffs and lavas (40–80 km³ of magma). Thus with presently available data, 80% or more of the estimated volume of subsidence can be attributed to eruption of the Bishop tuff and associated intracaldera volcanic rocks.

EARLY RHYOLITES

K-Ar ages of 0.73–0.63 m.y. indicate that almost immediately after subsidence, eruptions resumed within the caldera. During this time crystal-poor rhyolite tuffs, domes, and flows accumulated on the floor to a thickness of at least 500 m. These rocks, informally designated the 'early rhyolites,' are exposed in tilted and uplifted fault blocks in the central part of the caldera.

The tuffs contain abundant inclusions of Bishop tuff and basalt and, less commonly, fragments of granitic and metamorphic rocks, indicating that all of these rock types occur within the cauldron block. Many of the rhyolite tuffs show varying degrees of reworking by water: low-amplitude cross-bedding, sorting, and grading. Although ripple marks are absent, the tuffs were very likely deposited, at least partly, in an early formed caldera lake.

The rhyolite domes and flows associated with the tuffs typically contain abundant jet black obsidian and have less than 3% phenocrysts of quartz, plagioclase, biotite, and hypersthene. The low crystal content of these lavas indicates that they erupted at near-liquidus temperatures. They also appear to have been unusually fluid for rhyolites, as some units less than 50 m thick flowed as far as 6 km. Three mineralogical facies have been mapped [*Bailey*, 1974]; in order of increasing phenocryst content and, in general, decreasing age, they are: (1) aphyric rhyolite, (2) pyroxene rhyolite, containing phenocrysts of quartz, plagioclase, hypersthene, and Fe-Ti oxide, and (3) biotite rhyolite, containing phenocrysts of quartz, plagioclase, hypersthene, biotite, and Fe-Ti oxide. Scarce phenocrysts of fayalite and augite also have been identified in some samples of biotite rhyolite. Available chemical data [*Rinehart and Ross*, 1964, Table 9; *Jack and Carmichael*, 1968, Table 1; R. A. Bailey, unpublished data, 1974] indicate that the early rhyolites typically contain about 75% silica and that the three facies are not appreciably different chemically, suggesting that the succession represents progressive crystallization of the same magma.

Twelve eruptive centers for the early rhyolites, many of them aligned on and offset by northwest-trending faults, are exposed in the central part of the caldera. Additional vents probably are buried in the caldera moat. *Kane et al.* [1976] interpret the arcuate chain of secondary lows in their gravity model as local accumulations of low-density materials. These lows quite possibly represent accumulations of coarse pumice around early rhyolite vents on outer caldera ring fractures. Evidence that early rhyolites are buried in the moat include (1) lithic aphyric rhyolite debris in the phreatic deposits of the Inyo craters; (2) aphyric rhyolite tuff uplifted on the side of a large rhyodacite dome in the southwest moat; and (3) pyroxene rhyolite beneath younger basalts in the northwest moat at 200 m depth in U.S. Geological Survey heat-flow hole (Figure 3, DC).

K-Ar measurements on 8 of the 12 early rhyolite domes and flows give ages of 0.73–0.63 m.y. (Table 1 and Figure 4). With only one exception the ages are consistent with the mapped stratigraphic succession: the exception is the apparent age of 0.73 m.y. on pyroxene rhyolite (location 6), which at the 95% confidence level is significantly older than the ages of either of the three dated aphyric rhyolites (locations 1, 10, and 13). None of the K-Ar ages of the early rhyolites are significantly older than the age of the Bishop tuff. The data indicate that (1) the early rhyolites were erupted during a span of no more than 100,000 yr and perhaps as little as 40,000 yr after eruption of the Bishop tuff and collapse of the caldera and (2) the pyroxene rhyolites may have been contemporaneous in part with the aphyric and biotite rhyolites.

RESURGENT DOMING

Contemporaneous with emplacement of the early rhyolites, the west central part of the caldera floor was uplifted and deformed into a subcircular structural dome. This resurgent dome [*Smith and Bailey*, 1962, 1968] is 10 km in diameter and consists of a mosaic of fault-bounded blocks that rise 500 m above the surrounding moat. The dome is transected by a 5-km-wide complexly faulted keystone graben that trends northwest. The early rhyolites exposed in the dome are tilted radially outward as much as 30°, and detailed mapping of flow foliations and lineations [*Chelikowsky*, 1940; *Bailey*, 1974] shows that most of the extrusive units flowed radially away from the geometric center of the dome. Evidence that the dome is the result of positive central uplift rather than differential collapse of the moat is as follows: (1) lake terraces tilted outward on the dome at elevations as much as 35 m higher than the highest terrace on the caldera walls; (2) scattered beach pebbles as much as 80 m higher on the dome than on the caldera walls; and (3) 1- to 2-m-diameter blocks of granitic and metamorphic rocks, interpreted as ice-rafted glacial erratics from the Sierra Nevada [*Rinehart and Ross*, 1964, p. 68], 200 m higher on the dome than the highest terrace on the caldera walls and 60 m higher than the lowest part of the caldera rim during early postcaldera time. These features also indicate that the resurgent dome was an island in a caldera lake during much of its history (see Figure 5).

The orientation of the keystone graben in the resurgent dome is undoubtedly controlled by the dominant northwest trend of regional structures along the east front of the Sierra Nevada. The eccentric location of the resurgent dome is thought to be controlled by lines of structural weakness within the Mount Morrison roof pendant, which probably continues in the basement northwestward through the cauldron block to exposures of metamorphic rock on the north wall of the caldera near Big Springs. Several major precaldera faults within and bounding the roof pendant, the Hilton Creek, McGee Mountain, and Laurel-Convict faults [*Rinehart and Ross*, 1964, Plate 1] (Figure 3), undoubtedly contributed to the weakness of this zone.

Decrease in the amount of radial tilting of progressively younger flow units on the dome suggests that uplift was waning toward the close of eruption of the early rhyolites. However, no units between 0.63 and 0.51 m.y. old have been dated, so the time of termination of doming is not precisely known. The top of a 0.51-m.y.-old hornblende-biotite rhyolite dome (location 12) on the north flank of the resurgent dome slopes gently to the north, but whether this is due to posteruption tilting or to slumping during extrusion onto a preexisting slope is uncertain. A 2280-m (7500 ft) lake terrace that laps against this dome does not appear to be tilted, nor do the many other lower terraces and strandlines down to 2140 m (7000 ft) on the north slope of the resurgent dome. Thus doming, which began shortly after collapse of the cauldron, continued until about

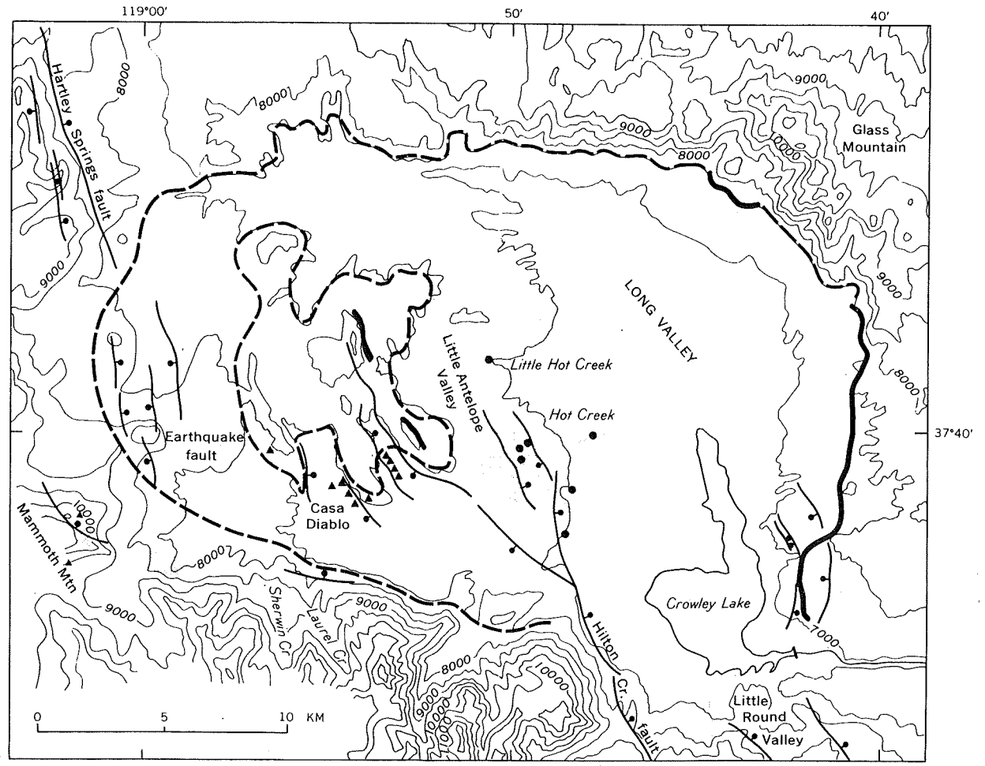

Fig. 5. Maximum extent of Pleistocene Long Valley Lake and distribution of hydrothermal activity. The heavy solid line represents remnants of highest (2320 m (7600 ft)) lake terrace; heavy dashed line, inferred position of highest shoreline and maximum extent of lake; triangles, active fumaroles; solid circles, active hot springs; dotted area, distribution of fossil gas vents and hydrothermal alteration; and solid thin lines, recently active faults. Contour interval is ~150 m (500 ft).

0.63 m.y. ago but probably did not persist much beyond 0.51 m.y. ago.

MOAT RHYOLITES

After resurgence, coarsely porphyritic hornblende-biotite rhyolite erupted from three groups of vents in the caldera moat. These rhyolites, informally designated the 'moat rhyolites,' are highly pumiceous and contain as much as 20% phenocrysts of hornblende, biotite, quartz, sanidine, and plagioclase. A single chemical analysis from a dome in the west moat indicates that they have silica contents of about 72% [*Rinehart and Ross*, 1964, Table 1]. They typically form steep-sided domes or thick flows of limited extent. Their crystal content and geomorphic form indicate that they were more viscous and probably erupted at lower temperatures than the early rhyolites.

The oldest hornblende-biotite rhyolites erupted on the north flank of the resurgent dome where two of four centers have been dated at 0.509 ± 0.011 m.y. (location 12) and 0.468 ± 0.010 m.y. (location 11). A second group of five erupted in the southeast moat, three of which have been dated at 0.349 ± 0.006 m.y. (location 25), 0.324 ± 0.010 m.y. (location 5), and 0.28 ± 0.03 m.y. (S17 of *Doell et al.* [1966]). A third group of four, with K-Ar ages of 0.113 ± 0.004 m.y. (location 17), 0.106 ± 0.003 m.y. (location 7), 0.103 ± 0.002 m.y. (location 9), and 0.094 ± 0.006 m.y. (location 8), occurs in the west moat. Thus the three groups erupted about 0.5, 0.3, and 0.1 m.y. ago in clockwise succession around the resurgent dome. These rocks are temporally, spatially, and petrographically analogous to the ring domes of the Valles caldera, New Mexico [*Smith and Bailey*, 1968; *Doell et al.*, 1968], and their distribution is probably controlled by ring fractures that bound the resurgent dome. The presence of hydrous minerals and the greater vesicularity of the moat rhyolites suggest that their extrusion and reopening of the ring fractures may have been caused by the concentration of volatiles accompanying crystallization of the magma and consequent increase in volatile pressure in the chamber. The apparent 0.2-m.y. periodicity of the groups may be a measure of the time required to build up sufficient pressure to reopen the ring fractures.

The restriction of the centers to three distinct areas in the ring fracture zone may be due to the fact that in these areas the ring fractures intersect major northwest-trending precaldera faults within the cauldron block. This suggestion is further supported by the northwest alignment of some of the domes within the groups. In the northern group, four vents are spaced at 1.5-km intervals on a northwest trend that may be either an arc concentric to the margin of the resurgent dome or a northwest extension of the Hilton Creek fault. The five vents of the southeast group appear to be randomly distributed, but they also are in the general area of intersection of the Hilton Creek fault with the ring fracture zone. The three main domes of the

western group are aligned north-northwest parallel to minor intracaldera faults that are in line with the Hartley Springs fault northwest of the caldera. The fourth dome in this group, Deer Mountain, although isolated from the other three, is aligned with the younger Inyo domes, which also trend north-northwest parallel to the Hartley Springs fault.

RIM RHYODACITES

Hornblende-biotite rhyodacites, less silicic and richer in crystals than the hornblende-biotite rhyolites of the caldera moat, occur at three localities on the caldera rim or in the outer part of the caldera moat: (1) Mammoth Mountain on the southwest, (2) Deadman Creek on the northwest, and (3) the foot of Glass Mountain on the northeast. A fourth unvented rhyodacite (?) intrusion probably occurs at the foot of Bald Mountain on the north, where cemented conglomeratic sediments capped with travertine have been punched upward into a steep-sided structural dome about 1 km in diameter. It is difficult to account for this structure other than by intrusion of a small igneous plug. Because of their peripheral location and semiarcuate distribution, these rhyodacites are informally designated the 'rim rhyodacites.'

Mammoth Mountain, the largest and most imposing of these rhyodacite centers, is a complex cumulo-volcano, consisting of many superimposed domes and short thick flows. At least 10 major eruptive vents can be identified on the mountain, most of which occur within an arcuate zone parallel to the caldera wall. The northeast face of the mountain has been oversteepened by glaciation and also in part by faulting. Displacement of lavas across a conspicuous cleft high on the northeast side of the mountain suggests that the northeast half of the mountain has subsided (see section on postcaldera tectonic activity).

The lavas of Mammoth Mountain have silica contents ranging from 74 to 66% [*Huber and Rinehart*, 1967, pp. D14–D15, Figure 5]. Recent mapping by R. P. Koeppen (personal communication, 1973) shows an upward succession from biotite rhyolite through biotite-augite rhyodacite to hypersthene-hornblende rhyodacite, indicating a trend toward more mafic compositions with time and suggesting that the lavas may have erupted from a high-level differentiated cupola.

The rhyodacites of Deadman Creek were mapped by *Rinehart and Ross* [1964] and *Huber and Rinehart* [1967] as 'olivine-bearing quartz latite.' These rocks comprise three small lava domes and a flow. The three domes are hornblende-biotite rhyodacites mineralogically similar to those of Mammoth Mountain and have silica contents of 63–67%. The associated flow, the only unit that contains olivine, has a lower silica content, 59–61% (N. K. Huber and C. D. Rinehart, personal communication, 1974), and is mineralogically heterogeneous, with olivine, augite, hypersthene, biotite, hornblende, plagioclase, sanidine, and quartz crystals, all in varying stages of reaction with the enclosing brown glass. Such relations suggest that the rock is the product of intermixing of rhyodacitic and basaltic liquids, a distinct likelihood since the K-Ar data indicate that basalts and rhyodacites were erupted contemporaneously in the western moat.

The small rhyodacite dome at the base of Glass Mountain has been described by *Gilbert* [1941, p. 799] as 'andesite,' but its mineralogy indicates that it is more silicic than typical andesites of the region. The rock contains abundant small crystals of hornblende and plagioclase in a light gray glassy matrix; its composition probably does not differ much from the rhyodacites of Deadman Creek and Mammoth Mountain.

It is probably not accidental that the two largest accumulations of rhyodacite, Mammoth Mountain and the Deadman Creek domes, occur where the caldera rim is intersected by a north-trending fracture system that also localized the more widely distributed, contemporaneous basalts described in the following section. The intersection of this fracture system with the outer caldera rim fractures undoubtedly was a zone of weakness that preferentially channeled magma to the surface. However, the fact that one and possibly two other rhyodacite centers occur along the north wall of the caldera, well to the east of this fracture zone, suggests that the rhyodacites are genetically related to the Long Valley magma chamber and not to the more deeply derived basalts.

Four rhyodacites have been dated in this study, two of which are among the youngest in the Mammoth Mountain complex. One from the summit dome (location 29) has an apparent sanidine age of 0.050 ± 0.010 m.y., and one from a flow midway down the northern flank (location 30) gives a biotite age of 0.118 ± 0.048 m.y. Two additional rhyodacites near Mammoth Mountain, a dome (location 27) and a flow (location 26), give K-Ar ages on biotites of 0.138 ± 0.079 m.y. and 0.145 ± 0.029 m.y., respectively. Previously published K-Ar ages from Mammoth Mountain include one of 0.148 ± 0.049 m.y. on biotite [*Curry*, 1971] and two on the same dome, 0.18 ± 0.09 m.y. on biotite [*Huber and Rinehart*, 1967] and 0.37 ± 0.04 on plagioclase [*Dalrymple*, 1964*a*]. Petrographic studies indicate that the plagioclase phenocrysts in the Mammoth Mountain rocks have had complex histories and probably have xenocrystic cores. Preliminary results of K-Ar dating of coexisting biotite and plagioclase from other Mammoth Mountain rocks show that K-Ar ages of plagioclase are more variable and consistently older than those on coexisting biotite, suggesting that biotite ages more closely reflect eruptive ages. If so, the rocks on Mammoth Mountain probably are no older than 0.18 ± 0.09 m.y.

These age data indicate that Mammoth Mountain was active for a minimum of about 100,000 yr and that rhyodactic volcanism was partly contemporaneous with the western group of moat rhyolites, as well as with the basalts described below.

LATE BASALTIC VOLCANISM

The west moat of Long Valley caldera contains many basaltic flows and cinder cones that are part of a more extensive chain of mafic volcanic rocks extending from southwest of Mammoth Mountain 45 km northward into Mono basin. This chain includes the trachybasaltic rocks of the Devils Postpile [*Huber and Rinehart*, 1967], the trachyandesite cinder cones and flows of the June Lake area [*Putnam*, 1949], and the sublacustrine cinder cone of Black Point on the north shore of Mono Lake [*Christensen and Gilbert*, 1964; *Lajoie*, 1968]. These rocks appear to have erupted from a north-trending fracture system consisting of north-northwest-trending en echelon segments that parallel the east front of the Sierra Nevada. Chemically and mineralogically, the rocks are similar to Cenozoic mafic rocks that occur throughout the Basin and Range province [*Leeman and Rogers*, 1969], and presumably they have a similar origin.

In general, the ages of the rocks decrease northward in the chain. The oldest rocks are from the Devils Postpile area, where K-Ar measurements on two different plagioclase separates from the same sample give ages of 0.63 ± 0.35 m.y. [*Huber and Rinehart*, 1967] and 0.94 ± 0.16 m.y. [*Dalrymple*, 1964*b*]. K-Ar ages on nine intracaldera basalts and

trachyandesites range from about 0.2 to 0.06 m.y. (Table 1, Figure 4). North of the caldera, the trachyandesite near June Lake overlies Tahoe till and is overridden by Tioga till [*Putnam*, 1949]; hence it is probably between 75,000 and 20,000 yr old [*Curry*, 1971]. The Black Point cinder cone on the north shore of Mono Lake is dated at 13,300 ± 500 yr by ^{14}C on ostracods from interbedded sediments [*Lajoie*, 1968].

The K-Ar ages of the basaltic rocks within Long Valley caldera indicate that basaltic volcanism was contemporaneous with the younger hornblende-biotite rhyolites of the western moat as well as with the rim rhyodacites. Since it is unlikely that liquid basalt could have penetrated any part of the rhyolitic magma chamber that had not already solidified, the distribution and age of the intracaldera basaltic centers are important indicators of the extent of crystallization of the Long Valley chamber. The innermost basaltic center in the western moat is 4 km from the caldera walls and is dated at 0.222 ± 0.080 m.y. (location 18). Thus at that time the chamber presumably had solidified inward at least 4 km from its margins and roof. The dimensions and geometry (thickness-diameter ratio) of the resurgent dome [*Smith and Bailey*, 1968, p. 646] suggest that at the close of resurgence about 0.6 m.y. ago the roof of the chamber probably was not deeper than 5 km and possibly was as shallow as 2 or 3 km. Thus about 0.2 m.y. ago the chamber had congealed to a depth of 6–9 km from the surface.

Of special interest to the glacial geology of the area are K-Ar ages of three basaltic flows exposed in the south moat. A till, named the Casa Diablo till by *Curry* [1971], is found between the middle and lower of these flows. On the basis of single K-Ar ages of 0.192 ± 0.035 m.y. on the upper flow, 0.280 ± 0.067 m.y. on the middle flow, and 0.441 ± 0.040 m.y. on the lower flow, Curry assigned the Casa Diablo till an age of about 0.4 m.y. and a stratigraphic position between the Sherwin till [*Sharp*, 1968] and the Mono basin till of possible Illinoian age [*Sharp and Birman*, 1963]. We have made duplicate measurements on the upper and lower of these three flows and obtained considerably different results. On the basis of our data the age of Curry's Casa Diablo till is between 0.062 ± 0.013 m.y. (location 23) and 0.126 ± 0.025 m.y. (location 22) and therefore may be equivalent in age to Mono basin till.

HOLOCENE RHYOLITIC VOLCANISM

The youngest volcanic features in Long Valley caldera are the Inyo craters and domes, [*Mayo et al.*, 1936], which are aligned on an apparent north-trending fracture extending from the west moat to the Mono craters along the east front of the Sierra Nevada. The Inyo domes are five rhyolitic to rhyodacitic lava domes, the three largest of which are the youngest (less than 720 ± 90 yr old on the basis of ^{14}C dating [*Wood*, 1975]). The Inyo craters are three phreatic explosion pits on the south flank of Deer Mountain (the moat rhyolite just south of the southernmost Inyo dome) and have been dated by ^{14}C at 650 ± 200 yr [*Rinehart and Huber*, 1965]. No primary ash or lava was expelled during formation of the craters, and very probably they were caused by rhyodacitic magma rising to shallow depth and flashing groundwater to steam. Thus it is possible that residual rhyodacitic magma was present in the Long Valley chamber as recently as 450 yr ago (see also *Steeples and Iyer* [1976]).

The Inyo domes are of particular interest because they are chemically and physically heterogeneous [*Lajoie*, 1968, p. 140; *Jack and Carmichael*, 1968, p. 22]. The three youngest domes are fluidal mixtures of two distinctly different rock types: (1) light, coarsely porphyritic hornblende-biotite rhyodacite that tends to be pumiceous, and (2) dark, sparsely porphyritic rhyolitic obsidian. The rhyodacite mineralogically and texturally resembles the rhyodacites of Long Valley caldera, whereas the rhyolitic obsidian resembles that of the Mono craters. Moreover, from north to south approaching Long Valley caldera, the proportion of pumiceous rhyodacite in successive domes increases noticeably at the expense of the obsidian, a relation that suggests that the Inyo domes represent the mixing along a north-south fissure of magmas from the Long Valley chamber and a chamber beneath the ring fracture zone of the Mono craters (Figure 1) [*Kistler*, 1966*b*, p. E48]. The age (about 12,000–1300 yr) and frequency of eruption of the Mono craters [*Dalrymple*, 1967; *Friedman*, 1968] suggest that the subjacent chamber may be actively rising and capable of feeding further eruptions.

PLEISTOCENE LONG VALLEY LAKE

After caldera subsidence the Long Valley depression was filled with water to form Pleistocene Long Valley Lake [*Mayo*, 1934]. Although normal runoff within the drainage basin was probably sufficient to fill the depression in a relatively short time, it is likely that glaciers were present in the Sierra Nevada at that time and that runoff was greatly accelerated by melting caused by the blanket of hot ash laid down during eruption of the Bishop tuff. This caldera lake rose to a level of at least 2320 m (7600 ft), as indicated by remnants of terraces on the northeast and east walls of the caldera (Figure 5). Terraces and strandlines are exceptionally well developed along the east wall, where they can be traced continuously for 14 km and where they have been downwarped southward and locally faulted. The terraces are veneered with coarse sand and gravel, consisting predominantly of well-rounded cobbles and pebbles of obsidian and lithoidal rhyolite, locally cemented with carbonate. This detritus was derived from the reworking of the tuffs and epiclastic sediments of Glass Mountain, which are exposed in the east rim and wall of the caldera. The gravels also contain scattered, large, angular blocks of coarsely porphyritic Cathedral Peak–type granite and metavolcanic rocks. The only source for these blocks is in the Sierra Nevada southwest of the caldera [*Huber and Rinehart*, 1965], so they must have been ice-rafted across Long Valley Lake. As noted in a preceding section, erratics of apparently similar origin are found on the west and south flanks of the resurgent dome within the caldera. These are the windward flanks against which icebergs from the Sierran glaciers would most likely have lodged.

Calcareous cement is common in the gravels of the lower terraces, and on the lowest terraces, dense, finely crystalline, calcareous tufa deposits are extensively developed. The increase in the amount of cementation and in the thickness of tufa on successively lower terraces suggests either more enduring lower lake stands, increased algal activity, or progressive increase in alkalinity and salinity of the lake water with time, the latter possibly due to late Pleistocene desiccation or to increased introduction of alkalies and salts from hot springs during the later part of the caldera history. Absolute dating of the terraces using the hydration rind method [*Friedman and Smith*, 1960] on obsidian pebbles is in progress and perhaps will provide further information on the history of the lake and its chemical evolution.

Draining of the caldera lake was attributed by *Mayo* [1934] and *Putnam* [1960] to headward cutting by the Owens River, but it is more likely that drainage was initiated by overflow of

the lake, as was believed by F. E. Matthes [see *Putnam,* 1960, p. 248]. The lake probably rose rapidly, forming no terraces during its rise to the lowest point on the caldera rim, which at that time was at about 2380-m (7800 ft) elevation and near the present lake outlet. It then began overflowing across the surface of the Bishop tuff, cutting rapidly downward through the upper 60 m or so of nonwelded to partly welded tuff, until it reached the densely welded zone at 2320 m (7600 ft), where the lake level became temporarily stabilized. (An ancient stream valley preserved in the surface of the Volcanic Tableland 20 km to the southeast [*Bateman,* 1965, p. 167] was probably cut by this early outflow stream.) The 2320-m (7600 ft) level coincides with the highest terrace recognized on the northeast caldera wall. (A figure of 2410 m (7900 ft) has been repeatedly cited in the literature for the highest lake terrace, but the surface rising to this elevation is an alluvial fan, not a terrace; the highest well-rounded beach pebbles indicating a lake strand are at 2320 m (7600 ft).) Since initial stabilization of the lake, overflow has been controlled by downwarping and intermittent movement on faults that bound the east front of the Sierra Nevada and intersect the caldera rim. (See section on postcaldera tectonic activity.)

That the lake reached a high level early in its history is indicated by the fact that many of the early rhyolites exposed in the resurgent dome are pervasively hydrated, suggesting their eruption into the caldera lake. Critical in this respect are two flows on the north flank of the resurgent dome, one being a pervasively perlitized biotite rhyolite flow and the other an overlying obsidian-bearing pyroxene rhyolite flow (location 14) dated at 0.634 ± 0.013 m.y. The pyroxene rhyolite, the youngest dated flow on the resurgent dome, is not greatly tilted or uplifted and is exposed at elevations from 2320 m (7600 ft) to 2415 m (7920 ft). The perlitized biotite rhyolite apparently flowed into the lake, whereas the overlying pyroxene rhyolite did not. Thus the lake probably reached its highest level, presumably 2380 m (7800 ft), near the time of eruption of the biotite rhyolite and then receded to 2320 m (7600 ft) before eruption of the pyroxene rhyolite flow 0.63 m.y. ago.

The approximate position of successively lower and younger lake levels may be inferred from other dated volcanic units within the caldera (Figure 6). On the north flank of the resurgent dome, lake terrace deposits at an elevation of 2290 m (7500 ft) lap against the base of a hornblende-biotite rhyolite dome (location 12) dated at 0.509 ± 0.011 m.y. but do not occur on an adjacent agglutinate cone and lava flow (location 11) dated at 0.468 ± 0.010 m.y.; the highest terrace deposits on the latter occur at 2230 m (7300 ft). Thus the lake level apparently was near 2290 m (7500 ft) between 0.51 and 0.47 m.y. ago and receded to 2230 m (7300 ft) after 0.47 m.y. ago.

Lake sediments above and below the Hot Creek rhyolite flow (S17 of *Doell et al.* [1966]) in the southeast moat indicate that the lake surface was at about 2200 m (7200 ft) about 0.28 m.y. ago. Lack of evidence that the basalt in the north moat (location 20) flowed into water indicates that the lake was below 2135 m (7000 ft) 0.104 m.y. ago. Complete draining of the lake occurred sometime within the last 0.1 m.y. (Lake Crowley is not a remnant of Pleistocene Long Valley Lake but is impounded behind Crowley Dam, which was built in 1941.)

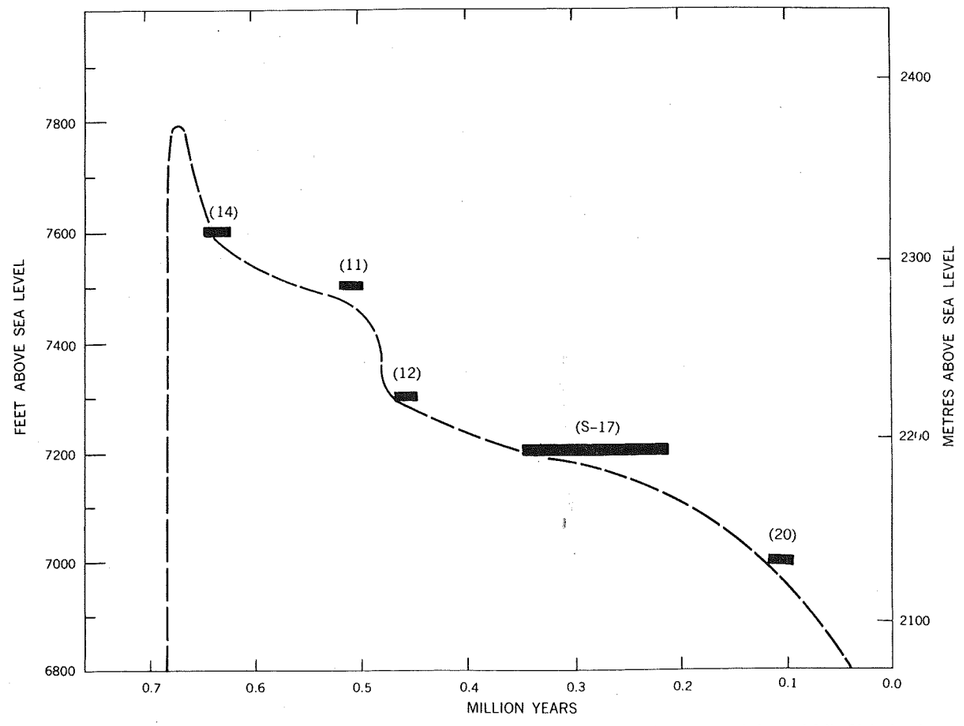

Fig. 6. Elevations and ages of Pleistocene Long Valley Lake levels. Dashed line shows general rise and fall of lake level with time, based on age of associated volcanic unit (solid bar). Numbers in parentheses are locality numbers of dated samples (Table 1 and Figure 3). Length of bar is analytical error of age determination.

LACUSTRINE SEDIMENTS

The sediments within Long Valley have been exposed to a depth of only 50 m by the dissection that followed draining of the caldera lake, and the deepest penetration of them by drilling is 305 m in U.S. Geological Survey drill hole LVCH-1 (Figure 3). Consequently, little is known of the character of the deeper sedimentary fill, although a large portion of it is undoubtedly lacustrine.

The upper 50 m of sediment exposed on the east flank of the resurgent dome are predominantly pebble conglomerate and coarse tuffaceous sandstone. They contain abundant clasts of early rhyolite indicating that they were derived mainly from erosion of the resurgent dome. The sediments commonly exhibit deltaic structure with well-developed topset and foreset beds, the latter having dips as much as 30° and amplitudes of as much as 10 m [*Rinehart and Ross,* 1964, pp. 76–77, Figure 38]. The topset beds commonly grade upward into marsh deposits containing or locally consisting almost entirely of silicified reedlike plant stalks and rootlets. Eastward the marsh and deltaic deposits grade or interfinger with fine-grained buff to white diatomaceous sediments exposed in the lower parts of Long Valley. Ostracods are abundant in both marsh and diatomaceous deposits.

In drill hole LVCH-1 the sediments below 50 m tend to be somewhat coarser and more pumiceous, but the general lithology does not change conspicuously downward, and no particularly distinctive units were penetrated. The Bishop tuff was not intersected, and it undoubtedly lies at much greater depth. Below 150 m the sediments in the drill hole are zeolitized. The principal zeolite is clinoptilolite, which occurs as a replacement product of glass shards and pumice; below 250 m, heulandite is also present as fine crystals in cavities. The sediments penetrated by the drill hole dip gently, usually not more than 10°, but several zones, each about 5 m thick, show intensely contorted and thrusted bedding, suggesting that penecontemporaneous wet sediment slumping, possibly triggered by earthquakes, was an important sedimentation process.

HYDROTHERMAL ACTIVITY

On the east and southeast flanks of the resurgent dome the tuffaceous lacustrine sediments are locally intensely argillized as a result of acidic hydrothermal alteration by hot spring and fumarolic activity. This argillization is most intensely developed in the vicinity of Little Antelope Valley and upper Little Hot Creek, although smaller areas also occur near Hot Creek, Casa Diablo, and northeast of Mammoth Lakes on the southwest edge of the resurgent dome. These argillized areas have not been studied in detail as yet, but they apparently consist mainly of kaolinite with traces of montmorillonite and alunite [*Cleveland,* 1962]. The kaolin deposits near Little Antelope Valley are of commercial grade and have been actively mined since the early 1950's. In the deeper parts of the Little Antelope Valley clay quarry, tuffaceous and conglomeratic sediments, initially consisting of clasts of lithoidal rhyolite, obsidian, and pumice, are completely argillized, yet bedding and clastic textures are almost perfectly preserved. In the upper part of the quarry the sediments are also opalized, and layers of opal become progressively thicker and more abundant upward. The origin of this type of zonation has been explained by *Schoen et al.* [1974] as the result of incongruent dissolution of primary minerals above the groundwater table by downward percolating sulfuric acid waters generated by near-surface oxidation of H_2S-bearing fumarolic gas. This process apparently ceased some time ago in the Little Antelope Valley area, as there are no active fumaroles nearby at present, although temperatures are rather high (110°C) at depths of 165–200 m in U.S. Geological Survey drill hole LVCH-6, 1 km south of the clay quarry [*Lachenbruch et al.,* 1976*b*].

Surrounding and locally overlying these areas of acid alteration, the lacustrine sediments are thoroughly cemented with opal but are otherwise unaltered. They form a hard, resistant cap rock as much as 15 m thick. The temporal and genetic relation between these silica-cemented sediments and those that are argillized and partly replaced by opal is unclear, but the silica-cemented sediments contain myriads of vertical pipelike or honeycomblike structures (illustrated by *Cleveland* [1962, Figure 8]) that have been identified as fossil gas vents (L. J. P. Muffler, personal communication, 1972). These interesting structures suggest that the sediments were deposited over an active fumarolic area, possibly during a temporary rise of the caldera lake. Also, locally interbedded with these silica-cemented sediments, mainly along faults, are now-inactive siliceous sinter deposits.

The wide distribution of these fossil gas vents, ancient sinter deposits, and areas of acid alteration (Figure 5) indicates that surficial hydrothermal activity within the caldera was more extensive as well as more intensive in the past than at present, and we suspect that parts of Long Valley were formerly as active as some of the Yellowstone geyser basins are today. The apparent decline and areal restriction of surficial hydrothermal activity are probably due to the general reduction in permeability of the intracaldera rocks and sediments by silicification, argillization, and zeolitization. These 'self-sealing' processes [*White et al.,* 1971] have progressed to a depth of at least 300 m, as indicated by the impermeability of sediments cored in drill hole LVCH-1. Although in detail the interrelations between these three types of alteration appear to be complex in the field, their general distribution and relative depths suggest a zonation downward from silicification at the surface through argillization to zeolitization at depth. This zonation is probably a function mainly of increasing temperature with depth, and the complexities observed probably are due to fluctuations in groundwater levels related to rising and falling of the caldera lake and to recurrent fracturing of the cap rock by tectonic activity.

Rinehart and Ross [1964, p. 80] have pointed out that most of the active hot springs and fumaroles are located on or near north- to northwest-trending faults. The only apparent exception is the springs along Hot Creek, which are aligned northeast along the bottom of the gorge. These springs, however, are confined within a shallow, 2-km-wide, northwest-trending graben, and their northeast alignment is the result of their flowing from the permeable, brecciated base of the Hot Creek rhyolite flow, which is confined to the gorge bottom. Significantly, the hottest springs, some of which are boiling, occur only near the two main faults bounding the graben; the cooler springs in the center of the graben are probably the result of lateral migration of fluid through the basal breccia of the flow or along minor graben fractures, where mixing with cold surface waters occurs.

Most of the hot springs and fumaroles in Long Valley are on active extensions of the Hilton Creek fault, which suggests that their location is related to disruption of the 'self-sealed' moat sediments by this relatively active Sierra Nevada frontal fault. An apparent temporal as well as spatial relation between faulting and hot spring activity was dramatically demonstrated recently when new boiling springs and ephemeral geysers

erupted along Hot Creek within hours of two earthquakes on August 25, and October 17, 1973. Although the epicenters were 20–40 km distant and not on the Hilton Creek fault, it seems likely that tremors disturbed the delicate plumbing of springs on the Hilton Creek system. The activity of the new springs and geysers has diminished markedly since their outbreak, but many of the older springs along Hot Creek and on Little Hot Creek, 3.5 km to the north, have shown marked increases in flow, and some an increase in temperature also, suggesting that their channels have been selectively enlarged since the earthquakes. With the data of *Haas* [1971] the salinities (~0.1%) and the geochemically indicated reservoir temperatures (~200°C) of the new hot spring waters [*Mariner and Willey,* 1976] suggest that they originated from a depth of at least 150 m. The presence of detrital zeolite particles in the new spring waters suggests a similar minimum depth of origin, as zeolites occur only below 150 m in drill hole LVCH-1, 1.5 km north of the new springs.

Although more sparsely distributed than in the east and south, hydrothermal activity also occurs locally in the western part of the caldera. Active fumaroles and abundant acid alteration occur on Mammoth Mountain [*Huber and Rinehart,* 1967, p. D19], a zone of hydrothermal alteration parallels the southwest caldera wall near the base of Mammoth Rock [*Rinehart and Ross*, 1964, p. 81], and pyritized rhyolite occurs at a depth of 210 m in U.S. Geological Survey heat-flow drill hole DC in the northwest moat (Figure 3). The apparent paucity of hydrothermal activity at the surface in the western moat does not necessarily indicate a lack of activity at depth because the thick sequence of young basalts in the western moat and the abundant subsurface flow of cold water from the Sierra Nevada may mask it.

Although individual hot springs and fumaroles are associated locally with north- to northwest-trending faults and fractures, the general distribution of hydrothermal activity within the caldera is in an arcuate zone peripheral to the resurgent dome, suggesting that the dominant controlling structures at depth are the caldera ring fractures. It is noteworthy that fumaroles in Long Valley caldera are restricted to fractures within the keystone graben of the resurgent dome, whereas hot springs are at lower elevations marginal to the dome where the groundwater table is near or at the surface.

Although fumaroles and hot springs probably have been active locally to a minor degree throughout the history of the caldera, the extensive development of hydrothermal activity in lacustrine sediments that are about 0.3 m.y. old, judging from the 0.28-m.y. age of the interbedded Hot Creek rhyolite flow, suggests that the geothermal system may have reached maximum development at about that time. This notion seems to be supported by the paucity of evidence for hydrothermal activity directly associated with the 0.73- to 0.63-m.y. early rhyolites and the 0.5-, 0.3-, and 0.1-m.y. moat rhyolites. This implies that the geothermal system is not related to the individual postcaldera eruptive groups but to the main magma chamber, which is a deeper and larger heat source. It also suggests that development of the geothermal circulatory system may have required considerable time and been completed only during the latter part of the caldera history.

Postcaldera Tectonic Activity

Matthes [1933, 1939], *Christensen* [1966], *Bateman and Wahrhaftig* [1966], and others have concluded that the rise of the Sierra Nevada crest was essentially completed before the advent of Pleistocene glaciation and that development of the eastern escarpment is the result of downfaulting of the region to the east during the past 3 m.y. Long Valley caldera lies across the faulted front of the Sierra and is intersected on the northwest and southeast by major frontal faults that have been active in both precaldera and postcaldera time. Because it is almost certain that the Long Valley magma chamber was substantially molten during this time, it is of interest to consider how the chamber responded to and how it may have influenced this tectonic activity locally.

The northwest caldera wall is intersected by the Hartley Springs fault (Figure 5), which has displaced precaldera andesites of the Tertiary San Joaquin Mountain complex by 450 m and the Bishop tuff by about 300 m. The topographic relief on the escarpment is about 600 m. This fault scarp terminates at the northwest caldera rim; southward within the western caldera moat several minor en echelon faults project on strike with it and form an ill-defined, incipient graben that terminates in the 'earthquake fault' [*Benioff and Gutenburg,* 1939] near the northeast base of Mammoth Mountain. These en echelon faults displace 0.2-m.y.-old trachyandesites by about 15 m, 0.1-m.y.-old moat rhyolite by about 10 m, and 650-yr-old Inyo crater phreatic deposits by about 5 m. Topographic evidence also indicates that the floor of western moat east of these faults is about 60 m lower than to the west. However, there is no suggestion of displacement in the west moat of 600 m as on the Hartley Springs fault outside the caldera. Thus the intracaldera segment or trace of the Hartley Springs fault appears not to have been active until fairly recent time.

The southeast caldera rim is intersected by the Hilton Creek fault, which forms an 1100-m escarpment at the mouth of McGee Creek. What part of this escarpment can be attributed to postcaldera movement is not precisely determinable, but if the fault has been continuously or intermittently active, it probably amounts to several hundred meters, as displacement on Tioga lateral moraines and outwash at the mouth of McGee Creek is as much as 15 m [*Putnam,* 1962, p. 200]. Like the Hartley Springs fault, the Hilton Creek fault terminates as a major escarpment at the caldera wall; within the caldera it splinters into several minor diverging faults that die out northward. The largest and most continuous of these splinters displaces by about 15 m 0.3-m.y.-old moat rhyolites, as well as 0.6- to 0.7-m.y.-old early rhyolites. Thus the maximum age of faulting is 0.3 m.y. However, since the intracaldera displacement about equals that on the Tioga deposits at McGee Creek, outside the caldera it probably is very much younger than 0.3 m.y. and may be in large part post-Tioga in age.

Thus both northwest and southeast of the caldera, major Sierra Nevada frontal faults having several hundred meters of postcaldera displacement show large and abrupt decreases in displacement at the caldera margins, and their intracaldera continuations apparently have been active only in very recent time. Where and how this postcaldera displacement was accommodated within the caldera is an enigma. Possibly it was accommodated on cross-caldera faults that have since been buried by younger lavas and sediments, but in the central part of the caldera where 0.6- to 0.7-m.y.-old early rhyolites are exposed, east-dipping faults with significant displacement are conspicuously absent. There is, however, some evidence of postcaldera movement on the south and southwest sectors of the caldera boundary fault. Although Pleistocene glacial deposits and steep alluvial fans have buried the actual boundary fractures on all sides of the caldera, on the south wall at Laurel and Sherwin creeks, older morainal ridges, thought to be of Mono basin age, are truncated by an apparent east-west fault

(Figure 5). Also, as noted in a preceding section, the northeast face of Mammoth Mountain, on the southwest caldera rim, is truncated by a fault that parallels the caldera wall. In contrast, the east and north walls of the caldera show no evidence of postcaldera movement on the boundary fractures. These relations suggest that during early postcaldera time, when the Long Valley magma chamber was shallow and its roof relatively thin and weak, displacement on the Sierra Nevada front between the south end of the Hartley Springs fault and the north end of the Hilton Creek fault was accommodated along the south and west sectors of the caldera boundary fault. More recently, with increased crystallization of the chamber and consequent thickening and strengthening of the roof, tectonic stresses have begun to be transmitted through the cauldron block, as indicated by the recent development of faults crossing the caldera floor on strike with the frontal faults.

This suggestion is reinforced by analysis of the deformation immediately east of the Sierra Nevada front. *Russell* [1899, p. 302] noted that the youngest shorelines of Pleistocene Mono Lake are depressed toward the range front, and *Gilbert et al.* [1968, p. 313] have described the area between Mono Lake and Long Valley as a broad, warped, faulted, grabenlike depression along the front. Southeast of Long Valley a similar depression occurs along the east base of the Wheeler Crest escarpment, where the Bishop tuff is downwarped as much as 300 m into Round Valley [*Bateman,* 1965]. Downwarping is evident also along the east and southeast rim and wall of the caldera where Pleistocene Long Valley Lake terraces are downwarped from 2320-m (7600 ft) elevation south of Glass Mountain to 2130 m (7000 ft) east of Lake Crowley (Figure 5) [*Rinehart and Ross,* 1957; *Putnam,* 1960; *Christensen,* 1966].

This zone of downwarping along the east front of the Sierra Nevada between Mono Lake and Round Valley (Figure 7*a*) constitutes a zone of backtilting or 'reverse drag' [*Hamblin,* 1965] that apparently developed simultaneously with the formation of the Sierra escarpment. A substantial amount of this downwarping postdates the caldera, but it does not appear to be continuous through the caldera (Figure 7*b*). Its continuity may be obscured partly by the resurgent dome, but the dome formed during a very short time interval immediately following caldera collapse, and any subsequent imposition of 200–300 m of downwarp should be discernible. The lack of evidence for major down-to-east faulting within and the discontinuity of 'reverse drag' across the caldera suggests that the cauldron block adjusted independently of the faulting immediately to the north and south. If postcaldera tectonic movements were restricted along the south and west sectors of the caldera boundary fault, possibly they were absorbed in the subjacent molten magma chamber, and any tendency for development of 'reverse drag' within the cauldron block was impeded by hydrostatic adjustments in the magma.

Summary and Discussion

The structure, stratigraphy, and geochronology of Long Valley caldera are summarized in Figures 8 and 9. Volcanism in the vicinity of Long Valley began about 3.2 m.y. ago with the eruption of basalt and andesite from widely scattered centers. Subsequently, 3.0–2.7 m.y. ago, rhyodacite erupted from two main areas: the Two Teats–San Joaquin Mountain and the Bald Mountain areas, respectively west and north of Long Valley. This mafic to intermediate volcanism probably occurred during the last major rise of the Sierra Nevada and before development of the eastern Sierra Nevada escarpment. The subsequent episode of rhyolitic volcanism associated with

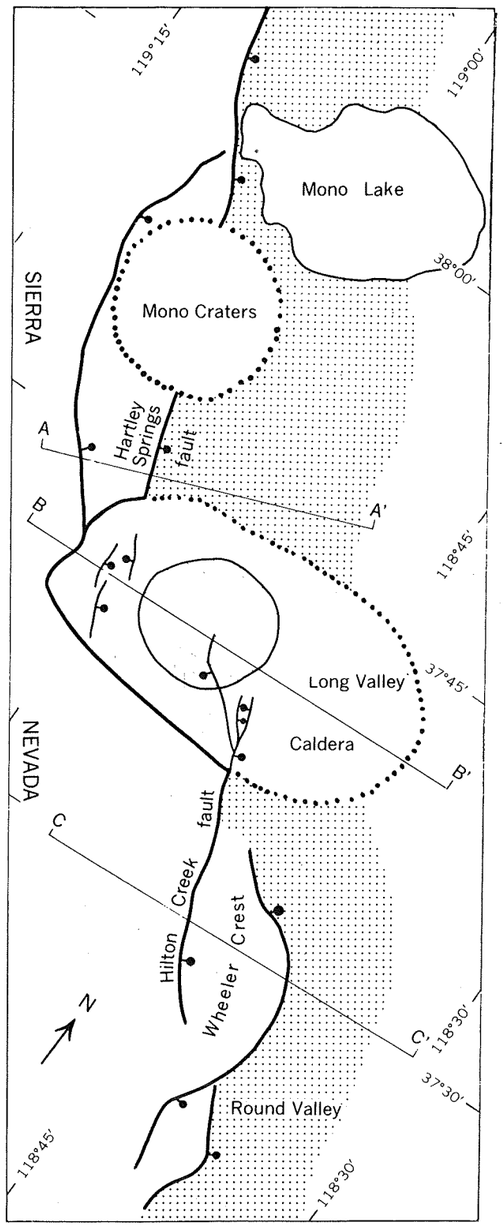

Fig. 7*a*. Tectonic map of Long Valley–Mono basin area. Heavily dotted area is zone of 'reverse drag' on Sierra Nevada front. Lined area is resurgent dome in Long Valley caldera. Solid lines represent faults (ball on downthrown side).

Long Valley caldera apparently accompanied development of the escarpment, and this fundamental change in tectonic activity may have provided the conditions necessary for the generation and accumulation of large volumes of silicic magma.

Rhyolitic volcanism began about 1.9 m.y. ago northeast of

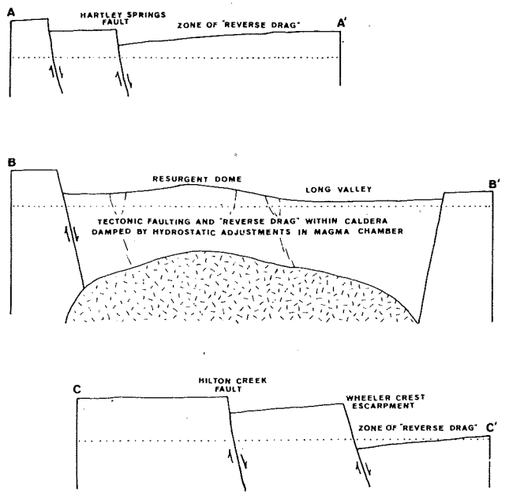

Fig. 7*b*. Schematic cross sections across the Sierra Nevada escarpment (Figure 7*a*) showing the contrast in postcaldera tectonic deformation within Long Valley caldera (BB′) and to the north (AA′) and south (CC′). Note the absence of major tectonic faults and associated 'reverse drag' within the caldera. The dotted line is an arbitrary reference level common to all three sections.

Long Valley. Sparsely porphyritic rhyolite, typically containing 77% silica, erupted over a period of 1 m.y. and accumulated in the immense edifice of Glass Mountain with its flanking pyroclastic fans. The eruptive centers of Glass Mountain are on a 13-km arcuate zone that probably coincides with an early incipient ring fracture related to development of the Long Valley magma chamber.

About 0.7 m.y. ago the Long Valley magma chamber was eviscerated by a series of explosive eruptions during which about 600 km³ of coarsely porphyritic biotite rhyolite magma containing 76% silica was ejected, mainly as ash flows, to form the Bishop tuff. Contemporaneous collapse of the roof of the chamber resulted in formation of the Long Valley caldera, an elliptical depression about 15 by 30 km and 2–3 km deep. Eruptions from at least 12 vents near the center of the caldera and possibly from others near its margins continued for 40,000–100,000 yr after collapse. During this time, at least 500 m of aphyric to sparsely porphyritic rhyolite, typically containing 75% silica, accumulated on the caldera floor. Contemporaneously with eruption of these early rhyolites the west central part of the caldera floor was uplifted into a subcircular resurgent dome about 10 km in diameter, and along its crest a 5-km-wide keystone graben formed parallel to the dominant northwest-trending precaldera structures of the region.

After resurgent doming, coarsely porphyritic hornblende-biotite rhyolite, typically containing 72% silica, erupted from three groups of centers in the caldera moat peripheral to the central resurgent dome. These three groups of moat rhyolites erupted in clockwise succession in the north, southeast, and west at 0.2-m.y. intervals about 0.5, 0.3, and 0.1 m.y. ago. About 0.2 m.y. to 50,000 yr ago, coarsely porphyritic hornblende-biotite rhyodacites containing 70–64% silica erupted on the southwest caldera rim and near the base of the northwest and north caldera walls. These rim rhyodacites constitute an outer arc of less silicic extrusions concentric with the moat rhyolites and the early rhyolites.

This concentric zonation of the postcaldera eruptives may be explained as a consequence of progressive downward crystallization of a magma chamber that was vertically zoned from rhyolite in its upper part to rhyodacite in its lower part as shown in Figure 8. The continuous decrease in silica content with time from 75% in the early rhyolites to 64% in the rim rhyodacites may be inferred to reflect intermittent tapping of the chamber at progressively greater depths along ring fractures that formed successively outward and extended downward into the congealing melt, possibly as a result of minor subsidence associated with the volume decrease that accompanied its consolidation. The upper, most silicic part of the chamber (77% silica) was erupted as the rhyolite of Glass Mountain, and during eruption of the Bishop tuff and collapse of the caldera, the chamber was drained of the zone of magma containing 76% silica. The abrupt decrease in crystal content of the magma from 20–30% in the Bishop tuff to less than 3% in the immediately subsequent early rhyolites may be the result either of phenocryst resorption caused by decompression of the chamber following eruption of the Bishop tuff or of resurgence of hotter, near-liquidus magma from deeper in the chamber. Successive tapping of deeper levels in the chamber at later times brought progressively more crystallized magma to the surface in the form of the moat rhyolites and rim rhyodacites. The simultaneous eruption of rhyolite in the west moat and rhyodacite on the rim is possibly a function of deeper consolidation on the outer edge of the magma chamber, which would require tapping of deeper, more mafic levels by outer ring fractures and of shallower, silicic levels by inner ring fractures.

Complete consolidation of a magma chamber of this type would result in a pluton zoned from granite to granodiorite downward. Documented examples of such plutons are few, the more usual zonation being concentric from more mafic to more silicic inward, but two notable examples can be cited as possible analogues: (1) the Cruachan 'granite' of the Etive and Glen Coe igneous ring complexes, Scotland, which is a binary granite on high peaks and adamellite in valley sides and floors [*Bailey and Maufe,* 1960, pp. 170, 220–221; *Anderson,* 1937], and (2) the outer 'granite' of Ben Nevis, Scotland, which in a vertical exposure of 1300 m grades from granite at high levels to granodiorite at low levels [*Anderson,* 1935, pp. 252, 264]. It is noteworthy that this latter intrusion shows the same tendency toward more coarsely porphyritic textures with apparent time as the postcaldera lavas of Long Valley.

Thermal calculations [*Lachenbruch et al.,* 1976*a*] indicate that the Long Valley magma chamber must have been replenished with heat to have sustained volcanism for more than 1 m.y.; thus the above model is probably an oversimplification. Because further refinement of it must await completion of petrochemical and mineralogical studies presently under way, discussion of the various possible mechanisms for heat replenishment seems unwarranted at this time.

During the late stages of solidification of the Long Valley chamber, basaltic and trachyandesitic lavas and pyroclastic rocks erupted from a system of north-trending fissures extending from south of the caldera through the western moat to the north shore of Mono Lake. These eruptions, possibly triggered by late faulting along the east front of the Sierra Nevada, probably tapped mafic magma from a much deeper source than the Long Valley chamber. A rare instance of the interaction of these mafic lavas with the silicic magma of the Long

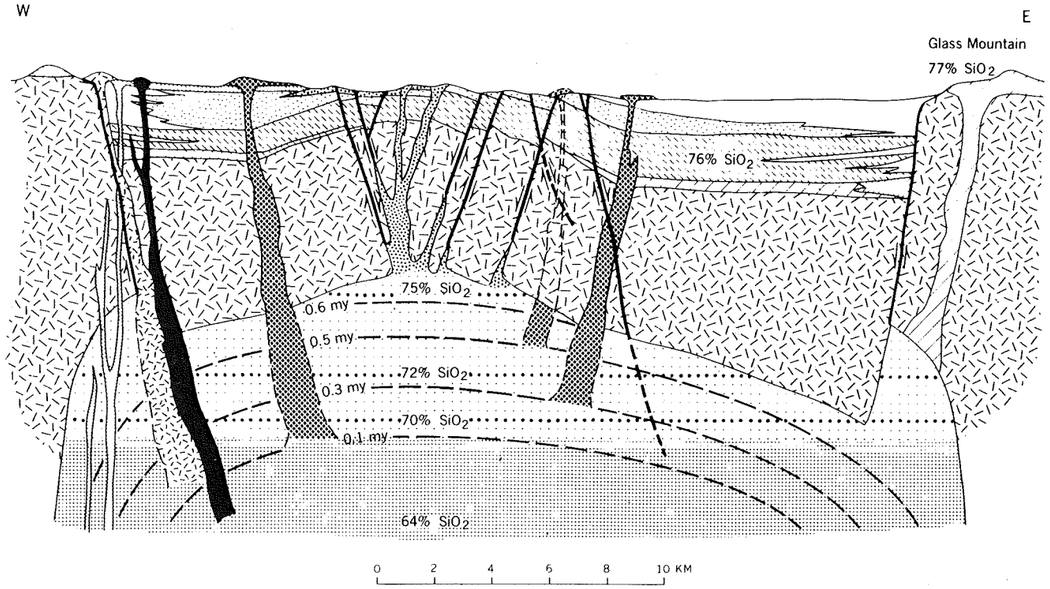

Fig. 8. Schematic east-west cross section through Long Valley caldera and its subjacent magma chamber showing hypothetical changes in chemical composition and depth of crystallization with time. The heavily dotted part of the chamber is rhyodacite magma; lightly dotted part is rhyolitic magma. Horizontal dotted lines show silica gradient in the vertically zoned chamber. Curved dashed lines show depth of crystal-liquid interface (depth to residual magma) at specified times (millions of years ago). Formation patterns are the same as in Figure 3, except that basement plutonic and metamorphic rocks (hachured) are undivided. The vertical scale is unspecified because of uncertainties in thickness of intracaldera units and depths in chamber.

Valley chamber is recorded in the mineralogically heterogeneous olivine-bearing rhyodacite of Deadman Creek.

The most recent volcanic rocks within Long Valley caldera are the Inyo domes, the youngest of which are less than 720 yr old. These domes are fluidal mixtures of rhyolitic and rhyodacitic lava that have erupted on a north-trending fissure between Long Valley caldera and the Mono craters. We interpret them as representing the mixing of rhyodacitic magma from the Long Valley chamber with rhyolitic magma from a chamber thought to underlie the Mono craters ring fracture zone. The Inyo craters, three phreatic explosion craters at the south end of the chain of Inyo domes, were possibly caused by the rise of rhyodacitic magma to very shallow depth, causing subsurface waters to flash explosively to steam. The craters may be as young as 450 yr, indicating that residual magma possibly was present in the Long Valley chamber that recently. The young age and frequency of eruptions along the Inyo-Mono volcanic chain indicate an active volcanic zone; eruptions of similar kind and magnitude could occur in the future.

Throughout most of its history, the Long Valley caldera was occupied by a lake that probably reached its highest level prior to 0.63 m.y. ago, then overflowed at the southeast rim, and subsequently was progressively lowered by tectonic faulting and warping of the rim near the outlet. Calcareous tufa deposits on the lower lake terraces indicate that in the latter part of its history the lake was alkaline and saline in composition.

Hydrothermal activity within the caldera probably reached maximum intensity about 0.3 m.y. ago. The decline of surface activity since then is probably due to 'self-sealing' of the intracaldera rocks by silicification, argillization, and zeolitization. Present thermal activity is mainly on or near recently rejuvenated segments of Sierra Nevada frontal faults that extend across the caldera and have ruptured the self-sealed cap rock. Although individual springs and fumaroles are located on or near north- to northwest-trending faults, the general distribution of hydrothermal activity is peripheral to the resurgent dome, suggesting that it is controlled at depth by the caldera ring fractures. These relations further suggest that thermal waters may be more extensive at depth than is suggested by the present surface activity.

Downfaulting on the Sierra Nevada front has continued throughout postcaldera time, but the major Sierra Nevada frontal faults that intersect the caldera rim have not displaced the caldera floor until very recently. During early postcaldera time when the magma chamber was shallow, movement on the front apparently was accommodated along the southern and western sectors of the caldera boundary fault. As the magma cooled and solidified, the cauldron block thickened and eventually became rigid enough to transmit tectonic stresses. The absence within the caldera of 'reverse drag,' present elsewhere along the Sierra Nevada front, suggests that until recently vertical tectonic stresses within the cauldron block have been absorbed by hydrostatic adjustments in the subjacent magma chamber. The manner in which the Sierra Nevada faults change from single, continuous fractures outside the caldera to branching, en echelon fractures inside suggests, however, that the cauldron block is still considerably less rigid than the surrounding crust and that it may still be partially underlain by magma.

A tentative history of the rise and consolidation of the Long Valley magma chamber can be reconstructed from several different sources of information on depth. The following esti-

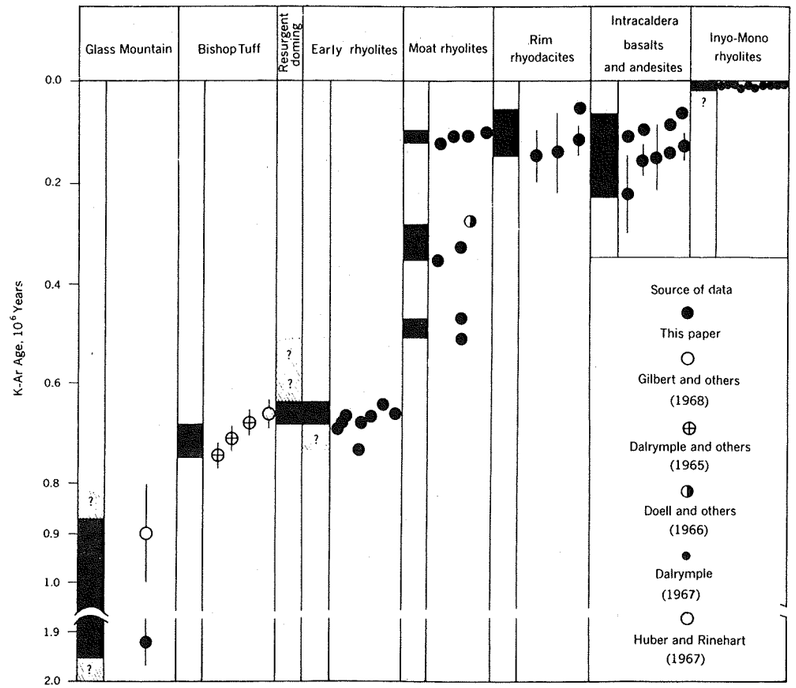

Fig. 9. K-Ar ages and inferred geochronology of volcanic events associated with Long Valley caldera. The dark bars indicate the approximate time and duration of frequent activity; lined bars with queries indicate uncertainty.

mates, although of uncertain and variable accuracy and subject to revision, are internally consistent and hence seem worth summarizing at this time. Geochemical data [*Hildreth and Spera,* 1974] suggest that at the time of eruption of the Bishop tuff 0.7 m.y. ago, the top of the chamber was at a depth of about 6 km. Structural analysis of the resurgent dome suggests that at the close of resurgence about 0.6 m.y. ago, the top of the chamber had risen to at least 5-km depth and possibly to 2 or 3 km. By about 0.2 m.y. ago the lateral encroachment of basaltic dikes on the chamber suggests that it had congealed inward and downward 4 km to a depth of 6 to possibly 9 km. Teleseismic and seismic refraction studies [*Steeples and Iyer,* 1976; *Hill,* 1976] suggest that an anomalously hot or partially molten mass still persists below 7 or 8 km. Geochemical data from the Inyo domes [*Carmichael,* 1967] indicate that lava from the Mono craters magma chamber erupted under pressures of 6.6–2.7 kbar, which suggests depths of 22–6 km.

Thus in summary, the Long Valley magma chamber appears to have developed and risen through the crust over a period of at least 1.3 m.y. (from 1.9 to 0.6 m.y. ago), during which time the rhyolites of Glass Mountain, the Bishop tuff, and the early rhyolites erupted. It then apparently achieved isostatic equilibrium in the upper crust, probably due to loss of mass. During the past 0.6 m.y. it has been cooling and congealing downward, periodically building up sufficient volatile pressure by crystallization to extrude the moat rhyolites and rim rhyodacites. Within the last 12,000 yr there has been an insurgence of new rhyolitic magma immediately to the northwest of the Long Valley chamber beneath the Mono craters, and there is some evidence in the Inyo domes that this magma has intermingled to a minor extent with the rhyodacitic residua in the Long Valley chamber.

In conclusion, volcanological, geochronological, and structural evidence indicates that large sources of heat exist at sufficiently shallow depth in the Long Valley–Mono craters area to be of importance as potential geothermal resources.

Acknowledgments. We wish to thank N. K. Huber and C. D. Rinehart for freely sharing their knowledge of the area from previous studies and for providing unpublished data and sample information that greatly facilitated the early stages of this project. We are also grateful to D. E. White for offering many helpful suggestions during the course of the fieldwork, particularly concerning the hydrothermal activity and alteration and other features associated with Pleistocene Long Valley Lake. The many exchanges of observations in the Mammoth Lakes area with S. R. Lipshie are also gratefully acknowledged. Special thanks are due to R. P. Koeppen for assistance with the mapping and sample collecting; to J. C. Von Essen, A. H. Atkinson, B. M. Myers, S. J. Kover, L. B. Schlocker, D. A. Williams, and J. Y. Saburomaru for assistance with the K-Ar analyses, and to P. C. Bateman, R. L. Christiansen, M. M. Clark, N. K. Huber, S. D. McDowell, R. P. Sharp, and D. E. White for critically reviewing the manuscript and offering many constructive suggestions.

REFERENCES

Anderson, J. G. C., The marginal intrusions of Ben Nevis, the Coille Lianachain Complex, and the Ben Nevis dyke swarm, *Trans. Geol. Soc. Glasgow, 19,* 225–269, 1935.

Anderson, J. G. C., The Etive granite complex, 4, *Quart. J. Geol. Soc. London, 93,* 487–533, 1937.

Bailey, E. B., and H. B. Maufe, The geology of Ben Nevis and Glen Coe and the surrounding country, *Mem. Geol. Surv. Scot.*, 1–307, 1960.

Bailey, R. A., Postsubsidence volcanism and structure of Long Valley Caldera, California, *Geol. Soc. Amer. Abstr. Programs, 5,* 7, 1973.

Bailey, R. A., Preliminary geologic map and cross sections of the Casa Diablo geothermal area, Long Valley Caldera, Mono County, California, open file map, 2 pp., U.S. Geol. Surv., Reston, Va., 1974.

Bateman, P. C., Geology and tungsten mineralization of the Bishop district, California, *U.S. Geol. Surv. Prof. Pap. 470,* 208 pp., 1965.

Bateman, P. C., and C. Wahrhaftig, Geology of the Sierra Nevada, Geology of Northern California, *Calif. Div. Mines Geol. Bull., 190,* 107–172, 1966.

Bateman, P. C., L. D. Clark, N. K. Huber, J. G. Moore, and C. D. Rinehart, The Sierra Nevada batholith: A synthesis of recent work across the central part, *U.S. Geol. Surv. Prof. Pap. 414-D,* D1–D46, 1963.

Benioff, V. H., and B. Gutenberg, The Mammoth 'earthquake fault' and related features, *Bull. Seismol. Soc. Amer., 29,* 333–340, 1939.

Byers, F. M., Jr., P. P. Orkild, W. J. Carr, and W. D. Quinlivan, Timber Mountain tuff, southern Nevada, and its relation to cauldron subsidence, *Geol. Soc. Amer. Mem., 110,* 87–97, 1968.

Carmichael, I. S. E., The iron-titanium oxides of salic volcanic rocks and their associated ferromagnesian silicates, *Contrib. Mineral. Petrol., 14,* 36–64, 1967.

Chelikowsky, J. R., Tectonics of the rhyolite in the Mammoth embayment, California, *J. Geol., 48,* 421–435, 1940.

Christensen, M. N., Late Cenozoic crustal movements in the Sierra Nevada of California, *Geol. Soc. Amer. Bull., 77,* 163–182, 1966.

Christensen, M. N., and C. M. Gilbert, Basaltic cone suggests constructional origin of some guyots, *Science, 143,* 240–242, 1964.

Christiansen, R. L., and H. R. Blank, Volcanic evolution of the Yellowstone rhyolite plateau and eastern Snake River plain, U.S.A., in *International Association of Volcanology Symposium on Volcanoes and Their Roots,* International Association of Volcanology, Oxford, England, 1969.

Cleveland, G. B., Geology of the Little Antelope Valley clay deposits, Mono County, California, *Calif. Div. Mines Geol. Spec. Rep., 72,* 1–28, 1962.

Cox, A., and G. B. Dalrymple, Statistical analysis of geomagnetic reversal data and the precision of potassium-argon dating, *J. Geophys. Res., 72,* 2603–2614, 1967.

Curry, R. R., Glaciation about 3,000,000 years ago in the Sierra Nevada, California, *Science, 154,* 770–771, 1966.

Curry, R. R., Glacial and Pleistocene history of the Mammoth Lakes Sierra, California: A geologic guidebook, *Univ. Mont. Geol. Ser. Publ. 11,* 1–49, 1971.

Dalrymple, G. B., Potassium-argon dates of some Cenozoic volcanic rocks of the Sierra Nevada, California, *Geol. Soc. Amer. Bull., 74,* 379–390, 1963.

Dalrymple, G. B., Cenozoic chronology of the Sierra Nevada, California, *Univ. Calif. Berkeley Publ. Geol. Sci., 47,* 1–41, 1964*a*.

Dalrymple, G. B., Potassium-argon dates of three Pleistocene interglacial basalt flows from the Sierra Nevada, California, *Geol. Soc. Amer. Bull., 75,* 753–757, 1964*b*.

Dalrymple, G. B., Potassium-argon ages of Recent rhyolites of the Mono and Inyo Craters, California, *Earth Planet. Sci. Lett., 3,* 289–298, 1967.

Dalrymple, G. B., and M. A. Lanphere, *Potassium-Argon Dating*, pp. 53–85, W. H. Freeman, San Francisco, Calif., 1969.

Dalrymple, G. B., A. Cox, and R. R. Doell, Potassium-argon age and paleomagnetism of the Bishop Tuff, California, *Geol. Soc. Amer. Bull., 76,* 665–673, 1965.

Doell, R. R., G. B. Dalrymple, and A. Cox, Geomagnetic polarity epochs, Sierra Nevada data 3, *J. Geophys. Res., 71,* 531–541, 1966.

Doell, R. R., G. B. Dalrymple, R. L. Smith, and R. A. Bailey, Paleomagnetism, potassium-argon ages, and geology of rhyolites and associated rocks of the Valles Caldera, New Mexico, *Geol. Soc. Amer. Mem., 116,* 211–248, 1968.

Friedman, I., Hydration rind dates rhyolite flows, *Science, 159,* 878–880, 1968.

Friedman, I., and R. L. Smith, A new dating method using obsidian, I, The development of the method, *Amer. Antiquity, 25,* 476–493, 1960.

Gilbert, C. M., Welded tuff in eastern California, *Geol. Soc. Amer. Bull., 49,* 1829–1862, 1938.

Gilbert, C. M., Late Tertiary geology southeast of Mono Lake, California, *Geol. Soc. Amer. Bull., 52,* 781–816, 1941.

Gilbert, C. M., M. N. Christensen, Y. Al Rawi, and K. R. Lajoie, Structural and volcanic history of Mono Basin, California-Nevada, *Geol. Soc. Amer. Mem., 116,* 275–329, 1968.

Haas, J. L., Jr., The effect of salinity on the maximum thermal gradient of a hydrothermal system at hydrostatic pressure, *Econ. Geol., 66,* 940–946, 1971.

Hamblin, W. K., Origin of 'reverse drag' on the downthrown side of normal faults, *Geol. Soc. Amer. Bull., 76,* 1145–1164, 1965.

Hildreth, W., and F. Spera, Magma chamber of the Bishop Tuff: Gradients in T, P_{total}, and P_{H_2O}, *Geol. Soc. Amer. Abstr. Programs, 6,* 795, 1974.

Hill, D. P., Structure of Long Valley Caldera, California, from a seismic refraction experiment, *J. Geophys. Res., 81,* this issue, 1976.

Huber, N. K., and C. D. Rinehart, Geologic map of the Devils Postpile quadrangle, California, *Map GQ-437,* U.S. Geol. Surv., Reston, Va., 1965.

Huber, N. K., and C. D. Rinehart, Cenozoic volcanic rocks of the Devils Postpile quadrangle, eastern Sierra Nevada, California, *U.S. Geol. Surv. Prof. Pap. 554-D,* D1–D21, 1967.

Ingamells, C. O., Lithium metaborate flux in silicate analysis, *Anal. Chim. Acta, 52,* 323–334, 1970.

Izett, G. A., R. F. Wilcox, H. A. Powers, and G. A. Desborough, The Bishop ash bed, a Pleistocene marker bed in the western United States, *Quaternary Res., 1,* 121–132, 1970.

Jack, R. N., and I. S. E. Carmichael, The chemical 'fingerprinting' of acid volcanic rocks, *Calif. Div. Mines Geol. Spec. Rep., 100,* 17–32, 1968.

Kane, M. F., D. R. Mabey, and R.-L. Brace, A gravity and magnetic investigation of the Long Valley Caldera, Mono County, California, *J. Geophys. Res., 81,* this issue, 1976.

Keefer, W. R., The geologic story of Yellowstone National Park, *U.S. Geol. Surv. Bull., 1347,* 1–92, 1972.

Kistler, R. W., Geologic map of the Mono Craters quadrangle, Mono and Tuolumne quadrangles, California, *Map GQ-462,* U.S. Geol. Surv., Reston, Va., 1966*a*.

Kistler, R. W., Structure and metamorphism in the Mono Craters quadrangle, Sierra Nevada, California, *U.S. Geol. Surv. Bull., 1221-E,* 1–52, 1966*b*.

Lachenbruch, A. H., J. H. Sass, R. J. Monroe, and T. H. Moses, Jr., Geothermal setting and simple magmatic models for the Long Valley Caldera, *J. Geophys. Res., 81,* this issue, 1976*a*.

Lachenbruch, A. H., M. L. Sorey, R. E. Lewis, and J. H. Sass, The near-surface hydrothermal regime of Long Valley Caldera, *J. Geophys. Res., 81,* this issue, 1976*b*.

Lajoie, K. R., Late Quaternary stratigraphy and geologic history of Mono Basin, Ph.D. thesis, 271 pp., Univ. of Calif., Berkeley, 1968.

Leeman, W. P., and J. J. W. Rogers, Late Cenozoic alkali-olivine basalts of the Basin-Range province, U.S.A., *Contrib. Mineral. Petrol., 25,* 1–24, 1969.

Lipman, P. W., and T. A. Steven, Reconnaissance geology and economic significance of the Platoro Caldera, southeastern San Juan Mountains, Colorado, *U.S. Geol. Surv. Prof. Pap. 700-C,* C19–C29, 1970.

Lipman, P. W., T. A. Steven, R. G. Luedke, and W. S. Burbank, Revised volcanic history of the San Juan, Uncompahgre, Silverton, and Lake City Calderas in the western San Juan Mountains, Colorado, *U.S. Geol. Surv. J. Res., 1,* 627–642, 1973.

Mankinen, E. A., and G. B. Dalrymple, Electron microprobe evaluation of terrestrial basalts for whole-rock K-Ar dating, *Earth Planet. Sci. Lett., 17,* 89–94, 1972.

Mariner, R. H., and L. M. Willey, Geochemistry of thermal waters in Long Valley, Mono County, California, *J. Geophys. Res., 81,* this issue, 1976.

Matthes, F. E., Geography and geology of the Sierra Nevada, in *XVI International Geological Congress Guidebook,* vol. 16, part C-1, pp. 26–40, Government Printing Office, Washington, D. C., 1933.

Matthes, F. E., History of faulting movements at the east front of the Sierra Nevada, as indicated by dislocated moraines (abstract), *Geol. Soc. Amer. Bull., 50,* 1955, 1939.

Mayo, E. B., The Pleistocene Long Valley Lake in eastern California, *Science, 80,* 95–96, 1934.

Mayo, E. B., L. C. Conant, and J. R. Chelikowsky, Southern extension of the Mono Craters, California, *Amer. J. Sci., 32,* 81–97, 1936.

Muffler, L. J. P., and D. L. Williams, Geothermal investigations of the U.S. Geological Survey in Long Valley, California, *J. Geophys. Res., 81,* this issue, 1976.

Noble, D. C., M. K. Korringa, C. E. Hedge, and G. O. Riddle, Highly differentiated subalkaline rhyolite from Glass Mountain, Mono County, California, *Geol. Soc. Amer. Bull., 83,* 1179–1184, 1972.

Pakiser, L. C., Gravity, volcanism, and crustal deformation in Long Valley, California, *U.S. Geol. Surv. Prof. Pap. 424-B,* B250–B253, 1961.

Pakiser, L. C., M. F. Kane, and W. N. Jackson, Structural geology and volcanism of Owens Valley, California—A geophysical study, *U.S. Geol. Surv. Prof. Pap. 438,* 1–68, 1964.
Putnam, W. C., Quaternary geology of the June Lake district, California, *Geol. Soc. Amer. Bull., 60,* 1281–1302, 1949.
Putnam, W. C., Origin of Rock Creek and Owens River Gorges, Mono County, California, *Univ. Calif. Berkeley Publ. Geol. Sci., 34,* 221–280, 1960.
Putnam, W. C., Late Cenozoic geology of McGee Mountain, Mono County, California, *Univ. Calif. Berkeley Publ. Geol. Sci., 40,* 181–218, 1962.
Ratté, J. C., and T. A. Steven, Ash flows and related volcanic rocks associated with the Creede Caldera, San Juan Mountains, Colorado, *U.S. Geol. Surv. Prof. Pap. 524-H,* H1–H58, 1967.
Rinehart, C. D., and N. K. Huber, The Inyo Crater Lakes—A blast in the past, *Calif. Div. Mines Geol. Miner. Inform. Serv. 18,* 169–172, 1965.
Rinehart, C. D., and D. C. Ross, Geology of the Casa Diablo quadrangle, California, *Map GQ-99,* U.S. Geol. Surv., Reston, Va., 1957.
Rinehart, C. D., and D. C. Ross, Geology and mineral deposits of the Mount Morrison quadrangle, Sierra Nevada, California, *U.S. Geol. Surv. Prof. Pap. 385,* 1–106, 1964.
Russell, I. C., Quaternary history of Mono Valley, California, *Annu. Rep. 8,* pp. 261–394, U.S. Geol. Surv., Reston, Va., 1889.
Schoen, R., D. E. White, and J. J. Hemley, Argillization by descending acid at Steamboat Springs, Nevada, *Clays Clay Miner., 22,* 1–22, 1974.
Sharp, R. P., Sherwin Till-Bishop Tuff geological relationships, Sierra Nevada, California, *Geol. Soc. Amer. Bull., 79,* 351–364, 1968.
Sharp, R. P., and J. H. Birman, Additions to the classical sequence of Pleistocene glaciation, Sierra Nevada, California, *Geol. Soc. Amer. Bull., 74,* 1079–1086, 1963.
Sheridan, M. F., The mineralogy and petrology of the Bishop Tuff, Ph.D. thesis, 165 pp., Stanford Univ., Palo Alto, Calif., 1965.
Sheridan, M. F., Double cooling-unit nature of the Bishop Tuff in Owens Gorge, California (abstract), *Geol. Soc. Amer. Spec. Pap. 115,* 351, 1968.
Smith, R. L., and R. A. Bailey, Resurgent cauldrons: Their relation to granitic ring complexes and large volume ash-flow fields, in *IAV International Symposium on Volcanology,* pp. 67–68, Japan Science Council, Tokyo, 1962.
Smith, R. L., and R. A. Bailey, Resurgent cauldrons, *Geol. Soc. Amer. Mem., 116,* 613–662, 1968.
Smith, R. L., R. A. Bailey, and C. S. Ross, Structural evolution of the Valles Caldera, New Mexico, and its bearing on the emplacement of ring dikes, *U.S. Geol. Surv. Prof. Pap. 424-D,* D145–D149, 1961.
Smith, R. L., R. A. Bailey, and C. S. Ross, Geologic map of the Jemez Mountains, New Mexico, *Misc. Invest. Map I-571,* U.S. Geol. Surv., Reston, Va., 1970.
Steeples, D. W., and H. M. Iyer, Low-velocity zone under Long Valley caldera as determined from teleseismic events, *J. Geophys. Res., 81,* this issue, 1976.
Suhr, N. H., and C. O. Ingamells, Solution technique for analysis of silicates, *Anal. Chem., 38,* 730–734, 1966.
White, D. E., L. J. P. Muffler, and A. H. Truesdell, Vapor-dominated hydrothermal systems compared with hot-water systems, *Econ. Geol., 66,* 75–97, 1971.
Williams, H., and G. Goles, Volume of the Mazama ash-fall and the origin of Crater Lake caldera, *Oreg. Dep. Geol. Miner. Ind. Bull., 62,* 37–41, 1968.
Wood, S. H., Mono and Inyo Crater eruptions, eastern California—Radiocarbon dating and trace element correlations of Late Pleistocene tephra, *Geol. Soc. Amer. Abstr. Programs, 7,* 389, 1975.
U.S. Geological Survey, Geologic map of Yellowstone National Park, *Misc. Geol. Invest. Map I-711,* Reston, Va., 1972.

(Received February 20, 1975;
revised September 11, 1975;
accepted September 12, 1975.)

Structure of Long Valley Caldera, California, From a Seismic Refraction Experiment

DAVID P. HILL

U.S. Geological Survey, Office of Earthquake Research, Menlo Park, California 94025

Two seismic refraction profiles crossing the Long Valley caldera in approximately east and north directions indicate that the crystalline basement with P wave velocities of 6.0 ± 0.4 km/s has been downdropped by 2.5–3 km across normal faults along the north and northwest sides of the caldera and 1–2 km along the south and east sides. Basement depths beneath the caldera floor range from between 3 and 4 km in the north and east sections to about 2 km in the central and south sections. Relief on the basement within the caldera suggests that the caldron block was partially disrupted during collapse, although a steplike offset in the eastern part of the basement may be due in part to precollapse displacement along the Hilton Creek fault. The distribution of P wave velocities in the caldera fill suggests that the Glass Mountain rhyolite and Bishop tuff have velocities of 4.0–4.4 km/s and the postcollapse rhyolite, rhyodacite, and basalt flows have velocities of 2.7–3.4 km/s. Domelike relief on the 4.0- to 4.4-km/s horizon indicates that postcollapse resurgence elevated the west central part of the caldera by about 1 km. Evidence for the roof of the magma chamber is contained in later arrivals tentatively identified as reflections from a low-velocity horizon at a depth of 7–8 km. Evidence for anomalous scattering or absorption properties associated with the region of shallow hydrothermal alteration and hot spring activity is contained in relative attenuation of high frequencies in a guided wave propagating through this region.

INTRODUCTION

Two seismic refraction profiles were shot across the Long Valley caldera during the last part of May 1973 as part of the U.S. Geological Survey's multidisciplinary investigation of this geothermal resource area. The primary objective of the seismic refraction experiment was to define the structure of the upper 5–10 km of the crust as a basis for a more complete understanding of the nature and development of what has been identified as the Long Valley resurgent caldron [*Smith and Bailey,* 1968; *Bailey et al.,* 1976]. Most of this paper is devoted to a description of the experiment and an interpretation of its results in terms of the subsurface structure of the caldera.

A secondary objective of the experiment involved an examination of the recorded wave forms for any evidence that may reflect the presence of a geothermal reservoir within the caldera or a possible magma chamber (either crystallized or molten) at depth. Little has been published on the application of active seismic methods to the study of geothermal systems [*Hayakawa,* 1970; *Hochstein and Hunt,* 1970], although recent developments in the recording and interpretation of seismic data offer considerable promise in this regard. The physical conditions thought to prevail in geothermal reservoirs, which include high temperatures, high porosity, fracture zones, etc. [*White,* 1973], suggest that the associated elastic properties should include relatively low seismic wave velocities, high attenuation (low Q), and local velocity heterogeneities resulting in anomalous wave scattering. *Hayakawa* [1970] cites evidence for some of these properties in data from the detailed seismic reflection survey in the Matsukawa geothermal field in Japan. This secondary objective met with at least partial success in that evidence in the seismograms was found for the roof of a magma chamber at a depth of 7–8 km as well as for near-surface effects of the hydrothermal area in the eastern section of Long Valley.

A number of geophysical studies in the Long Valley region are described in the literature. Most of this work involves seismic and gravity surveys by L. C. Pakiser and his colleagues as part of a continuing study of the tectonics and volcanism of the Owens Valley–Mono Lake region [*Pakiser et al.,* 1960; *Pakiser,* 1961; *Pakiser et al.,* 1964; *Pakiser,* 1968]. The regional crustal structure in the Long Valley–Mono Lake area is outlined by long-range seismic refraction profiles between Mono Lake and Lake Mead, Nevada [*Johnson,* 1965], and between China Lake and Mount Shasta [*Eaton,* 1966]. These studies indicate that the crust in the vicinity of Long Valley is characterized by (1) P wave velocities of 6.0–6.2 km/s near sea level (about 2 km below the surface) increasing to 6.4 km/s at depths of 25–30 km, (2) P wave velocities of 6.8–7.2 km/s in the lower 10–20 km of the crust, (3) a total crustal thickness of 40–50 km, and (4) upper mantle P wave (Pn) velocities of 7.8–7.9 km/s.

DESCRIPTION OF THE EXPERIMENT

The experiment consisted of two profiles crossing the caldera in roughly north and east directions. Locations of shot points and recording units along the two profiles, AA′ and BB′, are shown in Figure 1. Also shown are the caldera floor outline [*Bailey et al.,* 1976] and 10-mGal gravity contours adapted from *Pakiser et al.* [1964] and *Kane et al.* [1976]. Profile AA′ extends in an ESE direction from the Deadman shot point at the northwest edge of the caldera to the Hammil shot point near the foot of the White Mountains. Profile BB′ extends northward from the Convict shot point near the southern edge of the caldera to the Mono shot point 3 km south of Mono Lake. The profiles intersect near the center of the caldera in Little Antelope Valley; shot point Antelope is common to both profiles.

Data were obtained by 10 seismic refraction recording units held in fixed positions along a given profile as the individual shots along the profile were fired at half-hour intervals. Recording unit K at the Antelope shot point and units I and T at the east edge of the caldera were held in the same locations for all shots along both profiles. Recording units are the standard eight-channel U.S. Geological Survey seismic refraction trucks described by *Warrick et al.* [1961]. Each unit records the output of six vertical component seismometers in a linear array 2.5 km long together with WWV and WWVB time

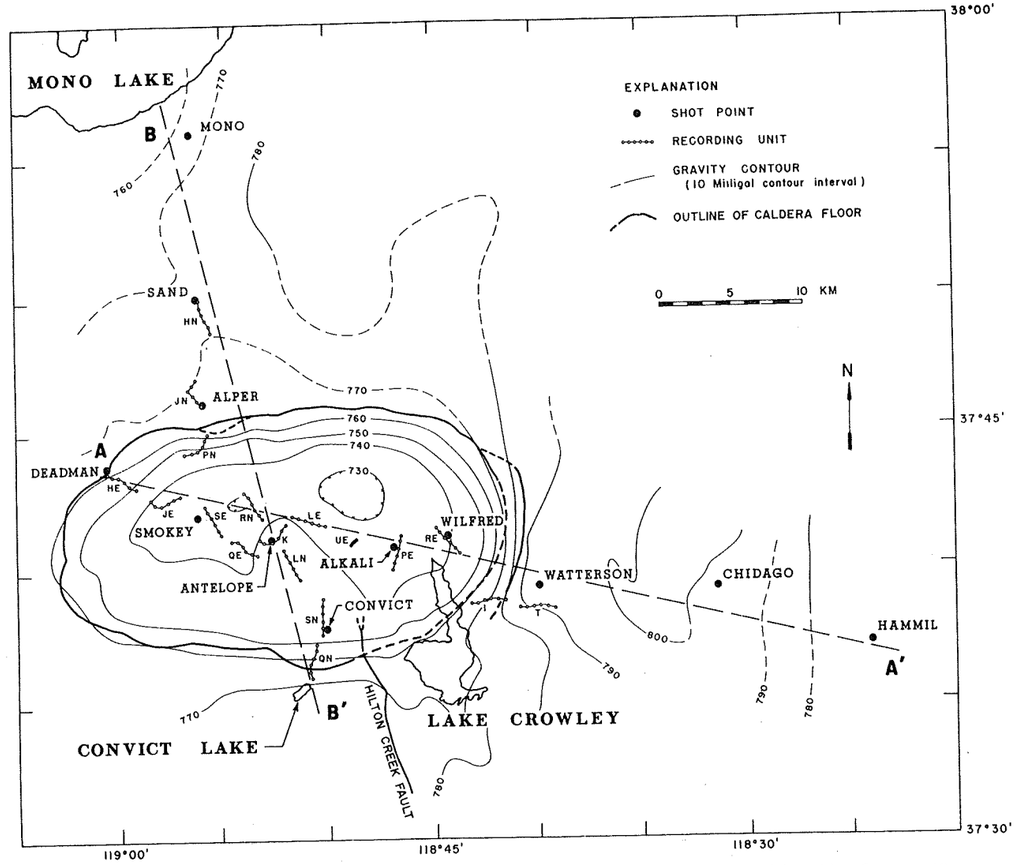

Fig. 1. Map showing locations of shot points and recording units with respect to the outline of the caldera floor and 10-mGal gravity contours. Caldera faults are closely associated with caldera floor outline [see *Bailey et al.*, 1976].

signals. Two horizontal component seismometers provide a three-component station at one of the verticals in the array. A Union Oil reflection crew operating in the area also recorded shots and provided analog copies of their records.

Shot times were determined to within ±0.01 s by recording the cap break and the output of an up-hole seismometer on two of the eight channels in an adjacent seismic refraction unit or on a special three-channel shot point recorder. Because of an equipment malfunction, however, the shot time at Smokey could only be determined to within 1 s. The shot at Hammil was weak and did not produce usable first arrivals on any of the recording units.

Travel times of first arrivals picked from analog records are plotted in Figures 2 and 3 for profiles AA′ and BB′. In addition, record sections for each shot point were generated by computer from digitized magnetic tapes. Examples of these record sections are shown in Figures 4, 5, and 6 for shot points Deadman, Alkali, and Mono, respectively. Locations, travel times, and a complete set of record sections are compiled in the report by *Hill and McHugh* [1975].

INTERPRETATION

The geometry of the experiment is such that intersecting profiles, which individually provide two-dimensional information, are used to obtain a first approximation to the three-dimensional structure of the caldera. A basic assumption in the interpretation of the experiment is that the structure along each profile can be approximated by a series of homogeneous layers bounded by plane interfaces with dips parallel to the trend of the profile. The possibility of a change in dip of a given interface along the profile is included. Accordingly, the travel time data in Figures 2 and 3 were fitted with a series of straight line segments.

Figure 1 suggests the limitations inherent in the two-dimensional design and interpretation of this experiment. The distribution of shot points and recording units, which was constrained by topography, existing roads, and permitting considerations, deviates somewhat from forming linear profiles. This, coupled with the three-dimensional character of the structure implied by the gravity data, indicates that the nominally reversed travel time branches cannot necessarily be associated with reversed subsurface propagation paths and, further, that interfaces may have dips that deviate significantly from the vertical plane of the profile. The interpretation should be recognized for these limitations while at the same time it should be recognized that a more elaborate interpretation would require additional assumptions not justified by the available data.

By using the above assumption, models of the velocity structure along each profile were constructed by (1) applying standard equations for plane dipping layers [*Mota*, 1954] to the travel time branches between adjacent shot points to approximate the near-surface (upper 1–2 km) velocity structure, (2) establishing the P wave velocity for the basement refractor based on reversed travel time branches judged to have propagated along nearly reversed subsurface paths, and (3) using apparent velocities of travel time branches to establish dips on the basement surface together with graphical two-dimensional ray tracing to establish basement depths consistent with total travel times and the near-surface structure determined under (1).

The resulting velocity models along profiles AA′ and BB′ are shown in Figures 7 and 8, respectively.

Interfaces that can reasonably be interpreted as having subsurface reversal between adjacent shot points are indicated by heavy lines. Interfaces indicated by thin lines probably do not have subsurface reversal for reasons mentioned above. Extrapolated interfaces or interfaces based on secondary arrivals are indicated by dashed lines. The shot points are too widely separated to define continuous variations in the near-surface structure along the profiles, and details of how the near-surface structure between adjacent pairs of shot points should join remain unresolved.

The basement P wave velocity is shown as a uniform 6.0 km/s in the velocity models. This value is based on the reversed and overlapping travel time branches on profile BB′ north of the caldera between the Sand and Alper shot points, where the propagation paths probably approach true subsurface reversal. *Johnson* [1965] reports a similar value (6.15 km/s) at a depth of 1.6 km south of Mono Lake. Efforts to determine the basement P wave velocities within the caldera, assuming that the reversed and overlapping travel time curves on profile AA′ provide true subsurface reversal, lead to velocities of 5.6 km/s west of Antelope and 6.4 km/s east of Antelope. There is no a priori reason to reject lateral velocity variations of this size within the basement; indeed, L. C. Pakiser (personal communication, 1974) reports a P wave velocity of 5.35 km/s for the uppermost basement at depths of 1–2 km beneath Mono Lake only 25 km to the north. Because of the limitations mentioned above, however, it seems most reasonable to interpret the apparent lateral velocity variation in Long Valley as a ±0.4-km/s uncertainty in the 6.0-km/s value for the basement P wave velocity under the caldera. The associated uncertainty in depth to the basement is approximately ±3%, the lower velocity giving a greater depth.

Two solutions for the basement interface within the caldera are shown in Figures 7 and 8. They result from assuming a uniform basement velocity (6.0 km/s) and admitting that arrivals on the reversed travel time curves may have propagated along different paths within the basement. Solution A in Figure 7, for example, is based on the reversed travel time branches between Deadman and Antelope with apparent

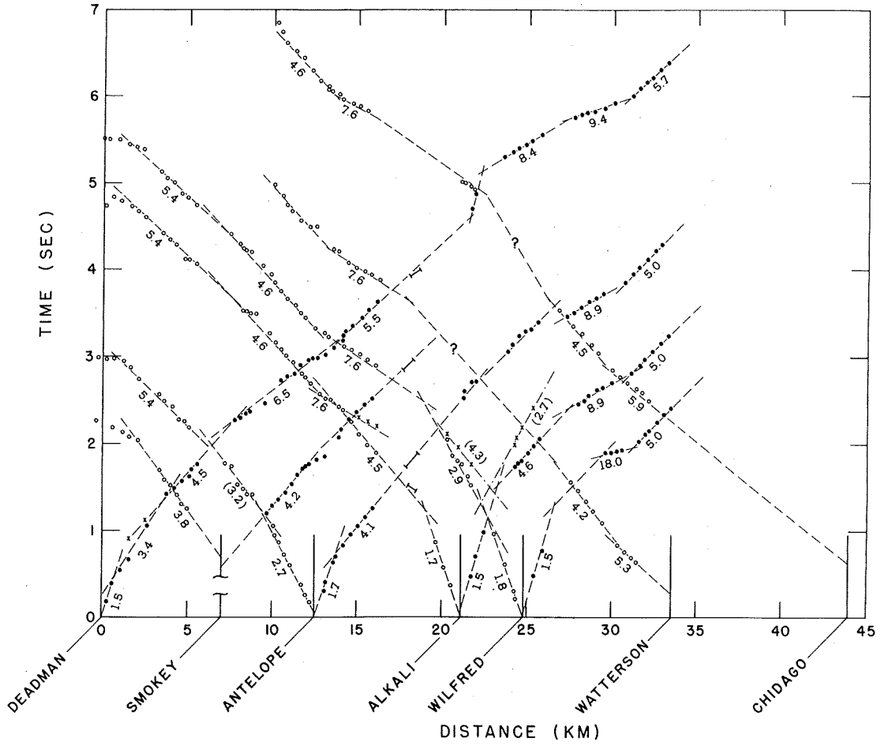

Fig. 2. Travel time curves along profile AA′. Circles and dots are first arrivals for waves propagating to the left and right, respectively. The crosses are later arrivals. The bars represent first arrivals recorded by the Union Oil reflection unit. Numbers are apparent velocities in kilometers per second. Parentheses indicate apparent velocities based on later arrivals or extrapolated travel time branches.

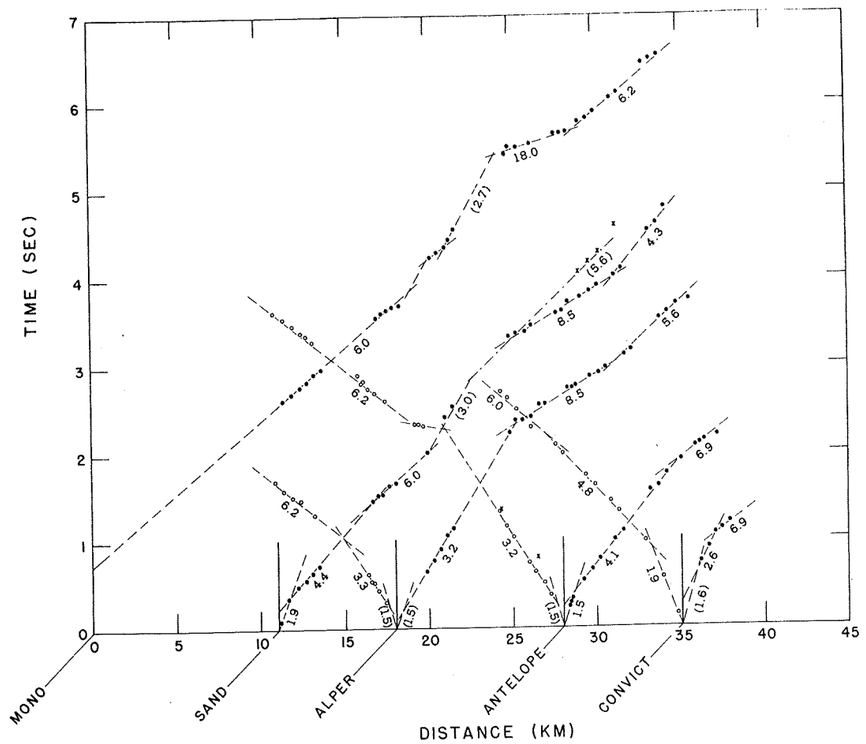

Fig. 3. Travel time curves along profile BB′. Symbols are the same as in Figure 2.

velocities of 6.5 and 5.4 km/s. The shot points and receivers lie nearly along a straight line in this interval (Figure 1). Solution B is based on overlapping travel time branches from Alkali and Wilfred with apparent velocities of 4.6 and 5.4 km/s. The distribution of shot points and recording units shown in Figure 1 suggests that these arrivals have propagated along paths that sample the basement somewhat closer to the gravity low on the north side of the caldera than those between Deadman and Antelope. The greater depth for solution B is generally consistent with the gravity gradient and the dip on the basement north of Antelope shown in profile BB′ (Figure 8).

Factors such as the possible lateral propagation of waves in the three-dimensional caldera structure and subjective judgments in drawing travel time branches through the plotted points make a strictly quantitative assessment of the accuracy of the velocity models in Figures 7 and 8 difficult. My estimate

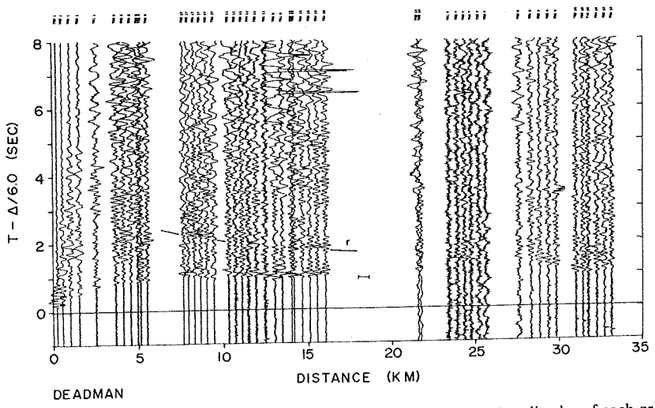

Fig. 4. Record section of seismograms recorded from the Deadman shot point. Amplitudes of each group of six traces from a given recording unit are normalized independently. Bar represents first arrivals recorded by Union Oil reflection unit; *r* indicates arrival, tentatively identified as a deep reflection.

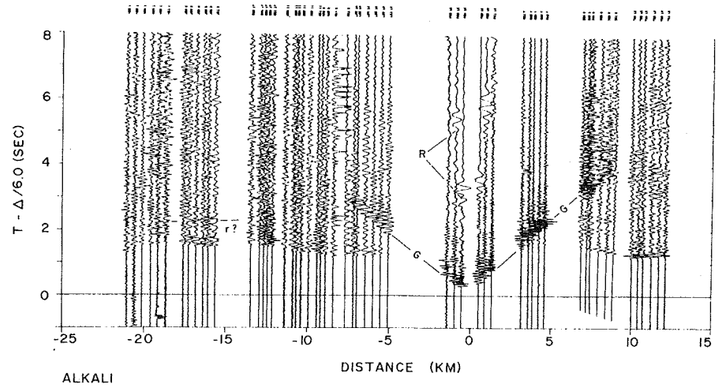

Fig. 5. Record section of seismograms recorded from the Alkali shot point. G indicates shallow guided wave group; R indicates surface wave.

of the overall accuracy of the models on the basis of experience with a number of different assumptions and solutions is that the *P* wave velocities of the various horizons are probably good to within ±10% and the depths of the interfaces are probably good to within ±20%.

Discussion

The velocity models in Figures 7 and 8 indicate that the upper surface of the basement within the caldera is at depths between 3 and 4 km beneath the north and east parts of the caldera and 1.5–2 km beneath the west central and southwest parts of the caldera. *P* wave velocities in the caldera fill overlying the basement increase from 1.5 km/s at the surface to 4.4 km/s at depth. Material with velocities from 4.0 to 4.4 km/s forms a continuous layer 1–2 km thick at the base of the caldera fill. Relief on the surface of this layer resembles a broad dome centered over the west part of the caldera. A layer with velocities between 2.7 and 3.4 km/s overlies the 4.0- to 4.4-km/s material and tends to be thickest over parts of the caldera where the basement is relatively deep. A surficial layer with velocities between 1.5 and 1.9 km/s and a thickness of 50–200 m overlies most of the west part of the caldera and is at least 0.5 km thick in the east part of the caldera.

P wave velocities and rock units. The subsurface distribution of major rock units illustrated in the east trending cross section through the caldera drawn by *Bailey et al.* [1976] on the basis of geologic field relations is remarkably similar to the distribution of seismic velocity horizons in profile AA′ (Figure 7). This similarity suggests the following association between seismic *P* wave velocities and rock units: 6.0 ± 0.4 km/s, Jurassic-Cretaceous granitic and Paleozoic-Mesozoic metamorphic basement rocks; 4.0–4.4 km/s, Bishop tuff and Glass Mountain rhyolite; 2.6–3.4 km/s, postcollapse rhyolites, rhyodacites, and basalts; 1.5–1.9 km/s, highly jointed near-surface volcanic rocks (weathered layer) in the west part of the caldera and alluvium and glacial, lake, and marsh deposits in the east.

Basement relief and gravity. Basement depths in the seismic velocity models along profiles AA′ and BB′ and the two-layer density model obtained by a three-dimensional interpretation of the gravity data by *Kane et al.* [1976] are also in reasonably close agreement. Evidently, the 0.45-g/cm³ density contrast used in the gravity interpretation is a good approximation of the average density contrast between the caldera fill and the basement.

The velocity models indicate a rather abrupt change in basement depth in the vicinity of the bounding caldera faults and steep gravity gradients. This relief on the basement is most clearly defined in profile BB′ just south of Alper where the depth to basement increases by 2.5–3 km in a distance of 5 km or less (see Figure 8). The solid line in this model represents the basement determined from Sand and Alper travel time curves, whereas the dashed line represents the basement determined from the Mono travel time curve (see Figure 3). High apparent velocities recorded near Deadman also indicate a steep dip on the basement at the west end of profile AA′, although the travel time data do not resolve the total relief on the basement. Granitic basement is exposed immediately west of the Deadman shot point, however, and if the 6.0-km/s horizon represents the top of the buried granitic basement, vertical relief across the caldera fault is 2.5–3 km here as well.

The moderate dip (about 15°) on the basement at the eastern edge of the caldera in the model for profile AA′ poses a problem in terms of the steep gravity gradient associated with the bounding faults. A profile across the gravity gradient, for example, can be fitted by a model with a 5 ± 2 km vertical step

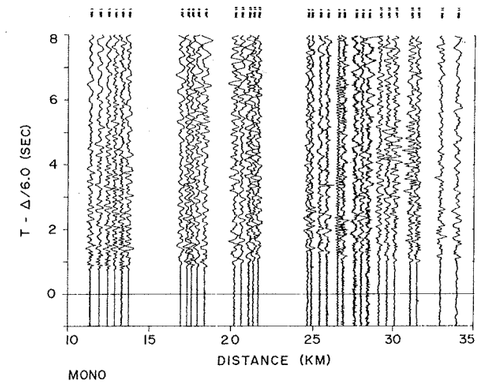

Fig. 6. Record section of seismograms recorded from the Mono shot point.

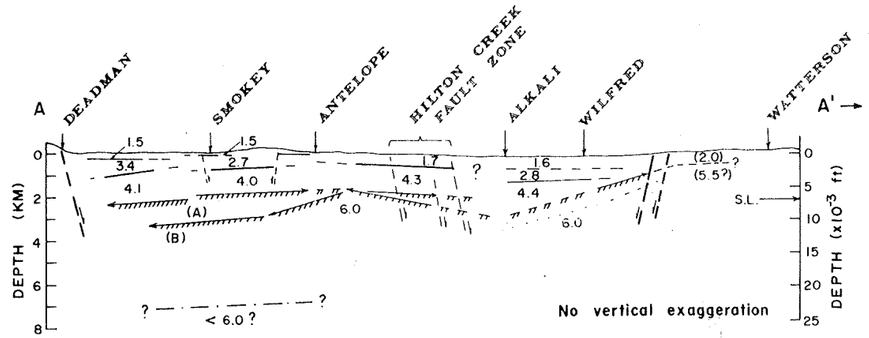

Fig. 7. Cross section showing P wave velocity structure under profile AA'. Numbers are P wave velocities in kilometers per second. Depths are with respect to average surface elevation (2.1 km); S.L. indicates sea level. Heavy lines indicate horizons with reversed subsurface coverage. Light lines indicate horizons with one-way subsurface coverage; arrows indicate propagation direction of subsurface waves along the horizon. Dashed lines indicate horizons based on later arrivals or extrapolated horizons. Basement horizon is indicated by hachures. Faults are indicated by steeply dipping dashed lines with arrows showing sense of displacement.

in the basement and a density contrast of 0.4 g/cm³ between the basement and the caldera fill [*Pakiser,* 1961; *Pakiser et al.,* 1964]. A more recent interpretation of the gravity field [*Kane et al.,* 1976] using a density contrast of 0.45 g/cm³ gives vertical relief in the basement across this zone of 3.3 km over a distance of about 2.5 km with an average dip of more than 50°. Resolution of this apparent discrepancy between the seismic and gravity interpretations may lie in the following explanations.

1. The locations of the recording units at the east end of the caldera depart from a simple profile normal to the gravity gradient, which tends to result in lower apparent velocities across the recording spreads than if the arrivals had propagated directly 'up dip.' The apparent continuity of travel time segments on the Deadman travel time curve recorded between Wilfred and Watterson, however, seems to preclude abrupt changes in basement depth in this interval.

2. The bulk density of the thick accumulation of low-velocity near-surface material in the east part of the caldera (Figure 2, also profile 6 in the work by *Pakiser et al.,* 1964] is not known but may be less than 2.0 g/cm³. Thus a significant part of the gravity low at the east end of the caldera could be attributed to these deposits. A similar explanation has resolved, in part at least, discrepancies between interpretations of the basement depth beneath Mono Lake [*Pakiser,* 1968; *Christensen et al.,* 1969; *Pakiser,* 1970].

Along similar lines, the 2.8- to 3.4-km/s layer may have a lower bulk density than might normally be associated with these P wave velocities. The rhyolites and rhyodacites presumed to form this horizon were erupted into a moat formed between the resurgent dome and the bounding caldera walls while the moat was occupied by the Pleistocene Long Valley Lake. Accordingly, there may be substantial thicknesses of lake and marsh deposits interbedded with the lava flows together with relatively coarse scree deposits from the steep, fault-controlled walls of the caldera (R. A. Bailey, personal communication, 1974). Such deposits would form low-velocity lenses within the 2.7- to 3.4-km/s layer that could not be detected by seismic refraction measurements on the scale of this experiment. If this is the case, then the average density of the caldera fill around the north and east sides of the caldera may be significantly lower than that in the west central part. The effect of correcting for such a lateral variation in the bulk density of the caldera fill would be to reduce the depths to the basement along the north and east margins of the caldera from those required in the single-density contrast gravity model.

Structural implications. Relief on the basement within the caldera can be attributed to (1) precollapse topography, (2) partial disruption or differential tilting during collapse of the caldera, (3) postcollapse resurgence, and (4) continuing tectonic displacement on throughgoing faults.

Bailey et al. [1976] suggest that the NNW trend of the gravity contours in the central part of the caldera [see *Kane et al.,* 1976] reflects precollapse displacement on the Hilton Creek fault that is preserved within the caldron block. The 0.5-s delay in the Deadman travel time curve in the vicinity of Alkali (Figure 2) indicates a vertical offset in the basement of about 1.5 km just west of Alkali that is consistent with displacement on the Hilton Creek fault (Figure 7). This offset, however, is somewhat east of the inferred location of the Hilton Creek fault zone and the maximum gravity gradient (Figure 1). How much of the vertical offset in the basement can be attributed to precollapse relief on the Hilton Creek fault is not clear. Some offset may have occurred during collapse as differential subsidence of the caldron block along this preexisting weak zone. Any offset due to postcaldera tectonic displacement on the fault should be reflected in the shallower horizons as well. Unfortunately, the solutions for the near-surface structure between Alkali and Antelope are ambiguous in this regard (see Figure 7).

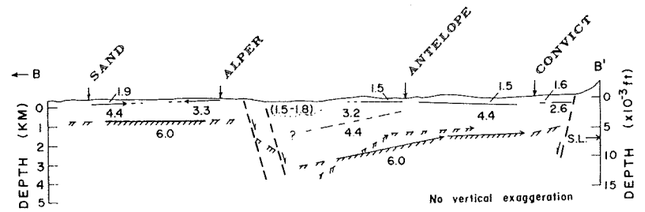

Fig. 8. Cross section showing P wave velocity structure under profile BB'. Symbols are the same as in Figure 7.

The general configuration of the basement in Figures 7 and 8 suggests that the caldron block partially broke up during collapse. In particular, it appears that a north section of the block tilted to the north and the eastern section tilted to the west, some differential subsidence occurring across the preexisting Hilton Creek fault.

Relief on the top of the 4.0- to 4.4-km/s layer (the Bishop tuff?) describes a broad dome centered over the west part of the caldera. The geometry of this dome supports the pattern of resurgence associated with eruption of the central rhyolites inferred by *Bailey et al.* [1976] from dips on central rhyolite tuffs and elevations of fossil shore lines of Pleistocene Long Valley Lake. The velocity models (Figures 7 and 8) suggest that maximum uplift in the center of the resurgent dome is between ½ and 1 km. A smooth connection of the 4.3- and 4.4-km/s layers on either side of Alkali (see Figure 7) would be consistent with this resurgence and in turn would eliminate the necessity for significant postcollapse tectonic displacement on the Hilton Creek fault within the caldera.

Possible evidence for a magma chamber. A set of later arrivals, following the first arrivals by 1.2–0.7 s is clearly evident on the Deadman record section (Figure 4) over the distance interval 7–16 km. These arrivals have a somewhat higher apparent velocity than the first arrivals; they also appear to be 180° out of phase with respect to the first arrivals. The latter can be demonstrated by tracing the first arrivals in the distance range 15–16 km and matching the later arrivals with the tracing inverted. Evidence for a similar, but weaker, set of arrivals can be seen on the Alkali record section in the distance range −12 to −17 km. The least complicated interpretation of these arrivals is that they have been reflected from a horizon within the basement at a depth of 7–8 km (Figure 7) across which the velocity decreases with depth.

Such a reflecting horizon is a likely candidate for association with the roof of the magma chamber that fed the eruption of the Bishop tuff and subsequent rhyolite eruptions. *Bailey et al.* [1976] infer from the geometry of the resurgent dome that the roof of the magma chamber at the time of resurgence was at a maximum depth of 5–7 km. *Steeples and Iyer* [1976] find evidence in teleseismic P wave delays for a volume beneath the caldera extending from depths of approximately 5–25 km in which the average P wave velocity is 15% lower than the surrounding crust. The character of the later arrivals is consistent with either a reflection from a solid-melt interface or from a solid-solid interface, the deeper solid having a lower P wave velocity (i.e., a crystallized residual melt fraction?).

The secondary arrivals identified as deep reflections may, of course, have other explanations. They could, for example, be lateral reflections or refractions from a steeply dipping boundary out of the plane of the profile. The most likely alternative is that they are multiple refractions from the basement involving one reflection from the earth's surface. Such arrivals would also have a 180° phase shift with respect to the first arrivals, but they should also have the same apparent velocity as the first arrivals. The higher apparent velocity of the later arrivals in the record section thus supports their identification as deep reflections.

Evidence for the hydrothermal system. The shot at Alkali generated a strong set of secondary arrivals that were recorded to a distance of 7–9 km on either side of the shot point (G in Figure 5). These arrivals have an apparent velocity of 1.9 km/s and form essentially continuous travel time curves with the first arrivals, which have apparent velocities of 1.5 and 1.7 km/s (Figure 2). The large amplitudes and extended coda of these arrivals suggest that they are generated by a series of supercritical reflected and refracted waves propagating between the base of the 0.5-km-thick, 1.5- to 1.9-km/s layer and the free surface. There is a close analogy between these arrivals and the $\bar{P}$ phase in crustal seismology.

One of the more striking aspects of these secondary arrivals is the pronounced difference in frequency content between wave groups on either side of the shot point; the waves propagating to the west are notably deficient in high-frequency energy with respect to those propagating to the east. The amplitude spectra of the wave groups from seismograms recorded at approximately 5 km on either side of the shot point plotted in Figure 9 emphasize this difference. Note in particular the rapid falloff of spectral amplitudes above about 8 Hz in the wave group that propagated to the west. The spectrum of the wave group that propagated to the east peaks at about 15 Hz. (The computed spectral amplitudes are not reliable for frequencies below 1–2 Hz; thus the apparent difference in spectral amplitudes between the two wave groups below about 3 Hz is of questionable significance.) The waves

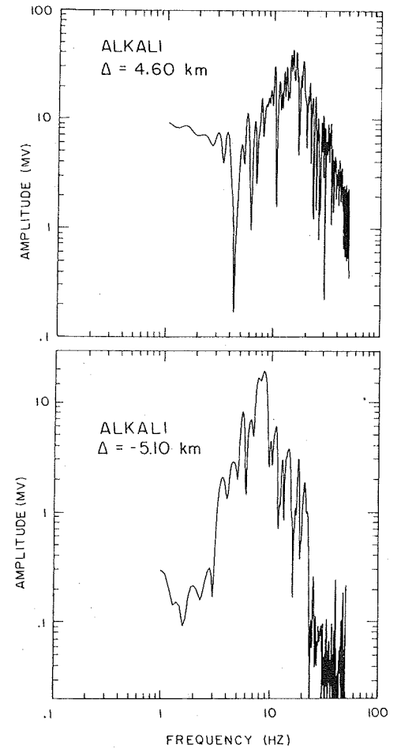

Fig. 9. Amplitude spectra of 1.9-km/s wave group from seismograms recorded 4.60 km east of Alkali (upper) and 5.10 km west of Alkali (lower) (see Figure 5). Ordinate is output of seismometer in millivolts. Amplitudes are not reliable for frequencies below about 2 Hz.

on the west side of the shot point have propagated across the main zone of shallow hydrothermal alteration and current hot spring activity in Long Valley (see Figure 5 in the work by *Bailey et al.* [1976]). The observed differences in the wave groups are very likely due to shallow scattering or attenuation properties of the hydrothermal area, the location of which is apparently controlled by north to northwest trending faults in the Hilton Creek fault zone [*Rinehart and Ross,* 1964]. Heterogeneities such as the vertical honeycomb or pipelike structures that are widespread in the hydrothermal area [*Bailey et al.,* 1976] would certainly provide a scattering mechanism, as would the fault zone itself. Although these data do not provide obvious clues to the deeper, poorly understood parts of the Long Valley hydrothermal system, it is encouraging to find what appears to be clear modification of the wave forms by shallow properties of the system.

As an aside, it is of interest to note the surface wave pulse recorded on the first two seismometers on either side of the Alkali shot point (R in Figure 5). The group velocity of this pulse is approximately 0.16 km/s, and its dominant period is about 0.3 s. This is virtually the same as the dominant group velocity and period associated with the microseismic noise in the east part of Long Valley described by *Iyer and Hitchcock* [1976] in their investigation of geothermal noise. Published dispersion curves from surface wave studies of shallow and sedimentary structures [*Dobrin et al.,* 1951] suggest that these waves may be an Airy phase of fundamental mode Rayleigh waves propagating in the lake and marsh deposits (the 0.5-km-thick layer with P wave velocities of 1.5–1.9 km/s).

CONCLUSIONS

The seismic refraction data obtained in this experiment provide a good first approximation to the P wave velocity structure of the upper 5–6 km of the crust beneath the Long Valley caldera. Tentative identification of horizons in the P wave velocity model with major rock units recognized in the caldera leads to the following conclusions.

1. The Sierran basement rocks in the caldron block (Cretaceous granitic rocks and Paleozoic to Mesozoic metamorphic rocks with P wave velocities of 6.0 ± 0.4 km/s) have been downdropped 2.5–3 km along normal faults bounding the north and northwest sides of the caldera. Displacement of the basement along normal faults bounding the south and east sides of the caldera is not well defined by the seismic data but generally appears to be between 1 and 2 km. There is an apparent discrepancy between the steep gravity gradients and the relatively small displacements and shallow dips of the basement suggested by the seismic data at the east margin of the caldera that may be explained in part by relatively thick accumulations of low-density sediments in that area.

2. Relief on the basement within the caldera suggests that the caldron block was partially disrupted during the collapse accompanying eruption of the Bishop tuff with the north part of the block tilting to the north and the east part of the block tilting to the west. A steplike displacement in the basement associated with the northward extension of the Hilton Creek fault into the caldera may be partly due to precollapse displacement along the Hilton Creek fault and partly due to differential settling of the basement during collapse along the preexisting weak zone formed by the fault.

3. The top of the 4.0- to 4.4-km/s layer, which overlies the basement and is tentatively identified with the Bishop tuff and Glass Mountain rhyolite, has a broad domelike structure centered over the western part of the caldera. This structure reflects postcollapse resurgence accompanying eruption of the central rhyolites. Maximum relief on the dome is from ½ to 1 km. Similar doming tends to be reflected in the basement as well, although it is partly obscured by relief on the basement.

4. The layer with P wave velocities of 2.7–3.4 km/s that overlies the 4.0- to 4.4-km/s layer is thickest in the moat between the resurgent dome and the caldera walls. This layer corresponds to the postcollapse rhyolites, rhyodacites, and basalt flows described by *Bailey et al.* [1976]. Substantial lake and marsh deposits from Pleistocene Long Valley Lake as well as clastic alluvial and glacial deposits are probably interbedded with these lava flows. Such interbedded deposits would result in a relatively low bulk density for this layer and may contribute significantly to the pronounced gravity lows observed along the north and northeast parts of the caldera. The permeability associated with substantial clastic deposits interbedded with the lava flows would also make the thicker sections of the 3.3- to 3.4-km/s layer filling the moat along the north and northwest margins of the caldera potentially favorable reservoirs for geothermal fluids.

5. The generally favorable agreement for basement depth in the caldera between the seismic refraction and three-dimensional gravity interpretations suggests that 0.45 g/cm^3 is a good approximation to the average density contrast between the caldera fill and the basement. The possibility that the 2.7- to 3.4-km/s material filling the moat may have a lower than average bulk density, however, suggests that the gravity lows may not require the deep depressions in the basement along the northern and northeast parts of the caldera shown in the single-density contrast model [*Kane et al.,* 1976]. The effect of the relatively thick, low-velocity (and presumably low-density) lake and marsh deposits in the east part of the caldera will also tend to reduce the depth to the basement shown in the gravity model.

6. Clear secondary arrivals on the Deadman record section are tentatively identified as a reflection from a low-velocity horizon at a depth of 7–8 km beneath the western section of the caldera. This horizon may be associated with the roof of the magma chamber beneath the caldera in the form of a trapped melt or a crystallized lens of low-velocity residual material.

7. And finally, the relative deficiency of high-frequency energy observed in a group of shallow guided waves provides evidence for anomalous scattering or attenuation associated with the region of hydrothermal alteration and hot spring activity in the eastern part of the caldera.

Acknowledgments. I am grateful to Wayne Jackson and Gene Taylor for their invaluable help with the logistics of the field program and to Stuart McHugh for his careful handling of the initial data reduction. I am particularly grateful to L. C. Pakiser for his encouragement and interest in all phases of the experiment. L. C. Pakiser and Roy A. Bailey critically reviewed the manuscript and suggested a number of improvements.

REFERENCES

Bailey, R. A., G. B. Dalrymple, and M. A. Lanphere, Volcanism, structure and geochronology of Long Valley Caldera, Mono County, California, *J. Geophys. Res., 81,* this issue, 1976.

Christensen, M. N., C. M. Gilbert, K. R. Lajoie, and Y. Al-Rawi, Geological-geophysical interpretation of Mono Basin, California-Nevada, *J. Geophys. Res., 74,* 5221–5239, 1969.

Dobrin, M. B., R. F. Simon, and P. L. Lawrence, Rayleigh waves from small explosions, *Eos Trans. AGU, 32,* 822–832, 1951.

Eaton, J. P., Crustal structure in northern and central California from seismic evidence, Geology of Northern California, edited by E. H. Bailey, *Calif. Div. Mines Geol. Bull., 190,* 419–426, 1966.

Hayakawa, M., The study of underground structure and geophysical state in geothermal areas by seismic exploration, *Geothermics, Spec. Issue 2, 2,* 347–357, 1970.

Hill, D. P., and S. McHugh, A compilation of data from the 1963 Long Valley seismic-refraction experiment, open file report, U.S. Geol. Surv., Menlo Park, Calif., 1975.

Hochstein, M. P., and T. M. Hunt, Seismic gravity and magnetic studies, Broadlands geothermal field, New Zealand, *Geothermics, Spec. Issue 2, 2,* 333–346, 1970.

Iyer, H. M., and T. Hitchcock, Seismic noise survey in Long Valley, California, *J. Geophys. Res., 81,* this issue, 1976.

Johnson, L. R., Crustal structure between Lake Mead, Nevada, and Mono Lake, California, *J. Geophys. Res., 70,* 2863–2872, 1965.

Kane, M. F., D. R. Mabey, and R. L. Brace, A gravity and magnetic investigation of Long Valley caldera, Mono County California, *J. Geophys. Res., 81,* this issue, 1976

Mota, L., Determination of dip and depths of geological layers by the seismic-refraction method, *Geophysics, 19,* 242–254, 1954.

Pakiser, L. C., Gravity, volcanism, and crustal deformation in Long Valley, California, *U.S. Geol. Surv. Prof. Pap. 424-B,* B250–B253, 1961.

Pakiser, L. C., Seismic evidence for the thickness of Cenozoic deposits in Mono Basin, California, *Geol. Soc. Amer. Bull., 79,* 1833–1838, 1968.

Pakiser, L. C., Structure of Mono Basin, California, *J. Geophys. Res., 75,* 4077–4080, 1970.

Pakiser, L. C., F. Press, and M. F. Kane, Geophysical investigation of Mono Basin, California, *Geol. Soc. Amer. Bull., 71,* 415–447, 1960.

Pakiser, L. C., M. F. Kane, and W. H. Jackson, Structural geology and volcanism of the Owens Valley region, California—A geophysical study, *U.S. Geol. Surv. Prof. Pap. 438,* 68 pp., 1964.

Rinehart, C. D., and D. C. Ross, Geology and mineral deposits of the Mount Morrison quadrangle, Sierra Nevada, California, *U.S. Geol. Surv. Prof. Pap. 385,* 106 pp., 1964.

Smith, R. L., and R. A. Bailey, Resurgent cauldrons, *Geol. Soc. Amer. Mem., 116,* 613–662, 1968.

Steeples, D. W., and H. M. Iyer, Low-velocity zone under Long Valley as determined from teleseismic events, *J. Geophys. Res., 81,* this issue, 1976.

Warrick, R. E., D. B. Hoover, W. H. Jackson, L. C. Pakiser, and J. C. Roller, The specification and testing of a seismic-refraction system for crustal studies, *Geophysics, 26,* 820–824, 1961.

White, D. E., Characteristics of geothermal resources in *Geothermal Energy,* edited by P. Kruger and G. Otte, pp. 69–94, Stanford University Press, Palo Alto, 1973.

(Received January 29, 1975;
revised July 22, 1975;
accepted July 24, 1975.)

A Gravity and Magnetic Investigation of the Long Valley Caldera, Mono County, California

MARTIN F. KANE, DON R. MABEY, AND ROSA-LEE BRACE

U.S. Geological Survey, Denver, Colorado 80225

Gravity studies show that the subsurface part of the Long Valley caldera is a coincident steep-sided depression filled with porous epiclastic and volcanic materials to a depth of as much as 3 km. The depression contains two major basins, a larger and deeper one making up much of the eastern part and a somewhat smaller, more shallow one to the west; a positive feature underlying the central part of the depression separates the two basin areas. The east side of this feature is linear in plan and coincides with the extension of the Hilton Creek fault which is mapped within and beyond the south edge of the caldera. The indicated relief on the postulated subsurface Hilton Creek fault together with difference in depth of the eastern and western basinal areas indicates that the eastern basin is downdropped in relation to the western one. Gentle gravity gradients outside the caldera but sloping towards it are interpreted as evidence of a low-density mass located below the caldera fill. We conclude that it is probably related to the magma source. Aeromagnetic data indicate that a northwest-trending belt of metasedimentary rocks on the south flank of Long Valley may extend into the caldera proper and form much of the bedrock floor of the western part of the caldera. A magnetic low of shallow source in the hot spring region in the southwest is thought to be caused by hydrothermal alteration of the ferrimagnetic minerals in the underlying rocks. A broad positive magnetic anomaly near the center of the caldera may be caused by a thick section of magnetic volcanic flow lying east of the projected Hilton Creek fault and underlying much of the eastern basin.

INTRODUCTION

Gravity and aeromagnetic surveys were conducted in Long Valley, California, during 1954–1957 as part of a regional geophysical study of the Owens River drainage basin. The results of these surveys were reported in a comprehensive paper by *Pakiser et al.* [1964]. Since that study was completed, more detailed and different kinds of geophysical and geological surveys have been made in Long Valley, and improved techniques for interpreting gravity and magnetic data have been developed. In addition, further insights into the nature of caldera fill have come to light as a result of extensive studies of ash flow-related calderas, for example, *Smith et al.* [1961, 1970]. We have therefore re-examined the gravity and magnetic data in an attempt to refine and extend the earlier interpretations, placing particular emphasis on features that relate to the potential geothermal resources of the valley.

As interest in geothermal resources has increased, a need has emerged for reconnaissance geophysical techniques suitable for identifying target areas for more intense exploration. In this regard, regional gravity and magnetic data are available for many areas and, where they are not available, can usually be obtained more economically than other geophysical data. In the case presented here, distinctive gravity and magnetic anomalies are shown to be associated with the Long Valley caldera and appear to reflect to some extent the geothermal system which is thought to underlie the caldera.

The geology of Long Valley is described elsewhere [*Bailey et al.*, 1976] and is discussed herein only as it relates directly to the gravity and magnetic anomalies. On geological grounds alone, two major anomalous masses with associated gravity anomalies might be anticipated as being approximately coextensive with the valley: (1) the porous volcanic and epiclastic rocks filling the caldera and (2) a postulated intrusive body or magma chamber located at some depth below the caldera fill. Both of these features would be expected to represent relatively negative mass anomalies and would therefore produce gravity lows. In addition, density variations within the caldera fill and shallow intrusive bodies penetrating the fill might cause intracaldera gravity variations. The sum of the local gravity anomalies associated with the Long Valley caldera is superimposed on a relatively complex regional anomaly consisting of two parts: (1) decreasing Bouguer anomaly values toward the west, reflecting isostatic compensation of the Sierra Nevada, and (2) somewhat more localized bedrock anomalies due to the density contrast between the granitic rocks of the Sierra Nevada batholith and the denser older metasedimentary and metavolcanic rocks [*Oliver et al.*, 1961].

Most of the magnetic highs or lows observed in the area can be related to the volcanic rocks of Cenozoic age in which remanent magnetization is probably the predominant factor. Magnetic anomalies are also associated with igneous units within the Sierra Nevada batholith and with some terrains underlain by metasedimentary and metavolcanic rocks.

The gravity map of Long Valley (Figure 1) is based primarily on the data from *Pakiser et al.* [1964] as shown on the Mariposa sheet of the gravity map of California [*Oliver and Robbins*, 1973]. The procedures for the gravity survey and data reduction are described in the work by *Pakiser et al.* [1964]. A second more detailed map was prepared from the data of *Pakiser et al.* [1964] by addition of new data measured by D. L. Peterson of the U.S. Geological Survey in 1973. From the latter map we prepared a residual map (Figure 2) by passing an approximately plane surface through the field such that the residual was zero at a distance of about 6 km beyond the valley margin.

Two separate aeromagnetic surveys were made by the U.S. Geological Survey [*Pakiser et al.*, 1964; *U.S. Geological Survey*, 1974]. The first was a low-level reconnaissance of the valley area made along east-west flight lines 1–1.5 km apart and 0.7 km above the land surface. The data were compiled as a total intensity map relative to an arbitrary datum (Figure 6). The second survey (Figure 7) was part of a high-level regional study with flight lines 1.7 km apart and 4 km above sea level. The data from this survey were compiled as a residual map by removing the 1965 international geomagnetic reference field (IGRF) updated to 1973.

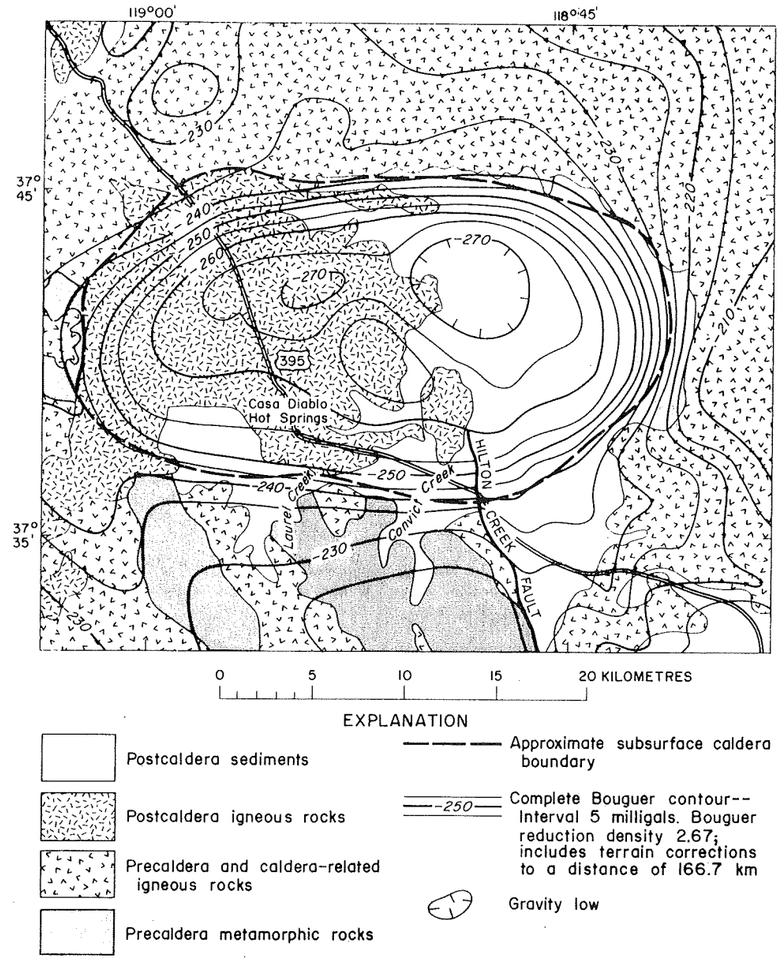

Fig. 1. Combined generalized geology and complete Bouguer gravity map of Long Valley caldera and vicinity. Geology is generalized from R. A. Bailey (written communications, 1974). Gravity is modified from *Oliver and Robbins* [1973].

GRAVITY

A major gravity low with a relative amplitude of more than 50 mGal coincides with the Long Valley caldera (Figure 1). As reported by *Pakiser et al.* [1964], much of the low is undoubtedly caused by the density contrast between the porous caldera fill and the compact enclosing crystalline rocks. Judging from the bedrock exposed around the valley the bulk of the rock enclosing the caldera probably approaches granite in composition with a corresponding average density of about 2.7 g/cm³. The average density of the caldera fill depends on many poorly known factors and can only be estimated with considerable uncertainty. Much of the porous sediment probably has a density of about 2.0 g/cm³, but some of the volcanic units have densities that equal or exceed the density of the enclosing crystalline rocks. Pumiceous sediments may be extremely anomalous in density with values considerably less than 2.0 g/cm³. We estimate that the average density of the caldera fill is about 2.25 g/cm³, yielding a density contrast of 0.45 g/cm³. This estimate may be as much as 50% in error on the average and even more in local areas. But, as will become clear in the following discussion, many other uncertainties in the models derived from the gravity data make the assessment of a more accurate value unwarranted.

Using the assumed average density of 0.45 g/cm³, we inverted the residual gravity anomaly (Figure 2) to a corresponding distribution of caldera fill (Figure 3) by using the method of *Cordell and Henderson* [1968]. Two constraints were imposed in the technique that was used, namely, that the top of the fill was at the surface and that the sides were within the boundary formed by the zero isogal; i.e., the walls of the caldera dip vertically or inward from within the zero isogal. As might be predicted, the thickness contours of the fill are like those of the gravity map but with considerable detail added in the central (deeper) part of the fill. A cursory inspection suggests that the northern and eastern walls of the caldera are steeper than those to the south and west. An apparent maximum thickness (depth) of 5.5 km is reached in the tight

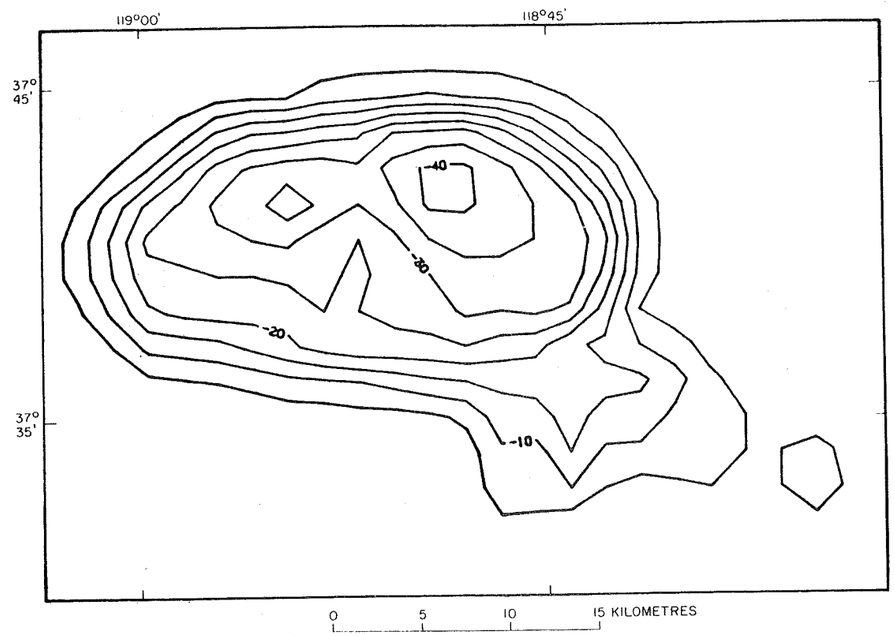

Fig. 2. Residual Bouguer gravity map of Long Valley area. Contour interval is 5 mGal.

gradient closure in the northwest part of the caldera, and a nearly equivalent thickness (depth) occurs in the broader closure just to the east. A series of apparent deeps occur along the west, east, and north rim of the basin; two apparent deeps of lesser magnitude are present in the south central part of the caldera. A central area of relatively positive relief, or platform, in the caldera floor divides the model into what might be regarded as separate eastern and western basinal areas. A well-defined peak in the central part of the platform reaches to within 1 km of the surface and forms the shallowest part of the

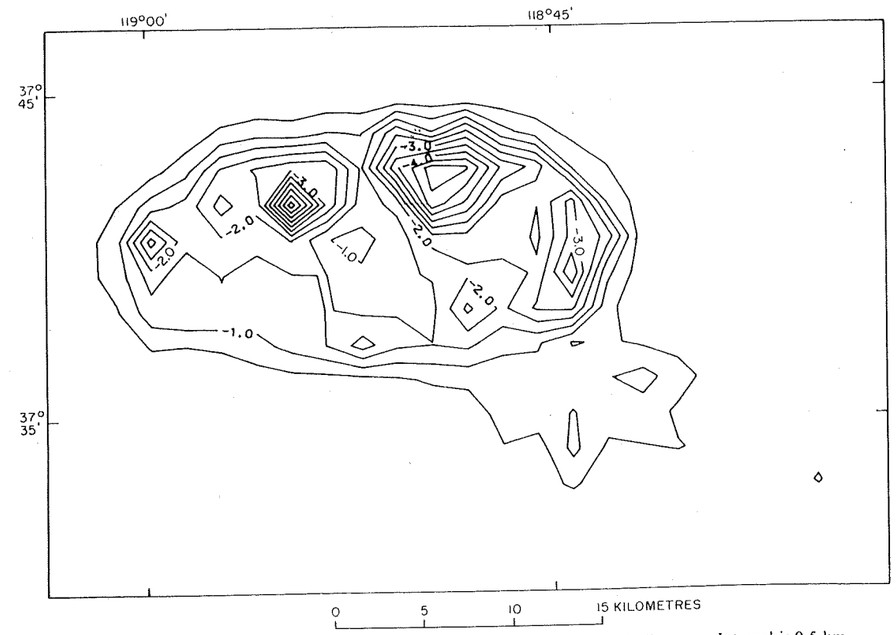

Fig. 3. Model of caldera fill showing depth to bottom of structure, Long Valley area. Interval is 0.5 km.

interior of the caldera. The eastern side of the platform is linear in plan and is approximately coincident with the mapped extension of the Hilton Creek fault in the caldera proper. An apparent shallow area is indicated in the vicinity of the Casa Diablo hot spring.

The shallow lobe southeast of the caldera proper indicates a bedrock trough attaining depths as great as 1 km. A somewhat shallower extension (indicated by the secondary lobe on the gravity contour map of Figure 2) must extend farther southeast to enclose the small isolated closure but is not shown because it is less deep than the contour interval of 0.5 km.

In the preceding discussion, two principal sources limit the validity of the quantitative conclusions. First, the selection of the regional surface is somewhat arbitrary. *Pakiser et al.* [1964] chose a surface such that the residual amplitude was higher, thereby leading to a greater average thickness for the fill. Second, in general, it is not possible to locate with any precision the bottom of models derived from gravity data alone, owing to problems of density contrast and to the separation of the anomaly from fields arising from other sources. Our choices, we believe, are reasonable but are certainly subject to revision if further relevant data, particularly on density contrast, become available. The model is most valid perhaps for the comparison of intracaldera features. Even the latter picture, however, is affected by lateral density variations in the fill, and we discuss these in the following paragraphs.

Variations in the density of caldera fill result mainly from three factors: (1) mode of deposition and degree of compaction of sedimentary units, (2) emplacement of igneous units of contrasting density, and (3) induration and alteration produced by hydrothermal alteration. The density of the epiclastic sediments will be determined largely by the degree of sorting, with coarse poorly sorted materials (less porous, more dense) near the source areas and finer ones (more porous, less dense) in the centers of depressions. The sediments will be compacted and therefore denser with depth. Both extrusive and intrusive rocks occur in the caldera and represent positive mass anomalies, except for pumiceous sediments. The density of the latter can be extremely low. Hot solutions bearing dissolved minerals and moving horizontally and vertically through porous zones can deposit minerals in pore spaces, thereby increasing the density.

When lateral sorting effects on clastic sediments are not accounted for in gravity-derived models of intermontane basins, it can be shown [*Kane and Pakiser,* 1961] that the walls of the model must dip less and be displaced somewhat more basinward than the actual subsurface walls of the basins. Thus to the extent that sorting affects the sediments of Long Valley, the walls of the model of Figure 3 can be considered to have dips equal to or less than actual dips and to have locations at or inside the valley walls.

Direct evidence of an intracaldera density variation—the second factor—is shown in the plot of the difference in values between the measured gravity field (Figure 2) and the field calculated for the model (Figure 4). The 2-mGal negative difference shown in the northeastern part of the caldera represents a steep gradient local anomaly which cannot be accounted for by adding a mass deficiency at the base of the model. The anomaly reflects the presence of a shallow mass which has a density contrast (porosity) higher than the model density (0.45 g/cm³). This clearly identified area of relatively low density raises the possibility that most, if not all, of the apparent deeps shown by the model have an equal probability of being caused by local increases in the porosity of the fill. The model contours in these areas may therefore also be considered as qualitative indications of possible variations in fill porosity.

The third factor variation which needs to be considered is related to the effect of the percolation of hydrothermal waters through porous sediments. Detailed geophysical measurements in the Raft River area of Idaho [D. R. Mabey, personal communication, 1974] indicate that the passage of water of this type through porous sediments can result in the deposition of minerals in the pore spaces, leading to an effective increase in density. This type of density variation may be the cause of the apparent thin part of the model in the southwest region of the caldera where Casa Diablo hot spring is located.

The model of caldera fill as modified conceptually in the preceding paragraphs has four salient features. (1) It confirms the earlier interpretation [*Pakiser et al.,* 1964] that the caldera is bounded by high-angle faults. The faults may have an equal or steeper dip and may lie somewhat outside those shown by the model. (2) If allowance is made for the suggested porosity variations in basin fill, the maximum thickness of the fill is more probably that shown by the contours exclusive of the local deeps, that is, about 3 km. This depth is appreciably less than that given by *Pakiser et al.* [1964], but the difference is due to the smaller residual that was chosen and the identification of the probable local concentrations of high-porosity fill. The lesser thickness is also in better agreement with the interpretation by *Hill* [1976]. (3) Two basinal areas are defined, the eastern one being estimated as about 3 km deep and the western one about 2 km deep. (4) The shallow region in the southwest part of the caldera may be deeper than shown if an allowance is made for an increase in fill density caused by pore deposition of minerals from percolating hydrothermal waters.

Two geological inferences may be drawn from the modified model. The first is that the local accumulations of high-porosity fill may be pumiceous sediments. Moreover, the locations of these accumulations about the margin of the caldera may mark volcanic centers; i.e., the deeps shown by the uniform density model (Figure 3)—at least the major deeps—may be the manifestation of these centers. The second geological inference is that even when allowance is made for local variations in fill porosity, two basinal areas divided by a relatively high central platform are present. The platform may represent a basement ridge between two areas where the basement has collapsed over separate magma chambers. It should be pointed out, however, that there is positive three-dimensional relief on the platform suggesting either the presence of a coincident igneous feature or residual relief left by erosion at some time prior to collapse of the caldera. The eastern side of the platform is linear and coincides with the location of the Hilton Creek fault. It seems reasonable to assume that the linear part of the model reflects subsurface throw on the fault. This feature together with the difference in depth of the two basins indicates that the eastern basin may have been downdropped relative to the western one along the Hilton Creek fault and the faults which bound the eastern part of the caldera.

The southeast lobe of the model is underlain primarily by Bishop tuff. The most direct interpretation is that the anomaly reflects pre-Bishop tuff topography and gives a measure of the thickness of the tuff. An alternate source for the lobe is a deeper intrabedrock mass, perhaps a lobe of intrusive rock whose emplacement is related to the formation of the caldera.

As will be shown below, the evidence of a gravity source that is significantly deeper than the caldera fill must be sought well outside the caldera boundary. The evidence should take the

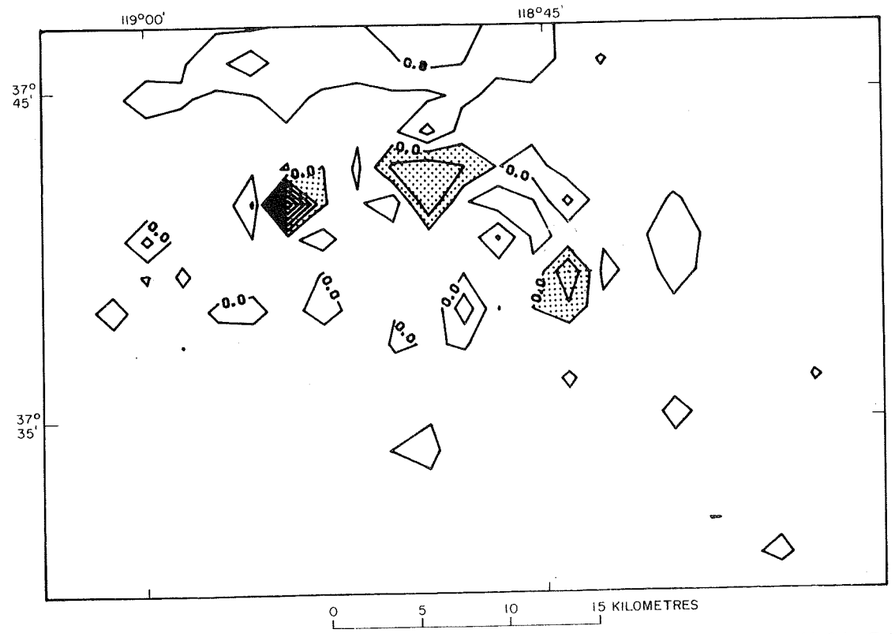

Fig. 4. Difference between measured and calculated values for the model of caldera fill (Figure 3). Interval is 0.4 mGal. Dotted areas are negative.

form of a gradient which persists beyond the region where it could reasonably be attributed to a shallow source, namely, the caldera fill. Because the dip of the regional trend is dominantly westward, the most likely areas to seek a manifestation of the deep-source gradient are north and south of the caldera. Figure 1 shows that a gentle gradient does exist to the north and south of the caldera and that it has an average value in excess of 1 mGal/km.

In order to examine the quantitative aspects of the gradients more closely we have plotted measured gravity profiles over the south edge of the caldera (Figures 5*a* and 5*b*) from the gravity map by *Pakiser et al.* [1964, Plate 1]. We chose the south edge for two reasons. First, north of the caldera the considerable thicknesses of alluvial and volcanic rock which overlies the granitic and sedimentary bedrock might substantially perturb the regional gradient. Second, the juxtaposed belts of metasedimentary and igneous rocks south of the caldera parallel the profile direction so that gravity effects due to bedrock density contrasts tend to be minimized. For comparison we show calculated profiles for a sequence of disc-shaped bodies [*Nettleton,* 1942] in Figures 5*c,* 5*d,* and 5*e*. The point of common reference is the edge of the caldera.

Figure 5*c* is the gravity profile over two concentrically arranged discs where the top of the upper disc coincides with the ground surface; the upper disc is 8 km in radius and 1.2 km thick, and the lower is 6 km in radius and 1.2 km thick. The representation of the caldera fill by the discs is sufficiently accurate for a close quantitative examination of the gradients outside the caldera boundary. Figures 5*d* and 5*e* are profiles of discs with radii of 8 km and maximum gravity amplitudes of about 10 mGal, tops being located at 6- and 10-km depth, respectively.

Comparing the profiles discloses that the interval 6–12 km of the measured profiles (Figures 5*a* and 5*b*) matches the same interval of profile *c* much more closely than that of profiles *d* and *e*; in fact, the gradients of the measured profiles are somewhat more steep than that of profile *c*. This comparison demonstrates that a major part of the observed anomaly must be caused by a shallow source as simulated by the discs of Figure 5*c*, in other words, the caldera fill. The overwhelming effect of the shallow caldera fill precludes separating the effects of deep and shallow sources in the interval 0–10 km, that is, from the center of the caldera to about 2 km beyond its boundary.

Apparently, the critical interval in which to seek evidence of a deep source for a feature of the size and geometry of the Long Valley caldera is 10–12 km, or 2–4 km beyond the caldera boundary. As shown in Figure 5*c* (the disc model of caldera fill), the calculated gradient for a shallow source in the interval 10–12 km is about 1 mGal/km; moreover, the amplitude at 12 km is 1.5 mGal, or roughly 4% of the maximum amplitude. The gravity gradients in the interval 10–12 km for the deep sources of the model profiles *d* and *e* are both about 0.6 mGal/km, but the amplitudes at 12 km are about 30% and 50% of maximum for *d* and *e* respectively.

In the uppermost measured profile (Figure 5*a*) the apparent gradient from 10 to 12 km is nearly 7 mGal, or about 3.5 mGal/km. The dashed part of the profile, however, is estimated from nearby stations, and the well-established part of the profile centered around 10 km is along a moderately wide valley where alluvial fill may be significantly affecting the gradient. We therefore view the gradients of this profile as possibly suspect. The second measured profile along Laurel Creek has a gravity change of 3 mGal between 10 and 12 km, yielding a gradient of about 1.5 mGal/km. This value is 50% larger than that calculated for a shallow source (profile *c*) and is considered to be significant.

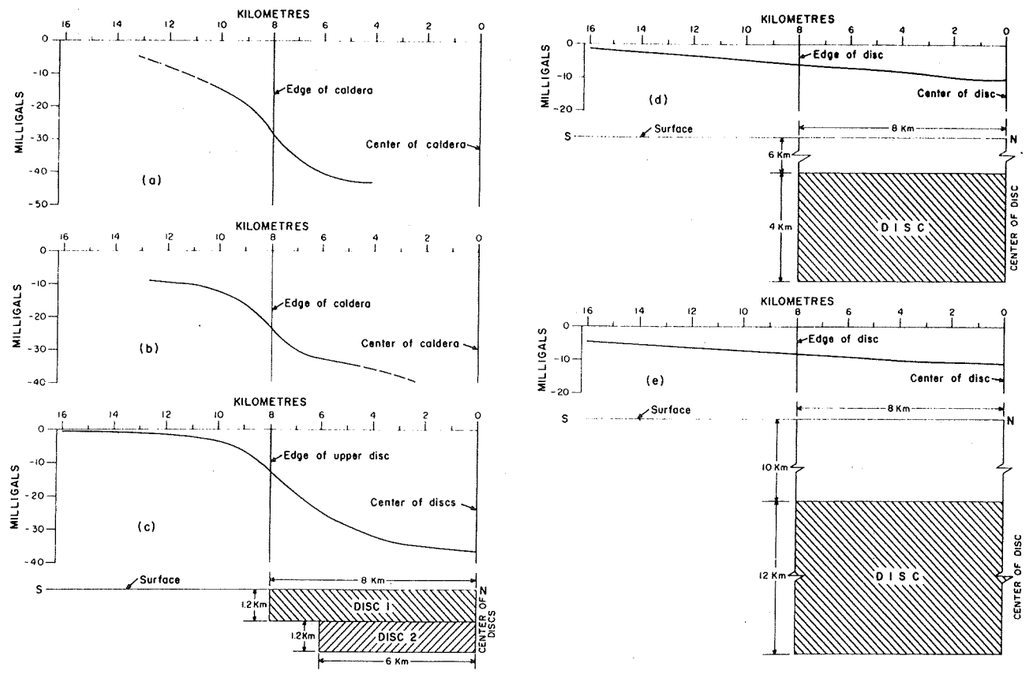

Fig. 5. Measured and calculated gravity profiles over edge of caldera: (*a*) measured gravity profile over south edge of caldera along Convict Creek, (*b*) measured gravity profile over south edge of caldera along Laurel Creek, (*c*) calculated gravity anomaly over edge of two circular, concentrically arranged discs centered at zero (both discs have a density contrast of 0.45 g/cm³), (*d*) calculated gravity anomaly over edge of circular disc centered at zero (disc has density contrast of 0.45 g/cm³), and (*e*) calculated gravity anomaly over edge of circular disc centered at zero (disc has density contrast of 0.45 g/cm³).

From these observations we draw four conclusions. (1) A source about 8 km in radius constrained above 3-km depth and with an amplitude of about 40 mGal should not exhibit a gradient steeper than about 1 mGal/km in the interval 2–4 km beyond the boundary of the source. (2) When the shallow-source steep gradients are integrated over the length of the profile inside and near the caldera boundary, they account for most of the amplitude, and so only a small fraction of that part of the anomaly can be attributed to a deep source, say, less than 10 mGal. (3) Because of the limit on amplitude for a deep source the corresponding deep-source gradient should not exceed 0.6–0.9 mGal/km in the interval 2–4 km beyond the caldera boundary. (4) Therefore a well-established gradient of 1.5–2.0 mGal/km in the interval 2–4 km beyond the caldera is evidence of a deep source. As shown by profiles *d* and *e*, a more direct measure of a deep source would be the observation of a persistent gradient of about 0.5 mGal/km in the interval 12–16 km, or a one-half to full radius beyond the caldera edge. Data in this region were not available for measured profiles *a* and *b* (Figure 5).

Profiles *a* and *b*, if taken at face value, indicate a deep source, although the dashed gradient for measured profile *a* is obviously much too large. The gradient of profile *b* is what would be predicted for a combined shallow source of about 35-mGal amplitude and a deep source of 10-mGal amplitude. Both profiles, however, should be viewed with some caution because they were measured along valleys underlain by an undetermined amount of alluvial fill. Terrain corrections were made for both profiles, but the stations are in relatively high terrain where accuracy of the terrain correction tends to fall off. Despite these reservations we feel that it is reasonable to conclude that the data indicate a deep source perhaps centered at a depth of 8–16 km causing an anomaly of about 10 mGal. Because of the depth, the thickness and density contrast parameters of the body cannot be separated with any precision.

In reviewing Figure 1 in light of the comments about profiles *d* and *e* (Figure 5) it can be seen that a definite gradient appears to persist beyond 4 km from the caldera boundary, particularly on the north. If bedrock density variation is not a factor, this gradient may also be taken as evidence of a deep low-density mass which might be a magma chamber or a pluton.

In general, the gravity evidence of a deep source is sketchy but affirmative. Additional field measurements in key areas outside the caldera and a fuller evaluation of the effect of variable density in the bedrock are needed to substantiate fully the tentative conclusions drawn here.

If it is assumed that all of the caldera fill originates from the immediate vicinity of the caldera (including volcanic material derived from the subsurface), then the porosity volume causing the negative gravity anomaly is an approximate measure of absent subsurface mass. Using Gauss' theorem, we calculate that the mass corresponding to the integrated negative anomaly (Figure 2) is 3.33×10^{17} g. For a rock density of 2.67 g/cm³ we calculate 125 km³ for empty pores and 200 km³ for pores filled with water. Our estimate of absent subsurface material is much less than *Pakiser's* [1961] because we have restricted our integration to the anomaly in the immediate

vicinity of the caldera. Much of the difference between the two figures would be attributed by us to the deep source.

MAGNETICS

The low-level magnetic survey (Figure 6) defines two major magnetic anomalies in Long Valley, a broad magnetic high present over much of the northeastern part of the valley and a rather complex magnetic low in the southwest in the vicinity of Casa Diablo hot spring. *Pakiser et al.* [1964, p. 41] estimated that a broad magnetic mass approximately outlined by the 1750 gamma contour underlies the area at a depth of about 1 km. In commenting on the two positive closures superposed on the broader high, they postulate two possible causes: The first is 'rock of intermediate magnetic susceptibility into which have been intruded, or from which have been segregated, the two smaller bodies composed of more highly magnetic rock.' The second, 'an alternative interpretation, which is preferred by the writers and is more consistent with the gravity data, would regard the smaller more highly magnetic masses as volcanic necks that were sources of a sequence of flows that express the broader feature.' In general we would agree with *Pakiser et al.* [1964] in their preference of the latter alternative and would further add that the magnetic mass appears to be bound on the west by the projected Hilton Creek fault.

Pakiser et al. [1964] did not interpret the low at Casa Diablo hot spring. The tightened contours in several places show gradients that indicate a near-surface source. The source could be reversely magnetized volcanic rock or possibly rock in which the magnetite has been altered by hydrothermal solutions. Because of the proximity of the anomaly to known hot springs and an approximately coextensive resistivity low [*Stanley et al.*, 1976] the interpretation as a zone of alteration is thought to be the more likely one.

The higher level of the regional survey (Figure 7) provides a somewhat different perspective of the magnetic anomalies. The outlines of the caldera are indicated by a change in magnetic gradients across the caldera boundary, lower gradients being present over the caldera where the magnetic rocks are farther below the flight level of the survey. The magnetic high in the northeast part of the valley has a similar form on both surveys

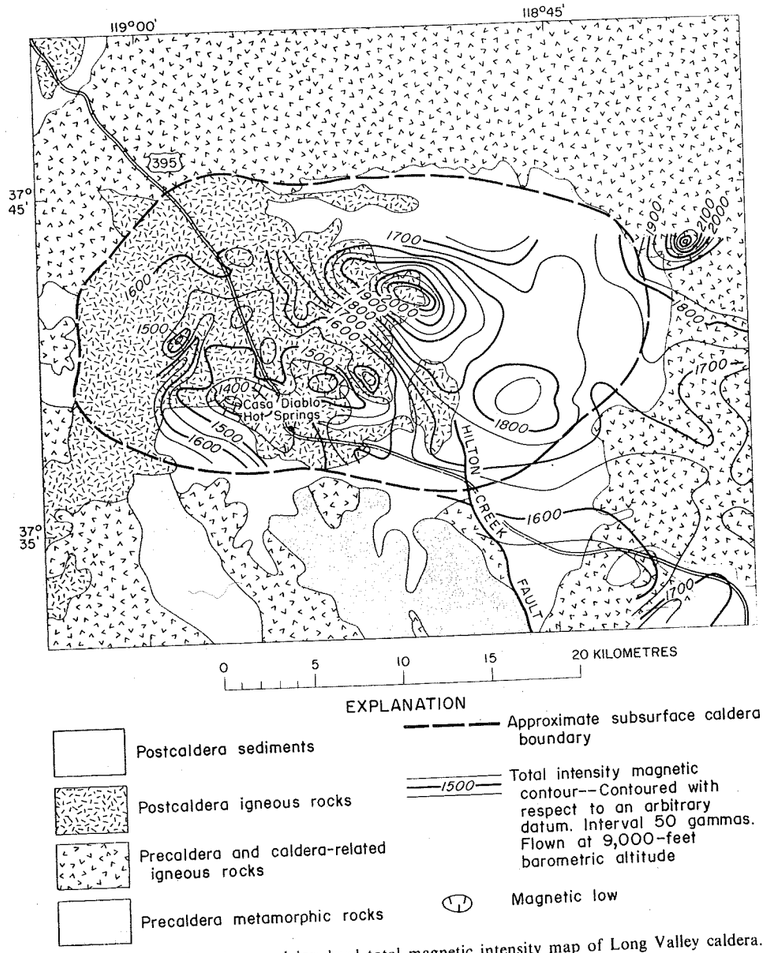

Fig. 6. Combined generalized geology and low-level total magnetic intensity map of Long Valley caldera. Magnetic contours from *Pakiser et al.* [1964].

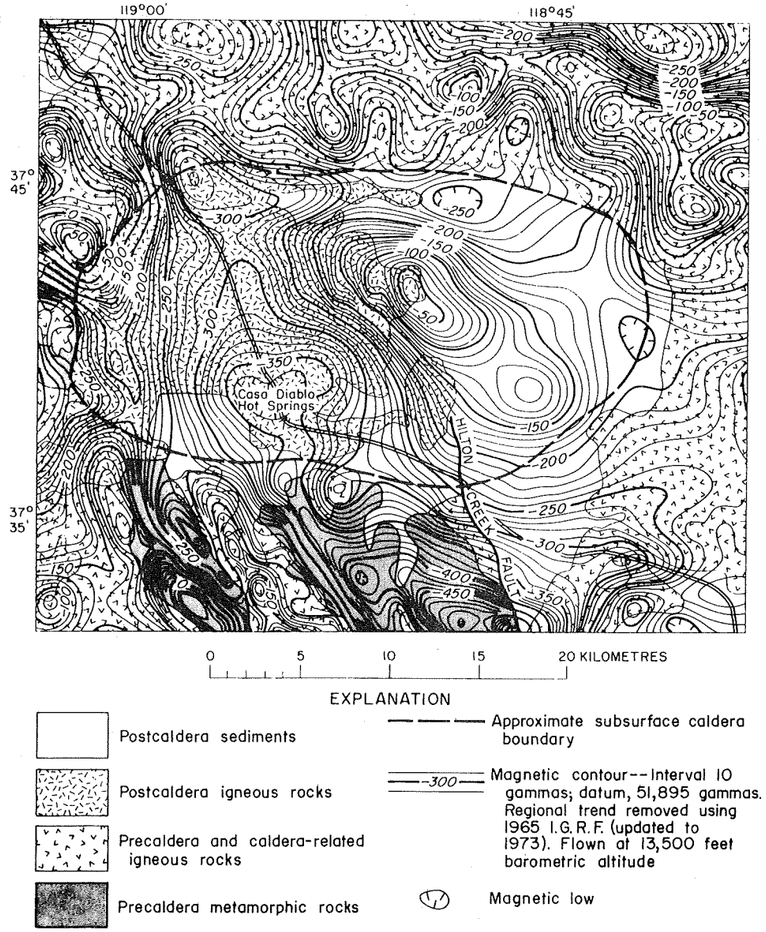

Fig. 7. Combined generalized geology and high-level residual magnetic intensity map of Long Valley area [*U.S. Geological Survey*, 1974].

because the dimensions of the source are large in comparison with the aircraft height above source. The near-surface anomaly at Casa Diablo hot spring, in contrast to the magnetic high, merges into a more intensive regional low on the higher-level survey. The regional feature, in contrast with the local low shown on Figure 6, extends to the north and south beyond the margins of the valley. To the south the regional low coincides with the belt of metasedimentary rocks enclosed within the granitic rocks of the Sierra Nevada batholith, suggesting that the western floor of the caldera may be underlain primarily by a belt of metasedimentary rocks.

SUMMARY

The regional gravity and magnetic surveys of Long Valley illustrate a type of reconnaissance exploration for geothermal systems in the western United States. They show that large features, like calderas, are clearly identified and that much information about the structure of the features can be derived from the geophysical data. The calculated anomalies reveal that evidence for deep sources, perhaps more directly linked to a primary geothermal source such as a magma chamber, must be sought in a region well outside any surface feature. The evidence for a deep source at Long Valley is marginal but affirmative and indicates that a deep source may be detectable by the gravity method under the right conditions, that is, where near-surface gravity variations do not mask the somewhat subtle but persistent gradients caused by the deep source. The calculations also show that the depth of the source is related to the extent of the gradient; i.e., a deeper source will cause the gradient to persist over a larger area. For sources deeper than several kilometers it is probably not possible to separate the thickness and density contrast parameters of a body with any degree of precision. The mass contrast of the body, however, is calculable from Gauss' theorem if the anomaly is reasonably well defined. If the density contrast can be estimated from theoretical or experimental data, then the volume of the postulated magma can be derived. Perhaps the most important point to be made from the calculations is that careful gravity surveys must be conducted over a broad region

around a postulated deep source before substantive conclusions are made about its presence.

Acknowledgment. We wish to express our appreciation to L. C. Pakiser, who conducted the original geophysical research in this area and who has graciously provided commentary and advice in the preparation of this manuscript.

REFERENCES

Bailey, R. A., G. B. Dalrymple, and M. A. Lanphere, Geology and geochronology of Long Valley caldera, Mono County, California, *J. Geophys. Res., 81,* this issue, 1976.

Cordell, L., and R. G. Henderson, Iterative three-dimensional solution of gravity anomaly data using a digital computer, *Geophysics, 33,* 596–601, 1968.

Hill, D. P., Structure of Long Valley caldera from seismic refraction experiments, *J. Geophys. Res., 81,* this issue, 1976.

Kane, M. F., and L. C. Pakiser, Geophysical study of subsurface structure in southern Owens Valley, California, *Geophysics, 26,* 12–26, 1961.

Nettleton, L. L., Gravity and magnetic calculations, *Geophysics, 7,* 293–309, 1942.

Oliver, H. W., and S. L. Robbins, Complete Bouguer gravity map of the Mariposa and part of the Goldfield 1° by 2° quadrangles, California-Nevada, open file report, U.S. Geological Survey, Reston, Va., 1973.

Oliver, H. W., L. C. Pakiser, and M. F. Kane, Gravity anomalies in the central Sierra Nevada, California, *J. Geophys. Res., 66,* 4265–4271, 1961.

Pakiser, L. C., Gravity volcanism, and crustal deformation in Long Valley, California, *U.S. Geol. Surv. Prof. Pap. 424-C,* B250–B253, 1961.

Pakiser, L. C., M. F. Kane, and W. H. Jackson, Structural geology and volcanism of Owens Valley, California—A geophysical study, *U.S. Geol. Surv. Prof. Pap. 438,* 1–68, 1964.

Smith, R. L., R. A. Bailey, and C. S. Ross, Structural evolution of the Valles caldera, New Mexico, and its bearing on the emplacement of ring dikes, *U.S. Geol. Surv. Prof. Pap. 424-D,* D145–D149, 1961.

Smith, R. L., R. A. Bailey, and C. S. Ross, Geologic map of the Jemez Mountains, New Mexico, *Misc. Invest. Map I-571,* U.S. Geol. Surv., Denver, Colo., 1970.

Stanley, W. D., D. B. Jackson, and A. A. R. Zohdy, Deep electrical investigations in the Long Valley geothermal area, California, *J. Geophys. Res., 81,* this issue, 1976.

U.S. Geological Survey, Aeromagnetic map of parts of the Walker Lake and Mariposa 1° by 2° quadrangles, eastern California, open file report, *U.S. Geological Survey,* Reston, Va., 1974.

(Received February 4, 1975;
revised August 21, 1975;
accepted September 12, 1975.)

The Near-Surface Hydrothermal Regime of Long Valley Caldera

ARTHUR H. LACHENBRUCH AND M. L. SOREY

U.S. Geological Survey, Menlo Park, California 94025

R. E. LEWIS

U.S. Geological Survey, Garden Grove, California 92643

J. H. SASS

U.S. Geological Survey, Menlo Park, California 94025

Temperatures at the 5- to 10-m depth from 29 shallow holes in Long Valley caldera can be contoured systematically; they correlate well with the character of the thermal gradient to 30 m. Where the temperature at a depth of 10 m is less than 11°C (group I), the gradients to 30 m are practically zero; where the 10-m temperature is between 11°C and 16°C (group II), the gradients are 200°–400°C/km and uniform, corresponding to conductive heat flows of 4–8 HFU (1 HFU = 1×10^{-6} cal/cm² s). Where the 10-m temperatures exceed 16°C (group III), gradients are larger and irregular, with local heat flows to 50 HFU. Thermal considerations suggest that the first group is characteristic of regions of hydrologic recharge, that the second group is probably characteristic of regions with conductive regimes to substantial depth, and that the third group is characteristic of regions of hydrologic discharge. This interpretation is supported by limited drilling to depths up to 300 m. Regimes in group I occur in the peripheral portion of the caldera, suggesting that this is an area of recharge. The hot springs discharge in a fault zone characterized by near-surface regimes in groups II and III; chemical evidence indicates that their source reservoir is at about 200°C. Evidently, the springs are fed by local fractures; if the background regime is conductive, their reservoirs are probably less than 1 km deep. Hydrologic and isotopic data indicate that gross circulation in the hydrothermal system is from west to east, suggesting that the hot springs gain their heat in the western caldera. The large estimates of heat being removed from the caldera by flowing water and the geologic inference that hydrothermal activity was more intense in the past support the view that the Long Valley system was resupplied with heat from deep magmatic sources during its eruptive history.

INTRODUCTION

As part of an investigation of the thermal state of the Long Valley geothermal area, we have measured temperatures in 29 holes drilled to depths up to 30 m and in 7 deeper holes (up to 300 m) within the caldera (Figure 1). A limited number of thermal conductivity measurements were made to permit rough estimates of conductive heat flow, but the detailed measurements of thermal and hydrologic parameters needed to calculate local heat and mass flux were not undertaken. Our aim was to see if inexpensive near-surface measurements could be used to obtain useful information about the hydrothermal system at greater depth.

Geothermal areas are generally characterized by large and locally variable surficial thermal gradients and by various forms of hot spring activity indicating that heat is crossing the earth's surface at an anomalous rate. At some points beneath these areas, we can expect anomalously high temperatures which might represent exploitable concentrations of geothermal energy. Such concentrations are generally at depths of ½–3 km; deeper sources would be costly to exploit, and shallower ones have insufficient pressure to permit the high enthalpy desired. The process by which heat is transferred to the surface from these depths can be complex. The farther beneath the surface we extend our observations, the more we can expect to learn about the hydrothermal system associated with the potential resource, but the more costly and time consuming each observation becomes. Hence, it is of interest to examine the near-surface hydrothermal regime in a geothermal area in which more comprehensive studies are anticipated; inferences about conditions at greater depth eventually can be tested, and the role of shallow observations in geothermal exploration can be evaluated.

MEASUREMENTS OF TEMPERATURE

Temperature measurements, particularly in geothermal areas, can be sensitive to details of the construction of observation wells. Our measurements were made in two types of wells: (1) 'shallow holes' to a maximum depth of 30 m and (2) 'core holes' to a maximum depth of 300 m. Their locations are shown by the small and large dots, respectively, in Figure 1.

The shallow holes were drilled with a hollow stem auger rig and completed with 5-cm PVC pipe. In those wells where the depth to the water table was greater than about 3 m, a second 1.9-cm pipe was placed inside the 5-cm pipe and sealed at the bottom. It was filled with water and allowed to equilibrate to facilitate temperature measurement above the water table. The core holes were drilled to 14.3-cm diameter with hydraulic rotary equipment and completed with 3.2-cm black iron pipe that was sealed at the bottom. The annulus outside the 3.2-cm pipe was filled with cement to the surface to prevent vertical water circulation. Cores were obtained at selected intervals where feasible; their thermal conductivities were measured in the laboratory [*Sass et al.,* 1974].

Temperatures were measured repeatedly to millidegree precision with equipment described by *Sass et al.* [1971]. Representative values are shown in Figures 2, 3, 4, and 5 (for a preliminary compilation of the data, see *Sass et al.* [1974]). Five of the core holes were drilled at the sites of shallow holes, thereby permitting a comparison of effects of the two different types of hole construction on measured temperature. System-

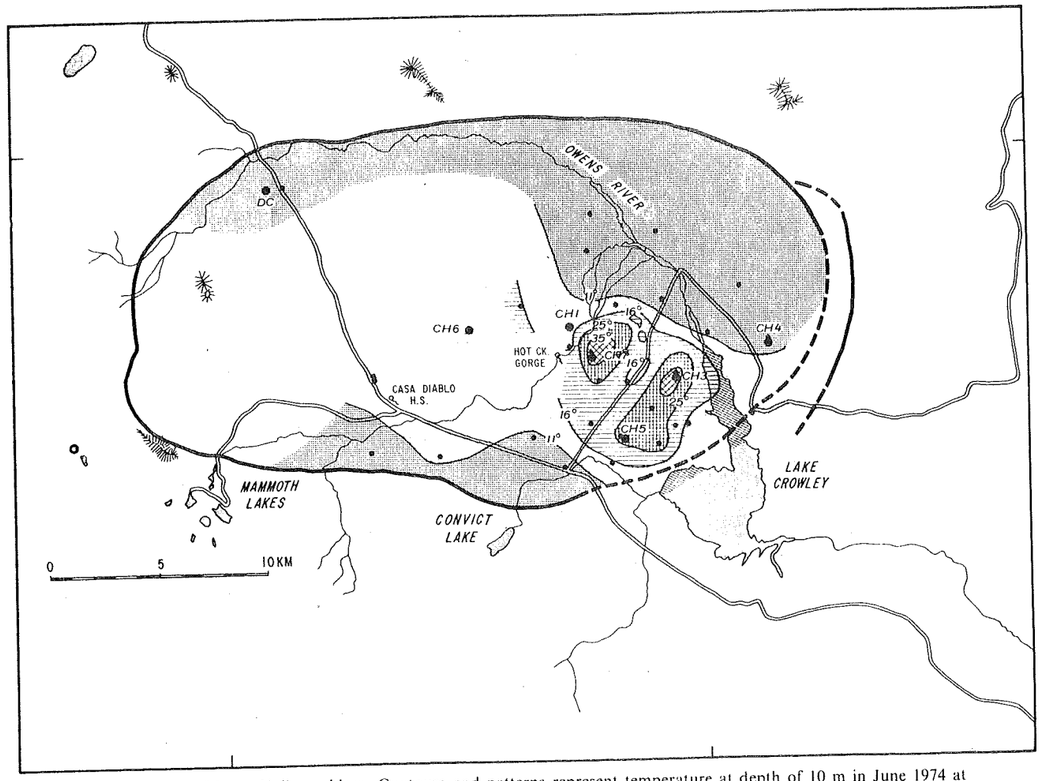

Fig. 1. Map of Long Valley caldera. Contours and patterns represent temperature at depth of 10 m in June 1974 at shallow hole locations indicated by small black circles. Large black circles indicate core hole locations.

atic differences were observed at all sites, but at only one of them, CH-3, were the differences large enough to affect the gross interpretation. At CH-3, temperatures above 45°C persist to within 3 m of the surface (Figure 4), whereas those in the adjacent shallow hole (LV-6) diverge from the core hole temperatures and fall rapidly in the upper 15 m. The difference is probably caused by relatively cool water leaking downward outside the pipe at LV-6 and then moving laterally into a permeable zone known to occur there. This disturbance would result in an underestimation of conductive flux to the surface by an order of magnitude. The vertical flow is blocked in CH-3 by cement in the annulus. In CH-1, slow upward water movement produced a systematic temperature disturbance in the upper 200 m until the annulus was cemented a year after completion. Subsequently, the disturbance decayed conductively; the equilibrium condition is represented by the data for CH-1 shown in Figure 5.

Temperature Patterns

We shall consider the shallower temperature observations first and then proceed to the deeper ones, investigating what types of information might be obtained from each. Figure 1 shows that temperatures in the shallow holes at a depth of 10 m can be contoured in a fairly simple way. We should like to know what this systematic pattern might mean in terms of the thermal regime at greater depths and whether the same information might have been obtained from temperature observations at smaller depths. Partial answers and a useful perspective are provided by the complete temperature profiles shown for two dates (June and October) in Figure 2*a*. (The individual curves can be identified with their respective hole locations from the compilation of *Lewis* [1974].) Figure 2*b* indicates the gradients that would be associated with steady conductive heat flows from 1 to 40 HFU (1 HFU = 10^{-6} cal/cm² s = 41.8 mW m^{-2}) for an assumed conductivity of 2 mcal/cm s °C (0.84 W/m °K).

With some notable exceptions (probably due to local water movements), the observed seasonal variation extends only to a depth of about 10 m (Figure 2*a*), roughly consistent with what we might anticipate from a simple model of conductive damping. At greater depth the profiles can be subdivided somewhat arbitrarily into three groups, denoted by the roman numerals in Figure 2*a* and illustrated by examples in Figure 3. In group I the steady gradients in the upper 30 m are small, generally representing heat flows less than 1 HFU. In group II, gradients lie typically in the range of 200°–400°C/km, representing conductive heat flows of about 4–8 HFU. In group III the gradients are generally larger, ranging to over 1000°C/km and representing conductive heat flows up to 50 HFU locally. The gradients in group III tend to be quite variable with depth, and although it is not obvious from the selected data in Figure 2*a*, they are also subject to more variation with time than gradients in the other groups. Figure 2*a* shows that these groups are distinguishable at the 10-m depth; in fact, the 11°C contour in Figure 1 separates groups I and II, and the 16°C contour separates groups II and III. As long as synoptic observations are used at these sites, essentially the same pattern emerges for contours at the 6-m depth, and much of it persists at 3 m. Hence at this locality, temperature observations at depths of a few meters contain some information on conditions to depths of a few tens of meters.

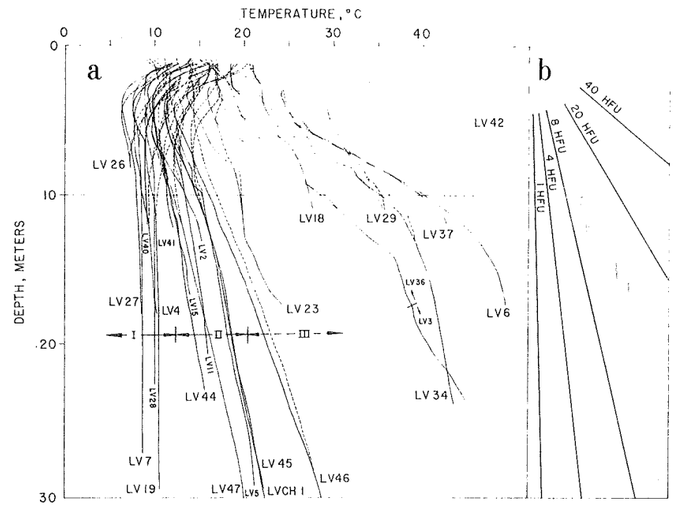

Fig. 2. (*a*) Temperatures to 30 m in Long Valley caldera in June 1974 (solid curves) and October 1974 (dashed curves). Roman numerals denote the three groups discussed in the text. Symbols (e.g., LV-34) are hole designations [see *Lewis*, 1974]. (*b*) Theoretical temperature profiles for steady conductive heat flows from 1 to 40 HFU (1 HFU = 10^{-6} cal/cm² s = 41.8 mW/m²). Assumed thermal conductivity is 2 mcal/cm s °C = 0.84 W/m °K.

What is the nature of this information? The general seasonal uniformity of temperatures below 10 m in group I suggests that the local heat transfer in the upper 30 m is predominantly by conduction. The vanishingly small gradients suggest that heat from greater depth is being absorbed by moving groundwater, a characteristic condition in or near zones of hydrologic recharge. Hence the peripheral part of the caldera, where 10-m temperatures are less than 11°C (Figure 1), may be an area of general recharge. The actual downward flow from the surface is probably localized; at least it does not generally occur near the holes in group I, or we should have seen seasonal temperature variation throughout their depth (Figure 2*a*). Similarly, we infer from the large and variable gradients that near-surface thermal conditions in group III are characteristic of areas of regional discharge in the sense that the groundwater beneath them is giving up heat as it moves generally to regions of lower ambient rock temperature. The magnitude and uniformity of gradients at group II sites suggest that they overlie regions less disturbed by water flow. The heat flows at group II sites are comparable to the hydrologically undisturbed value of about 4 HFU measured in granitic rock at site DP just beyond the western caldera rim (Figure 1; *Lachenbruch et al.* [1976]), although this agreement is probably fortuitous. Figures 1 and 6 show that the region in which the hot springs discharge is characterized by near-surface thermal regimes in groups II and III. Group II sites occur within 1 km of Casa Diablo Hot Springs and Hot Creek Gorge Springs, suggesting that the upflow is confined to local fracture systems.

The core hole observations expand our depth range another order of magnitude (Figure 5) and provide additional information on the meaning of the near-surface measurements. Two of the core holes, DC and CH-4, were drilled at opposite ends of the caldera (Figure 1) in the region in which the shallow hole profiles are in group I. They indicate that the low temperatures and small conductive heat flows persist at depth (Figure 5). A temperature minimum near the 100-m depth in DC implies that heat is being absorbed by lateral water flow there, but the small conductive heat flow (1.5 HFU) in the bottom of DC suggests that hydrologic heat sinks occur also at greater depth. Hence the fragmentary data from all holes taken collectively suggest that beneath the region around the periphery of the caldera delineated by 10-m temperatures less than 11°C (Fig-

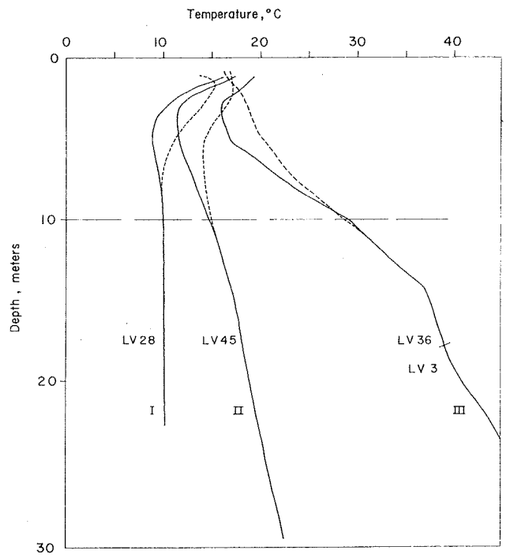

Fig. 3. Typical examples of the three groups indicated in Figure 2.

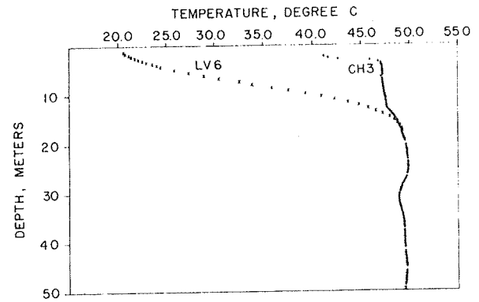

Fig. 4. Comparison of temperatures in LV-6 with uncemented annulus and CH-3 with cemented annulus. Holes are 20 m apart.

ure 1), heat is being absorbed by recharging groundwater to depths of at least 200 m or so.

Three of the core holes, CH-3, CH-5, and CH-7 (Figure 5), were drilled in the region in which shallow profiles were in group III. They show the influence of lateral and vertical circulation of hot water in permeable layers or fractures. As it liberates heat to the surrounding rock, the moving water causes high conductive heat flow above and sometimes gradient reversals below. Data from CH-5 suggest that water discharged at or near the surface in the hot springs is moving laterally in a shallow aquifer overriding colder recharge water, this suggestion being consistent with one by *Mariner and Willey* [1976]. One core hole, CH-6, was drilled in Little Antelope Valley, where no local shallow temperature information was previously available. The near-surface regime is in group III; the nearly isothermal part of the temperature profile below 165 m indicates that circulation of hot groundwater is influencing the thermal regime in the upper 200 m. It is clear from this group of results that deepening any of these holes by 50 or 100 m could lead to surprises and that downward extrapolation of near-surface temperatures is hazardous.

One of the core holes, CH-1, was drilled in a region in which the nearby shallow temperature was in group II, and it shows little or no effect of hydrothermal circulation. The change in gradient from about 250°C/km in the upper half to about 175°C/km in the lower half could be caused by a systematic variation in thermal conductivity or by very slight vertical water movements; the thermal conductivity sampling was insufficient to permit a distinction. (Limited conductivity data from CH-1 [*Sass et al.*, 1974] indicate a conductive heat flow of 3–5 HFU.) In any case, temperatures in CH-1 seem consistent with the speculation that regions in Figure 1 in which the 10-m temperature lies between 11°C and 16°C might be underlain by predominantly conductive regimes to depths of hundreds of meters.

DISCUSSION

Some tentative generalizations regarding the Long Valley geothermal system are suggested by combining the foregoing results with findings of related studies reported in this volume.

It has been pointed out that the present area of major hot spring discharge lies within the region in which the 10-m temperatures were above 11°C (Figure 6). This region includes areas (in group III) where thermal profiles in the upper 200 m are strongly influenced by lateral and vertical circulation of water at temperatures up to at least 110°C. It also includes areas (in group II) where the thermal regime is largely conductive with intermediate gradients to 30 m, and in at least one location (CH-1), to 300 m. The hot springs are probably fed by fractures, as they are located on or near the intracaldera extensions of the Hilton Creek fault (Figure 6) [*Bailey et al.*, 1976]. From chemical evidence it has been estimated that the reservoirs feeding these springs have a temperature of about 200°C [*Mariner and Willey*, 1976; *Sorey and Lewis*, 1976]. Even if we allow for an increase in conductivity with depth, this temperature would occur at a depth of about a kilometer or less according to extrapolation of group II gradients. Some justification for the extrapolation is provided by the fact that Casa

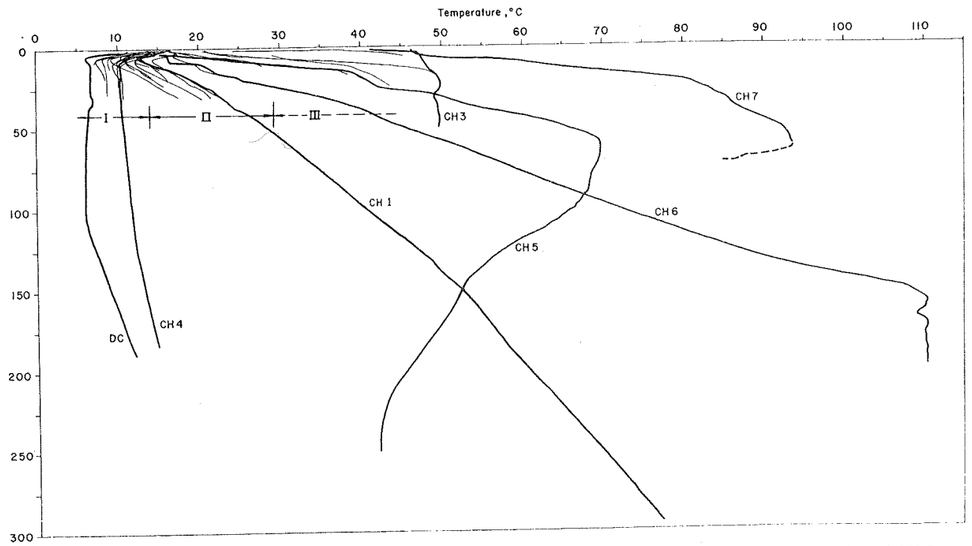

Fig. 5. Temperature profiles from the core holes (heavy lines) and shallow holes (light lines). Dashed portion of CH-7 represents approximate temperatures (±2°C) obtained before caving.

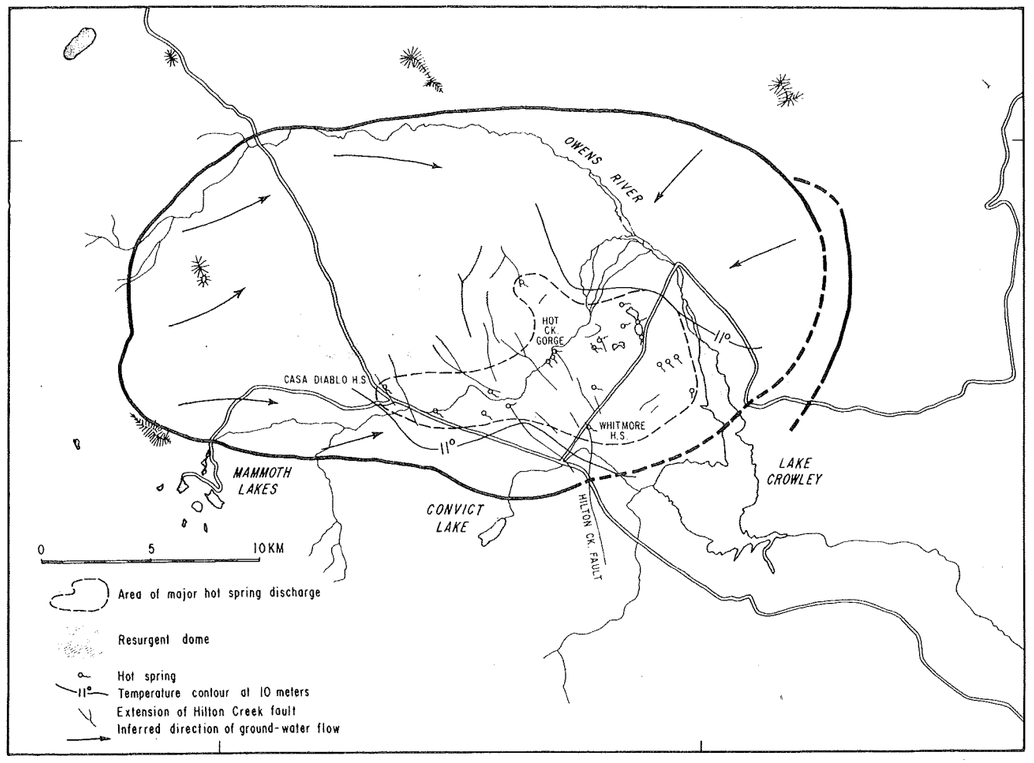

Fig. 6. Map of Long Valley caldera showing relations among groundwater flow, hot spring discharge, 10-m temperatures, and the resurgent dome (crosshatched).

Diablo Hot Springs and the Hot Creek Gorge Springs lie very close to shallow holes with regimes in group II (Figure 1), implying that flow in the conduits of the springs may produce only local perturbations to a predominantly conductive regime. However, the limited information in Figure 5 clearly indicates that many measurements to greater depths will be needed before the circulation beneath the hot springs can be delineated with confidence.

The topography indicates that surface drainage in the caldera is primarily from the Sierra Nevada Mountains in the west towards Lake Crowley in the east, interrupted locally by higher elevations on the resurgent dome. Limited data on water table elevations [*Lewis*, 1974] indicate that flow in the shallow groundwater system follows the topographic slope. Moreover, the supply of water available for recharge to the groundwater system is considerably larger in the mountains around the western and southern rims than around the eastern rim of the caldera. Thus it is reasonable to expect that the gross circulation of groundwater in the caldera is from west to east, towards the areas of hot spring discharge and Lake Crowley.

The limited information on ground temperatures indicates that cool recharge water occurs around the rim of the caldera to depths of at least 200 m. Isotopic data on concentrations of ^{18}O and D, as presented by *Mariner and Willey* [1976], suggest that water which emerges in the hot springs originated in the Sierra Nevada Mountains to the west; shallow groundwater from the peripheral regions evidently flows laterally towards the hot springs, mixing in varying proportions with the upflowing hot water. For this reason and the ones given in the previous paragraph we have indicated in Figure 6 that the direction of flow in the hydrothermal system is generally from west to east with discharge in the hot spring area in the southeastern part of the caldera. If this is so, the input of heat required to raise the temperature of the circulating meteoric water from approximately 10°C to temperatures above 200°C occurs at depth in the western half of the caldera.

The above inference is consistent with studies of heat flow and magmatic history, which suggest that the greatest heat at depth is likely to occur in the western part of Long Valley caldera [*Lachenbruch et al.*, 1976]; the magnitude of the mean conductive flux there is still unknown. From geochemical mixing models and measured spring discharges, *Sorey and Lewis* [1976] have estimated that water is presently removing heat at a rate greater than 10 HFU integrated throughout the entire caldera. A similar calculation by *White* [1965, p. 8] based on an estimate of the total boron discharged by the Long Valley thermal waters leads to an even larger value of about 16 HFU. The significance of such heat loss to the thermal budget of the heat source beneath Long Valley depends, of course, upon how long it has been going on at the measured rate.

If we assume that the heat removed by water flow comes ultimately from a magmatic source, it must be supplied to the surface by conduction and circulatory hydrothermal convection through the overlying roof rocks and possibly in addition by some direct contribution of magmatic fluids. A mean

flux of 10 HFU could be supplied by steady state conduction from a molten magma chamber through about 5 km of crystalline roof rocks (conductivity ~6 mcal/cm s °C). Circulatory hydrothermal convection would increase the required roof thickness by some fraction of the depth to which it was effective. If 15% of the hypothetical 200°C water contributing convective heat to the springs were supplied directly by magmatic fluids, less conductive flux would be required, and the estimate of roof thickness might be doubled [see, e.g., *White*, 1957]. However, if the magma underlies only half of the caldera [*Lachenbruch et al.*, 1976], the above estimate of roof thickness would be halved.

The time constant for propagation of a temperature disturbance by conduction through 5 km or so of roof rocks above a magma chamber is $\sim 10^6$ yr [see *Lachenbruch et al.*, 1976, Table 2]. Hydrothermal flow events of shorter duration could be removing heat stored at shallower depths. As an extreme example an additional 10 HFU could be supplied for 10,000 yr by convectively flushing the top 1 km of an otherwise conductive rock column; time would be insufficient for the gradient disturbance to propagate to the roof of a magma chamber a few kilometers below [see *Lachenbruch et al.*, 1976, curve I, Figure 10*a*]. Thus the present-day estimates of 10 HFU or greater need not constrain the depth to magma if they represented a flushing of the caldera by such short-term effects on flow as might be caused by post-Pleistocene deglaciation or new fracture openings from recent faulting. However, according to *Bailey et al.* [1976], hydrothermal activity in the caldera began at least 0.3 m.y. ago, and it was formerly much more extensive than it is today. As *White* [1968] has pointed out, heat loss associated with such prolonged activity would place large demands on a magmatic source; evidence for this activity supports the conclusion [*Lachenbruch et al.*, 1976] that the Long Valley system was resupplied with heat from deep magmatic sources throughout its eruptive history. This resupply could be achieved by any combination of (1) hydrothermal circulation in progressively deepening fractures, (2) convection in a magma chamber extending downward through the lower crust, or (3) repeated upper crustal intrusions.

Acknowledgments. We are grateful to Donald White, Alfred Truesdell, William Diment, Franklin Omsted, David Blackwell, Mary O'Neil, and Patrick Muffler for comments on the manuscript.

REFERENCES

Bailey, R. A., G. B. Dalrymple, and M. A. Lanphere, Volcanism, structure, and geochronology of Long Valley caldera, Mono County, California, *J. Geophys. Res., 81,* this issue, 1976.

Lewis, R. E., Data on wells, springs, and thermal springs in Long Valley, Mono County, California, open file report, 52 pp., U.S. Geol. Surv., Garden Grove, Calif., January 1974.

Lachenbruch, A. H., J. H. Sass, R. J. Munroe, and T. H. Moses, Jr., Geothermal setting and simple heat conduction models for Long Valley caldera, *J. Geophys. Res., 81,* this issue, 1976.

Mariner, R. H., and L. M. Willey, Geochemistry of thermal waters in Long Valley, Mono County, California, *J. Geophys. Res., 81,* this issue, 1976.

Sass, J. H., A. H. Lachenbruch, R. J. Munroe, G. W. Greene, and T. H. Moses, Jr., Heat flow in the western United States, *J. Geophys. Res., 76,* 6376–6413, 1971.

Sass, J. H., A. H. Lachenbruch, and R. J. Munroe, Thermal data from heat flow test wells near Long Valley, California, open file report, 43 pp., U.S. Geol. Surv., Menlo Park, Calif., 1974.

Sorey, M. L., and R. E. Lewis, Convective heat flow from hot springs in the Long Valley caldera, Mono County, California, *J. Geophys. Res., 81,* this issue, 1976.

White, D. E., Thermal waters of volcanic origin, *Geol. Soc. Amer. Bull., 68,* 1637–1658, 1957.

White, D. E., Geothermal energy, *U.S. Geol. Sur. Circ., 519,* 17 pp., 1965.

White, D. E., Hydrology, activity, and heat flow of the Steamboat Springs thermal system, Washoe County, Nevada, *U.S. Geol. Surv. Prof. Pap. 458-C,* 109 pp., 1968.

(Received February 28, 1975;
revised September 15, 1975;
accepted September 15, 1975.)

Geothermal Setting and Simple Heat Conduction Models for the Long Valley Caldera

ARTHUR H. LACHENBRUCH, J. H. SASS, ROBERT J. MUNROE, AND T. H. MOSES, JR.

U.S. Geological Survey, Menlo Park, California 94025

Heat flow and heat production measurements have been made in the vicinity of Long Valley from 0–30 km from the rim of the caldera and up to 30 km on either side of the boundary of the Basin and Range province at the eastern scarp of the Sierra Nevada. The search for a thermal anomaly associated with magma is complicated by the location of the caldera at the boundary between these two provinces with strongly contrasting regional heat flows and by unknown effects of hydrothermal circulation. The data show no conspicuous effect of the province transition, possibly a small local heat flow anomaly near the east rim of the caldera, and a very substantial anomaly near the west rim. Simple heat conduction models suggest that Long Valley caldera is the surface expression of a deep magmatic system; an upper crustal magma chamber could not have sustained molten material throughout the 2-m.y. eruptive history unless it were resupplied with heat from deep crustal or subcrustal magmatic sources. If the heat were supplied by crustal intrusion of mantle basalt, the crust would thicken rapidly unless magmatic activity were accompanied by accelerated local crustal spreading. To generate a viable silicic magma chamber by sill injection in the upper 5–8 km of crust, minimum intrusion rates of the order of 1 m per century are probably required. Thermal models for the near-normal heat flow at the east rim suggest that magma beneath the eastern part of Long Valley caldera might have been exhausted during eruption of the Bishop Tuff 0.7 m.y. ago and that the resurgent dome, which subsequently formed in the west central caldera, marks the location of a residual chamber more circular in plan. High heat flow indicated by the single measurement near the west rim can be attributed to a simple shallow magma chamber beneath the western caldera or to recent local magmatism along the Sierra frontal fault system. Additional heat flow and hydrologic measurements are necessary for a confident interpretation of the thermal history and the present state of the caldera region.

INTRODUCTION

As part of an investigation of the Long Valley region we have measured heat flow in 11 holes drilled to depths of 150–300 m in terrain surrounding the caldera (Figures 1 and 2). Our aim was to investigate any detectable effects that magmatic events associated with the caldera might have had on the conductive thermal regime of the surroundings. Because of the long time required for a thermal disturbance to equilibrate by conduction in earth materials, measurements of heat flow, unlike other geophysical measurements, can contain direct information on past geologic events. However, with the introduction of the time variable, the inverse problem of reconstructing the cause from an observation of its effects takes on an added dimension of ambiguity. Near hot spring areas a further complication in the interpretation of heat flow measurements is the uncertainty of the role played by hydrothermal convection. Indeed, the large estimates of sustained heat discharge from hot springs in Long Valley caldera and similar volcanic regions [*White*, 1965; *Sorey and Lewis*, 1976] indicate either that the magmatic source must be very close to the surface or, more reasonably, that convective transport must dominate conduction to considerable depth beneath these regions [*Lachenbruch et al.*, 1976]. Nevertheless, if heat is transferred primarily by conduction in the crystalline rocks surrounding Long Valley caldera, it should be possible to confirm this with internally consistent heat flow measurements beyond the caldera rim. Analysis of these measurements could, in principle, provide limiting information on the distribution, history, and present state of magmatic sources that might extend to the edge of the caldera or beyond. In any case, if we neglect heat transfer by hydrothermal convection, useful limits can be calculated for the time required for any hypothetical magma source to cool. Simple conduction models are used in this paper to make approximate calculations of these kinds (i.e., of present state and maximum cooling time). Analytical results are presented in a general graphical form somewhat more complete than is warranted for interpretation of our preliminary measurements near Long Valley; the problems are general, and it is expected that the results might be useful for similar calculations applicable elsewhere.

The new thermal data are summarized in Table 1; they were obtained by procedures described by *Sass et al.* [1971*a*, *b*]. The heat production (A_0) was measured by our colleague Carl Bunker, using the methods of *Bunker and Bush* [1966, 1967]. The heat flows (q) are based on linear least squares temperature gradients (Γ) over the specified depth intervals, corrected (to Γ_c) where appropriate for the effects of topography, uplift, erosion, and glaciation, and multiplied by harmonic mean thermal conductivities ($\langle K \rangle$). Inasmuch as a significant fraction of the data is based on temperature profiles acquired shortly after the access pipe was grouted in, we have omitted the customary formal statistical estimates of scatter from the least squares mean gradients and consequently from estimates of mean thermal conductivity, heat flow, and radiogenic heat production (A_0). Adjustments to these preliminary values based on equilibrium temperature gradients and an increased number of conductivity and heat production measurements are anticipated. The units of heat flow (HFU), units of heat production (HGU), and units of thermal conductivity (CU) are defined in Table 1.

The latest temperature measurements from each of the new holes is shown in Figure 3*a*. In Figure 3*b*, profiles from the 10 holes in granitic rock are plotted in such a way that the portions used to determine heat flow extrapolate to a common origin at the surface.

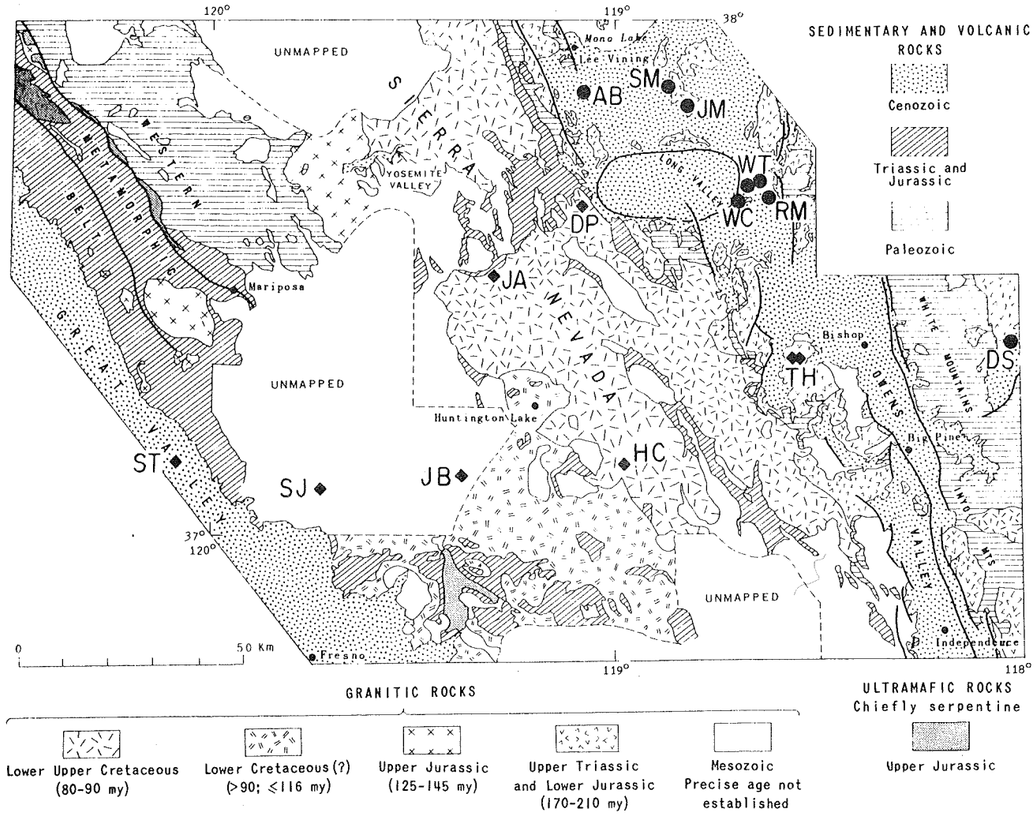

Fig. 1. Geologic sketch map [after *Bateman and Eaton,* 1967] showing outline of the Long Valley caldera and locations of heat flow stations. Square symbols are identified with the Sierra Nevada physiographic province; circles, with the Basin and Range province. (Results from ST, SJ, JB, HC, and DS have been published previously.)

Thermal Setting of Long Valley

As explained by *Bailey et al.* [1976], the Long Valley caldera lies nearly astride a major fault system that separates the tectonically active Basin and Range province to the east from the relatively stable Sierra Nevada tectonic province to the west. The Basin and Range province is characterized by extensive Cenozoic normal faulting and volcanism, high seismicity, a thin crust, and a low upper mantle seismic velocity; none of these characteristics obtain in the Sierra Nevada [*Thompson and Burke,* 1974; *Bateman and Eaton,* 1967; *Pakiser and Robinson,* 1966]. Consistent with these tectonic indicators, the contrast in regional heat flow across this boundary is one of the most abrupt known on the North American continent [*Roy et al.*, 1968, 1972; *Sass et al.*, 1971*a*]. While this location makes Long Valley an interesting subject for study, the transition zone compounds the problem of establishing the regional heat flow upon which any local anomaly might be superimposed.

The problem of establishing the background heat flow is simplified somewhat by the observation that heat flow q from granitic rocks in each province generally depends to a first approximation on the radiogenic heat production A_0 of the rock locally exposed at the surface according to the following relation [*Birch et al.*, 1968; see also *Roy et al.*, 1968; *Lachenbruch,* 1968*a*].

$$q = q^* + DA_0 \qquad (1)$$

The parameters (q^*, D) have the respective dimensions of heat flow and depth, and they may be viewed as uniform throughout each province (although the relation is much less certain for the Basin and Range [*Roy et al.*, 1968, 1972; *Blackwell*, 1971]). For the Sierra Nevada the values are 0.4 HFU and 10 km, and for the Basin and Range they are 1.4 HFU, 10 km. The second term in (1) is equivalent to the steady heat flux that would be produced by a uniform 10-km slab of the rock currently exposed locally at the surface [*Roy et al.*, 1968]. It is determined by multiplying by 10 km the heat production (per cubic kilometer) determined by a laboratory measurement on core or surface samples. The expected heat flow is then determined by adding 0.4 HFU (q^*, equation (1)) if the station is in the Sierra Nevada or 1.4 HFU if it is in the Basin and Range province. Hence this unexpected relation implies that the rock exposed locally at the surface contains information on the heat flow and thermal regime of the entire crust.

It seems unlikely that granites of greatly varying age in a given province would all have the same thickness D (in these cases, 10 km). It has been shown, however, that (1) will not be affected by differential erosion in any province if (and only if) the neat production, instead of being uniform to depth D, varies with depth z according to $A_0 e^{-z/D}$ [*Lachenbruch*, 1968*a*,

Geothermal Setting and Simple Heat Conduction Models for the Long Valley Caldera

ARTHUR H. LACHENBRUCH, J. H. SASS, ROBERT J. MUNROE, AND T. H. MOSES, JR.

U.S. Geological Survey, Menlo Park, California 94025

Heat flow and heat production measurements have been made in the vicinity of Long Valley from 0–30 km from the rim of the caldera and up to 30 km on either side of the boundary of the Basin and Range province at the eastern scarp of the Sierra Nevada. The search for a thermal anomaly associated with magma is complicated by the location of the caldera at the boundary between these two provinces with strongly contrasting regional heat flows and by unknown effects of hydrothermal circulation. The data show no conspicuous effect of the province transition, possibly a small local heat flow anomaly near the east rim of the caldera, and a very substantial anomaly near the west rim. Simple heat conduction models suggest that Long Valley caldera is the surface expression of a deep magmatic system; an upper crustal magma chamber could not have sustained molten material throughout the 2-m.y. eruptive history unless it were resupplied with heat from deep crustal or subcrustal magmatic sources. If the heat were supplied by crustal intrusion of mantle basalt, the crust would thicken rapidly unless magmatic activity were accompanied by accelerated local crustal spreading. To generate a viable silicic magma chamber by sill injection in the upper 5–8 km of crust, minimum intrusion rates of the order of 1 m per century are probably required. Thermal models for the near-normal heat flow at the east rim suggest that magma beneath the eastern part of Long Valley caldera might have been exhausted during eruption of the Bishop Tuff 0.7 m.y. ago and that the resurgent dome, which subsequently formed in the west central caldera, marks the location of a residual chamber more circular in plan. High heat flow indicated by the single measurement near the west rim can be attributed to a simple shallow magma chamber beneath the western caldera or to recent local magmatism along the Sierra frontal fault system. Additional heat flow and hydrologic measurements are necessary for a confident interpretation of the thermal history and the present state of the caldera region.

Introduction

As part of an investigation of the Long Valley region we have measured heat flow in 11 holes drilled to depths of 150–300 m in terrain surrounding the caldera (Figures 1 and 2). Our aim was to investigate any detectable effects that magmatic events associated with the caldera might have had on the conductive thermal regime of the surroundings. Because of the long time required for a thermal disturbance to equilibrate by conduction in earth materials, measurements of heat flow, unlike other geophysical measurements, can contain direct information on past geologic events. However, with the introduction of the time variable, the inverse problem of reconstructing the cause from an observation of its effects takes on an added dimension of ambiguity. Near hot spring areas a further complication in the interpretation of heat flow measurements is the uncertainty of the role played by hydrothermal convection. Indeed, the large estimates of sustained heat discharge from hot springs in Long Valley caldera and similar volcanic regions [*White*, 1965; *Sorey and Lewis*, 1976] indicate either that the magmatic source must be very close to the surface or, more reasonably, that convective transport must dominate conduction to considerable depth beneath these regions [*Lachenbruch et al.,* 1976]. Nevertheless, if heat is transferred primarily by conduction in the crystalline rocks surrounding Long Valley caldera, it should be possible to confirm this with internally consistent heat flow measurements beyond the caldera rim. Analysis of these measurements could, in principle, provide limiting information on the distribution, history, and present state of magmatic sources that might extend to the edge of the caldera or beyond. In any case, if we neglect heat transfer by hydrothermal convection, useful limits can be calculated for the time required for any hypothetical magma source to cool. Simple conduction models are used in this paper to make approximate calculations of these kinds (i.e., of present state and maximum cooling time). Analytical results are presented in a general graphical form somewhat more complete than is warranted for interpretation of our preliminary measurements near Long Valley; the problems are general, and it is expected that the results might be useful for similar calculations applicable elsewhere.

The new thermal data are summarized in Table 1; they were obtained by procedures described by *Sass et al.* [1971*a, b*]. The heat production (A_0) was measured by our colleague Carl Bunker, using the methods of *Bunker and Bush* [1966, 1967]. The heat flows (q) are based on linear least squares temperature gradients (Γ) over the specified depth intervals, corrected (to Γ_c) where appropriate for the effects of topography, uplift, erosion, and glaciation, and multiplied by harmonic mean thermal conductivities ($\langle K \rangle$). Inasmuch as a significant fraction of the data is based on temperature profiles acquired shortly after the access pipe was grouted in, we have omitted the customary formal statistical estimates of scatter from the least squares mean gradients and consequently from estimates of mean thermal conductivity, heat flow, and radiogenic heat production (A_0). Adjustments to these preliminary values based on equilibrium temperature gradients and an increased number of conductivity and heat production measurements are anticipated. The units of heat flow (HFU), units of heat production (HGU), and units of thermal conductivity (CU) are defined in Table 1.

The latest temperature measurements from each of the new holes is shown in Figure 3*a*. In Figure 3*b*, profiles from the 10 holes in granitic rock are plotted in such a way that the portions used to determine heat flow extrapolate to a common origin at the surface.

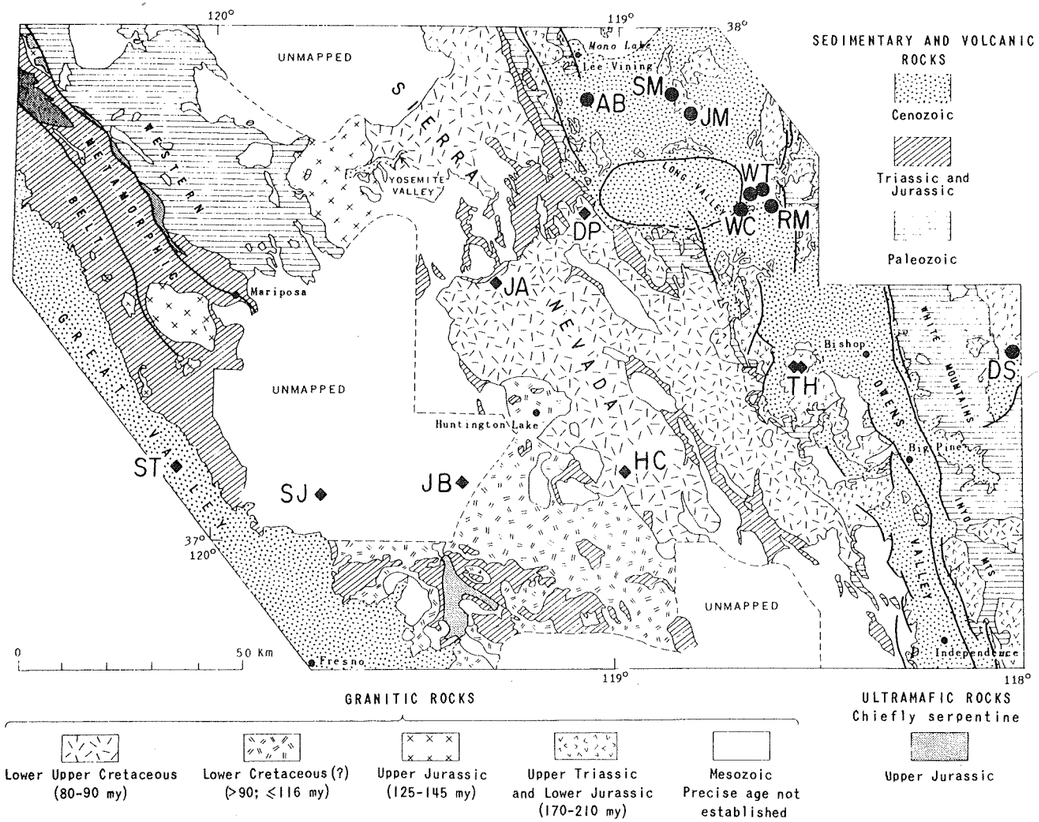

Fig. 1. Geologic sketch map [after *Bateman and Eaton,* 1967] showing outline of the Long Valley caldera and locations of heat flow stations. Square symbols are identified with the Sierra Nevada physiographic province; circles, with the Basin and Range province. (Results from ST, SJ, JB, HC, and DS have been published previously.)

THERMAL SETTING OF LONG VALLEY

As explained by *Bailey et al.* [1976], the Long Valley caldera lies nearly astride a major fault system that separates the tectonically active Basin and Range province to the east from the relatively stable Sierra Nevada tectonic province to the west. The Basin and Range province is characterized by extensive Cenozoic normal faulting and volcanism, high seismicity, a thin crust, and a low upper mantle seismic velocity; none of these characteristics obtain in the Sierra Nevada [*Thompson and Burke,* 1974; *Bateman and Eaton,* 1967; *Pakiser and Robinson,* 1966]. Consistent with these tectonic indicators, the contrast in regional heat flow across this boundary is one of the most abrupt known on the North American continent [*Roy et al.*, 1968, 1972; *Sass et al.*, 1971*a*]. While this location makes Long Valley an interesting subject for study, the transition zone compounds the problem of establishing the regional heat flow upon which any local anomaly might be superimposed.

The problem of establishing the background heat flow is simplified somewhat by the observation that heat flow q from granitic rocks in each province generally depends to a first approximation on the radiogenic heat production A_0 of the rock locally exposed at the surface according to the following relation [*Birch et al.*, 1968; see also *Roy et al.*, 1968; *Lachenbruch,* 1968*a*].

$$q = q^* + DA_0 \qquad (1)$$

The parameters (q^*, D) have the respective dimensions of heat flow and depth, and they may be viewed as uniform throughout each province (although the relation is much less certain for the Basin and Range [*Roy et al.*, 1968, 1972; *Blackwell,* 1971]). For the Sierra Nevada the values are 0.4 HFU and 10 km, and for the Basin and Range they are 1.4 HFU, 10 km. The second term in (1) is equivalent to the steady heat flux that would be produced by a uniform 10-km slab of the rock currently exposed locally at the surface [*Roy et al.*, 1968]. It is determined by multiplying by 10 km the heat production (per cubic kilometer) determined by a laboratory measurement on core or surface samples. The expected heat flow is then determined by adding 0.4 HFU (q^*, equation (1)) if the station is in the Sierra Nevada or 1.4 HFU if it is in the Basin and Range province. Hence this unexpected relation implies that the rock exposed locally at the surface contains information on the heat flow and thermal regime of the entire crust.

It seems unlikely that granites of greatly varying age in a given province would all have the same thickness D (in these cases, 10 km). It has been shown, however, that (1) will not be affected by differential erosion in any province if (and only if) the neat production, instead of being uniform to depth D, varies with depth z according to $A_0 e^{-z/D}$ [*Lachenbruch*, 1968*a*,

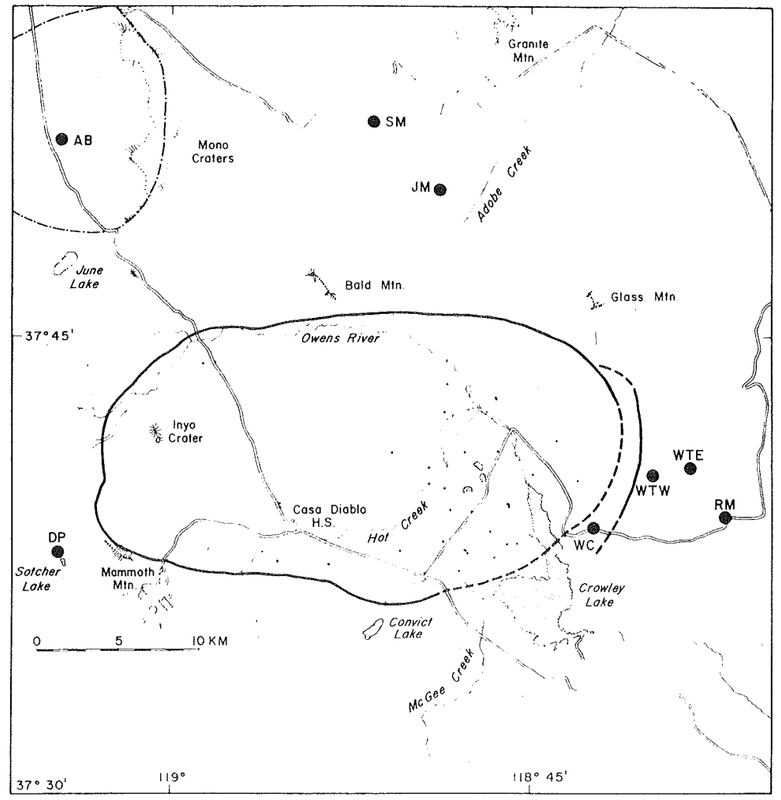

Fig. 2. Sketch showing the location of close-in heat flow stations relative to the caldera rim and other major physiographic features. Chain-dotted line at upper left outlines the ring fracture zone of *Kistler* [1966]. The small dots inside the caldera show the locations of heat flow and hydrological data discussed by *Lachenbruch et al.* [1976].

1970]. With this interpretation, q^* is most naturally identified as the contribution from the mantle. A knowledge of the province parameters (q^*, D) and an assumption of conductivity then lead to a complete crustal temperature profile from a knowledge of surface heat flow or heat production. Such profiles are shown in Figure 4 for the Sierra Nevada and the Basin and Range for the extremes of heat production normally found in plutonic rocks (0–10 HGU) and for

TABLE 1. Summary of Preliminary Geothermal Data Near Long Valley, California

Site	Elevation, m	Depth Range, m	Γ, °C/km	Γ_c, °C/km	⟨K⟩, CU	q, HFU	A_0, HGU	Q_S,* HFU	Q_{BR},† HFU	Distance Beyond Rim, km
Jackass Creek (JA)	2100	60–190	17.7	18.7	7.26	1.36	9.6	0	(−1.0)	28 (SW)
Devils Postpile (DP)	2316	150–250	56.8	51.4	7.30	3.75	6.0	2.75	(1.75)	3 (WSW)
Tungsten Hills (THE)	1737	160–189	15.1	14.7	6.35	0.93	3.1	0.2	(−0.8)	30 (S)
Tungsten Hills (THW)	1760	100–138	15.1	14.4	8.8	1.27	6.8	0.2	(−0.8)	30 (S)
Aeolian Buttes (AB)	2240	25–124	31.2	31.2	6.98	2.18	8.7	(0.9)	−0.1	13 (NNW)
Watterson Canyon (WC)	2133	110–140	30.0	30	7.44	2.23	4.2	(1.4)	0.4	0 (SE rim)
Watterson Trough (WTW)‡	2316	50–113	78.1	78.1	2.7	2.1				1 (E)
Watterson Trough (WTE)	2393	90–128	23.0	25.0	6.70	1.68	4.4	(0.8)	−0.2	3 (E)
Round Mountain (RM)	2225	125–209	24.3	24.0	7.91	1.90	7.7	(0.7)	−0.3	6 (E)
Johnny Meadow (JM)	2637	100–168	6.08	6.1	6.75	0.41	6.4	(−0.6)	−1.6	6 (N)
Sagehen Meadow (SM)	2560	150–271	9.20	9.3	7.79	0.72	9.3	(−0.6)	−1.6	11 (N)

1 conductivity unit (CU) = 1 mcal cm^{-1} s^{-1} °C^{-1} = 0.418 W m^{-1} °K^{-1}; 1 heat flow unit (HFU) = 1 μcal cm^{-2} s^{-1} = 41.8 mW m^{-2}; 1 heat generation unit (HGU) = 10^{-13} cal cm^{-3} s^{-1} = 0.418 μW m^{-3}.

* Q_S is heat flow anomaly relative to the Sierra Nevada norm. Values in parentheses are for sites in the Basin and Range physiographic province.

† Q_{BR} is heat flow anomaly relative to the Basin and Range norm. Values in parentheses are for sites in the Sierra Nevada physiographic province.

‡ Drilled in rhyolitic tuff; all other holes were drilled in granitic rocks.

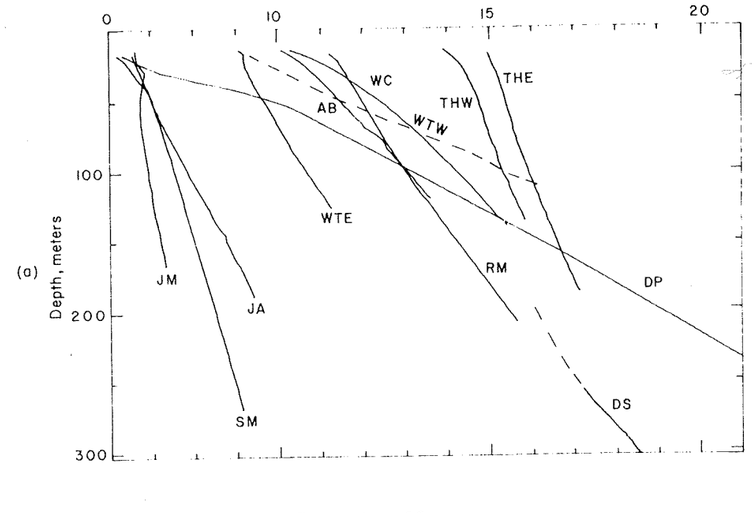

Fig. 3. Temperature profiles from holes near Long Valley: (*a*) all profiles and (*b*) profiles from holes in granite with their extrapolated surface temperatures adjusted to a common origin.

assumed conductivities believed reasonable for each province. For the same surface heat production, heat flow will generally be greater by 1 HFU at sites in the Basin and Range. For the same surface heat flow (e.g., 1.4 HFU, Figure 4) crustal temperatures are much higher in the Basin and Range because a larger proportion of the heat originates at great depth there.

In Figure 5, measured values of (q, A_0) are plotted for each of the stations in granitic rock shown in Figure 1. The straight lines represent relation (1) with the appropriate slope and intercept parameters (D and q^*) for each province. These parameters were determined previously from published observations of q and A_0 at many locations in each province [*Roy et al.*, 1968; *Lachenbruch*, 1968*a*; *Sass et al.*, 1971*a*], only five of which (Sherman Thomas (ST), San Joaquin (SJ), Jose Basin (JB), Helms Creek (HC), and Deep Springs (DS)) occur in the map area of Figure 1. The stations represented by squares in Figures 1 and 5 lie southwest of the physiographic boundary between the Sierra Nevada and the Basin and Range; those represented by circles lie northeast of it. This assignment to province is unambiguous at all stations except perhaps at the two sites at Tungsten Hills (THE and THW). Table 1 lists the 11 new sites, roughly in order of increasing distance from the physiographic boundary, distance within the Sierra Nevada province being considered negative.

The departure of the circles and squares in Figure 5 from their respective province norms (the straight lines) can be viewed as the measure of a local heat flow anomaly. The anomaly may reflect several contributing causes, some perhaps of opposite sign. First, the data from the Basin and Range generally show considerable local scatter about their curve; the five upper circles in Figure 5 are not atypical. Second, many of the points lie close to the boundary of the two provinces,

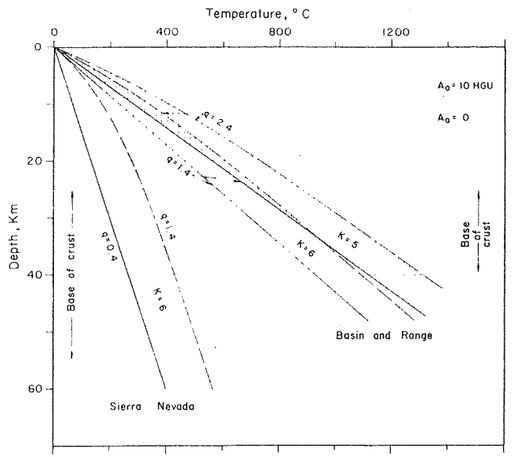

Fig. 4. Theoretical steady state crustal temperature profiles based on the exponential source model and the heat flow–heat production relationship inferred for the Sierra Nevada and Basin and Range heat flow provinces [*Lachenbruch*, 1970]. Horizontal screen represents an assumed thermal conductivity of 6 CU, vertical screen represents 5 CU. A_0 and q represent surface heat production in heat generation units and surface heat flow in heat flow units, respectively. (For definitions of units, see Table 1.)

where the deep crustal heat flow (q^*) must change by a factor of 3 or more. As this change must be transitional in some degree, we should expect such points normally to lie between the two province curves. Third, very slight systematic movements of groundwater can cause substantial anomalies (positive or negative) in the conductive heat flow. Where the upper crust contains local anomalous sources of heat, such circulation is more likely to be important. Finally, most of the points in Figure 5 are based on preliminary data, and their plotted positions may be revised when additional measurements are made. With these qualifications it is still rather surprising that with the exception of Johnny Meadow (JM), Sagehen Meadow (SM), and Devils Postpile (DP), Figure 5 does not show conspicuous anomalies. In Table 1 the anomalies relative to the Sierra and Basin and Range norms are tabulated, respectively, under Q_S and Q_{BR}.

It is not surprising that ST, SJ, JB, and HC lie on the Sierra curve because they were among the previously published points used to define it [*Roy et al.*, 1968; *Lachenbruch*, 1968*a*]. It is surprising that THE and THW, which lie almost on the physiographic boundary, do not show a stronger effect of the transition. However, they are based upon incomplete conductivity and heat production data. The new site at Jackass Creek (JA) in the central Sierra Nevada lies precisely on the previously established Sierra curve. This observation not only provides important confirmation for (1), but it also establishes that at this site, 28 km southwest of Long Valley caldera, there are no detectable thermal effects of the Long Valley igneous activity, the basaltic volcanism that preceded it by 2 or 3 m.y., or any transition to the Basin and Range thermal regime. The Sierra point, DP, at Devils Postpile (Figures 1 and 2) 25 km northwest of JA and 3 km from the caldera rim, shows a very conspicuous anomaly, as it lies 2.75 HFU above the Sierra curve (Figures 3 and 5; Table 1). The conductive heat flow at DP is well determined in homogeneous competent rock by a smooth and uniform gradient (Figure 6). The slight curvature in the upper half of the profile in quartz monzonite at this important site can be accounted for by local topography.

We have mentioned that the departure of the five upper circles (Figure 5) from the Basin and Range line is not atypical for the province. This group includes sites whose distance from the caldera varies from ~0 at Watterson Canyon (WC) to 70 km at DS and whose distance from the physiographic boundary varies from less than 10 km at Aeolian Buttes (AB) to 35 or 40 km at DS. Thus there is no compelling evidence to suggest that the circles a bit below the Basin and Range line are transitional because of their proximity to the province boundary. The fact that the highest heat flow (2.2 HFU) in the Basin and Range group occurs at the site (WC) on the eastern caldera rim seems to suggest that a small local conductive anomaly might occur there. The value of 2.1 HFU in nearby tuff at Watterson Trough (WTW) (Table 1), though uncertain, lends a little support to that view. However, at these locations near the rim, effects of thermal refraction could easily account for local variations of a few tenths of a HFU [see, e.g., *Lachenbruch*, 1968*b*, p. 399]; corrections for them are not warranted because of the other sources of uncertainty. The two very low heat flows at SM and JM are puzzling and evidently reflect hydrologic effects. Our inability to account for them at this time serves as a reminder of the uncertainty in these results.

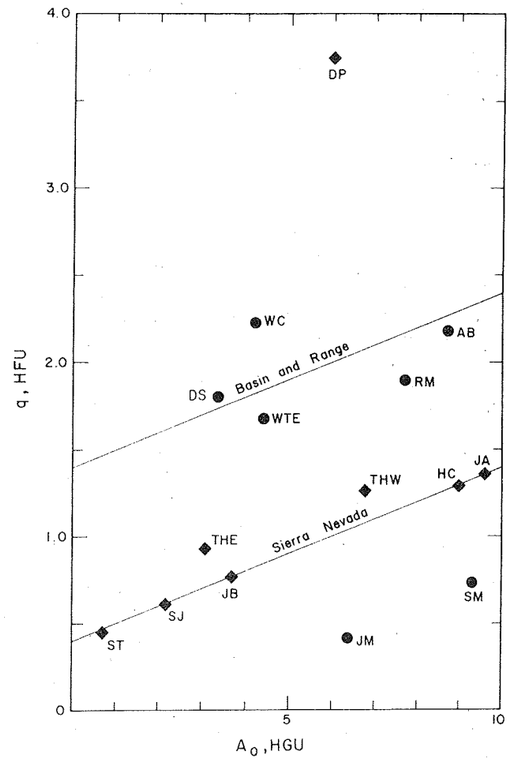

Fig. 5. Heat flow versus heat production for granitic rocks in the region surrounding Long Valley. Square symbols are identified with the Sierra Nevada physiographic province; circles, with the Basin and Range province. The straight lines represent previously determined relationships (equation (1)) for the two provinces [*Roy et al.*, 1968; *Lachenbruch*, 1968*a*].

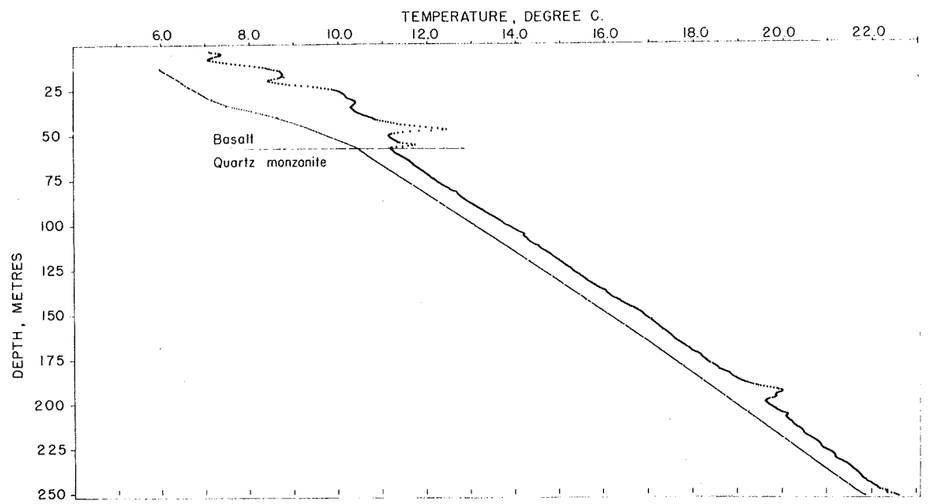

Fig. 6. Temperature profiles from DP. The upper profile (showing thermal effects of cementing) was obtained a day after completion of the hole; the lower profile, 9 months later.

In summary, the preliminary thermal data show no conspicuous effect of the province transition, possibly a very small local conductive anomaly at the east rim of Long Valley caldera, and a very substantial one a few kilometers beyond the west rim. Recognizing that these generalizations are tentative, in the next section we shall attempt to analyze some of their implications with the aid of geologic information relating to the history of the caldera.

Implications for the Magmatic History of Long Valley Caldera

Some relevant geologic information. According to *Bailey et al.* [1976], Long Valley caldera resulted from the collapse of the roof of a magma chamber during the explosive eruption of a layer of partially crystallized magma (the Bishop Tuff) perhaps 2 km thick about 0.7 m.y. ago. The Long Valley magma chamber is thought to be more or less congruent in plan with the caldera structure, an ellipse with axes of about 20 and 30 km. The oldest evidence for the existence of the Long Valley magma chamber is Glass Mountain on the northeast rim of the present caldera; silicic volcanism began there almost 2 m.y. ago and continued intermittently up to the time of collapse. Shortly after the collapse a resurgent dome formed in the west central part of the caldera, and silicic and intermediate volcanic material has been discharging in and around it virtually up to the present time. The most recent activity has been concentrated near the western rim along the Sierra Nevada frontal fault system, and little or no material has been discharged in the eastern half of the caldera during the past 0.3 m.y. Basaltic volcanism in the vicinity of Long Valley predated caldera formation by as much as 3 m.y. or so, and recent basaltic volcanism along the Sierra frontal faults is evidently almost contemporaneous with the most recent silicic extrusion from the Long Valley system. Largely on the basis of mechanical arguments relating to collapse and resurgence [*Bailey et al.*, 1976; *Smith and Bailey*, 1968], the roof above the magma chamber is estimated to have been about 5 km thick. On the basis of geochemical arguments the magmatic temperature was probably about 800°C [*Hildreth and Spera*, 1974; R. L. Christiansen, personal communication, 1974].

Given this information and the preliminary heat flow results outlined above, we should like to know whether it is possible to place any useful constraints on the history of the hypothetical chamber and its present state from theoretical considerations. The problem of thermal effects of igneous intrusion is extremely complex, involving conductive and convective transport of heat in inhomogeneous geometrically complicated systems little known in detail. It is the subject of several extensive discussions [e.g., *Lovering*, 1935; *Shaw*, 1965; *Jaeger*, 1964; *Simmons*, 1967*b*] which we make no attempt to review in this preliminary study. The related problem of hydrothermal convection beneath hot springs, largely neglected in this discussion, is also the subject of an extensive literature. We consider only some simple limiting heat conduction models, most of which are well known, in an attempt to investigate the consistency of the geologic and geothermal observations and inferences to date.

Some simple conduction models. The time progression of temperature for three simple one-dimensional models of a magmatic heat source is shown schematically in Figure 7. In these models the magma chamber is a slab extending infinitely in the horizontal directions, and a represents the depth of its roof beneath the surface. In model I the magma raises the temperature of its roof Θ_0 degrees above its surroundings at time $t = 0$, and it maintains this condition thereafter ($t > 0$), as might be expected in an idealized convecting chamber. Model II is the instantaneous source model wherein magma of thickness Δ is assumed to move instantaneously into place at time $t = 0$ at a temperature Θ_0 above its surroundings; thereafter the magma stagnates and loses its heat by conduction from its upper and lower boundaries. In model III, heat is liberated at a constant rate Q_0 cal/cm² s starting at time $t = 0$ on the plane $z = a$, which represents the chamber roof. The physical significance of model III will be discussed below.

We define Q_0 as follows:

$$Q_0 = K(\Theta_0/a) \tag{2}$$

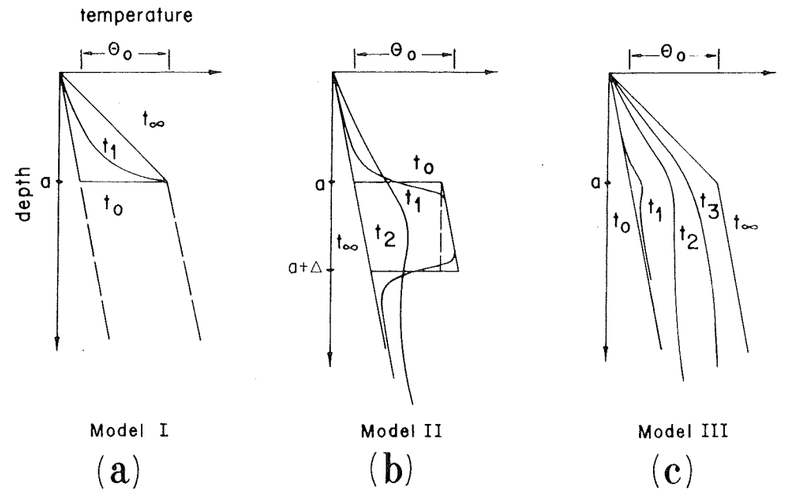

Fig. 7. Schematic representation of the time progression of temperature from the initial condition (t_0) to the steady state condition (t_∞) for three one-dimensional conduction models of a magmatic heat source (see text).

where K is thermal conductivity, assumed to be uniform. Hence after equilibrium is established, the rate of upward heat loss from models I and III will be the same.

It is convenient to discuss these heat conduction models in terms of a characteristic 'conduction length' $l(t)$ defined by

$$l(t) \equiv (4\alpha t)^{1/2} \tag{3}$$

where α, the thermal diffusivity, is the ratio of the thermal conductivity to the volume specific heat of the principal materials through which heat is being conducted. Generally, $l(t)$ represents a characteristic distance from the source of a temperature disturbance to which a perturbation is likely to be appreciable after the passage of time t. Representative values of l are presented for selected values of t and α in Table 2. The first column, denoted by l', might be appropriate for calculations principally involving conduction within the liquid magma, and possibly through the roof materials above it as well, if porous volcanic rocks and sediments predominate. The second column, l'', represents an average for conduction paths including heated and cool crystalline rocks and the more poorly conducting materials just mentioned. It may be appropriate for conduction paths related to close-in thermal edge effects around the caldera rim and also for conduction through the roof if it contains an appreciable amount of crystalline rock. The last column, l''', represents crystalline rock at average temperatures not exceeding a few hundred degrees. The fact that the thermal properties probably contrast significantly among materials in, above, and surrounding the magmatic system poses problems for simple homogeneous models. Actually, the properties of all of the materials in the system affect the temperature in any one of them, sometimes in subtle ways, and the effects of inhomogeneities might have to be considered in more refined treatments. However, a more serious problem is likely to be the neglected effect of hydrothermal convection in permeable materials surrounding the magma.

For convenience and in order to specify notation we give some mathematical results for the three one-dimensional models of Figure 7 and for some related two- and three-dimensional cases. The graphical representation of the solutions will be somewhat more complete than is required by the immediate needs of the present discussion. We have found them to be a useful guide to intuition in problems relating to Long Valley and similar thermal areas. The relations are expressed in terms of conduction length $l(t)$ (Table 2) rather than the time t, so that all of the independent variables have the same dimensions.

For model I the anomalous heat flow $Q(l)$ on the ground surface $z = 0$ above the magma chamber is given at any time by [see, e.g., *Uyeda and Horai*, 1964; *Carslaw and Jaeger*, 1959, p. 313]

$$Q(l)/Q_0 = \left[1 + 2\sum_1^\infty (-1)^n \exp\left(\frac{-n^2\pi^2 l^2}{4a^2}\right)\right] \tag{4}$$

$$n = 0, 1, 2, \cdots$$

It is represented by the dashed curve in Figure 10*a*.

For model II the anomalous temperature $\Theta(l, z)$ at any time and depth is given by [*Carslaw and Jaeger*, 1959, p. 62]

$$\frac{1}{\Theta_0}\Theta(l, z) = \frac{1}{2}\left[\operatorname{erf}\frac{\Delta + a - z}{l} - \operatorname{erf}\frac{\Delta + a + z}{l} - \operatorname{erf}\frac{a - z}{l} + \operatorname{erf}\frac{a + z}{l}\right] \tag{5}$$

The temperature Θ_c at the center of the cooling magma, obtained by setting $z = a + \Delta/2$ in (5), is represented in terms of roof thickness a in Figure 8*b* and in terms of magma thickness Δ in Figure 8*a*. This is a convenient measure of the temperature in the deep interior of a cooling magma, although the actual depth of maximum temperature will be displaced downward somewhat depending upon the roof thickness a and the vertical gradient in the undisturbed country rock. The vertical dashed line in Figure 7*b* is a more realistic representation of the initial magma temperature for instantaneous intrusion; the excess temperature Θ_0 will have to be adjusted accordingly in applications of model II to the cooling of thick bodies. The anomalous heat flow at the ground surface above the chamber is

TABLE 2. Conduction Length $l \equiv (4\alpha t)^{1/2}$ km

Time t, m.y.	l'	l''	l'''
0.01	0.7	1.0	1.4
0.1	2.2	3.2	4.5
0.3	3.9	5.5	7.8
0.7	6.0	8.4	12
1	7.1	10	14
2	10	14	20
4	14	20	28
10	22	32	45
20	31	45	64
30	39	55	78

For l', $\alpha = 0.004$; for l'', $\alpha = 0.008$; and for l''', $\alpha = 0.012$, where α is thermal diffusivity (in square centimeters per second or 10^{-4} m^2 s^{-1}).

$$\frac{1}{Q_0} Q(l) = \frac{2}{(\pi)^{1/2}} \frac{a}{l} \left\{ \exp\left(-a^2/l^2\right) - \exp\left[-a^2/l^2\left(1 + \frac{\Delta}{a}\right)^2\right]\right\} \qquad (6)$$

It is represented graphically in Figure 8*c*. The maximum surface heat flow cannot exceed $\frac{1}{2}Q_0$ (see Figure 10*a*); for $\Delta \lesssim a$ the maximum is substantially less, and it probably occurs after the magma has completely solidified (see Figures 8*b* and *c*).

These one-dimensional results for model II are easily generalized to the case of initial temperature Θ_0 in a rectangular parallelepiped of thickness Δ beneath a roof of thickness a. The result has been used widely in discussions of cooling igneous bodies [e.g., *Lovering*, 1935; *Van Orstrand*, 1944; *Jaeger*, 1964; *Simmons*, 1967*b*; *Blackwell and Baag*, 1973]. It is more convenient than the corresponding result for the sphere [*Rikitake*, 1959; *Carslaw and Jaeger*, 1959, p. 257] because the aspect ratios of the chamber can be adjusted, and it is a bit simpler analytically. The three-dimensional results are obtained by multiplying the results for the slab (e.g., (5) and (6)) by an edge effect factor E that depends only on x, y, l, and the horizontal dimensions of the chamber. We consider only the case of a square prism of horizontal width $2m$, which will be referred to as model II*a* (Figure 9, inset). The edge effect factor along the vertical plane of symmetry ($y = 0$) is

$$E(x, l, m) = \frac{1}{2} \operatorname{erf} \frac{m}{l} \left[\operatorname{erf} \frac{m}{l}\left(1 - \frac{x}{m}\right) + \operatorname{erf} \frac{m}{l}\left(1 + \frac{x}{m}\right)\right] \qquad (7)$$

This result is shown graphically in Figure 9.

Results for model III, a uniform distribution of continuous heat sources on the infinitely extended plane $z = a$, are given in the appendix (equation (A6)). A generalization, model III*a* (Figure 10*a*, inset), where the sources occur only on the half plane $x' < 0$, $z = a$, is useful for considering edge effects (equations (A4)). The heat flow at the ground surface is represented by the family of curves in Figure 10*a*; the curve $x'/a = -\infty$ represents model III. By subtracting the result for a second value of x' the effect of a continuous strip source of finite width can be obtained from the figure. Subtracting the result for a second value of time (i.e., l) gives the effect of a continuous source of finite duration.

A generalization of model III in cylindrical coordinates is called model III*b*. As illustrated by the curves in Figure 10*b*, it represents the heat flow anomaly above the center of a uniform continuous circular source of radius R at depth a. Heat flow above the apex of a pie slice of central angle λ is obtained by multiplying the result for the circle by $\lambda/2\pi$. Results for various finite and infinite regions including the useful sector of a circular annulus (Figure 10*b*, inset and equation (A5)) can be obtained by combining results from Figure 10*b* for various values of R and λ. Discussions of models III*a* and III*b* are given in the appendix.

Depth of the Long Valley magma chamber. The geologic inference that Long Valley was a source of silicic volcanism for a period of about 2 m.y. extending virtually to the present has implications for the depth of the associated magmatic system.

If we assume that the magma temperature was 800°C, the roof thickness a was initially 5 km, and the ambient geothermal gradient was 25°C/km, then at the top of the chamber the ambient temperature was initially 125°C, and the excess temperature of the magma was $\Theta_0 \sim 675°$. If the thermal conductivity K of the overlying heated rock and sediments averaged 4.5 mcal/cm s °C, then the equilibrium upward-conducted anomalous flux would be (equation (2))

$$Q_0 \sim 6 \text{ HFU} \qquad (8a)$$

$$Q_0 \sim 200 \text{ cal/cm}^2 \text{ yr} \qquad (8b)$$

This value could reasonably be adjusted upward to about 10

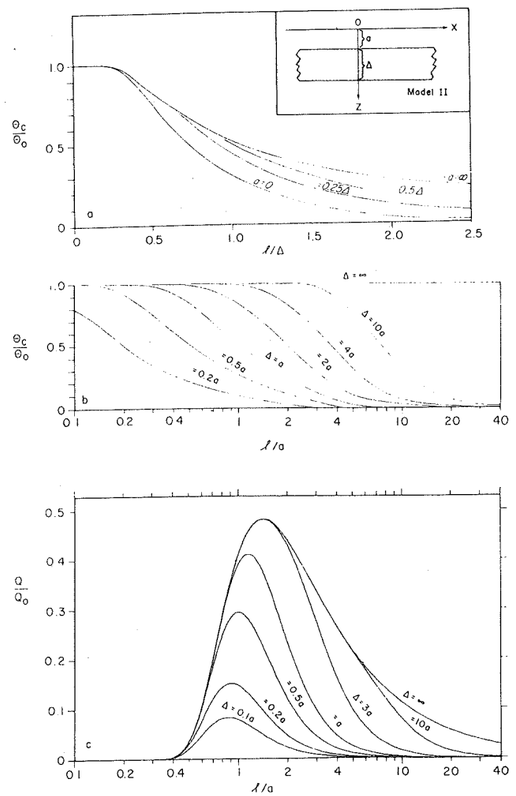

Fig. 8. Model II. The instantaneous slab source with initial temperature excess Θ_0, where l represents 'conduction length' (Table 2): (*a*) central temperature Θ_c in terms of magma thickness Δ, (*b*) central temperature Θ_c in terms of roof thickness a, and (*c*) anomalous surface heat flow Q.

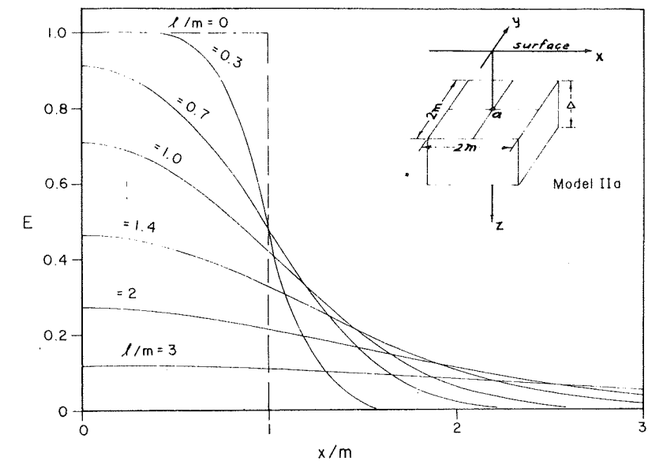

Fig. 9. Model II*a*. Edge effect factor E (equation (7)) for heat flow and temperature on the plane $y = 0$ for a square prism. The effect is independent of depth (z).

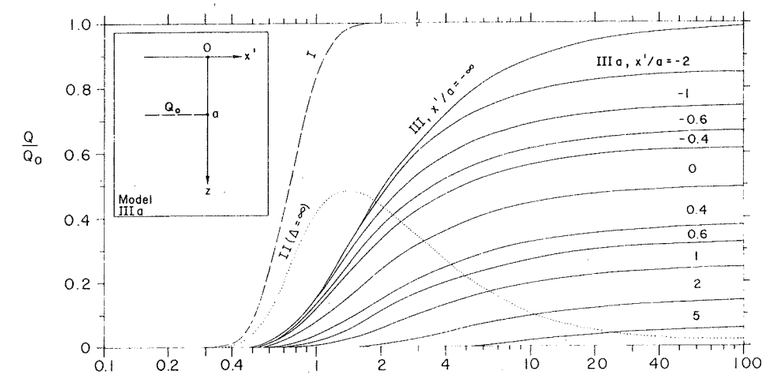

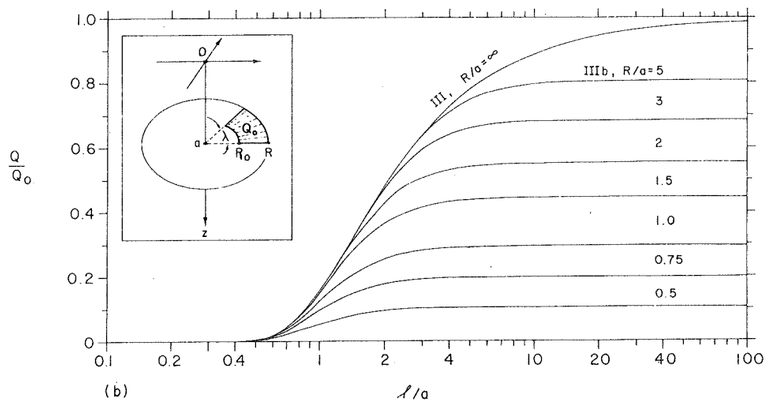

Fig. 10. Surface heat flow from continuous sources of constant strength Q_0 in a region of the horizontal plane $z = a$. (*a*) Solid curves (model III*a*) represent surface heat flow at x' for sources in the negative half plane (inset). The special case $x'/a = -\infty$ represents model III. Results for model I (dashed curve) and model II, $\Delta = \infty$ (dotted curve), are shown for comparison. (*b*) Surface heat flow (model III*b*) at origin from sources in the circle $\rho < R$. Inset shows a more general case obtainable by superposition. The special case $R/a = \infty$ represents model III.

HFU or downward to perhaps 4 HFU depending on the assumed ambient temperature, conductivity, and roof thickness. The total heat flow is obtained by adding the regional value, probably 1½–2 HFU. If the latent heat of crystallization of the silicic magma were 65 cal/g [*Harris et al.,* 1970] and the density were 2.5 g/cm³, crystallization of a layer about 1.2 cm thick each year could supply heat at this rate. Thus heat loss from the upper surface at the rate Q_0 since the start of Long Valley volcanism (~2 m.y. ago) would remove enough heat to crystallize 24 km of silicic magma. If hydrothermal circulation in the roof rocks were appreciable, the heat loss and crystallization rate would have to be increased accordingly [see, e.g., *Lachenbruch et al.,* 1976]. Consider the extreme case in which the Long Valley chamber was a convecting slab of thickness Δ isolated from sources of resupply from below and assume that as crystals formed, they settled, and the roof $z = a$ was continually maintained at 800°C. Neglecting any superheat of the magma, the chamber would have to extend virtually to the base of the crust in order to have been a source of extrusive materials up to the present time. This represents a model like model I (Figure 7) except that the extra heat loss during warming of the roof is neglected; the problem of heat loss during emplacement is, of course, circumvented by the assumed initial condition. If the chamber extended to the base of the crust where the ambient temperature in the Basin and Range province (Figure 4) is not far from the melting curve, the assumption that the chamber was isolated from sources of resupply would not seem reasonable. Thus if the chamber behaved according to this simple extreme, which maximizes heat loss, the duration of extrusive activity at Long Valley would be inconsistent with the view that the chamber was an isolated blister in the upper crust.

We now consider a model that represents slow cooling; it is extreme but not necessarily bracketing. A magma slab of thickness Δ is emplaced at $t = 0$ beneath $z = a$ at a temperature exceeding its surroundings by Θ_0; thereafter it is isolated from its source and cools by homogeneous conduction, inside and outside of the chamber (Figure 7*b*, model II). As gradual accumulation (at excess temperature Θ_0) prior to $t = 0$ would give some of the material a head start in cooling, the initial condition assumed would tend to overestimate the value of t for complete crystallization. The effect of neglecting convection by magma in the isolated cooling chamber and convection by water in fractured roof rocks is also to overestimate the crystallization time. The chief problem is how to cope with the effects of latent heat of crystallization, the theory of which has been discussed in considerable detail by J. C. Jaeger [e.g., *Jaeger,* 1964, 1959, 1961; *Carslaw and Jaeger,* 1959, chap. 11]. He has presented relations that account for contrasting thermal properties of magma, newly crystallized material, and country rock; for latent heat release over a finite melting interval; for intrusion at temperatures above the liquidus; and, to some extent, for geometric irregularities. Each of these effects can significantly influence the crystallization time and the thermal regime within and immediately around the chamber. However, application of these relations is not warranted, as it involves many parameters, most of which have not yet been carefully considered for Long Valley. In any event, results would be uncertain because of neglected effects of hydrothermal circulation. We shall use a scheme contrived to yield very approximate results from inspection of Figures 8 and 9. We suppose that crystallization is complete when the central part of the chamber has cooled by such an amount ($\delta\Theta$, calculated by neglecting latent heat) that the heat withdrawn locally is equivalent to the latent heat. Thus

$$\delta\Theta = (L/c) \sim 215°C \tag{9}$$

where L is the latent heat, assumed to be 65 cal/g, and c is the specific heat of the magma, assumed to be 0.3 cal/g °C. Hence we shall consider crystallization to be complete when the central temperature Θ_c calculated from model II falls to

$$\Theta_c \sim \Theta_0\left[1 - \frac{L}{c\theta_0}\right] \tag{10a}$$

$$\Theta_c \sim \Theta_0\left[1 - \frac{215°C}{\theta_0}\right] \tag{10b}$$

The model is most likely to be reasonable if Θ_0 is close to the liquidus temperature and the temperature interval for crystallization is small, as in the case of freezing along the cotectic curve [e.g., *Winkler and Lindemann,* 1972]. In this case the true central temperature at the time of complete crystallization will still be at or near Θ_0, and the central temperature Θ_c used for estimating crystallization time will be 215°C less. If the crystallization interval is large, say 200°C, the model could underestimate the crystallization time. The total heat loss from the magma computed by the approximation will generally be somewhat less than the true heat loss during complete crystallization, but the crystallization time will be overestimated by it for many cases of practical interest. This is possible because latent heat has two opposing effects on the cooling of a chamber: it increases the amount of heat that must be removed, but it also increases the rate at which heat is lost.

Figure 8*a* shows that as long as the magma thickness is greater than the conduction length ($l/\Delta \lesssim 1$) and is not greater than twice the roof thickness ($a > 0.5\Delta$), proximity to the earth's surface does not affect the decay of the central temperature. In this case (by symmetry) we can identify Θ_0 with the excess temperature at the level of the midpoint of the intrusive ($z = a + \frac{1}{2}\Delta$). For an 800°C magma with its midpoint at the 10-km depth in a region with an undisturbed gradient of 25°C/km, we obtain $\Theta_0 = 550°C$. Equation (10*b*) then gives $\Theta_c/\Theta_0 \sim 0.6$, and according to Figure 8*a*, crystallization is essentially complete when $l/\Delta \sim 0.8$. Choosing the lowest value of α in Table 2 as a conservative estimate of properties in the magma, we find for a 0.7-m.y.-old chamber that $l' \sim 6$ km and consequently $\Delta \sim 7\frac{1}{2}$ km. Thus a 7½-km-thick magma that intruded beneath a 6-km roof at the time of eruption of the Bishop Tuff could not be a volcanic source today. If the intrusion had accumulated over some finite period prior to 0.7 m.y. ago, it would, of course, have solidified at some time before present. Crystallization would occur earlier also if, as seems likely, the chamber included portions of solid country rock or was partially crystallized at the time of intrusion; in that case, L and $\delta\Theta$ (equation (9)) would be overestimated. A less conservative estimate of properties (using α'' instead of α'; Table 2) would have led to crystallization of an intrusion 10 km thick beneath a 5-km roof for the same conditions.

More massive intrusions for which the present approximation is less satisfactory would, of course, be required to survive the 2-m.y. volcanic history at Long Valley without resupply from a deeper source. For such large values of time an appreciable amount of cooling takes place from the edges of the chamber. Taking $m = 10$ km in Figure 9 to approximate conditions at Long Valley, the appropriate horizontal temperature profiles through 1- and 2-m.y.-old prisms are given by the curves $l'/m = 0.7$ and 1.0, respectively (Figure 9 and Table 2). Hence the central temperature in the prism (at $z = a + \frac{1}{2}\Delta$, $x = y = 0$) is 90% of that in the slab after 1 m.y. and 70% after 2 m.y. These differences would substantially reduce one-dimensional estimates of crystallization time and further increase the initial thickness required for survival of melt in an intrusive chamber isolated from sources of resupply.

These results taken collectively suggest that an independent intrusive chamber with lateral dimensions of Long Valley caldera and a thickness up to perhaps 10 km would be crystallized by conductive heat loss no more than 1 m.y. or so after its magma supply was cut off. If the magma convected or if hydrothermal loss were appreciable, the time would be substantially less. The result is relatively insensitive to the thickness of the roof (for a given temperature contrast). For times longer than 1 m.y. the edge losses become substantial, and an uppercrustal silicic magma chamber probably could not sustain molten material as required by the geologic observations, unless it were repeatedly resupplied with heat from deep-crustal or subcrustal magmatic sources.

Present state of the Long Valley magma chamber. Judging from estimates of structural collapse and volumes of material removed during eruption of the Bishop Tuff [*Bailey et al.,* 1976], the entire area of the caldera was probably underlain by a magma layer at least 1 or 2 km deep for some unknown period prior to the eruption 0.7 m.y. ago. The resurgent structure forming shortly thereafter (0.6 m.y. ago) indicates a roof thickness of perhaps 5–7 km at that time. Recent volcanism [*Bailey et al.,* 1976] implies that a source of silicic magma probably still exists in the chamber today, at least in the western part. The question arises whether shallow molten material could still underlie the entire region occupied by the caldera. If heat transfer were primarily by conduction, surface heat flow measurements should provide a definitive answer. However, hydrothermal circulation precludes the application of heat conduction theory to measurements within the caldera [*Lachenbruch et al.,* 1976], and conductive heat flow measured in the surrounding rocks could be affected even if circulation were confined to the caldera proper. Effects of hydrothermal convection within the caldera on conductive flux beyond its rim could be of either sign depending upon details of the circulation. As these details are unknown, we shall neglect them and consider the present thermal state in terms of simple conduction models. Although this assumption renders the conclusions uncertain, the analysis provides a useful frame of reference.

We know from model III (Figure 7*c*) that if heat is released at some depth a in a nonconvecting solid at an average rate Q_0 (equation (2)), after an infinite amount of time the excess temperature there will reach Θ_0, the value required for a stable magma chamber. Thus if the average rate of heat release is greater than Q_0, a chamber will ultimately develop, and if it is less, a chamber will not develop. The quantity Q_0 is smaller at greater depth, both because a is larger and because Θ_0 is smaller (equation (2)). Hence it is generally easier to develop a stable magma chamber at greater depth. We might view the heat release Q_0 as the result of successive intrusion and crystallization at depth a of thin sills with a thickness $\Delta << a$. How the sensible and latent heat is conducted and convected away from a real sill depends upon the mechanics of intrusion and upon hydrologic conditions in the surrounding rock. In any case, solidification of a 1-meter sill every century would release latent heat at the average rate of about 7 HFU; in the early stages when the country rock was cool, sensible heat would be released at a comparable rate. Hence average intrusion rates of at least 1 m every century or so would probably be required to develop a stable chamber at the 5-km depth; at the 10-km depth the required rates would be roughly half as great. Where circulating water removes appreciable heat, estimates of Q_0 and intrusion rates must be increased accordingly. Sills that were fed at rates much greater than these minima might be expected to develop quickly into viable magma chambers; if their upper surfaces were kept in contact with magma by convection, temperatures above them would be represented by model I (Figure 7*a*). Comparison of the gradient at $z = a$ for the curves labeled t_1 in models I and III (Figure 7) shows that the upward heat loss is much greater from the early developing chamber; this, of course, is why the surface heat flow grows to the equilibrium value Q_0 much faster in model I than in model III (Figure 10*a*, curves I and III).

From the foregoing we expect model III to provide a lower limit to the surface heat flow above a developing or established magma chamber at depth a for the case of one-dimensional conductive transfer. The model has the advantage of being easily modified to consider heat flow across the edge of sources of limited lateral extent (models III*a* and III*b*). We assume that the limited source models apply at and beyond the rim of Long Valley caldera; whether the assumption is justified depends upon unknown effects of hydrothermal circulation. For a 1-m.y.-old chamber at the depth $a = 5$ km we have $l''/a = 2$ (Table 2). Coincidence of the curves $R/a = 3$ and $R/a = \infty$ for $l/a \lesssim 2$ (Figure 10*b*) indicates that sources whose lateral distances from the heat flow station exceed 15 km will not contribute appreciably. Therefore for this example the magma sheet beneath the caldera can be represented by the semi-infinite region of model III*a* (Figure 10*a*). The position $x' = 0$ might be identified with the heat flow site WC on the eastern rim of the caldera, and Watterson Trough (WTE) and Round Mountain (RM) would correspond, respectively, to $x' = 3$ km and $x' = 6$ km (Table 1). For $a = 5$ km this model leads to heat flow anomalies at these sites of 1.4, 0.7, and 0.3 HFU, respectively. If the chamber had been developing under this region for the past 2 m.y., these values would be larger by 30–50%, and if it existed only for the past 0.7 m.y., they would be smaller by only 10–20%. Figure 5 and Table 1 show that no such anomalies are indicated at these sites if the Basin and Range norm applies for them. If the magma surface were represented (less conservatively) as a region of constant temperature at depth a, the edge effects would develop much more rapidly, and the predicted heat flow anomalies would be even larger. (Steady state results for the constant temperature case can be estimated from model III*b*; see appendix.) Although the model is uncertain chiefly because of neglected hydrothermal effects, it suggests that the measured heat flow is inconsistent with the continuous existence of magma only 5 km beneath the eastern portion of the Long Valley caldera throughout its recent eruptive history. A similar conclusion is probably justified for magma at a depth of 7 km. However, magma at the 10-km depth leads to substantially smaller anomalies and probably cannot be ruled out on present evidence by this model.

We now consider what magmatic history for the eastern caldera is consistent with the conditions that shallow magma occurred there 0.7 m.y. ago and that heat flow near the eastern rim is normal or nearly so today. The conduction time constant for a 5- to 7-km roof (i.e., the value of t for $l'' \sim 5$–7 km; Table 2) is less than 0.7 m.y.; hence substantial cooling could have occurred by conduction alone in the eastern caldera if the heat sources beneath it were removed with eruption of the

Bishop Tuff. Extension of the foregoing constant source model indicates that if a chamber developed 5–7 km beneath the eastern half of the caldera about 1 m.y. ago and was evacuated 0.3 m.y. later, a heat flow anomaly probably would not be detectable near the eastern rim today. A constant temperature conduction model of the magma would imply that the molten condition beneath the eastern rim was of shorter duration or possibly that the residual magma there was quenched by hydrothermal convection. In any case, it seems consistent to speculate that eruption of the Bishop Tuff may have largely exhausted the magma in the eastern part of the caldera, leaving a residual magma chamber more circular in plan under the western part of the caldera. By this view the asymmetric position of the resurgent dome would mark the location of this hypothetical residual chamber. These suggestions are speculative because of the unknown role of hydrothermal convection and the preliminary status of the heat flow data. Curve I (Figure 10*a*) shows that the absence of a heat flow anomaly does not preclude a more recent intrusion beneath the eastern part of the caldera, say, in the last 0.1 and 0.2 m.y. ($l''/a \lesssim 1/2$), although there is no present evidence that this has occurred.

The foregoing discussion depends upon the nearly normal heat flow to the east to tell us where the magma could not have been and upon geologic observations to tell us where it must have been. Inside the Long Valley caldera the thermal regime is strongly influenced by water movements [*Lachenbruch et al.,* 1976], and outside of it we have only one observation of an anomalously large heat flow, the site DP about 3 km beyond the western rim. This anomaly of 2.75 HFU could be the effect of a still molten, geometrically simple Long Valley magma chamber. If it is, a model of the type just discussed would suggest that the roof of the chamber is not deep (perhaps about 5 km) and that the chamber might even extend a few kilometers beyond the western caldera rim. It is interesting that at Valles caldera, New Mexico, whose size and recent eruptive history are rather similar to Long Valley's, a site similar to DP (3 km west of the rim in granitic rock) also yields a heat flow of 3.5–4.0 HFU [*Potter,* 1973]. This observation might lend some support to the foregoing simple explanation. Alternatively, the high value at DP might be a local effect of the extensive recent magmatic activity along the Sierra Nevada frontal fault system in the vicinity of Devils Postpile. If the second alternative is true, the observation at DP contains no information on the present state of the Long Valley magma chamber, and the best evidence for existence of a chamber is the very recent silicic extrusion attributed to it [*Bailey et al.,* 1976] and perhaps the hydrochemical estimates of large heat flux from the caldera [*White,* 1965; *Sorey et al.,* 1976; *Lachenbruch et al.,* 1976]. Additional heat flow measurements near the western rim of the caldera could provide a basis for selection between these alternatives.

Background heat flow near the province boundary and the measurement at AB. The foregoing examples illustrate how simple heat conduction models can be used with heat flow measurements near a volcanic area to guide speculation on the magmatic history and the present thermal state. Ignorance of the geometric distribution of thermal properties and of convective movements (both magmatic and hydrologic) throughout this history will often preclude the useful application of elaborate analytical or numerical thermal models, even if the distribution of heat flow in the vicinity is very well known. If the distribution of heat flow is not well known, as in the Long Valley study at its present stage, the implications of even the simple extreme models (e.g., Figures 8, 9, and 10) can be uncertain. This uncertainty has been illustrated by the foregoing discussion and particularly by the example of the single measurement DP near the west rim of the caldera. It is illustrated in another way by the measurement at Aeolian Butte and its bearing on the interpretation of the province transition and heat flow at the east rim sites.

The inference that heat flow is normal or nearly so near the east rim of the caldera is based on the supposition that the Basin and Range norm applies approximately to the background heat flow there. Under that condition the measured anomaly at the rim and at distances of 3 and 6 km beyond it would be +0.4, −0.2, and −0.3 HFU, respectively (Q_{BR} for WC, WTE, and RM, Table 1). We have pointed out that such variations from the norm are typical of sites interior to the Basin and Range province where there is no obvious association with very recent volcanism. The sites in question, however, lie an average of perhaps 15 or 20 km from the boundary of the Sierra Nevada physiographic province. It might be argued that the typical Basin and Range values measured near the east rim are a coincidence resulting from canceling effects of a regional transition to the lower heat flow characteristic of the Sierra and the anomalous heat from the Long Valley magma chamber. If we took the extreme position that the Sierra norm applied at the east rim, the anomalies there (Table 1, Q_S) would be larger by 1 HFU, and the effects of magmatic heat would be judged significant. However, there is no observational evidence to support this position. Apart from the measurement at JM and SM, which are probably controlled by hydrologic effects, we have two other measurements (DS and AB, Figures 1, 2, and 5) in granitic rocks of the Basin and Range province in the area. Both are too far from the caldera to be affected by it, and both yield data consistent with the Basin and Range norm. One site (DS) is about 10 km farther from the physiographic province boundary than the east rim, and the other (AB) is about 10 km closer to it. Although the normal Basin and Range value at AB (less than 10 km from the province boundary) deepens the puzzle of the province transition, it tends to confirm the validity of the Basin and Range norm at the east rim of the caldera.

Aeolian Butte is probably closer to the physiographic boundary than any other site yielding normal Basin and Range heat flow. The measured heat flow and heat production there are well-established values at a location in the center of a Mesozoic pluton. However, the site also lies in the center of *Kistler*'s [1966] ring fracture zone (Figure 2), which contains areas of very recent volcanism, including the Mono craters on its eastern rim. *Bailey et al.* [1976] have suggested that the ring fracture zone is probably underlain by a modern magma chamber. Thus we could speculate that the normal heat flow at AB is transitional and that AB falls on the Basin and Range curve by coincidence because of an anomaly from the hypothetical crustal magma source, a problem similar to that on the east rim of Long Valley.

We should like to know whether such a chamber exists, both as a matter of geologic interest and because of its bearing on the interpretation of background heat flow in the Long Valley area. With only one measurement near the ring fracture zone it is difficult to resolve this question, but if we assume it to be representative, some information can be obtained.

According to *Kistler* [1966, p. E48], faulting on the ring fracture occurred after the Sherwin glaciation (minimum age ~1 m.y. [*Dalrymple,* 1964]) and before the eruption of the Bishop Tuff 0.7 m.y. ago [*Bailey et al.,* 1976]. (More recent

displacements have also occurred on some parts of the fracture zone (R. A. Bailey, personal communication, 1975).) If the activity on the ring fracture is a mechanical effect of the hypothetical magma chamber beneath it, the chamber must be at least 0.7 m.y. old, and according to Table 2, $l'' \geq 8.4$ km and $l''' \gtrsim 12$ km; the most reasonable value in this case is probably closer to l'''. The radius of the ring fracture zone is about 6 km. If it were underlain by magma at a depth of 6 km, then by model III*b* the heat flow anomaly at AB would be $\gtrsim 0.25\ Q_0$ (Figure 10*b*, $R/a = 1$, $l/a \gtrsim 2$), i.e., probably greater than 1½ HFU in these crystalline rocks ($K \sim 6$ CU). But even if AB were interpreted in terms of the Sierra norm, the measured anomaly at AB would not exceed 0.9 HFU (Table 1, Q_S), and a more reasonable interpretation of the province transition would limit the anomaly further. Extension of the argument suggests that if a stationary chamber exists beneath the ring fracture, its roof is probably at least 8–10 km deep; it could be shallower if it had changed its position rapidly in recent times. If such a chamber supplied the very recent volcanism in the area, it probably did so along deep local conduits. Additional measurements of heat flow in this region might provide useful information on the nature of the local magmatic system and the province transition.

THERMAL IMPLICATIONS FOR MASS TRANSFER AND CRUSTAL SPREADING

It is unlikely that silicic melt can be maintained in the upper 5–8 km of the crust for periods of the order of a few million years without anomalous upward heat loss at the average rate of at least 5–10 HFU; this estimate allows little for hydrothermal circulation in the roof rocks. We suppose that this minimum condition obtained in those places with lateral dimensions of a few tens of kilometers where silicic volcanism was associated with caldera formation [*Smith and Bailey,* 1968]. If conductive transfer predominates, this thermal anomaly might not appear at the surface for several hundred thousand years; if hydrothermal convection occurs, the anomaly could be much larger, and it might never appear in the conductive flux at the earth's surface above the melt, as the heat could be discharged by hot springs. The Basin and Range crust is 30 km or so thick [*Thompson and Burke,* 1974], and hence 5–10 HFU cannot be transferred through it by conduction without prohibitively large subcrustal temperatures [*Blackwell,* 1969, 1971]. Therefore the large heat flux implies vertical transfer of mass through the crust; to maintain the molten condition the mass must deliver heat to the melt at temperatures at or above 800°C or so.

Christiansen and Lipman [1972] document the universal association of basalts with rhyolitic volcanism in the Basin and Range province and propose that the 'basalts represent the fundamental expression of deep-seated processes and that the rhyolites are directly related to the rise of basaltic magmas in the earth's crust.' This seems plausible as the high melting temperature, large latent heat, and low viscosity of basalt [*Shaw,* 1965; *Shaw et al.,* 1968] make it a most effective heat transfer fluid for crustal magmatic processes. Furthermore, temperatures represented by the Basin and Range norm (Figure 4) are consistent with the existence of basaltic melt at or slightly below the base of the crust [see also *Roy and Blackwell,* 1966; *Roy et al.,* 1972; *Blackwell,* 1971; *Archambeau et al.,* 1969; *Pakiser and Zietz,* 1965].

Basaltic sills (with latent heat of 100 cal/g, density of 3 g/cm³, and specific heat of 0.3 cal/g °C) intruding the crust at 1100°C and then crystallizing and cooling to 800°C at average rates of 1 cm/yr would supply heat at the rate of about 18 HFU. (The intrusions could, of course, be of any geometric form; we mention sills to emphasize that the calculation is one-dimensional.) Presumably their heat could mobilize or melt in place indigenous silicic material to produce the laterally extensive upper crustal melts implied by caldera collapse. Whether the basalt transferred its heat to the upper crustal melt by inducing convection in a deep silicic magma chamber, by melting silicic rock which ascended to replenish upper crustal sills, or by direct intrusion of the upper crust to rejuvenate crystallizing melt, only the heat available in the basalt above 800°C or so could contribute to the upward heat loss as required to preserve the upper crustal melt. To supply the estimated minimum heat loss from the top of the silicic melt for 2 m.y. by these processes would require the local addition to the crust (beneath the top of the melt) of a layer of basalt on the order of 10 km thick. (The requirement would be even greater if we allowed for heat lost to lower crustal rocks at temperatures below 800°C.) This would result in substantial crustal thickening unless the original crustal material were displaced downward into the mantle or sideways by local crustal spreading.

Simple calculations are possible if we assume somewhat arbitrarily that basaltic additions necessary to supply the excess heat are accommodated by local crustal spreading with little change in crustal thickness and that convective input from below and surface heat loss have achieved a steady state. In this case the anomalous heat flux and the local spreading strain rate are proportional to one another (as both are proportional to the upward flux of basalt). Such a process could be consistent with the model of *Thompson and Burke* [1974] in which passive basaltic dikes fill extension fractures at the base of the laterally spreading Basin and Range crust. In an area of active silicic volcanism, basaltic intrusion would be intense, and the locally weakened crust might relieve regional tectonic strain at an accelerated rate. This model would suggest that subcrustal intrusion and volcanism might cease after the accumulated regional strain is relieved locally. For a 30 km crust and the conditions assumed above, crustal area would increase at the rate of about 2% per million years per anomalous HFU. Thus anomalous heat loss of 5–10 HFU from the top of the Long Valley magma chamber for 2 m.y. would be associated with an area increase on the order of 20–40%, e.g., extension of a 25-km square by 5–10 km in one direction.

A similar calculation can be applied to the Basin and Range province as a whole if we assume that the excess regional flux is provided by distributed basaltic intrusions in the lower crust, cooling to the reasonable ambient temperature of 800°C (Figure 4). Although it is still uncertain, the anomaly in the flux (equation (1), q^*) from the lower crust of the Basin and Range province is estimated to be about 0.6 HFU relative to stable continental regions [*Roy et al.,* 1968]. If this anomalous thermal condition has persisted throughout the 15-m.y. history of the structural province, the foregoing model leads to an increase in its average area of about 20%. This would represent a total E-W extension throughout the life of the Basin and Range province of 150–200 km and a mean spreading rate of the order of 1 cm/yr. These tenuous results are within the range of values estimated by other means [*Thompson and Burke,* 1974].

Because of the likelihood of basaltic melt at or slightly below the base of typical Basin and Range crust, the Basin and Range heat flow 'norm' is, in a sense, a magmatic thermal anomaly. Near the edge of the province (e.g., in the Long

Valley area) the problem of distinguishing between the effects of the province transition and those of upper crustal magmatism is that of distinguishing between a deep magmatic anomaly and a shallow one. General availability of basaltic melt in the subcrust of the Basin and Range would make both types of anomalies likely, and this probably contributes to much of the variability of heat flow in the province. Curve I, Figure 10*a*, and Table 2 show that 'normal' Basin and Range heat flow would probably obtain no more than 5 or 10 m.y. after basaltic melt becomes established in the subcrustal region; if the formation of Basin and Range crust were initiated by silicic volcanism, the thermal 'norm' could be established faster. Development of the thermal edge effect by conduction in the deep-rooted crust of the adjacent Sierra Nevada province is a longer process. Thus the abrupt thermal transition across the province boundary might imply a westward encroachment of the Basin and Range province on the Sierra Nevada province in the last several million years [see also *Roy et al.*, 1972]. Unfortunately, the heat flow data near the province boundary are not yet adequate for an analytical discussion of this problem.

SUMMARY

Heat flow was measured at 11 sites in the vicinity of Long Valley caldera in a search for information on the local magmatic history and present thermal state. The problem is complicated by hydrothermal convection and by the location of Long Valley astride the boundary between the Sierra Nevada and Basin and Range physiographic provinces, the locus of one of the sharpest transitions in regional heat flow in North America. The locations of the new sites range 30 km or so on either side of the province boundary and 0–30 km (outward) from the caldera rim. Four previously published values from the Sierra Nevada and one from the Basin and Range extend the regional coverage. With three notable exceptions (two of which are attributed to moving groundwater) the values of heat flow and heat production are within the range expected at points interior to each province. Hence individual effects of either the province transition or of recent magmatic heat are not generally conspicuous. As these effects are of opposite sign in the Basin and Range, there is, of course, the possibility that they both occur and are self-canceling. Four measurements near the eastern rim of the caldera indicate that if an anomaly (relative to the Basin and Range norm) exists there, it is very local and probably not greater than a few tenths of a heat flow unit. An important exception to the normal pattern is the single value measured near the western rim where the anomaly is 2.75 HFU in relation to the Sierra norm. Although the new data are preliminary and their geographic distribution is sparse, it is useful to use them with simple heat conduction models and geologic information to explore possible constraints on the magmatic regime and to identify areas where additional observations might be most helpful.

According to *Bailey et al.* [1976] the region beneath Long Valley has been the source of silicic volcanic material over a period beginning about 2 m.y. ago and extending virtually up to the present. Simple heat conduction models suggest that such a source probably could not have survived crystallization unless it was resupplied with heat from deep crustal or subcrustal magmatic sources. In this sense, Long Valley caldera represents the surface expression of a deep magmatic system.

It seems likely that the heat supply at some stage involves the movement of basalt [*Christiansen and Lipman*, 1972], the most effective heat transfer fluid for crustal magmatic processes [*Shaw*, 1965; *Shaw et al.*, 1968]. This suggests an idealized model (following *Thompson* [1966]) in which mantle basalts replenish the spreading crust by intruding tensile openings in its base. They supply the anomalous heat loss which would therefore be proportional to local spreading strain rate if a steady state is approached. For the special conditions assumed in the text this leads to crustal extension of the order of 2% per million years per anomalous HFU; for a province-wide anomaly of 0.6 HFU this yields an average spreading rate across the Basin and Range province of the order of 1 cm/yr. In regions of active silicic volcanism the anomalous heat loss is an order of magnitude greater than the anomalous regional flux and by this simple model, so is the local rate of basaltic intrusion and crustal extension.

Judging from the collapse and resurgence following eruption of the Bishop Tuff, the Long Valley caldera was probably underlain by silicic magma at a depth of perhaps 5–7 km about 0.7 m.y. ago [*Bailey et al.*, 1976]. If magma had persisted at such depths throughout the recent eruptive history of Long Valley, we should expect a more conspicuous heat flow anomaly near the eastern rim than we infer from the observations. The time constant for decay of such an anomaly is a few hundred thousand years. Hence we speculate that eruption of the Bishop Tuff exhausted the magma source beneath the eastern caldera and that the subsequent resurgence in the western part identifies the position of a residual chamber, more circular in plan. This interpretation is consistent with the absence of silicic extrusion in the last 0.3 m.y. on the eastern side of the resurgent structure. A source of uncertainty in the interpretation is the unknown effect of hydrothermal circulation beneath the caldera. The high heat flow near the western rim can be interpreted in terms of a simple shallow magma chamber, possibly extending a bit beyond the caldera rim, or perhaps it is a local effect of recent magmatic activity along the Sierra frontal fault system. Additional heat flow measurements could help resolve this ambiguity.

Bailey et al. [1976] have suggested that a modern magma chamber underlies the ring fracture zone associated with Mono craters, about 15 km northwest of the Long Valley caldera. A geologic constraint on the age of the ring fracture and a heat flow measurement at its center imply that if a stationary chamber exists there, its roof is probably deeper than 8–10 km.

The general significance of an individual heat flow measurement is always uncertain, and the sparse distribution of observations in the Long Valley area together with incompletely understood hydrothermal effects leaves fundamental thermal questions subject to more than one plausible answer. However, this preliminary study suggests that investigation of heat flow can yield information not obtainable in other ways about the magmatic system at Long Valley and similar thermal areas.

APPENDIX: THE HEAT FLOW ANOMALY CAUSED BY CONTINUOUS SOURCES IN A FINITE REGION OF A BURIED HORIZONTAL PLANE

We wish to find expressions for the heat flow $Q(x, y, 0, t)$ at the surface, $z = 0$, when the region $z > 0$ is initially at zero temperature under the following condition: heat is generated at the constant rate Q_0 cal/cm² s in the region (S: x', y', a) of the plane $z = a > 0$ for $t > 0$ while the surface $z = 0$ is maintained at zero temperature.

The contribution to the gradient at time t at a point $(x, y, 0)$ on the surface $z = 0$ due to a unit instantaneous heat source at (x', y', a) liberated at time τ is given by [*Carslaw and Jaeger*, 1959, p. 370]

$$\frac{a}{8K(\pi\alpha)^{3/2}}(t-\tau)^{-5/2}\exp\left[\frac{-r^2}{4\alpha(t-\tau)}\right] \qquad \text{(A1)}$$

where $r^2 = (x - x')^2 + (y - y')^2 + a^2$. We can therefore express the solution to the problem as follows:

$$\frac{1}{Q_0}Q(x, y, 0, t) = \frac{a}{8(\pi\alpha)^{3/2}}\int_0^t\iint_S (t-\tau)^{-5/2} \cdot \exp\left[\frac{-r^2}{4\alpha(t-\tau)}\right] d\tau\, dx'\, dy' \qquad \text{(A2)}$$

We now consider a second problem. Find the temperature $T(x, y, a, t)$ at depth $z = a$ in the region $z > 0$ initially at zero temperature under the following condition: the region (S: x', y', 0) of the surface $z = 0$ is maintained at constant temperature T_0 for $t > 0$ while the rest of the surface $z = 0$ is maintained at zero temperature. It will be seen from the Green's function formulation of this problem [e.g., *Carslaw and Jaeger*, 1959, p. 371; *Birch*, 1950, equation (3); *Lachenbruch*, 1957*b*, equation (23)] that the solution is identical to (A2) if we replace Q by T and Q_0 by T_0. Thus for these two seemingly unrelated problems, we have the following: The temperature disturbance at (x, y, a, t) due to a uniform anomalous temperature in the region (S: x', y', 0) on $z = 0$ for $t > 0$ is the same as the heat flow disturbance at $(x, y, 0, t)$ due to a uniform continuous heat source distribution in the region (S: x', y', a) on $z = a$ for $t > 0$. The region is initially at zero temperature, and the surface temperature is zero except where otherwise specified.

Therefore results for the corresponding temperature anomaly problem can be applied to this problem of anomalous continuous sources.

Integration with respect to time in (A2) yields the general result

$$\frac{1}{Q_0}Q = \frac{1}{2\pi}\iint_S\left[\frac{2}{(\pi)^{1/2}}\frac{r}{l}\exp(-r^2/l^2) - \operatorname{erfc}\frac{r}{l}\right]d\Omega \qquad \text{(A3}a\text{)}$$

$$\frac{1}{Q_0}Q \to \frac{1}{2\pi}\Omega(x, y; S) \qquad t \to \infty \qquad \text{(A3}b\text{)}$$

where $d\Omega$ is the element of solid angle subtended by the surface element $dx'\,dy'$ in S at the field point $(x, y, 0)$ and Ω is the solid angle subtended by S there. Equation (A3*b*) is the well-known result from potential theory, widely used in the interpretation of gravity anomalies [see, e.g., *Nettleton*, 1942; *Simmons*, 1967*a*]. Equation (A3*a*) generalizes the result for transient heat conduction. The integrand is a simple time-dependent weighting factor, and the integral is easily evaluated numerically. (Related results have been obtained by *Birch* [1950].) The continuous source case for which S is the half plane $z = a$, $x' < 0$, has been solved for the corresponding anomalous boundary-temperature problem [*Lachenbruch*, 1957*a*, equation (5)]

$$\frac{1}{Q_0}Q(x, a, l) = \frac{1}{2}\operatorname{erfc}\frac{a}{l} - \frac{1}{\pi}\int_0^{x/a}\exp\left[-\frac{a}{l}(1+\beta^2)\right]\frac{d\beta}{1+\beta^2} \qquad \text{(A4}a\text{)}$$

$$\frac{1}{Q_0}Q \to \frac{1}{2} - \frac{1}{\pi}\tan^{-1}\frac{x}{a} \qquad t \to \infty \qquad \text{(A4}b\text{)}$$

Equations (A4*a*) and (A4*b*) represent model III*a* illustrated in Figure 10*a*. (There we have replaced x by x' to avoid confusion with the notation for model II*a*.) The integral in (A4*a*) has been tabulated [*Lachenbruch*, 1957*a*; *Smith*, 1953].

The corresponding problem in cylindrical coordinates (ρ, ϕ, z) has also been considered for the anomalous boundary-temperature case [*Lachenbruch*, 1957*b*]. The surface heat flow at $z = 0$, $\rho = 0$, due to a continuous uniform source distribution of strength Q_0 for $t > 0$ at depth $z = a$ in the region $R_0 < \rho < R$, $0 < \phi < \lambda$, is [*Lachenbruch*, 1957*b*, equation (33)]

$$\frac{Q}{Q_0} = \frac{\lambda}{2\pi}\left\{\left[1+\left(\frac{R_0}{a}\right)^2\right]^{-1/2}\operatorname{erfc}\frac{a}{l}\left[1+\left(\frac{R_0}{a}\right)^2\right]^{1/2} - \left[1+\left(\frac{R}{a}\right)^2\right]^{-1/2}\operatorname{erfc}\frac{a}{l}\left[1+\left(\frac{R}{a}\right)^2\right]^{1/2}\right\} \qquad \text{(A5)}$$

The geometric conditions for this result are illustrated by the inset in Figure 10*b*. The result for the circular region ($R_0 = 0$, $\lambda = 2\pi$) is shown graphically in Figure 10*b* as model III*b*. The circle of infinite radius ($R \to \infty$), of course, represents the one-dimensional case, model III.

$$Q/Q_0 = \operatorname{erfc}\frac{a}{l} \qquad \text{(A6)}$$

The steady state result ($l \to \infty$) is obtained by setting the complementary error functions to unity in (A5) and (A6). It can be used as an approximation (and lower limit) to the steady state heat flow above a horizontal plane region at constant temperature Θ_0 (equation (2)). The steady state is approached much faster above a constant temperature region than above a constant source region (e.g., compare curves I and III, Figure 10*a*).

Transient effects of continuous or intermittent sources in certain regions bounded by lines of the polar and Cartesian coordinate systems can be obtained by combining (A4) and (A5).

Acknowledgments. We are grateful to Carl Bunker for measurements of the content of U, Th, and K in our rock samples and to D. E. White, R. L. Christiansen, P. C. Bateman, G. B. Dalrymple, R. W. Kistler, R. A. Bailey, and S. P. Galanis, Jr., for helpful discussions. We also thank D. E. White, R. A. Bailey, D. D. Blackwell, W. H. Diment, D. L. Williams, Mary O'Neill, L. J. P. Muffler, and Gene Simmons for comments on the manuscript.

REFERENCES

Archambeau, C. B., E. A. Flinn, and D. G. Lambert, Fine structure of the upper mantle, *J. Geophys. Res., 74,* 5825–5865, 1969.

Bailey, R. A., G. B. Dalrymple, and M. A. Lanphere, Volcanism, structure, and geochronology of Long Valley caldera, Mono County, California, *J. Geophys. Res., 81,* this issue, 1976.

Bateman, P. C., and J. P. Eaton, Sierra Nevada batholith, *Science, 158,* 1407–1417, 1967.

Birch, F., Flow of heat in the Front Range, Colorado, *Geol. Soc. Amer. Bull., 61,* 567–630, 1950.

Birch, F., R. F. Roy, and E. R. Decker, Heat flow and thermal history in New England and New York, in *Studies of Appalachian Geology: Northern and Maritime,* edited by E. Zen, W. S. White, J. B. Hadley, and J. B. Thompson, Jr., pp. 437–451, Interscience, New York, 1968.

Blackwell, D. D., Heat-flow determinations in the Northwestern United States, *J. Geophys. Res., 74,* 992–1007, 1969.

Blackwell, D. D., The thermal structure of the continental crust, in *The Structure and Physical Properties of the Earth's Crust, Geophys. Monogr. Ser.,* vol. 14, edited by J. G. Heacock, pp. 169–184, AGU, Washington, D. C., 1971.

Blackwell, D. D., and C.-G. Baag, Heat flow in a 'blind' geothermal area near Marysville, Montana, *Geophysics, 38,* 941–956, 1973.

Bunker, C. M., and C. A. Bush, Uranium, thorium, and radium analyses by gamma-ray spectrometry (0.184-0.352 million electron volts), *U.S. Geol. Surv. Prof. Pap. 550-B,* B176–B181, 1966.

Bunker, C. M., and C. A. Bush, A comparison of potassium analyses by gamma-ray spectrometry and other techniques, *U.S. Geol. Surv. Prof. Pap. 575-B,* B164–B169, 1967.
Carslaw, H. S., and J. C. Jaeger, *Conduction of Heat in Solids,* 2nd ed., Oxford University Press, New York, 1959.
Christiansen, R. L., and P. W. Lipman, Cenozoic volcanism and plate-tectonic evolution of the Western United States, 2, Late Cenozoic, *Phil. Trans. Roy. Soc. London, Ser. A, 271,* 249–284, 1972.
Dalrymple, G. B., Potassium-argon dates of three Pleistocene interglacial basalt flows from the Sierra Nevada, California, *Geol. Soc. Amer. Bull., 75,* 753–758, 1964.
Harris, P. G., W. Q. Kennedy, and C. M. Scarfe, Volcanism versus plutonism—The effect of chemical composition, in *Mechanism of Igneous Intrusion, Geol. J. Spec. Issue 2,* edited by G. Newall and N. Rast, pp. 187–200, Gallery Press, Liverpool, England, 1970.
Hildreth, W., and F. Spera, Magma chamber of the Bishop tuff: Gradients in T, P_{total}, and P_{H_2O} (abstract), *Geol. Soc. Amer. Abstr. Programs, 6,* 795, 1974.
Jaeger, J. C., Temperatures outside a cooling intrusive sheet, *Amer. J. Sci., 257,* 44–54, 1959.
Jaeger, J. C., The cooling of irregularly shaped igneous bodies, *Amer. J. Sci., 259,* 721–734, 1961.
Jaeger, J. C., Thermal effects of intrusions, *Rev. Geophys. Space Phys., 2,* 443–466, 1964.
Kistler, R. W., Structure and metamorphism in the Mono Craters quadrangle, Sierra Nevada, California, *U.S. Geol. Surv. Bull., 1221-E,* 53 pp., 1966.
Lachenbruch, A. H., Thermal effects of the ocean on permafrost, *Geol. Soc. Amer. Bull., 68,* 1515–1530, 1957*a*.
Lachenbruch, A. H., Three-dimensional heat conduction in permafrost beneath heated buildings, *U.S. Geol. Surv. Bull., 1052-B,* 51–69, 1957*b*.
Lachenbruch, A. H., Preliminary geothermal model of the Sierra Nevada, *J. Geophys. Res., 73,* 6977–6989, 1968*a*.
Lachenbruch, A. H., Rapid estimation of the topographic disturbance to superficial thermal gradients, *Rev. Geophys. Space Phys., 6,* 365–400, 1968*b*.
Lachenbruch, A. H., Crustal temperature and heat production: Implications of the linear heat-flow relation, *J. Geophys. Res., 75,* 3291–3300, 1970.
Lachenbruch, A. H., M. L. Sorey, R. E. Lewis, and J. H. Sass, The near-surface hydrothermal regime of Long Valley caldera, *J. Geophys. Res., 81,* this issue, 1976.
Lovering, T. S., Theory of heat conduction applied to geological problems, *Geol. Soc. Amer. Bull., 46,* 69–94, 1935.
Nettleton, L. L., Gravity and magnetic calculations, *Geophysics, 7,* 293–310, 1942.
Pakiser, L. C., and R. Robinson, Composition and evolution of the continental crust as suggested by seismic observations, *Tectonophysics, 3,* 547–557, 1966.
Pakiser, L. C., and I. Zietz, Transcontinental crustal and upper-mantle structure, *Rev. Geophys. Space Phys., 3,* 505–520, 1965.
Potter, R. M., Heat flow of the Jemez Plateau (abstract), *Eos Trans. AGU, 54,* 1214, 1973.
Rikitake, T., Studies of the thermal state of the earth, 2, Heat flow associated with magma intrusion, *Bull. Earthquake Res. Inst. Tokyo Univ., 37,* 233–243, 1959.
Roy, R. F., and D. D. Blackwell, Heat flow in the Sierra Nevada and western Great Basin (abstract), *Eos Trans. AGU, 47,* 179–180, 1966.
Roy, R. F., D. D. Blackwell, and F. Birch, Heat generation of plutonic rocks and continental heat flow provinces, *Earth Planet. Sci. Lett., 5,* 1–12, 1968.
Roy, R. F., D. D. Blackwell, and E. R. Decker, Continental heat flow, in *The Nature of the Solid Earth,* edited by E. C. Robertson, pp. 506–543, McGraw-Hill, New York, 1972.
Sass, J. H., A. H. Lachenbruch, R. J. Munroe, G. W. Greene, and T. H. Moses, Jr., Heat flow in the western United States, *J. Geophys. Res., 76,* 6376–6413, 1971*a*.
Sass, J. H., A. H. Lachenbruch, and R. J. Munroe, Thermal conductivity of rocks from measurements on fragments and its application to heat flow determinations, *J. Geophys. Res., 76,* 3391–3401, 1971*b*.
Shaw, H. R., Comments on viscosity, crystal settling, and convection in granitic magmas, *Amer. J. Sci., 263,* 120–152, 1965.
Shaw, H. R., T. L. Wright, D. L. Peck, and R. Okamura, The viscosity of basaltic magma: An analysis of field measurements in Makaopuhi Lava Lake, Hawaii, *Amer. J. Sci., 266,* 225–264, 1968.
Simmons, G., Interpretation of heat flow anomalies, 1, Contrasts in heat production, *Rev. Geophys. Space Phys., 5,* 43–52, 1967*a*.
Simmons, G., Interpretation of heat flow anomalies, 2, Flux due to initial temperature of intrusives, *Rev. Geophys. Space Phys., 5,* 109–120, 1967*b*.
Smith, R. C. T., Conduction of heat in the semi-infinite solid, with a short table of an important integral, *Aust. J. Phys., 6,* 127–130, 1953.
Smith, R. L., and R. A. Bailey, Resurgent cauldrons, Studies in Volcanology, *Geol. Soc. Amer. Mem., 116,* 613–662, 1968.
Sorey, M. L., and R. E. Lewis, Convective heat flow from hot springs in the Long Valley caldera, Mono County, California, *J. Geophys. Res., 81,* this issue, 1976.
Thompson, G. A., The rift system of the western United States, in *The World Rift System, Geol. Surv. of Canada Pap. 66-14,* edited by T. N. Irvine, pp. 280–289, Department of Mines and Technical Surveys, Ottawa, Ontario, 1966.
Thompson, G. A., and D. B. Burke, Regional geophysics of the Basin and Range province, *Ann. Rev. Earth Planet. Sci., 2,* 213–238, 1974.
Uyeda, S., and K. Horai, Terrestrial heat flow in Japan, *J. Geophys. Res., 69,* 2121–2141, 1964.
Van Orstrand, C. E., Flow of heat from an intrusive body into country rock, *Amer. Inst. Mining, Met. Petrol. Eng. Tech. Publ., 1677,* 1–9, 1944.
White, D. E., Geothermal Energy, *U.S. Geol. Surv. Circ., 519,* 17 pp., 1965.
Winkler, H. G. F., and W. Lindemann, The system Qz-Or-An-H_2O within the granitic system Qz-Or-Ab-An-H_2O application to granitic magma formation, *Neues Jahrb. Mineral. Monatsh., 2,* 49–61, 1972.

(Received March 19, 1975;
revised September 15, 1975;
accepted September 15, 1975.)

Convective Heat Flow From Hot Springs in the Long Valley Caldera, Mono County, California

MICHAEL L. SOREY

U.S. Geological Survey, Water Resources Division, Menlo Park, California 94025

R. E. LEWIS

U.S. Geological Survey, Water Resources Division, Laguna Niguel, California 92677

The heat discharged by the hot spring system in Long Valley, California, has been estimated from measured spring discharges by using geochemical mixing models. Of the total flow of 1300 l/s from 11 thermal springs in the caldera, approximately 20% or 250 l/s is contributed by the hydrothermal system at depth with temperatures near 210°C. The effects of heat loss by conductive cooling, mixing, and boiling are quantified for the springs in Hot Creek Gorge, which are the major source of hot water discharge in the caldera. The estimated total convective heat discharge is 4.3×10^7 cal/s, which is in agreement with an estimate obtained from the rate of boron discharge from the caldera into Lake Crowley. To supply heat conductively to circulating water of meteoric origin at a rate of 4.3×10^7 cal/s requires a heat flux at depth in excess of 10 μcal/cm^2/s.

INTRODUCTION

The natural heat flow in potential geothermal areas is a useful parameter in assessing the potential for energy development. As discussed by *White* [1965, p. 4], the natural heat flow is a first approximation of the minimum rate at which heat can be withdrawn from the system in water or steam and is a reference base for evaluating effects of accelerated withdrawal from a developed geothermal field. The magnitude and distribution of heat flow in a 'hot' area are also useful in attempting to define the characteristics of the underlying heat source.

In the Long Valley area, preliminary temperature measurements indicated that the conductive heat flow in the upper 300 m was about 4 HFU (1 HFU = 1 μcal/s/cm^2) near the western rim of the caldera, 4 HFU in the center of the caldera, and 2 HFU near the eastern rim, as discussed by *Lachenbruch et al.* [1976]. The convective heat flow in hot spring water was estimated by *White* [1965, p. 7] to be 7×10^7 cal/s, based on the boron contributed to Lake Crowley from the thermal system. A convective heat flow of this magnitude implies that the total heat flux at depth averaged over the caldera is considerably greater than 4 HFU. This suggests that a more detailed study of the convective heat flow is desirable.

In this paper the rate of heat discharge in each of the major thermal springs in Long Valley is estimated. For the purposes of this paper, springs are classified as thermal if their discharge temperatures are above 10°C. Geochemical techniques are used to separate the surface flow of thermal water into hot water and cold water components. The hot water component is assumed to be contributed by the geothermal reservoir at depth and to have chemical characteristics and temperatures distinctly different from the colder, fresher water which mixes with it. In particular, the hot water has significantly greater concentrations of chloride, boron, and silica than the shallow ground water. The total of dissolved solids of the thermal springs is near 1400 mg/l, and that of the nonthermal springs is near 150 mg/l.

DISTRIBUTION OF HOT SPRINGS

Casa Diablo Hot Springs

In the literature, one of Long Valley's most widely cited areas of geothermal activity is the Casa Diablo area (Figure 1, T3S/R28E-32). Historically, hot spring discharge from the area has been substantial, as is noted by *Russell* [1889], *Lee* [1906], and *Blake and Matthes* [1938], and the springs were once used for bathing by Indians and travelers along the old highway between Bishop and Mono Lake. Presently, very little hot water is discharging from the area, although numerous steam vents and several mud pots are in evidence. In June 1972 an estimated discharge of 0.6 l/s of 82°C water was observed coming from the spring area at Casa Diablo west of the old highway. By June of the following year, however, no discharge was apparent, and the temperature of the water in the marshy spring area was ambient. Chemical characteristics of the spring water suggest that its source may be steam-heated groundwater and the ambient temperature condition noted in 1973 may be the result of the diluting effect of a local perched groundwater body which formed as a result of the above normal recharge.

Casa Diablo Hot Pool

Variously referred to as Casa Diablo Hot Pool by *Stearns et al.* [1937] and *Waring* [1915] and as Hot Bubbling Pool by the *California State Department of Water Resources* [1967] and *Rinehart and Ross* [1964], this shallow pool, about 650 m^2 in surface area, is located very near the eastern fault of the central graben mapped by *Bailey* [1974] in T3S/R28E-35. Temperature measured near one of the vents along the northern margin of the pool was 68°C. *Waring* [1915] recorded temperatures of 49°C and 82°C at vents near the margin of the pool. There is no apparent discharge from the pool; however, a small well-defined channel leading in the direction of Hot Creek indicates flow in the past. Calculations based on the work of *Bensemen* [1959] indicate that an inflow of about 6.5 l/s is necessary to maintain a surface temperature near 55°C in a pool of this size. Such a volume of water cannot be accounted

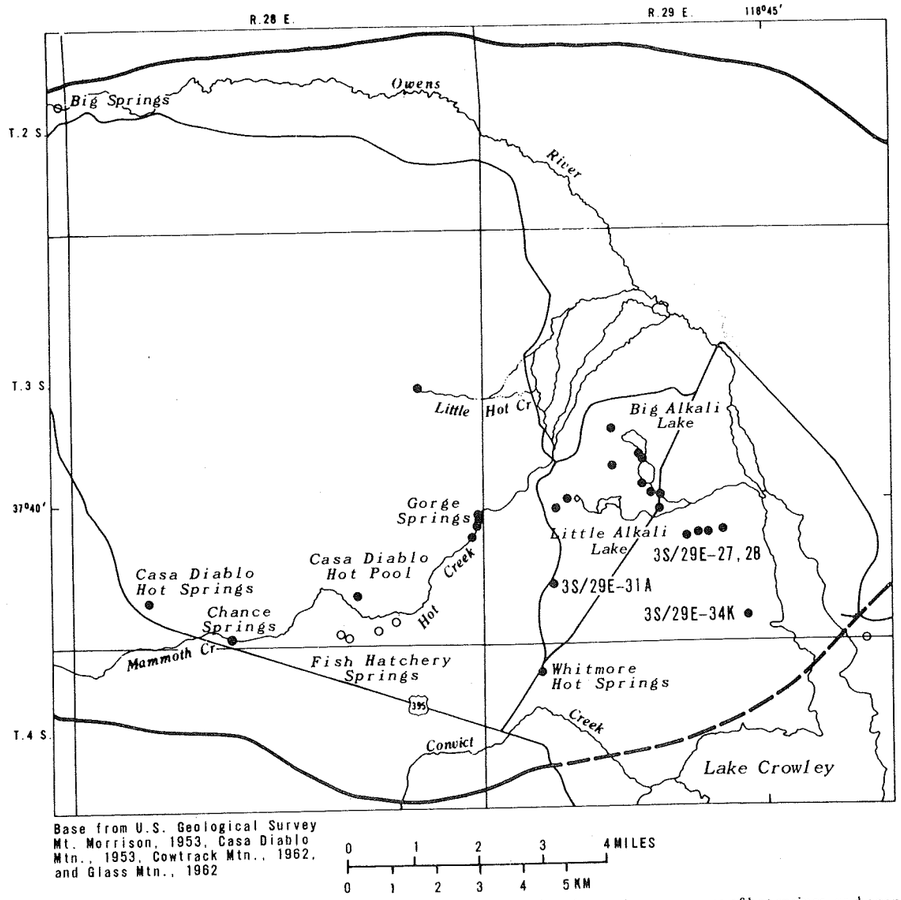

Fig. 1. Map of thermal springs in Long Valley caldera. Solid circles show hot springs or groups of hot springs, and open circles show cold or slightly thermal springs or groups of springs. The thick solid line is the caldera boundary, and it is dashed where the boundary is approximately located.

for by evaporation alone. Thus some combination of subsurface outflow and convective circulation is suggested. Over the bottom of the pool, numerous openings emit bubbles of what is apparently CO_2 gas and possibly some steam. Some carbonate material has precipitated from the water and is deposited along the edge of the pool.

Hot Creek Springs

Along a 1.6-km reach of Hot Creek, in the gorge in T3S/R28E-25, about 18 springs discharge nearly 250 l/s of thermal water into the creek. This discharge represents about 20% of the discharge of thermal water (above 10°C) in the caldera and is a mixture of shallow groundwater and hot water from the geothermal system. Springs along this reach of Hot Creek are among the hottest found in the Long Valley caldera and are the source of the greatest discharge of hot water from the geothermal system, accounting for 80% of the total (see Table 3). Most of the low-discharge springs along this reach are located on the banks above the creek and can be readily measured and sampled. Their combined discharge, however, is minor in relation to the total spring discharge into Hot Creek. Most of the thermal water contributory to Hot Creek discharges beneath the water surface. Techniques for estimating this flow are described in the next section.

Little Hot Creek

The springs of Little Hot Creek (Figure 1, T3S/R28E-13) are located in a small narrow canyon near the head of the creek; above the springs there is no perennial flow in the channel. Four main spring orifices discharge a total of about 12 l/s of thermal water at 68°C to 82°C into Little Hot Creek. Most of the flow disappears beneath the ground surface within about 0.8 km downstream from the hot springs and continues as underflow along a broad channel until it mixes with water from Hot Creek flowing toward the Owens River. Some variation in the flow of these springs has been observed during the period of this investigation, possibly in response to continuing tectonic activity or seasonal hydrologic events.

Fish Hatchery Springs

About eight main spring orifices make up the spring group at the California State Fish Hatchery (Figure 1, T3S/R28E-35). These springs are classified as thermal with temperatures between 12.5°C and 17°C throughout the year and are ideally suited for the raising of rainbow trout at the hatchery. The fish hatchery springs discharge about 570 l/s and comprise about 74% of the total thermal spring discharge in Long Valley. The actual amount of hot geothermal water contributed by these springs is small, however, and amounts to only about 7% of the total (see Table 3).

Alkali Lakes Springs

Springs in the vicinity of Big Alkali Lake and Little Alkali Lake (Figure 1) generally show low discharge between 0.07 and 2.5 l/s and moderate temperatures between 39°C and 63°C. Many of the very low discharge springs do not discharge at the surface but form seeps, and the entire area is one of broad flat grass-covered sometimes marshy terrain. Even in some of the moderately discharging springs, surface flows are not apparent for any great distance as the water quickly percolates into the unconsolidated sediments and joins the shallow groundwater in its movement toward Lake Crowley.

The existence of the Alkali lakes is evidently due in part to the near-surface water table in that area. The total measured and estimated warm spring discharge of about 12.7 l/s is insufficient to sustain the lake levels, particularly during the summer months. The high groundwater table remains fairly constant, being replenished by the subsurface discharge from the hot springs and subsurface inflow from Hot Creek.

Whitmore Hot Springs

Whitmore Hot Springs is located about 1.6 km from U.S. Highway 395 along the road to Owens River (Figure 1, T4S/R29E-6). Referred to in the early description of *Waring* [1915] as Whitmore Tub, the springs were later developed into a spa with the construction of several concrete pools, a bath house, and several other structures. With the development of bathing facilities at Hot Creek the Whitmore spa was shut down and has remained closed since. In the Whitmore group there are two large main spring openings and two small ones. The temperature and discharge of these springs have remained constant over the years. In the two large pools, *Waring* [1915] measured a maximum temperature of 38°C and a discharge of 28 l/s at the same time that the two smaller spring openings had equal discharge of 0.5 l/s and temperatures of 23.5°C and 37.8°C. Recent data by *Lewis* [1974] indicate a combined discharge of 25 l/s and temperatures of 32.5°C and 34.5°C in the two large springs and a discharge of 0.8 l/s and temperatures of 27°C and 35°C in the two small springs.

Other Spring Discharge

Several other springs or spring groups exist in the Long Valley caldera which have significant flow but contribute little water from the geothermal system because of the dilute nature of their waters. The Chance Springs (Figure 1, T3S/R28E-33) issue along the bank of Mammoth Creek several hundred meters downstream from U.S. Highway 395. About 23 l/s of water at 22.5°C discharge from three orifices formed by cooling joints in the basalt.

Between the Alkali lakes and Lake Crowley, about 17 springs discharge along a nearly east-west line (Figure 1, T3S/R29E-27, 28). The discharge of these springs is low, between 0.1 and 3.2 l/s, and the temperatures range between 18°C and 49°C. In addition to the springs, numerous seeps exist along the same line between the road and the lake. This broad grassy area is similar in appearance to the area around the Alkali lakes.

Big Springs (Figure 1, T2S/R27E-25) discharges water at about 11°C which flows into the upper Owens River near the northwest rim of the caldera. Although not measured in recent investigations, the discharge was estimated at about 6 l/s. Samples from this spring and other cold water springs provided data on the chemical characteristics of the shallow groundwater which mixes with the hot spring water.

MIXING MODELS

Variations in the chemical composition and temperature of thermal spring waters in Long Valley suggest that the hot water rising from depth is mixed with and diluted by cooler water from shallow aquifers before being discharged at the land surface. In addition, surface discharge conditions are affected by boiling in the upflowing column and heat conduction in the surrounding rocks. Thus to evaluate the amount and heat content of the hot water moving through the system, the effects of mixing, boiling, and conduction must be accounted for.

Methods

Several chemical techniques have been described by *Fournier and Truesdell* [1973, 1974] and *Fournier et al.* [1974] for estimating the temperature of water in geothermal reservoirs and the fraction of hot water mixed with cold water in hot spring systems. *Mariner and Willey* [1976] discuss the geochemistry of thermal water in Long Valley and the application of geothermometers on the basis of concentrations of silica and the cations sodium, potassium, and calcium. Their results show that calculations of reservoir temperatures based on the cation ratios were consistently higher and hence less affected by mixing than were the silica temperatures.

Mixing calculations based on the model of *Fournier and Truesdell* [1974] require data on the silica concentration and temperature of the mixed spring water and the cold fresh water. Results for samples from springs in Hot Creek Gorge and along Little Hot Creek give temperature estimates ranging from 170°C to 225°C [*Mariner and Willey,* 1976]. The range in temperature is due in large part to uncertainty as to the characteristics of the fresh water component.

An alternative mixing model, proposed by *Truesdell and Fournier* [1975], utilizes the ratio of the chloride concentration in the mixed water to the chloride concentration in the unmixed hot water to correct the silica geothermometer temperature and compute the mixing ratio. From a chloride balance the mixing ratio or the fraction of the total discharge which is from the hot water source is computed as

$$X = (Cl_m - Cl_c)/(Cl_h - Cl_c) \quad (1)$$

where X is the mixing ratio, Cl_m is the chloride concentration of mixed spring water, Cl_c is the chloride concentration of the cold water component, and Cl_h is the chloride concentration of the hot water component. If the spring is boiling, the chloride concentration at the surface must be corrected for the concentrating effect of boiling to obtain Cl_m. Otherwise, Cl_m is equal to the chloride concentration at the surface. In the Long Valley area the concentration of chloride in the nonthermal springs ranges from 1 to 6 mg/l compared with 280 mg/l in the hot water, as is discussed in the next section.

The enthalpy of the hot water source is computed as

$$h_h = (h_m - h_c)/X + h_c \quad (2)$$

where h_h is the enthalpy of the hot water source, h_m is the enthalpy of the mixed spring water, and h_c is the enthalpy of the cold water component. The enthalpy of the mixed spring

TABLE 1. Geochemical Data From Samples of Long Valley Hot Springs

Spring or Spring Area	Discharge, l/s	Surface Temperature T, °C	Boron, mg/l	Chloride, mg/l	T_{Si}, °C	$T_{Na-K-Ca}$, °C
Hot Creek Gorge*	6.7	90	10.3	225	153	192
Little Hot Creek	12.0	80	10.6	200	143	172
Casa Diablo Hot Pool	6.5†	60	13.0	250	209	189
Whitmore Hot Springs	26.0	34	3.5	74	75	...
Big Alkali Lake‡	8.8	56	7.7	150	196	200
Little Alkali Lake	3.8	66	8.8	200	150	...
Chance Spring	23.0	20	1.8	40	100	...
T3S/R29E-27, 28	3.8	49	8.6	150	193	200
T3S/R29E-34K	1.8	41	6.2	130	182	184
T3S/R29E-31A	1.5	58	8.1	176	161	176

*New spring discharging from bank.
†Calculated from evaporation rate.
‡Sample 3S/29E-21 PS1 [*Mariner and Willey*, 1976].

water is based on the temperature obtained from the silica geothermometer calculation, when no mixing is assumed. Where the mixing ratio is greater than about 0.7, the enthalpy of the cold water component in (2) can be neglected to yield

$$h_h = h_m/X \tag{3}$$

In the case of the springs along Hot Creek Gorge, most of the discharge occurs below the stream surface, a situation making discharge measurements and sampling impractical by standard techniques. Consequently, a seepage gain technique was used in this area and for the springs at the fish hatchery. Measurements of water discharge, temperature, and concentrations of boron and chloride were made above and below the hot springs to compute the net gain of boron and chloride by using

$$B_m = (B_2Q_2 - B_1Q_1)/(Q_2 - Q_1) \tag{4}$$

$$Cl_m = (Cl_2Q_2 - Cl_1Q_1)/(Q_2 - Q_1) \tag{5}$$

where B_1 and Cl_1 are the boron and chloride concentrations of the stream above the springs, respectively, B_2 and Cl_2 are the boron and chloride concentrations of the stream below the springs, respectively, Q_1 is the volumetric flow rate of the stream above the springs, and Q_2 is the volumetric flow rate of the stream below the springs. Boron and chloride were chosen as the constituents to be used because they are characteristic of water of volcanic association [*White*, 1957*a*, *b*] and are least likely to be affected by chemical precipitation, base exchange, and other factors [*White*, 1968, p. 83]. As is seen in subsequent tables, calculations of boron and chloride concentrations from the seepage gain technique agree well with data from a spring sample taken along the bank in Hot Creek Gorge.

In the results that follow, the component of the spring discharge which is of geothermal origin is computed from (1) by using boron and chloride concentrations for each of 11 spring systems with significant discharges. With the exception of the Hot Creek Gorge springs the discharge temperatures of these springs are well below 90°C, and hence the effects of boiling have been neglected. The magnitude of the boiling effect is considered later for the Hot Creek springs. Hot water temperatures were first computed from the silica and cation geothermometers and then corrected by using the mixing models as indicated in Table 3.

Thermal Water

Hot waters discharging in the Long Valley springs may originate from one regionally continuous reservoir or from several zones at various depths. In the course of this investigation a core hole to 305 m was drilled inside the caldera about 1.6 km northeast of Hot Creek Gorge. No evidence of a permeable reservoir with hot water was found. However, extrapolation of the measured temperature gradient of about 200°C/km indicated that water with temperatures in excess of 200°C might be found at depths near 1 km.

Ten geothermal wells were drilled at Casa Diablo hot springs by the Magma Power Company between 1959 and 1964 to a maximum depth of 324 m. Maximum temperatures of 177°C were found at a depth of 120 m [*McNitt*, 1963, p. 28]. Temperatures decrease below 120 m, a fact suggesting that the wells penetrate a fault underlying the Casa Diablo area and that hot water moving up the fault is intercepted by the wells at the 120-m depth. Thus water sampled from these wells may be relatively unmixed, although the measured temperatures may be below temperatures in the reservoir because of conductive cooling as the water moves up the fault.

Water sampled from one of the wells during the course of this investigation contained 280 mg/l of chloride and 15 mg/l of boron [*Willey et al.*, 1974]. The temperature of this water at depth, based on its silica content, is 220°C. Earlier analyses reported 276 mg/l [*McNitt*, 1963] and 285 mg/l of chloride and 13 mg/l of boron [*California State Department of Water Resources*, 1967] as average values for 11 samples. For the purposes of this paper it will be assumed that the geothermal waters underlying the hot spring areas in the caldera average 14 mg/l of boron and 280 mg/l of chloride. Constant Cl/B ratios [*Mariner and Willey*, 1976] and hot water temperatures from mixing model calculations consistently near 200°C indicate that the same hot water aquifer supplies each of the

TABLE 2. Results of Seepage Gain Measurements for Springs at Hot Creek Gorge and the Fish Hatchery

	Discharge, l/s	Calculated Concentration, mg/l	
		Boron	Chloride
Hot Creek Gorge			
October 17, 1972	303	9.23	199
January 17, 1973	218	12.28	221
March 25, 1973	227	9.33	220
April 17, 1973	275	9.06	225
September 25, 1973	212	15.29*	248
Average	247	11.04	223
Fish Hatchery			
October 17, 1973	843	0.25	4.8
September 25, 1973	1085	0.23	4.6
Average	964	0.24	4.7

*Calculated concentration exceeds upper limit established for boron in Long Valley thermal water.

major thermal springs in the caldera. However, the extent of regional continuity to this reservoir is as yet unknown. The area of present hot spring activity covers only about 15% of the total caldera area.

Geochemical Data

Table 1 presents pertinent geochemical data from samples of the major hot springs in Long Valley. Geothermometer calculations for springs with discharge temperatures greater than 90°C assume adiabatic cooling by boiling, whereas for springs with temperatures less than 90°C, conductive cooling is assumed.

Results of the seepage gain measurements for the springs at Hot Creek Gorge and the fish hatchery are shown in Table 2. The averages of calculated concentrations of boron and chloride for the Hot Creek springs are in close agreement with measured concentrations in Table 1 for the sample from the new spring along the bank.

Table 3 lists the results of mixing calculations for thermal water discharges and temperatures. The estimate of total discharge of hot water is 248 l/s from both boron and chloride calculations. Of this, approximately 80% is contributed by the springs in Hot Creek Gorge. Calculated temperatures of the hot water range from 184°C to 225°C and average 204°C.

CONVECTIVE HEAT DISCHARGE

Heat Content of Thermal Water

Hot water discharging in the Long Valley thermal springs is primarily of meteoric origin [*White*, 1968]. The water must be heated from approximately mean annual air temperature to temperatures in excess of 200°C by conduction from the surrounding rocks as it moves through the system. When a mean annual air temperature of 10°C and a reservoir temperature of 210°C are assumed, on the basis of the data in Table 3, the gain in heat content of the water can be calculated as

$$C = \rho_{210°}(h_{210°} - h_{10°})$$

$$= 0.86 \text{ g/cm}^3\ (214 - 10) \text{ cal/g} = 175 \text{ cal/cm}^3$$

where C is the gain in heat content per unit volume, ρ is fluid density, and h is fluid enthalpy.

As this water moves upward toward the discharge areas, heat is removed from the thermal reservoir at a rate given by

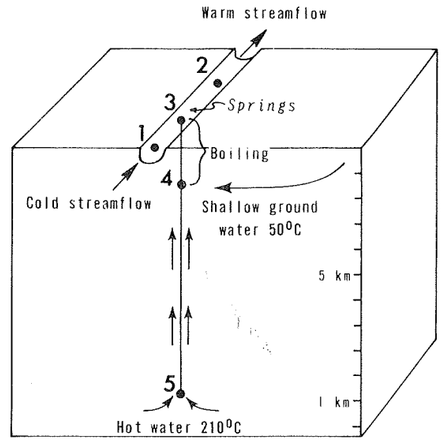

Fig. 2. Diagram of Hot Creek Gorge spring system.

CQ, where Q is the volumetric flow rate of hot water. From Table 3, Q = 248 l/s. Thus our estimate of the convective heat discharge from the system is 4.3×10^7 cal/s. *White* [1965, p. 7] used an estimate of the annual discharge of boron into Lake Crowley of 181 metric tons per year and assumed a boron concentration of 11 mg/l to compute a discharge of thermal water equal to 520 l/s. He then assumed a conservative reservoir temperature of 150°C to compute a total convective heat flow from the Long Valley springs of 7×10^7 cal/s. The difference between the two estimates of heat flow is due in part to subsurface discharge of hot water which was not measured in the present study. However, data obtained from the Los Angeles Department of Water and Power for the period 1960–1973 show an average discharge of boron from sources within the caldera of 136 metric tons per year. If we use this figure and a concentration of 14 mg/l, the hot water discharge would be 306 l/s. If we assume a reservoir temperature of 210°C, the convective heat flow estimate would be 5.4×10^7 cal/s or about 25% greater than the estimate based on measurements at individual hot springs.

TABLE 3. Summary of Hot Water Discharge From Long Valley Hot Springs

Spring	Discharge of Hot Water, l/s: With 14.0 mg/l B	With 280 mg/l Cl	Temperature of Hot Water, °C
Hot Creek Gorge	195.0	197.0	210*†
Fish hatchery	16.5	16.2	...
Little Hot Creek	9.0	8.5	214*
Whitmore Hot Springs	6.8	6.7	...
Casa Diablo Hot Pool	6.0	5.8	189‡
Big Alkali Lake	4.8	4.7	200‡
Chance Springs	3.2	3.2	...
Little Alkali Lake	2.7	2.5	210*
T3S/R29E-27, 28	2.0	2.0	200‡
T3S/R29E-34K	0.8	0.8	184‡
T3S/R29E-31A	0.8	0.8	225†
Total	248	248	

*Based on Si-Cl mixing model (A. H. Truesdell, personal communication, 1974).
†Based on Si mixing model [*Fournier and Truesdell*, 1974].
‡Based on Na-K-Ca geothermometer [*Fournier and Truesdell*, 1973].

Heat Balance for Hot Creek Gorge Springs

Because approximately 80% of the convective heat discharge from the caldera is from the springs along Hot Creek Gorge, it is of interest to consider this particular system in more detail. We wish to quantify the effects of conductive cooling, mixing, and boiling on the heat content of the upflowing water. A simplified diagram of the system is shown in Figure 2. From the seepage gain measurements at points 1 and 2 we have calculated an average spring flow of 247 l/s at a boiling temperature of 90°C at point 3 (Table 2). We also have an estimate of 196 l/s of hot water with a temperature of 210°C at point 5 (Table 3). The corresponding heat fluxes are 3.4×10^7 cal/s at point 5 and 1.9×10^7 cal/s at point 3. Thus a net loss of 1.5×10^7 cal/s occurs as the water flows to the land surface.

Considering first the conductive heat loss to the surrounding rocks, we note that the amount of heat lost and the resultant temperature drop in the fluid depend strongly on the geometry of the upflow channel. At one extreme would be a conduit whose lateral dimensions have been limited, say, by mineral deposition to an area similar to that of the spring discharge area. At the other extreme would be the slab configuration in

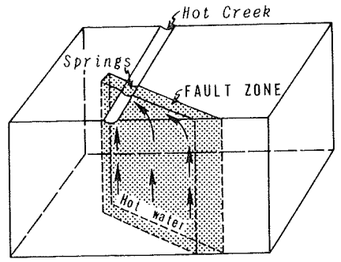

Fig. 3. Slab model for spring flow in Hot Creek.

Figure 3 which is suggested by the surface expression of the faults intersecting the gorge area and the evidence of hydrothermally altered rock along the faults at some distance from the gorge [*Bailey*, 1974]. With a lateral extent to the fault plane of 1 km and a depth of 1 km the heat loss from the plane would be considerably greater than that from the conduit.

From hydraulic considerations the fault plane model seems more likely. For example, Table 4 lists pressures in excess of hydrostatic pressure necessary to yield an upflow of 200 l/s for various combinations of area and permeability. The total head difference from artesian (elevation) and thermal artesian (density) effects is of the order of 300 m, although it is likely that only a fraction of this is available at point 5. From Table 4, unless the permeability of the fractured zone is considerably larger than 10 darcys, the available head would be insufficient for the cylindrical model but adequate for the slab model.

Numerical simulations of conductive cooling in upflowing hot spring systems, as described by *Sorey* [1975], can be used to estimate the temperature drop as a function of mass flow rate for the cylindrical conduit and fault plane models. For a flow rate of 200 l/s and the same dimensions as those used in Table 4 the temperature drop in the cylinder would be negligible, whereas the temperature drop in the fault plane would be about 10°C, with a corresponding conductive heat loss of 10^6 cal/s. Under steady state conditions this heat flows out at the land surface within a distance equal to about one conduit depth away from the spring.

On the assumption, then, that the hot water cools from 210°C to 200°C as it flows up to the shallow groundwater system, boiling would begin at a depth of about 160 m. There is evidence from cores and geophysical logs in the test well, located 1.6 km northeast of Hot Creek Gorge, of a permeable zone at 140 m which could provide water for mixing at point 4 in Figure 2 [*Lachenbruch et al.*, 1976]. The temperature at this depth in the test well is about 50°C. If this zone is the source of fresh water which dilutes the spring water and its boron and chloride concentrations are close to those in the nonthermal springs, we can calculate a mixing ratio of 0.80, using (1) and the boron and chloride concentrations in Table 2. The temperature of the mixture at point 4 would then be 160°C. Above this point, boiling would reduce the liquid flow rate by about 13%, and the formation of steam would account for about 1.8 $\times$ 10^7 cal/s of heat loss from the water as its temperature drops from 160°C to 90°C at the surface (point 3). This leaves a convective heat flow with the liquid discharge at point 3 of 1.9 $\times$ 10^7 cal/s, as was indicated previously. The fate of the steam which forms is uncertain. If it recondenses in the stream, then the heat added at this point would be closer to 3.9 $\times$ 10^7 cal/s. However, temperature and discharge measurements downstream at point 2 average 25°C and 1270 l/s in the fall and winter and 16°C and 3680 l/s during the spring runoff period. This represents a heat flow of between 1.9 $\times$ 10^7 cal/s and 2.2 $\times$ 10^7 cal/s and suggests that the steam either discharges as vapor at the land surface or recondenses in the shallow groundwater below the creek.

Conductive Heat Flow Requirements

Before considering the significance of our estimate for the convective heat discharge from the Long Valley thermal springs we first note some inherent assumptions in the chemical methods used in its derivation. Essentially, we have assigned a quantity of heat to various ions in the thermal spring waters and assumed a degree of regional continuity to a reservoir at depth in terms of uniform concentrations of B and Cl in the hot water underlying the area of hot spring discharge. Further, we refer to this estimate as the gain in heat content, assuming that the source of water was meteoric. In this regard it is possible that the thermal water includes a component of magmatic origin to account for the high concentrations of elements such as boron, chloride, and arsenic, as discussed by *White* [1968] for the Steamboat Springs, Nevada, area and by the *California State Department of Water Resources* [1967] for the Long Valley area. Thus an unknown portion of the heat gained by the circulating meteoric water could be supplied by this fluid of magmatic origin.

With these assumptions in mind, we note that our estimate for the convective heat discharge of 4.3 $\times$ 10^7 cal/s is somewhat less than the estimates based on boron discharge in Lake Crowley, a result suggesting that 4.3 $\times$ 10^7 cal/s is a minimum value which does not account for some subsurface discharge of hydrothermal water. The significance of this estimate can be seen by calculating from a simple hot plate model that if the heat gained by the circulating fluid at a rate of 4.3 $\times$ 10^7 cal/s were supplied conductively to a reservoir covering the entire caldera area of 450 km², an average heat flux of about 10 HFU would be required. For a reservoir of smaller lateral extent the required heat flux would be correspondingly greater. If similar rates of heat removal have persisted for a significant portion of the eruptive history of the caldera, the above calculations place constraints on the nature and intensity of the conductive heat source underlying the caldera, as is discussed by *Lachenbruch et al.* [1976]. Further test drilling to obtain additional thermal, hydrologic, and geochemical information is needed before a satisfactory model of the hydrothermal system and its related heat source is possible.

TABLE 4. Pressures Required to Cause Flow of 200 l/s Through Hot Creek Gorge Spring System

Model	Area Cross Section, m²	Permeability, darcys	Pressure Above Hydrostatic, bars	Head,* m
Cylinder	176	1	1,600	19,000
(diameter, 15 m)	176	10	160	1,900
Plane	16,000	1	17	210
(1.6 km $\times$ 10 m)	16,000	10	1.7	21

The depth of the spring system is 1 km, and its temperature is 210°C.
*Head is defined as pressure/ρg.

REFERENCES

Bailey, R. A., Preliminary geologic map and cross-sections of the Casa Diablo geothermal area, Long Valley caldera, Mono County, California, open file report, 2 pp., U.S. Geol. Surv., Reston, Va., 1974.

Bensemen, R. F., Estimating the total heat output of natural thermal regions, *J. Geophys. Res., 64*(8), 1057–1062, 1959.

Blake, A. H., and F. E. Matthes, The new Casa Diablo 'geyser,' *Sierra Club Bull., 23*(2), 82–83, 1938.

California State Department of Water Resources, Investigation of geothermal waters in the Long Valley area, report, 141 pp., Mono County, Calif., 1967.

Fournier, R. O., and A. H. Truesdell, An empirical Na-K-Ca geothermometer for natural water, *Geochim. Cosmochim. Acta, 37*, 1255–1275, 1973.

Fournier, R. O., and A. H. Truesdell, Geochemical indicators of subsurface temperature, 2, Estimation of temperature and fraction of hot water mixed with cold water, open file report, 43 pp., U.S. Geol. Surv., Reston, Va., 1974.

Fournier, R. O., D. E. White, and A. H. Truesdell, Geochemical indicators of subsurface temperature, 1, Basic assumptions, *U.S. Geol. Surv. J. Res., 2*(3), 259–262, 1974.

Lachenbruch, A. H., M. L. Sorey, R. E. Lewis, and J. H. Sass, The near-surface hydrothermal regime of Long Valley caldera, *J. Geophys. Res., 81*, this issue, 1976.

Lee, W. T., Geology and water resources of Owens Valley, California, *U.S. Geol. Surv. Water Supply Pap. 181*, 28 pp., 1906.

Lewis, R. E., Data on wells, springs, and thermal springs, in Long Valley, Mono County, California, open file report, 52 pp., U.S. Geol. Surv., Reston, Va., 1974.

Mariner, R. H., and L. M. Willey, Geochemistry of thermal waters in Long Valley, Mono County, California, *J. Geophys. Res., 81*, this issue, 1976.

McNitt, J. R., Exploration and development of geothermal power in California, *Spec. Rep. 75*, 44 pp., Calif. Div. of Mines and Geol., Sacramento, Calif., 1963.

Rinehart, C. D., and D. C. Ross, Geology and mineral deposits of the Mount Morrison quadrangle, Sierra Nevada, California with a section on: A gravity study of Long Valley by L. C. Pakiser, *U.S. Geol. Surv. Prof. Pap. 385*, 106 pp., 1964.

Russell, I. C., Quaternary history of Mono Valley, California, Eighth Annual Report of the United States Geological Survey, 1886–87, compiled by J. W. Powell, pp. 261–394, U.S. Geol. Surv., Reston, Va., 1889.

Sorey, M. L., Numerical modeling of liquid geothermal systems, Ph.D. dissertation, Univ. of Calif., Berkeley, 1975.

Stearns, N. D., H. T. Stearns, and G. A. Waring, Thermal springs in the United States, *U.S. Geol. Surv. Water Supply Pap. 679-B*, 59–206, 1937.

Truesdell, A. H., and R. O. Fournier, Calculation of deep reservoir temperatures from chemistry of boiling hot springs of mixed origin, paper presented at 2nd Symposium on Development and Use of Geothermal Resources, United Nations, San Francisco, Calif., May 20–29, 1975.

Waring, G. A., Springs of California, *U.S. Geol. Surv. Water Supply Pap. 338*, 410 pp., 1915.

White, D. E., Thermal waters of volcanic origin, 1, *Geol. Soc. Amer. Bull., 68*(12), 1637–1658, 1957*a*.

White, D. E., Magmatic, connate, and metamorphic waters, 1, *Geol. Soc. Amer. Bull., 68*(12), 1659–1682, 1957*b*.

White, D. E., Geothermal energy, *U.S. Geol. Surv. Circ. 519*, 17, 1965.

White, D. E., Hydrology, activity, and heat flow of the Steamboat Springs thermal system, Washoe County, Nevada, *U.S. Geol. Surv. Prof. Pap. 458-C*, 109 pp., 1968.

Willey, L. M., J. R. O'Neil, and J. B. Rapp, Chemistry of thermal waters in Long Valley, Mono County, California, open file report, 19 pp., U.S. Geol. Surv., Reston, Va., 1974.

(Received January 15, 1975;
revised August 22, 1975;
accepted September 12, 1975.)

Geochemistry of Thermal Waters in Long Valley, Mono County, California

ROBERT H. MARINER AND LAWRENCE M. WILLEY[1]

U.S. Geological Survey, Menlo Park, California 94025

Thermal springs and wells in Long Valley, California, issue sodium bicarbonate–chloride waters containing 1000–1420 mg/l of dissolved solids. Thermal waters of sodium bicarbonate–chloride composition are usually associated with hot-water reservoirs. Chloride concentrations and stable isotope data indicate that the thermal waters have had varied histories. All of the thermal springs issue a mixture of fluid from the thermal reservoir and less saline, cooler water from one or more shallow aquifers. The composition of springs in Hot Creek Gorge may have been further altered by minor subsurface boiling. Thermal springs between Hot Creek and Lake Crowley issue mixtures of fresh and thermal waters which have lost heat by conductive cooling and changed composition by reaction with rock in the shallow aquifer. The silica content of water from Magma Richie 5 and mixing calculations based on the concentrations of silica in thermal waters collected from springs in Hot Creek Gorge and along Little Hot Creek indicate a temperature of at least 200°C in the thermal reservoir. The sodium-potassium-calcium geothermometer yields a reservoir temperature estimate near 200°C for most of the thermal springs. If geothermal energy is developed in Long Valley, the high concentrations of arsenic (up to 2.2 mg/l), boron (up to 15 mg/l), and total dissolved solids in the thermal fluids will make it necessary to isolate the effluent of production wells from the freshwater system.

INTRODUCTION

The chemical composition of water from thermal springs and wells provides an indication of the temperature of the fluid in the reservoir and of the type of thermal system. The distinctive physical and chemical characteristics of hot-water and vapor-dominated systems have been discussed by *White et al.* [1971]. Hot-water systems occur in permeable rock, whereas vapor-dominated systems occur in impermeable rock. Springs associated with hot-water systems discharge chloride-rich water at an aggregate rate of several hundred to several thousand liters per minute. Individual springs associated with the hot-water system, however, may discharge as little as a few liters per minute, and low chloride, acid sulfate springs formed by steam separation may occur with the chloride-rich springs. Springs associated with vapor-dominated systems usually discharge acid sulfate waters at rates of less than 100 l/min. Some near-neutral sodium bicarbonate springs with less than 20 mg/l of chloride may also be associated with vapor-dominated systems. Although qualitative indicators of temperature in the thermal reservoir have been suggested by *Ellis* [1970], *Mahon* [1970], *Tonani* [1970], and *Fournier and Truesdell* [1970], only two quantitative geothermometers have been demonstrated to have widespread application. These quantitative geothermometers are based on silica concentration [*Fournier and Rowe,* 1966; *Mahon,* 1966] and the proportions of sodium, potassium, and calcium in the thermal fluid [*Fournier and Truesdell,* 1973]. Another quantitative geothermometer, based on the ratio of sodium to potassium [*Ellis,* 1970; *White,* 1965], has been largely superseded by the Na-K-Ca geothermometer. Qualitative chemical indices such as $Cl/(HCO_3 + CO_3)$ are, however, useful in delineating subsurface flow direction in thermal systems [*Fournier and Truesdell,* 1970; *Truesdell,* 1975].

Dilution of thermal water by fresh water (mixing) has been demonstrated in several ways. A proportional relationship between chloride concentration and spring temperature may be an indication of mixing [*Fournier and Truesdell,* 1974]. *Fournier et al.* [1974] have stated that springs of large flow rate, more than 100 l/min, should be considered to be issuing mixed water if the Na-K-Ca geothermometer indicates a reservoir temperature more than 25°C above the measured spring temperature. *Giggenbach* [1971] has demonstrated linear relationships between chloride concentrations and the isotope ratios of hydrogen and oxygen in the mixed waters of the Broadlands geothermal field.

The first detailed chemical sampling for water quality in Long Valley was carried out by the *California Department of Water Resources* [1967] to determine the effect of geothermal development on water quality in Long Valley and indirectly the impact of such development on the water supply for Los Angeles. The state report noted that (1) the fresh waters outside the caldera are calcium bicarbonate in character and have very low total dissolved solids; (2) the hot springs issue sodium bicarbonate to sodium bicarbonate–chloride waters, high in total dissolved solids, bicarbonate, chloride, and the trace elements boron, arsenic, and fluoride; (3) the alkali lakes contain sodium bicarbonate to sodium carbonate waters; and (4) the warm springs and shallow groundwater are intermediate between fresh and hot spring water in chemical characteristics. In the state report it was concluded that discharge of geothermal waste waters rich in arsenic, fluoride, and boron to Lake Crowley and its tributaries could cause serious degradation of the water quality and constitute a threat of pollution to the water supply of the Los Angeles–Owen River Aqueduct as well as the local water resources. Magma Power Company and its affiliates drilled some 20 exploratory wells to as much as 300-m depth in the vicinity of Casa Diablo Hot Springs during the period extending from 1959 to 1962. Temperatures up to 177°C were encountered in some of the wells.

The general water quality of Long Valley is described in the state report. However, no special care was taken in preparing water samples for silica, calcium, or bicarbonate. Recent sampling by *Willey et al.* [1974], which forms the basis for this report, was concentrated on the geothermally important constituents of silica, principal cations, gas composition, and isotope ratios of oxygen and hydrogen in the major hot springs.

[1]Now at Pent-A-Vate, Inc., Lindsay, California 93247.

Lewis [1974] has compiled the available chemical and hydrologic data for Long Valley.

METHODS AND PROCEDURES

Water samples were collected at points as close as possible to the orifice of the thermal springs or wells. If several springs issued in the same area, the spring with the highest temperature, specific conductance, and flow rate was sampled. Water was collected in a 12-l stainless steel pressure vessel and immediately pressure-filtered through a membrane filter of 0.45-μm effective pore diameter using nitrogen as a pressure source. The filtered water samples were collected and stored in plastic bottles which had been washed with acid prior to use. Ten milliliters of filtered sample were diluted to 100 ml with distilled deionized water to prevent the polymerization of silica. Samples for isotopic analyses were collected in glass bottles with polyseal caps.

Field determinations were made of barometric pressure, water temperature, conductivity, *p*H, and alkalinity. Water temperatures were determined with a thermistor probe while the conductivity was measured in the spring using a conductivity bridge with a temperature compensator. The *p*H was measured directly in the spring, and alkalinity was determined immediately after the sample was withdrawn from the spring [*Barnes,* 1964]. The water sample from Magma Richie 5 was not flashed to atmospheric pressure as are most water samples collected from 'wet' steam wells. The well was fully opened and allowed to flow for 4 hours previous to sampling. The well was then closed and 8 m of 0.64-cm-ID aluminum tubing was attached to the sampling valve on the well head. This tubing was coiled and placed in a 30-gal. (133-l) oil drum which was filled with crushed ice. The well was then reopened, and the steam and hot water issuing from it were cooled to 2°C. The resulting fluid was collected in a 12-l pressure vessel and treated as described above.

SAMPLE LOCATIONS

Surface expressions of thermal activity in Long Valley extend from Casa Diablo Hot Springs along Hot Creek through Hot Creek Gorge. Other hot springs issue along Little Hot Creek 3.2 km north of Hot Creek Gorge, and between Hot Creek and Lake Crowley (Figure 1).

Two freshwater samples were collected from Big Spring near Lookout Mountain, northwest quadrant, section 25, T. 2S, R. 27E, and an artesian well in the northwest quadrant, section 13, T. 3S, R. 29E.

WATER COMPOSITION

Hot springs in Long Valley discharge slightly saline sodium bicarbonate–chloride water. The chemical composition of hot springs sampled for detailed chemical analysis is given in Table 1. Cool fresh waters, springs 2SAS1 and the artesian well 13C1, issue nonsaline sodium bicarbonate waters (150 μmho). The fresh waters contain proportionally more calcium, more magnesium, and less chloride than the thermal spring waters (Figure 2). The *California Department of Water Resources* [1967] reported that in Long Valley the proportions of chloride and sodium increase as the total dissolved solids increase.

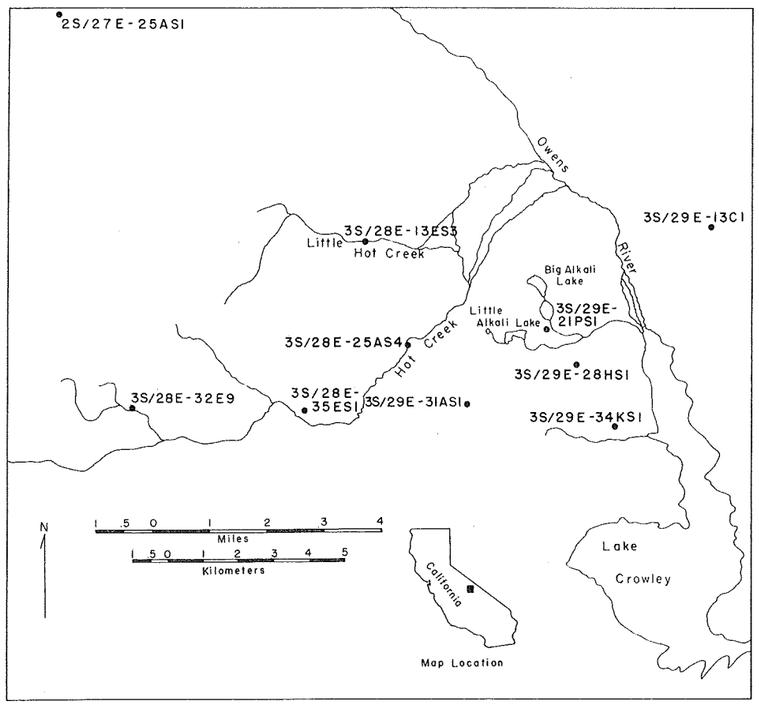

Fig. 1. Index map showing the locations of springs and wells sampled for detailed chemical analysis, Long Valley, California. The spring issuing in Hot Creek Gorge, designated 3S/28E-25AS4, was collected during August 1973. All other samples were collected during May 1972.

TABLE 1. Major Constituents of Selected Thermal and Meteoric Waters From Long Valley, California

	U.S. Public Health Water Standard Limits (Drinking Water)	3S/28E-13ES3	3S/28E-32E9	3S/28E-35ES1	3S/28E-21PS1	3S/29E-28HS1	3S/29E-31AS1	3S/29E-34KS1	3S/28E-25AS4	2S/28E-25AS1	3S/29E-13C1
Sodium (Na)		410	390	380	310	400	310	320	400	23	38
Potassium (K)		30	45	25	37	43	22	28	24	4.0	1.3
Calcium (Ca)		50	0.9	3.3	25	22	15	23	1.6	5.1	5.3
Magnesium (Mg)	125	0.6	0.1	0.1	0.6	0.6	0.4	1.2	0.1	5.9	0.2
Carbonate (CO_3)*		0.3	16.6	0.7	0.3	0.3	1.9	0.3	24.0	0	2.8
Bicarbonate (HCO_3)*		735	416	466	828	845	516	695	549	90	111
Sulfate (SO_4)	250	96	130	120	68	69	81	59	100	8.1	3.7
Chloride (Cl)	250	200	280	250	150	170	170	150	225	5.7	3.0
Lithium (Li)		2.8	2.8	2.5	1.5	1.7	2.0	1.6	2.3	0.04	0.14
Boron (B)		10.6	15	13	7.7	8.8	7.9	8.1	10.5	0.37	0.18
Fluoride (F)	1.7	8.4	12	11	4.6	4.8	7.5	4.6	9.6	0.5	0.6
Silica (SiO_2)		110	340	300	250	240	150	205	150	58	64
Arsenic (As)	0.01	0.74	2.2	0.34	0.46	0.34	0.84	0.36	···	0.02	0.02
Ammonia (as N)		0.40	0.40	0.15	0.20	0.10	0.09	0.15	···	0.13	0.35
Rubidium (Rb)		0.26	0.48	0.28	0.11	0.14	0.19	0.08	···	0.01	<0.01
Sulfide, total (H_2S)		2.3	10	1.4	0.8	0.7	0.8	0.9	···	<0.1	3.8
*p*H		6.5	9.2	7.2	7.9	6.5	6.6	7.5	6.6	6.8	8.8
Temperature, °C		79	94	60	56	49	58	41	90	11	10
Specific conductance, μmho at 25°C		1950	1920	1800	1770	1790	1900	1500	1630	182	191

Analysts were L. M. Willey, J. B. Rapp, and T. S. Presser.
Concentrations are in milligrams per liter.
*Total alkalinity distributed as carbonate (CO_3) and bicarbonate (HCO_3).

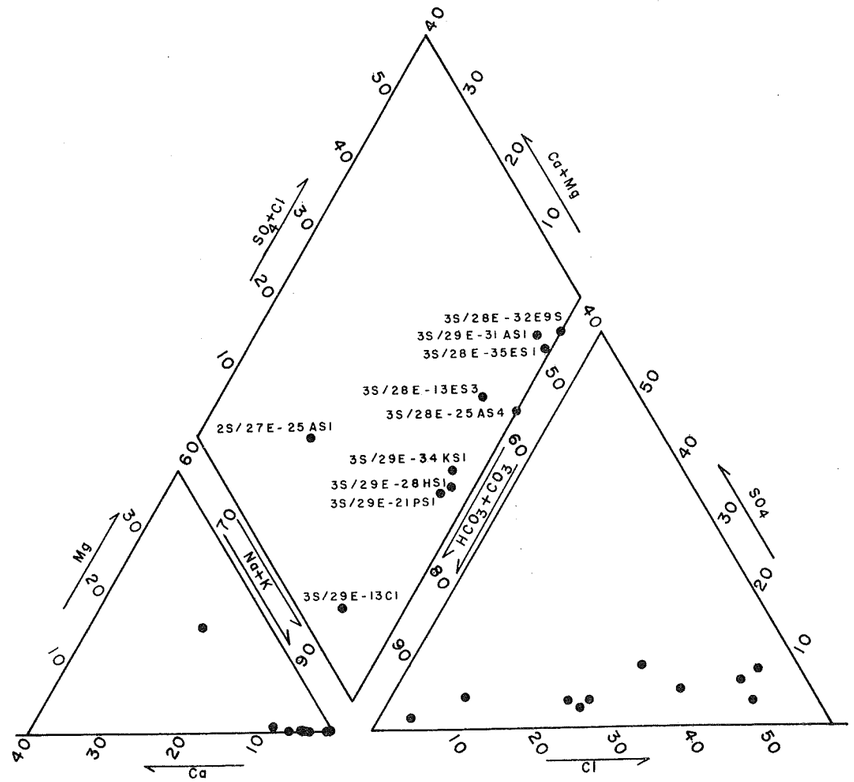

Fig. 2. Modified trilinear plot of waters collected for detailed analysis, Long Valley, California.

Progressing from the fresh waters to thermal waters, a marked decrease occurs in the proportion of the divalent cations, especially calcium, relative to the monovalent cations sodium and potassium.

Ratios of elements which may be useful in determining flow direction and extents of solution-rock interaction have varying patterns of distribution (Table 2). The high ratios of Cl/Ca and Cl/Mg in thermal waters from along Hot Creek are probably due to the loss of carbon dioxide and the precipitation of calcium carbonate at depth. The $(Ca^{1/2})$/Na ratios for these springs are less than 1 for the same reason. Springs with higher ratios of Cl/Ca and Cl/Mg generally have lower Ca/Mg ratios, perhaps indicating precipitation of magnesian calcite. $Cl/(HCO_3 + CO_3)$ ratios decrease as spring temperature decreases. *Truesdell* [1975] attributed a similar change in Shoshone Geyser Basin, Yellowstone Park, Wyoming, to the reaction

$$CO_2 + H_2O + \text{Na silicate} = HCO_3^- + Na^+ + \text{H silicate}$$

That is, as hot water cools in contact with alkali aluminosilicate (or silicate) minerals at constant activity of the alkali ions, the *p*H increases [*Hemley,* 1959] and more dissolved carbon dioxide is converted to bicarbonate with simultaneous introduction of alkali ions. If this reaction is controlling the $Cl(HCO_3 + CO_3)$ ratio, then the Cl/Na ratio should change in a similar manner, and the ratio of $Na/(Cl + HCO_3 + CO_3)$ should remain approximately constant. The Cl/Na ratios generally follow the $Cl/(HCO_3 + CO_3)$ ratios, although the $Na/(Cl + CO_3 + HCO_3)$ ratios range from 0.81 to 1.05. Thermal springs along Hot Creek and Little Hot Creek have constant ratios of $Na/(Cl + CO_3 + HCO_3)$, 0.98–1.01, indicating that solution of sodium feldspar and precipitation of clay may be controlling the ratio in this area. However, lower ratios of $Na/(Cl + CO_3 + HCO_3)$ and higher Cl/K ratios in the area between Hot Creek and Lake Crowley may indicate solution of something other than sodium feldspar or the precipitation of some sodium-potassium phases.

Low ratios of Na/K for thermal springs along Hot Creek may indicate that they are associated with a higher-temperature part of the thermal reservoir. *Orville* [1963] and *White* [1965] have shown that low Na/K ratios indicate high temperatures of equilibrium. The $(Ca^{1/2})$/Na ratios range from 0.28 for the steam well at Casa Diablo to 2.0 for the hot spring on Little Hot Creek. Ratios of Cl/Rb, Na/Rb, and Na/Li generally increase in hydrothermal areas as the fluids react with the country rock, producing hydrothermal minerals [*Ellis,* 1970]. In Long Valley, Cl/Rb, Na/Rb, and Na/Li ratios are smallest for hot springs along Hot Creek, increasing as spring temperatures decrease toward Lake Crowley. Perhaps thermal spring waters issuing in the area between Hot Creek and Lake Crowley have relatively less rubidium and lithium because of more extensive reaction with the country rock. The slight increase in Cl/Li and Cl/F as the spring temperatures decrease may indicate loss of these minor elements into alteration minerals. Low NH_3/Na ratios are found in the springs which are releasing gas. Ratios of Cl/SO_4 are nearly constant, increasing slightly from northwest to southeast with the highest ratios in thermal springs south of the alkali lakes.

Thermal springs in Long Valley have Cl/B ratios in the range 6.6–5.6. Cl/B ratios for springs in and near Hot Creek Gorge may be highest (6.4–6.6) because of phase separation with loss of boron into the vapor phase. Such phase separation is not uncommon in hot-water systems; this vapor phase con-

TABLE 2. Atomic Ratios of Major and Minor Elements in Thermal and Meteoric Waters From Long Valley, California

Spring	Cl/Ca	Cl/Mg	Cl/Na	Cl/K	Cl/SO_4	Ca/Mg	$Ca^{1/2}/Na$	Na/Li	Na/K	Cl/F	Cl/B	Na/NH_3	Cl/Li	Cl/Rb	Na/Rb	Cl / HCO_3+CO_3	Na / $Cl+HCO_3+CO_3$
3S/28E-13ES3	4.5	228	0.32	7.4	5.6	50.5	2.0	43	23	13	5.7	625	14	1890	5880	0.47	1.01
3S/28E-32E9	352	1920	0.47	6.9	5.8	5.5	0.28	42	15	15	5.7	588	20	1320	2860	1.55	1.31
3S/29E-31AS1	13	291	0.36	8.5	5.7	22.7	1.43	48	24	12	6.6	2000	17	2380	6670	0.56	1.01
3S/28E-21PS1	6.7	171	0.31	4.5	6.0	25.3	1.8	62	14	18	6.0	1000	20	4170	14,300	0.31	0.76
3S/29E-28HS1	8.7	194	0.28	4.4	6.7	22.2	1.3	71	16	19	5.9	2500	20	2380	9090	0.35	0.93
3S/29E-34KS1	7.4	86	0.30	5.9	6.9	11.6	1.7	83	20	18	5.6	1250	18	4170	14,300	0.37	0.89
3S/28E-35ES1	86	1714	0.43	11	5.6	20.0	0.55	59	26	12	5.8	1670	20	2330	5560	0.92	1.12
3S/28E-25AS4	159	2572	0.37	10	6.1	16.2	0.37	45	28	12	6.4	1250	19	2080	5880	0.62	1.04
2S/27E-25AS1	1.3	0.7	0.16	1.6	1.9	0.52	11.3	167	10	6.0	4.7	106	···	···	···	0.11	0.62
3S/29E-13C1	0.64	10	0.05	2.5	2.2	16.1	7.0	83	50	2.8	5.2	67	···	···	···	0.05	0.92
Steamboat Springs*	59	820	0.80	14	31	13.9	0.39	27	18	200	5.4	···	17	2940	3703	3.94	0.998
Broadlands†	1127	···	0.80	8.4	30	···	0.007	35	18	111	10.1	167	28	25,000	33,300	4.79	0.911

All ratios are molal ratios except $Cl/HCO_3 + CO_3$ and $Na/Cl + HCO_3 + CO_3$, which are equivalence ratios. Ratios were calculated with the aid of the computer program SOLMNEQ [*Kharaka and Barnes,* 1973]. Ratios containing carbonate or bicarbonate species are calculated from carbonate alkalinity, not total alkalinity (carbonate and bicarbonate) reported in Table 1.
*Data from *Mariner et al.* [1974].
†Spring 1 from *Browne and Ellis* [1970].

denses to produce acid sulfate springs. An analyzed acid sulfate spring from the Casa Diablo area has a Cl/B ratio of 0.12 [data from *Lewis*, 1974].

Ellis [1970] has shown that ratios of chloride, boron, and bicarbonate may be used to distinguish aquifers within the Ohaki-Broadlands geothermal field. Waters from the same aquifer have chemical compositions with almost constant Cl/B ratios regardless of the bicarbonate concentrations. Ratios of Cl/B are 5.7 ± 0.1 for most of the hot springs in the Long Valley area. The springs in and near Hot Creek Gorge which have higher Cl/B ratios may result from boron loss due to minor subsurface boiling. If the thermal waters come from the same aquifer, then differences in chloride concentration may be a function of the extent of mixing. In simple mixing, thermal fluids rising from depth mix with fresh water near the surface. If simple mixing without boiling or conductive cooling is controlling the chloride concentration and spring temperature, a plot of the chloride concentration versus the water temperature should be a straight line. However, a linear relationship between chloride concentration and water temperature does not exist in Long Valley (Figure 3). Springs which plot above the ideal mixing composition may result from vapor loss or conductive cooling. Springs with the largest chloride concentration and highest temperatures occur in Hot Creek Gorge.

Isotopic data for deuterium and oxygen 18 (Table 3 and Figure 4) are given in the standard δ values, parts per mil (‰). Hot springs in Long Valley range from −12.44 to −16.09 in $\delta^{18}O$ and from −111.0 to −124.9 in δD. The two fresh waters range from −15.89 to −17.07 in $\delta^{18}O$ and −115.4 to −129.5 in δD. Recharge water for the hot-spring system in Long Valley may have approximately the composition of the cold spring at Big Spring Campground ($\delta^{18}O$ = −15.9, δD = −115.4). The recharge water reacts with rock in the thermal reservoir until at least $\delta^{18}O$ = −14.2 is attained; then dilution by a fresh water of approximate composition $\delta^{18}O$ = −18.4 and δD = −135

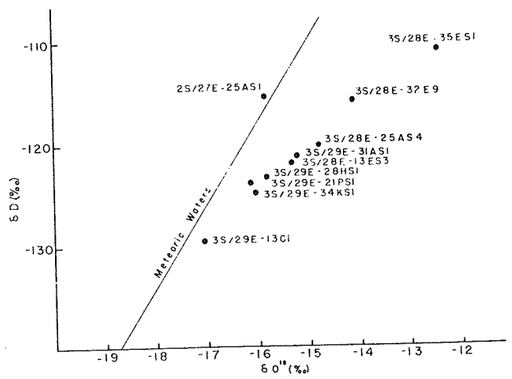

Fig. 4. Detailed plot of δD versus $\delta^{18}O$ for thermal springs and fresh waters in Long Valley, California. Fresh waters include 25AS1 and 13C1.

would produce the various thermal waters. The plots of δD-chloride and $\delta^{18}O$-chloride (Figure 5) emphasize the mixed character of most of the hot-spring waters. Thermal-spring waters from the Hot Creek Gorge area (31AS1 and 25AS4) show slight concentration of heavy isotopes. This could result from subsurface boiling, which was inferred from the Cl/B ratios. The hot pool (35ES1) located between Hot Creek Gorge and Casa Diablo Hot Springs has been strongly fractionated, probably by evaporation. The isotopic shift for thermal springs in Long Valley is less than for most other major thermal areas as shown in Figure 6 [modified from *Craig*, 1963]. The small $\delta^{18}O$ shift, similar to that observed at Wairakei, may indicate that the hot-spring system in Long Valley is moderately old and has isotopically well flushed conduits.

Gas escaping from thermal springs along Hot Creek and

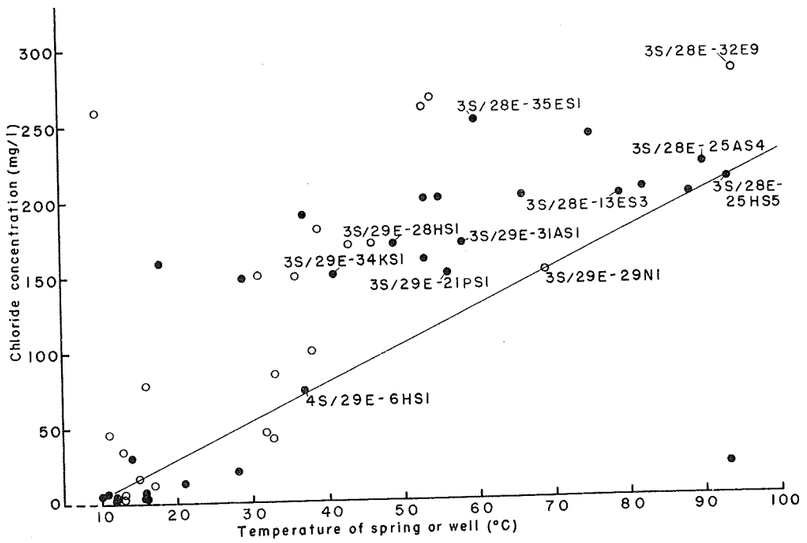

Fig. 3. Chloride concentration versus temperature of thermal springs and wells in Long Valley, California [data from *Willey et al.*, 1974, and *Lewis*, 1974]. Open circles represent wells, filled circles represent springs.

TABLE 3. Isotopic Composition of Thermal and Meteoric Waters in Long Valley, California

Sample	$\delta^{18}O$	δD
2S/27E-25AS1	−15.89	−115.4
3S/28E-13ES3	−15.34	−121.8
3S/28E-32E9	−14.16	−115.8
3S/28E-35ES1	−12.44	−111.0
3S/28E-25AS4	−14.83	−120.3
3S/29E-13C1	−17.07	−129.5
3S/29E-21PS1	−16.17	−123.9
3S/29E-28HS1	−15.85	−123.4
3S/29E-31AS1	−15.23	−121.2
3S/29E-34KS1	−16.08	−124.9

Analysts were L. A. Adami and S. J. Grigg.

Little Hot Creek is 89–93% carbon dioxide (Table 4). *Browne and Ellis* [1970] reported that the noncondensable fraction of five steam wells in the Ohaki-Broadlands field contained 92–95% carbon dioxide. Noncondensable gases from Steamboat Springs, Nevada, contain an even larger percentage of carbon dioxide, 98% [*White et al.*, 1963]. The increase in the nitrogen content of gas escaping from the cooler springs in Long Valley may result from water-rock reactions. *Truesdell* [1975] has shown that in Shoshone Geyser Basin, Yellowstone Park, Wyoming, the active gases such as carbon dioxide are removed by water-rock reactions as the water temperature decreases, producing an increase in the percent of nonreactive gases. The high carbon dioxide and low methane concentrations of gases escaping from the springs in Long Valley suggest that the thermal reservoir is in igneous rocks. Springs associated with thermal reservoirs in sedimentary or low grade metamorphic rock are rich in carbon dioxide and methane [*Ellis*, 1967].

Data in *Lewis* [1974] indicate that the surface of the zone of saturation generally parallels the topography, sloping toward Lake Crowley. Between Hot Creek and Lake Crowley the shallow aquifer has been contaminated by thermal fluid. Contamination is evident in the chemical composition and temperatures of springs and wells between Hot Creek and Lake Crowley. Chloride concentrations (Figure 7) indicate that chloride-rich water is being introduced into the zone of saturation in the Hot Creek Gorge and perhaps into the alkali lake area. This chloride-rich water is altering the chloride concentration of the zone of saturation for 7 or 8 km east and east-southeast of Hot Creek Gorge. The concentration of chloride in the zone of saturation decreases from 200 mg/l in the Hot Creek Gorge area to 50 mg/l within 7–8 km. Temperatures in springs and wells show a similar trend (Figure 8) with temperatures decreasing from 93° to 30°C within the same distance. Therefore the best area for mixing calculations should be along Hot Creek or Little Hot Creek, areas where water in the zone of saturation has not been contaminated.

GEOTHERMOMETERS

The qualitative and quantitative chemical geothermometers are valid only for hot-water systems. The high chloride content (200 mg/l) of the thermal springs in Long Valley indicates that they are associated with a hot-water system. Qualitative indicators suggested by *Ellis* [1970], *Fournier and Truesdell* [1970], *Mahon* [1970], and *White* [1970] are listed in Table 5. Qualitatively, these chemical indicators as well as the water temperatures indicate that the hot springs and steam well near Hot Creek (32E9, 25AS4, and 35ES1) should be associated with the hottest part of the geothermal system.

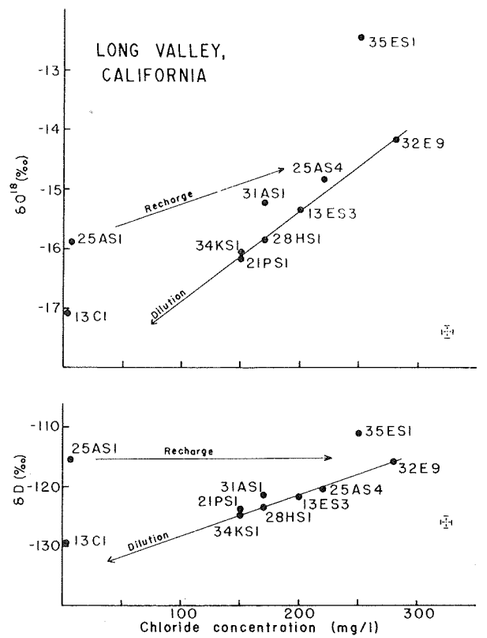

Fig. 5. Plots of δD-chloride and $\delta^{18}O$-chloride for springs and wells, Long Valley, California.

The chemical compositions of thermal spring or well waters can be used to estimate the last temperature at which the thermal fluid was in equilibrium with the reservoir rock. However, several of the thermal waters violate basic assumptions, discussed by *Fournier et al.* [1974], which must be fulfilled before the quantitative geothermometers can be meaningful. Mixing of thermal and fresh water has been demonstrated by stable isotope and chloride-temperature relationships. Reaction of thermal fluid with country rock has been implied from the reaction parameters $Cl/(HCO_3 + CO_3)$ and $Na/(Cl + HCO_3 + CO_3)$. Thus two of the basic assumptions of quantitative geothermometry, negligible mixing of thermal fluids with other waters and negligible water-rock interaction at lower temperatures, are violated. Temperatures estimated from the concentrations of silica and the cations (sodium, potassium, and calcium) are listed in Table 6. The conductive quartz curve was utilized for all samples except the new spring in Hot Creek Gorge, 25AS4, where the adiabatic curve was used because the spring was boiling. The steam-water mixture from the 'steam' well (32E9) was condensed without any steam loss, and the other springs were not boiling. Springs issuing at temperatures below boiling may be mixed waters and/or may have cooled by conduction. If the thermal fluids mix with dilute surface waters, the silica concentrations will be sharply decreased along with the temperature estimate based on the silica con-

TABLE 4. Compositions of Gases Escaping From Thermal Springs in Long Valley, California

Spring	O_2 + Ar	N_2	CH_4	CO_2	Total
3S/28E-13ES3	1.8	6.3	0.1	92.7	100.9
3S/28E-35ES1	1.6	10.7	0.0	88.8	101.1
3S/28E-25AS4	3.5	8.4	0.3	88.8	101.0
3S/29E-21PS1	6.0	65.1	0.3	37.2	108.6

Analyst was J. B. Rapp. Analysis is in volume percent.

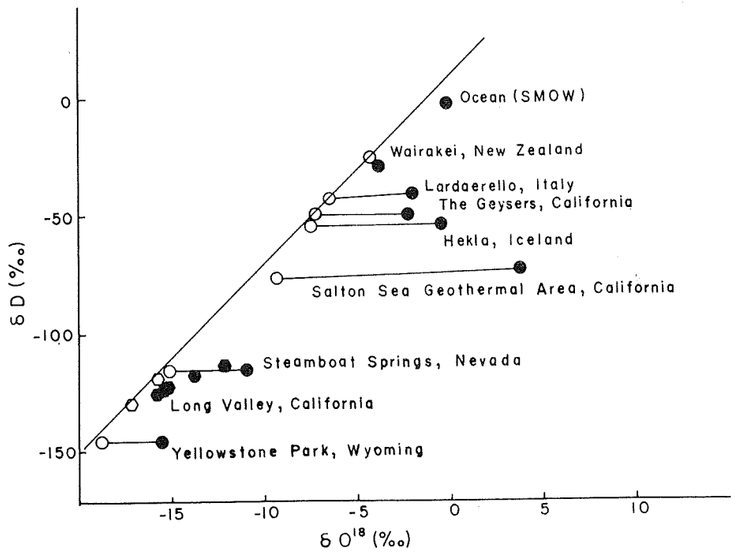

Fig. 6. Isotopic composition of some of the major thermal areas of the world as compared with that of Long Valley, California [after *Craig*, 1963]. Thermal springs are represented by filled symbols, fresh waters by open symbols. Waters from Long Valley are represented by hexagons, while other thermal areas are represented by circles.

centrations. However, mixing should affect the cation ratios less, and the cation geothermometer should produce an estimate nearer the true reservoir temperature. The Na-K geothermometer should not be used where the $(Ca^{1/2})/Na$ ratio is more than 1 [*Fournier and Truesdell*, 1973]. The $(Ca^{1/2})/Na$ ratio is greater than 1 for all the samples except the 'steam' well (32E9), the new spring (25AS4), and the hot pool (35ES1). The geothermometers are meaningless for the hot pool (35ES1) because of evaporation and precipitation of calcite. Loss of carbon dioxide from the well and the new spring may have resulted in the loss of calcium as calcium carbonate precipitated from the thermal fluid. For these samples, neither the Na-K-Ca nor Na-K geothermometer may give an accurate estimate of the temperature in the thermal reservoir.

The Na-K-Ca geothermometer for all the thermal springs (Table 6) indicates reservoir temperatures more than 25°C

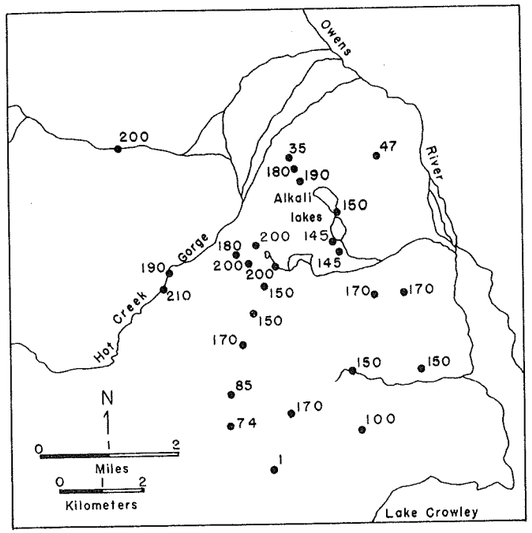

Fig. 7. Areal distribution of chloride in thermal springs and wells, Long Valley, California. Data from *Willey et al.* [1974] and *Lewis* [1974]. Chloride concentrations are in milligrams per liter.

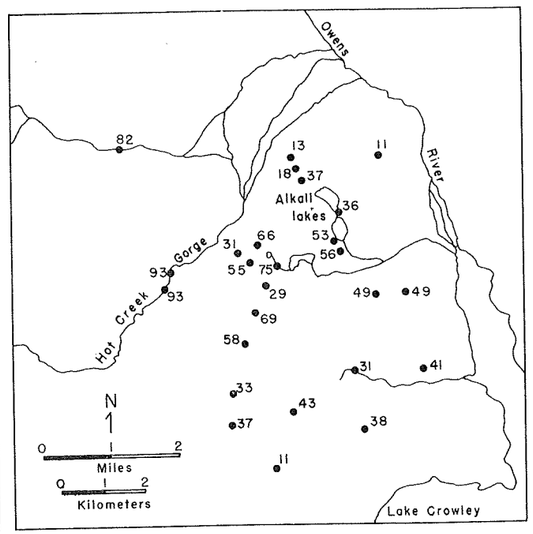

Fig. 8. Areal distribution of temperatures in thermal springs and wells, Long Valley, California. Data from *Willey et al.* [1974] and *Lewis* [1974]. Temperatures are °C.

TABLE 5. Qualitative Chemical Indicators of Thermal Reservoir Temperatures

Sample Designation	Ca*	HCO_3*	Mg/Ca†	Na/Ca‡	Cl/(HCO_3 + CO_3)§	Cl/F‖
3S/28E-13ES3	50	735	0.020	14.3	0.47	12.8
3S/28E-32E9	0.9	450	0.183	754	1.55	12.5
3S/28E-35ES1	3.3	466	0.050	200	0.92	12.3
3S/28E-21PS1	25	828	0.040	21.6	0.31	17.5
3S/29E-28HS1	22	845	0.045	31.7	0.35	19.0
3S/29E-31AS1	15	516	0.044	36.0	0.56	12.2
3S/29E-34KS1	23	695	0.086	18.8	0.37	17.5
3S/28E-25AS4	1.6	580	0.113	432	0.62	12.3
2S/27E-25AS1	5.1	90	1.910	7.8	0.11	5.9
3S/29E-13C1	5.3	111	16.0	12.5	0.05	2.8

*Low concentrations of calcium (Ca) and bicarbonate (HCO_3) in near-neutral *p*H waters may indicate high temperatures [*Ellis*, 1970].

†Low ratios of magnesium to calcium (Mg/Ca) may indicate high temperatures [*White*, 1970].

‡High ratios of sodium to calcium (Na/Ca) may indicate high temperatures [*Mahon*, 1970].

§Highest ratios of chloride to total carbonate (Cl/(HCO_3 + CO_3)) in waters from the same thermal system indicate the highest temperature in the thermal aquifer [*Fournier and Truesdell*, 1970]. Ratios were calculated with the aid of the computer program SOLMNEQ [*Kharaka and Barnes*, 1973] after noncarbonate alkalinity was removed.

‖Highest ratios of chloride to fluoride (Cl/F) may indicate high temperatures [*Mahon*, 1970].

above the measured spring temperatures, typical of thermal springs which issue mixed water. Calculations based on the mixing model of *Fournier and Truesdell* [1974] and assuming temperatures of fresh water from 10° to 17°C with possible silica concentrations from 32 to 64 mg/l indicate reservoir temperatures between 170° and 200°C for the thermal spring on Little Hot Creek. This range of possible reservoir temperatures is due to the uncertainty of the silica concentration and temperature of the cool-water component. Similar calculations for the new spring in Hot Creek Gorge, 25AS4, indicate temperatures of 200° to 225°C. Mixing calculations on 31AS1 located south of Hot Creek Gorge indicate a minimum temperature of 275°C. However, the chloride-temperature plot (Figure 3) may indicate conductive cooling from 76° to 58°C. Assuming that the spring temperature would be 76°C if it had not lost heat by conductive cooling reduces the estimated temperature to 225°C. The estimated reservoir temperature would be further reduced for springs in the Hot Creek Gorge area if some steam separation had occurred, as is indicated by isotope and Cl/B data.

The springs sampled for detailed analysis in the alkali lake area discharge waters with a complex history. Isotopic compositions indicate mixing with a fresh water. Chloride-temperature relationships indicate that the waters are mixed and may have lost heat by conduction. Mixing calculations using a fresh water of 10°C containing 60 mg/l silica produce an unacceptable calculated temperature (500°C). A possible explanation is that the thermal spring waters are in metastable equilibrium with amorphous silica in the shallow aquifer. All three springs have silica concentrations which would be in equilibrium with amorphous silica at temperatures 10°–15°C above the temperature of the respective spring waters. Cation geothermometers for these three springs estimate temperatures near 200°C.

The best estimate of reservoir temperature may be 220°C, based on the silica concentration in the condensate from the steam well (32E9). Isotopic data and reaction indices indicate that the condensate has not been appreciably altered by dilution, vapor loss, or reaction with the country rock.

Temperatures of 200°–220°C are reasonable minimum temperatures for the thermal reservoir based on the chemical composition of the hot springs. Higher temperatures are possible. On the basis of the silica and Na-K-Ca geothermometers, thermal springs in the Broadlands area of New Zealand

TABLE 6. Estimated Reservoir Temperatures

Sample Designation	Surface Temperature, °C	Discharge, l/min	Chemical Geothermometers*		
			Quartz	Na-K	Na-K-Ca
3S/28E-13ES3	79	280	143	150	172
3S/28E-32E9	94	...	219	201	238
3S/28E-35ES1	60	0	209	140	189
3S/28E-21PS1	56	100	196	205	200
3S/29E-28HS1	49	200	193	192	200
3S/29E-31AS1	58	190	161	147	176
3S/29E-34KS1	41	150	182	169	184
3S/28E-25AS4	90	400±	153	132	192
28/27E-25AS1	10	380	109	259	83
3S/29E-13C1	10	25	114	86	53

*Basic assumptions of quantitative geothermometry [after *Fournier et al.*, 1974]: (1) temperature dependent reactions in the thermal reservoir must control the water composition, (2) equilibrium must exist between the fluid in the thermal reservoir and the reservoir rock, (3) minerals which supply the constituents used as a basis for the geothermometers must occur in the reservoir rock, (4) negligible re-equilibrium must exist at lower temperatures, and (5) negligible mixing with other waters must occur as the thermal fluid rises to the surface.

should have been associated with a reservoir at a temperature of at least 220°C. Wells drilled near the springs intersect aquifers containing fluid up to 285°C [*Mahon and Finlayson,* 1972].

SUMMARY

The chloride concentrations, spring temperatures, and isotopic compositions indicate mixing of thermal and fresh waters in the Long Valley geothermal area. Some spring temperatures may be modified by conductive cooling. The thermal spring waters have chemical compositions which indicate a hot-water system similar to the New Zealand geothermal fields. The minimum estimated temperature of the thermal reservoir is 200°C, based on the silica and cation concentrations.

Thermal springs between Hot Creek and Lake Crowley have a different history than the springs along Hot Creek or Little Hot Creek. Possibly part of the thermal fluid rising along Hot Creek enters a shallow aquifer which feeds the springs and wells between Hot Creek and Lake Crowley. Some additional thermal fluid from the deep reservoir may enter the shallow aquifer near Big Alkali Lake. Conductive cooling of mixed thermal and fresh water in this shallow aquifer may control the spring temperature more than simple mixing. Therefore the main thermal reservoir is more directly associated with the thermal springs along Hot Creek and Little Hot Creek. Mixing may also have altered the chemical composition of these springs. Springs in the Hot Creek Gorge area may have been slightly concentrated by some vapor loss during near-surface boiling.

Acknowledgments. We thank A. H. Truesdell, F. H. Olmsted, and L. J. P. Muffler for critical reading of the manuscript. The comments of A. H. Truesdell were particularly helpful in clarifying the interpretation of the stable isotope data and reaction parameters.

REFERENCES

Barnes, I., Field measurement of alkalinity and *p*H, *U.S. Geol. Surv. Water Supply Pap. 1535-H,* 1–17, 1964.

Browne, P. R. L., and A. J. Ellis, The Ohaki-Broadlands hydrothermal area, New Zealand: Mineralogy and related geochemistry, *Amer. J. Sci., 269*(2), 97–131, 1970.

California Department of Water Resources, Investigation of geothermal waters in the Long Valley area, Mono County, California, 141 pp., Dep. of Water Res., Sacramento, Calif., 1967.

Craig, H., The isotopic geochemistry of water and carbon in geothermal areas, in *Nuclear Geology on Geothermal Areas—Spoleto 1963,* edited by E. Tongiorgi, pp. 17–53, Consiglio Nazionale Delle Ricerche, Laboratorio di Geologia Nucleare, Pisa, 1963.

Ellis, A. J., The chemistry of some explored geothermal systems, in *Geochemistry of Hydrothermal Ore Deposits,* edited by H. L. Barnes, pp. 465–514, Holt, Rinehart, and Winston, New York, 1967.

Ellis, A. J., Quantitative interpretation of chemical characteristics of hydrothermal systems, *Geothermics Spec. Issue 2,* 516–528, 1970.

Fournier, R. O., and J. J. Rowe, Estimation of underground temperatures from the silica content of water from hot springs and wet steam wells, *Amer. J. Sci., 264*(9), 685–697, 1966.

Fournier, R. O., and A. H. Truesdell, Chemical indicators of subsurface temperature applied to hot waters of Yellowstone National Park, Wyo., U.S.A., *Geothermics Spec. Issue 2,* 529–535, 1970.

Fournier, R. O., and A. H. Truesdell, An empirical Na-K-Ca geothermometer for natural waters, *Geochim. Cosmochim. Acta, 37*(5), 1255–1275, 1973.

Fournier, R. O., and A. H. Truesdell, Geochemical indicators of subsurface temperature, 2, Estimation of temperature and fraction of hot water mixed with cold water, *J. Res. U.S. Geol. Surv., 2*(3), 263–270, 1974.

Fournier, R. O., D. E. White, and A. H. Truesdell, Geochemical indicators of subsurface temperature, 1, Basic assumptions, *J. Res. U.S. Geol. Surv., 2*(3), 259–262, 1974.

Giggenbach, W., Isotopic composition of waters of the Broadlands Geothermal Field, New Zealand, *N. Z. J. Sci., 14*(4), 959–970, 1971.

Hemley, J. J., Some mineralogical equilibria in the system K_2O-Al_2O_3-SiO_2-H_2O, *Amer. J. Sci., 257*(4), 241–270, 1959.

Kharaka, Y. K., and I. Barnes, SOLMNEQ: Solution-mineral equilibrium computations, *Rep. NTIS PB 215-899,* 88 pp., U.S. Dep. Comm., Nat. Tech. Inform. Serv., Springfield, Va., 1973.

Lewis, R. E., Data on wells, springs, and thermal springs in Long Valley, Mono County, California, *Open File Rep.,* 51 pp., U.S. Geol. Surv., Reston, Va., 1974.

Mahon, W. A. J., Silica in hot water discharged from drillholes at Wairakei, New Zealand, *N. Z. J. Sci., 9*(1), 135–144, 1966.

Mahon, W. A. J., Chemistry in the exploration and exploitation of hydrothermal systems, *Geothermics Spec. Issue 2,* 1310–1322, 1970.

Mahon, W. A. J., and J. B. Finlayson, The chemistry of the Broadlands geothermal area, New Zealand, *Amer. J. Sci., 272*(1), 48–68, 1972.

Mariner, R. H., J. B. Rapp, L. M. Willey, and T. S. Presser, The chemical composition and estimated minimum thermal reservoir temperature of the principal hot springs of northern and central Nevada, *Open File Rep.,* 32 pp., U.S. Geol. Surv., Reston, Va., 1974.

Orville, P. N., Alkali ion exchange between vapor and feldspar phases, *Amer. J. Sci., 261,* 201–237, 1963.

Tonani, F., Geochemical methods of exploration for geothermal energy, *Geothermics Spec. Issue 2,* 492–515, 1970.

Truesdell, A. H., Chemical evidence of subsurface structure and fluid flow in a geothermal system, in *Proceedings of the International Symposium on Water-Rock Interaction,* Czechoslovak Geological Survey, 1975.

White, D. E., Saline waters of sedimentary rocks, Fluids in Subsurface Environments—A Symposium, *Amer. Ass. Petrol. Geol. Mem. 4,* 342–366, 1965.

White, D. E., Geochemistry applied to the discovery, evaluation, and exploitation of geothermal energy resources, *Geothermics Spec. Issue 2,* 58–80, 1970.

White, D. E., J. D. Hem, and G. A. Waring, Chemical composition of subsurface waters, *U.S. Geol. Surv. Prof. Pap. 440-F,* 1–67, 1963.

White, D. E., L. J. P. Muffler, and A. H. Truesdell, Vapor-dominated hydrothermal systems compared with hot-water systems, *Econ. Geol., 66*(1), 75–97, 1971.

Willey, L. M., J. R. O'Neil, and J. B. Rapp, Chemistry of thermal waters in Long Valley, Mono County, California, *Open File Rep.,* 19 pp., U.S. Geol. Surv., Reston, Va., 1974.

(Received January 13, 1975;
revised September 15, 1975;
accepted September 15, 1975.)

Audiomagnetotelluric Sounding as a Reconnaissance Exploration Technique in Long Valley, California

D. B. HOOVER, F. C. FRISCHKNECHT, AND C. L. TIPPENS

U.S. Geological Survey, Denver, Colorado 80225

An audiomagnetotelluric (AMT) sounding system developed by the U.S. Geological Survey appears to be an effective technique for reconnaissance exploration to detect shallow resistivity anomalies associated with geothermal reservoirs. The equipment operates within the frequency range of 8–18,600 Hz by using nine logarithmically spaced narrow band filters. The technique has been evaluated in Long Valley, California, where the results from dc resistivity and time domain electromagnetic surveys were available for control. The AMT method outlines two linear zones of low resistivity that correlate well with known hot springs in the area. Generally, good agreement was obtained with the results of other electrical methods.

INTRODUCTION

The audiomagnetotelluric method (AMT) has recently been used by the U.S. Geological Survey as a reconnaissance technique for the evaluation of potential geothermal areas. Initial testing of the technique, using newly developed equipment, was done in the Long Valley caldera, where extensive geothermal studies by the Geological Survey were in progress. The results of those studies are reported in the other 12 companion papers in this special issue and provide a unique opportunity for evaluation of this relatively new electromagnetic technique. Of particular importance in evaluating the AMT method was the work of *Bailey et al.* [1976] and that of *Stanley et al.* [1976].

Because the AMT method is an inductive electromagnetic technique, it emphasizes conductive bodies such as are commonly associated with the hot waters and alteration zones of geothermal reservoirs. Although large errors in depth estimation can occur due to very poor resolution of intermediate high-resistivity beds, in reconnaissance work it is usually sufficient to verify the existence of conductive anomalies, measure their approximate values, and gain some idea of their lateral extent. These tasks can be carried out rather easily by using AMT techniques for conductors relatively near the surface. The depth of exploration is quite variable depending on the geoelectric section but typically ranges from 200 to as much as 2000 m.

Because commercial equipment was unavailable for purchase, the results reported here were obtained from equipment and field techniques developed by the authors. We consider these methods and techniques only preliminary, and modifications to both equipment and field methods are continuing as more experience is gained.

THEORETICAL BASIS FOR AMT METHOD

The magnetotelluric method is one of three exploration techniques which use naturally occurring electromagnetic fields. The more familiar telluric and Afmag (audiofrequency magnetics) methods are the others, and all three suffer from being dependent upon the vagaries in the natural fields, as all who have worked with these methods know. In our work, selected narrow frequency bands were employed in the range from 8 to 18,600 Hz, and the technique is accordingly called audiomagnetotelluric (AMT) exploration. An excellent discussion of the method as applied to mineral exploration is given by *Strangway et al.* [1973]. The interested reader will find a more thorough discussion of the theory and nature of the source fields in their paper and in its listed references.

Electromagnetic fields penetrate into the earth to depths which vary depending on the earth conductivity and the frequency of the signals. The skin depth δ is a measure of this penetration and an approximate measure of the depth of exploration by the AMT method. It is given by (1) for a homogeneous earth:

$$\delta = (2\rho)^{1/2}/\mu\omega \qquad (1)$$

where ρ is resistivity, μ is permeability, and ω is the angular frequency $2\pi f$.

Using our system, then, over a 100-Ωm earth, we measured the resistivity from the surface to a depth of about 37 m at 18,600 Hz and to about 1800 m at 8 Hz. One should also remember that as the depth of exploration increases at the lower frequencies, so too does the lateral extent of exploration increase.

In employing the AMT method a usual assumption is that the electromagnetic energy propagates as a plane wave nearly vertically downward into the earth. For practical purposes this condition is met when the energy source is removed several wavelengths from the point of measurement and when displacement currents in the earth can be neglected.

Associated with this downward propagating plane wave are mutually orthogonal horizontal magnetic and electric fields. In the case of a homogeneous or horizontally stratified earth the electric field in the earth is radial, and the magnetic field is tangential to the source. Under these conditions the apparent resistivity of the earth is a function of these horizontal fields and the frequency and is given by the following equation [*Cagniard,* 1953]:

$$\rho_a = \frac{1}{5f}\frac{|E|^2}{|H|^2} \qquad (2)$$

where f is frequency in hertz, E is electric field in microvolts per meter, H is magnetic field in gammas, and ρ_a is apparent resistivity in ohm meters.

Because the skin depth and apparent resistivity are both functions of frequency, one can determine the variation of resistivity with depth by surface measurements of the electric and magnetic fields as a function of frequency. Thus in measuring apparent resistivity as a function of frequency, a sounding is made in much the same way as a dc geometric sounding

[*Keller and Frischknecht,* 1966] but without the bother of expanding an electrode array.

The principal source of natural electrical energy in the AMT range of frequencies is worldwide lightning storms, particularly in tropical regions, which account for the preponderance of the energy. *Bleil* [1964], *Ward* [1967], and *Strangway et al.* [1973] discuss in detail the temporal and spatial variations of these storm-stimulated signals. Briefly, these variations principally affect the method by restricting operations to good signal periods and by introducing scatter in the data. In regard to the temporal variations the energy is weakest during winter months, when storm activity is reduced. We have operated as late as October but noticed a decided decrease in energy toward the end of the month, particularly in the higher frequencies. Also the energy, particularly in the higher frequencies, tends to increase in the afternoon as thunderstorm activity comes closer to the recording site [*Strangway et al.,* 1973].

The presence of two or more major storm centers supplying energy during a given recording period will cause some data scatter and nonrepeatability of data, particularly where lateral inhomogeneities exist. The response of two- and three-dimensional structures varies with the orientation of the source fields and the sensor array orientation [*Strangway et al.,* 1973]. Thus data scatter is due to the varying source locations during a given recording period, and nonrepeatability is due to distinctly differing source locations at different recording times. While these problems preclude very precise analysis of the data in terms of a layered structure, they clearly emphasize that the earth usually does not fit the simple horizontally stratified model that we often assume.

Propagation in the earth-ionosphere wave guide produces spectral characteristics which impose other restrictions on the method. In the low-frequency range, wave guide resonances produce energy peaks at discrete frequencies. These are the Schumann resonances, the lowest frequency being at about 8 Hz. Above this frequency the energy wave guide has a strong absorption band which severely limits data acquisition in the 2000-Hz range.

Within the AMT frequency band, manmade signals are also present. Most troublesome are the fields from power lines at both the fundamental and many of the harmonics. The large amount of energy at these discrete frequencies constitutes a difficult noise problem in most cases, as the source generally cannot be assumed to be distant enough to produce a plane wave.

In the higher AMT frequency range, VLF radio signals are present and may be employed. In our system we used stations at 10,200 Hz and 18,600 Hz as a matter of convenience. During the rare periods when these stations were not transmitting, there was sufficient natural energy for operations.

Interpretation of Data

Where horizontal layering can safely be assumed, interpretation of data is similar to that of conventional resistivity interpretation techniques such as curve matching. For any postulated layered structure one can compute the corresponding sounding curve; thus matches to sounding curves may be made. The problem of intermediate high-resistivity layers being masked, however, seriously limits accurate depth interpretation and is discussed in detail by *Strangway et al.* [1973] and *Strangway and Vozoff* [1970]. As they point out, an intermediate high-resistivity layer must be 2–3 times as thick as the upper layer in order to be seen. In the present system the limited definition of the sounding curves also is a hindrance to interpretation. This limited definition is due, in part, to weak signal conditions near 2000 Hz, this situation being particularly bad during the winter months. In addition, with eight points typically defining the sounding over more than 3 decades, much detail is lost.

In mining and geothermal exploration, two- and three-dimensional structures are much more prevalent than are simple layered ones. Interpretation methods for this situation are severely limited, and most often simple anomaly maps are used as a basis for qualitative interpretation. We have chosen the anomaly map method to present our data. Some theoretical solutions for simple two-dimensional structures have been presented [*Strangway et al.,* 1973; *Strangway and Vozoff,* 1970; *Vozoff,* 1972; *Madden and Swift,* 1969], and limited three-dimensional data are available from model studies of *Frischknecht* [1973]. These studies permit some generalizations that are useful when AMT anomaly maps or sounding curves are examined.

For two-dimensional structures the most definitive measurements are made with the electric field oriented parallel and perpendicular to the strike of the structure. In general, '*E* perpendicular' measurements will define the boundaries very sharply, but the measured values near the boundaries will exhibit overshoot and undershoot. These edge effects can result in measured apparent resistivities both higher and lower than the actual resistivities present in the section. Near-surface conductive layers, however, tend to suppress the overshoot. In the case of '*E* parallel' measurements across a structure, the resistivity values will vary smoothly without edge effects but will only poorly define the boundaries. A common situation would involve an area in which approximately vertical conductive fault zones are present. In this case, if one were not within a fault zone, the *E* parallel measurements would be lower, and the *E* perpendicular measurements higher than the background resistivities of the area; if one were within a fault zone, just the opposite would tend to result with respect to the actual resistivities in the fault zone.

In a broad sense these same generalizations apply to three-dimensional structures. Thus measurements with the telluric line oriented perpendicular to the boundary are more definitive of that boundary than *E* parallel measurements. From these results one can conclude that spherical bodies will not give circular anomaly maps, as is evident from Frischknecht's [1973] data.

Equipment

Commercial AMT equipment is not yet available for purchase, so the equipment used was designed and fabricated by the U.S. Geological Survey. It is similar to that recently described by *Strangway et al.* [1973] except that we have provided a means of preserving phase information as well. Figure 1 is a block diagram of our instrumentation. To measure the horizontal electric field, two steel stakes, generally separated by 100 m, are used as electrodes. The voltage difference between the electrodes is amplified and prefiltered by using RC (resistance-capacitance) band-pass filters so as to prevent strong local noise sources from overdriving the first stages generating spurious signals. Narrow band active notch filters are used to remove 60- and 180-Hz power line signals, which are very strong when work is being done in the vicinity of power lines. The signals then enter a universal active filter connected in a high-Q band-pass configuration. Approximately constant, Q is maintained at all filter settings, the

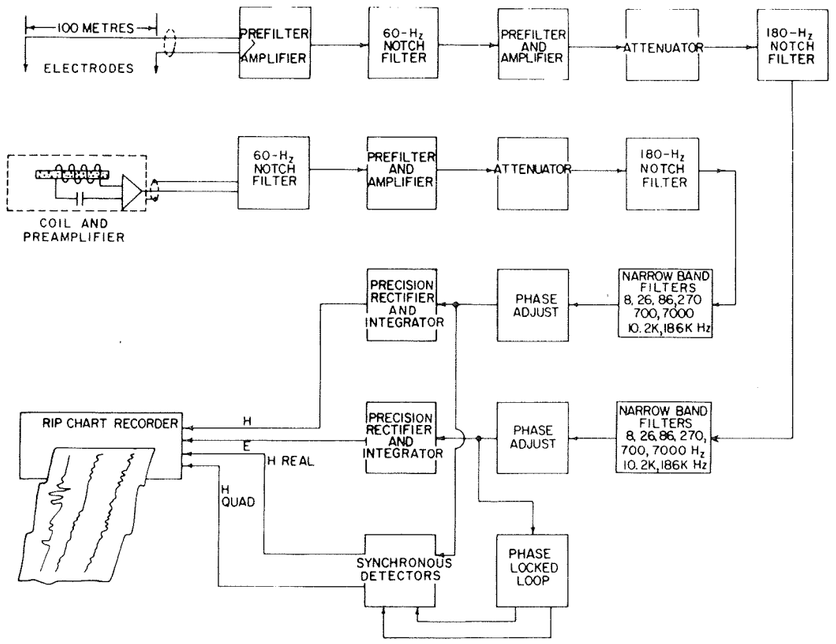

Fig. 1. Block diagram of the U.S. Geological Survey audiomagnetotelluric system.

6-dB bandwidth at 8 Hz being 0.3 Hz. To define a sounding curve, nine selected frequencies are used, these being spaced roughly logarithmically throughout the band but selected so as to avoid the midband harmonics of 60 Hz. At present, our operating frequencies are 8, 26, 86, 270, 700, 2000, 7000, 10,200 and 18,600 Hz. The output of the narrow band filter is rectified, integrated, and displayed on a strip chart recorder to show the envelope of the received energy.

An induction pickup is used for the horizontal magnetic field sensor and consists of a ferrite core upon which are wound many thousands of turns of wire. In order to span the broad range of frequencies we found it necessary to use two separate coils. One covers the frequency range from 8 to 700 Hz and the other covers from 2,000 to 18,600 Hz. The coils weigh 5.3 and 6.1 kg, respectively. The sensitivity of the large coil is 0.1 μV/mγ at 8 Hz. An integral part of each sensor is a low-noise preamplifier which feeds the magnetic field signal to a second channel nearly identical to that described for recording the electric field.

Phase information is preserved by means of a phase-locked loop and synchronous detectors as shown in Figure 1. The usefulness of the phase information is still being evaluated, so it will not be discussed further here.

Field Operations

The strip chart recorder and high-gain selective filters were operated from the back of a carryall van. The power was supplied by an inverter connected to the truck battery. The coil and common electrode of the electric line were located 30 m from the truck to avoid electrical noise in the vicinity of the truck. Signals are brought to the truck over coaxial cable.

The electric line is laid out in either an east-west or north-south direction, and the coil placed at the right angle to the line. System gains are adjusted so as to give 20 to 40-mm chart deflection of peak energy bursts on each channel. The amplitudes of corresponding electric and magnetic signals are measured, and their ratios are computed for a sufficient number of signals to obtain a reliable average ratio. The Cagniard resistivity [*Cagniard,* 1953] is then computed by using system gain values and (2).

Data are computed and plotted in the field while recording is under way. A sounding is obtained by switching through the various frequencies. The electric dipole and coil are then rotated 90°, and a second sounding is made and plotted. This permits the operators to correct any obvious errors and to check any data points that appear aberrant. The second sounding also provides information on lateral variations in conductivity or anisotropy of the earth.

Soundings were carried out by two persons, one acting as observer and the other acting as computer. Typical production was eight soundings (four stations) per day. Most of the time is spent waiting for a sufficient number of strong signals so as to provide a good statistical sample for the E/H ratio. Our experience has shown that the 8-Hz signals are often insufficient to provide strong samples; 700-Hz signals tend to be variable in strength, 2000-Hz signals are virtually nonexistent, and at 7000 Hz and greater the signals provide very good samples.

Figure 2 shows the locations of the 25 sounding stations used in this survey as well as the major faults and hot springs in the area, as adapted from *Bailey et al.* [1976]. Inasmuch as the AMT technique is being used for reconnaissance exploration, the object was to define the major conductive anomalies and not to detail them precisely. No attempt will be made here to review the geological setting or other pertinent geophysical data, as these are given in accompanying papers. The results reported here were obtained by two persons during 1 week of field work in June 1973.

Typical sounding curves are shown in Figures 3 and 4,

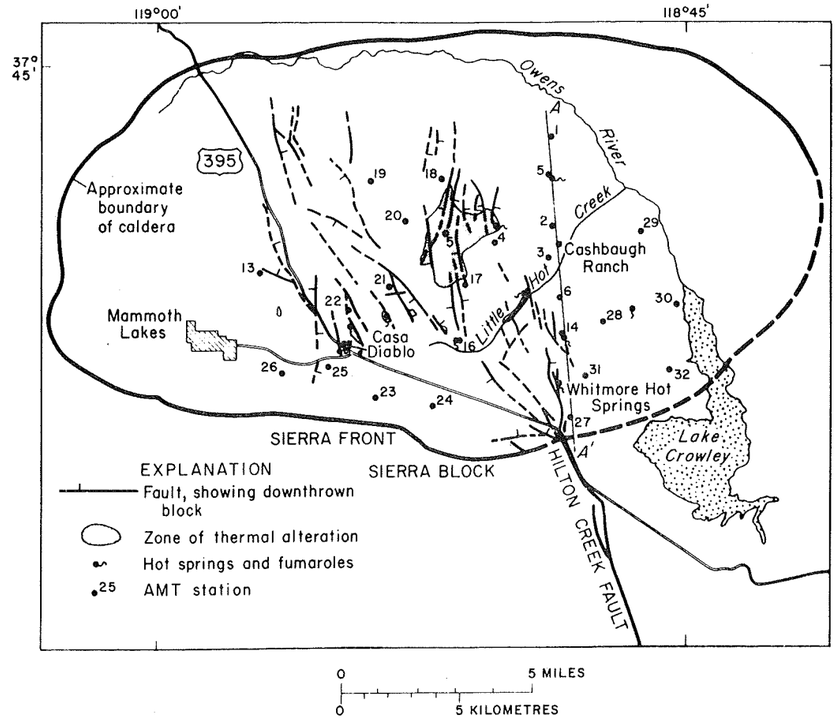

Fig. 2. AMT station location map, Long Valley, California.

which give data from stations 1, 14, and 16. Soundings for station 1 (Figure 3) show the typical reproducibility of the two soundings in which lateral effects are not pronounced. The soundings are plotted on a logarithmic base with frequencies increasing to the left. Although this is contrary to conventional presentation, it produces a sounding similar in appearance to Schlumberger sounding curves, thus providing easier reference to the work of *Stanley et al.* [1976].

Stations 14 and 16 are beside two hot springs associated with approximately north-trending faults, as shown in Figure

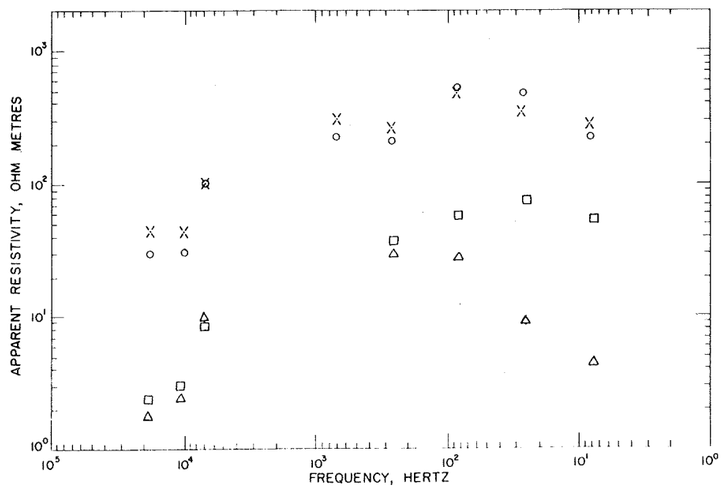

Fig. 3. Long Valley AMT soundings at stations 1 and 14. Crosses represent telluric line going east-west, station 1; circles represent telluric line going north-south, station 1; squares represent telluric line going east-west, station 14; and triangles represent telluric line going north-south, station 14.

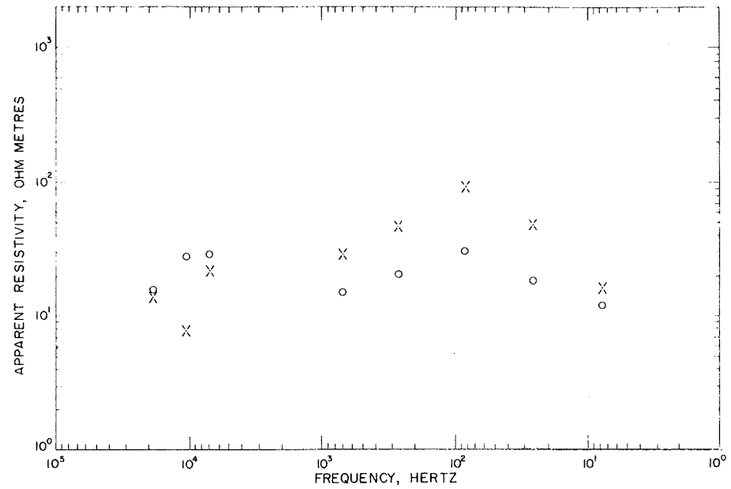

Fig. 4. Long Valley AMT soundings at station 16. Crosses represent telluric line going east-west, and circles represent telluric line going north-south.

2. These soundings (Figure 4) show very clearly the effect of lateral resistivity variations, the north-south (E parallel) orientation of the telluric line giving significantly lower apparent resistivities. At station 14, which was about 100 m west of the fault, the data begin to diverge significantly, showing the influence of the fault when the skin depth is greater than the offset. This type of behavior is to be expected outside of the conductive zone. The variation in apparent resistivity with orientation is not as great at station 16. Although this could be due to the relative orientation of the fault, these less pronounced variations at 16 are probably associated with less intensive alteration of the rocks, as the activity of the hot springs is considerably less there than at station 14.

Strangway and Vozoff [1970] note that in practice many more lateral variations are noted in this type of data than one might expect. This is quite evident in the Long Valley data, and, in fact, the north-south orientation of the telluric sensor usually, but not always, gives the lower resistivity values. This would be expected in Long Valley, where the predominant faulting is north to northwest trending and is of minor width; thus measurements would generally be made near but outside of the narrow conductive zones.

Because it is an inductive technique, the AMT method is excellent for locating conductors because it tends to 'look through' high-resistivity materials, and this is one of the principal reasons we are employing it in our geothermal program. However, its depth resolution is often poor, as was pointed out earlier. Because of both this problem and the evidence for lateral variations in the soundings themselves, interpretation in terms of horizontally layered structures was not attempted. Instead, the data presentation was limited to a set of anomaly maps at each frequency and some pseudosections.

Figure 5 is a map of apparent resistivity at 8 Hz. Where differences in apparent resistivity were obtained for the two sensor orientations, an average of the two values was used. Contouring of the data is logarithmic with four intervals per decade. This map represents information obtained at greatest depth in our survey, but the reader is cautioned not to think of the measurements as representing resistivity at a fixed depth across the map.

Despite the low station density, Figure 5 shows an anomaly pattern remarkably similar to the total-field resistivity anomaly of *Stanley et al.* [1976, Figure 6]. A small low, under 10 Ωm, is seen just south of the Cashbaugh Ranch, enclosed within a broader, V-shaped low under 100 Ωm. This V-shaped low encloses most of the hot springs in the caldera from Casa Diablo on the west and Whitmore Hot Springs on the east, to the head of Little Hot Creek in the northwest. In terms of reconnaissance, surveying the high-conductivity region has been adequately defined.

On the southern border of the caldera the 8-Hz map shows steep resistivity gradients as the Sierra front is approached. Resistivities of several thousand ohm meters are associated with the Sierra batholith and Paleozoic metasediments present in a nearby roof pendent. Intermediate resistivity values within the caldera are associated with volcanic fill, where there has evidently been little hydrothermal activity.

The total-field map of *Stanley et al.* [1976, Figure 6] shows a broader resistivity low in the vicinity of the Cashbaugh Ranch than is indicated by Figure 5. This discrepancy is due in part to the contour interval chosen and also to the differences in depth of exploration obtained with the two techniques. A 50-Ωm contour at 8 Hz would have included all of the anomalous area outlined by Stanley et al. near the Cashbaugh Ranch. Evidence to be discussed later indicates that the northern part of this conductive zone is slightly deeper than the rest of the zone and thus does not appear as prominently in Figure 5. Deepening of this zone is more clearly seen in the pseudosections across the anomaly (Figures 9 and 10).

At 26 Hz the signals are sufficiently strong, and so quite reliable data are obtained for both east-west and north-south orientations of the telluric line. To show the differences produced by lateral inhomogeneities, two maps have been prepared (Figures 6 and 7), one for each orientation. The two maps are generally similar to the 8-Hz map, showing the same V-shaped low centered on the hot springs and the steep resistivity gradient on the south. Either of the two maps adequately defines the anomalous area.

One major difference between the two maps lies in the significantly lower resistivity values associated with the north-

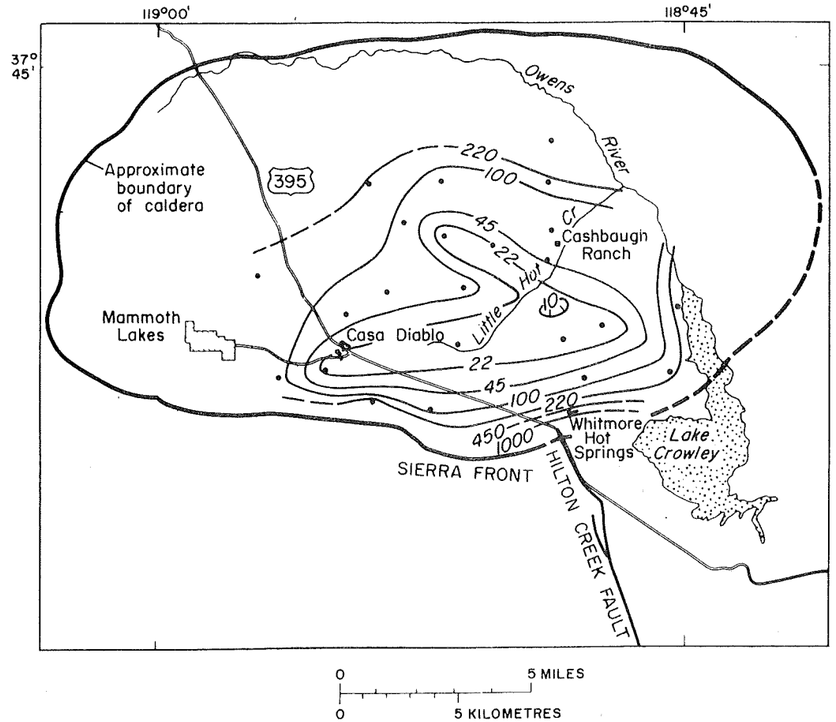

Fig. 5. The 8-Hz apparent resistivity map, Long Valley, California. Values are in ohm meters; contours are dashed where they are approximate.

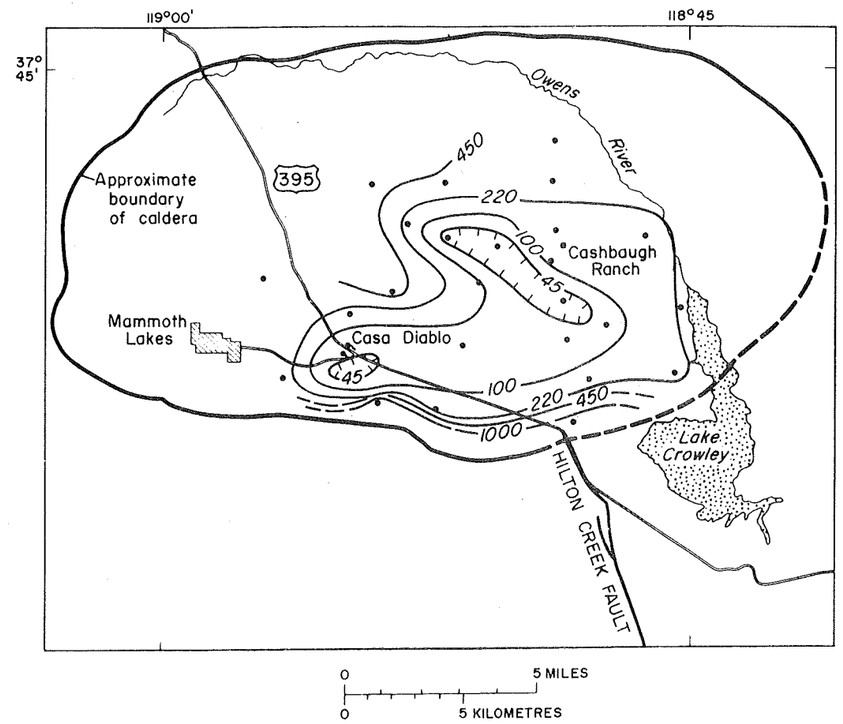

Fig. 6. The 26-Hz apparent resistivity map, Long Valley, California (electric line east-west). Values are in ohm meters; contours are dashed where they are approximate.

south telluric line orientation in the region of the anomaly. These lower values are believed to reflect the predominant north to northwest fault trend within the caldera, as was explained in the discussion of soundings at stations 14 and 16. Other differences between these two maps also are the result of lateral resistivity variations, but the low station density makes specific explanation or description of these variations impossible.

Mapped data at the higher frequencies continue to show the same general trends as the maps previously presented but with a smaller change in apparent resistivity across the map. Figure 8, the apparent resistivity at 7000 Hz, shows the near-surface resistivity variations in a general way. Although at the high frequency the volume of rock sampled at each station is quite small in comparison to the station spacing, the correlation of resistivity data with surface geology is quite good. The resistivity low now appears as a broad trough from Casa Diablo Hot Springs to the head of Lake Crowley. This is interpreted as the zone of most pervasive near-surface alteration and the region in which the saline hot spring waters discharge at the surface. The resistivities associated with the Sierra front are lower than those noted in the deeper data, showing the effect of weathering. On the 7000-Hz map the resurgent dome to the north of Casa Diablo has the highest resistivities in the mapped area; these resistivities do not differ much from values obtained at the lower frequencies. Rocks near the surface of the dome are young volcanics which have undergone little weathering.

In magnetotelluric work, electrical cross sections are often used as interpretational aids. These are called pseudosections and are usually plotted with frequency decreasing downward on a logarithmic scale. An obvious disadvantage of this type of pseudosection is the distorted idea of depth of exploration that is gives in areas where large changes in resistivity exist. We prefer a pseudosection plotted in terms of skin depth, which gives a better idea of the variation in exploration depth in complex areas. Figures 9 and 10 show skin depth pseudosections on a line oriented approximately north-south through Whitmore Hot Springs. Figure 9 was plotted for an east-west orientation of the telluric line. The major conductor is evident near Whitmore Hot Springs between stations 14 and 6 but continues somewhat deeper to the north under the Cashbaugh Ranch area. It is interesting to compare this figure with the total-field map which shows that the major low along the AMT line extends from station 31 to midpoint between stations 2 and 15. Figure 9 also shows clearly the large variation in exploration depth.

SUMMARY

The described AMT technique was developed for use as a reconnaissance geothermal exploration tool to search for conductive anomalies associated with hot saline waters and related altered rock. The exploration philosophy is that a survey using a relatively inexpensive technique such as AMT would be followed by a more definitive electrical surveying program in promising areas. Long Valley was used as a test area for the technique because of the extensive supporting studies.

The correlation of AMT results with other detailed electrical work in Long Valley is considered very good and provides evidence for the effectiveness of the technique. In fact, if the

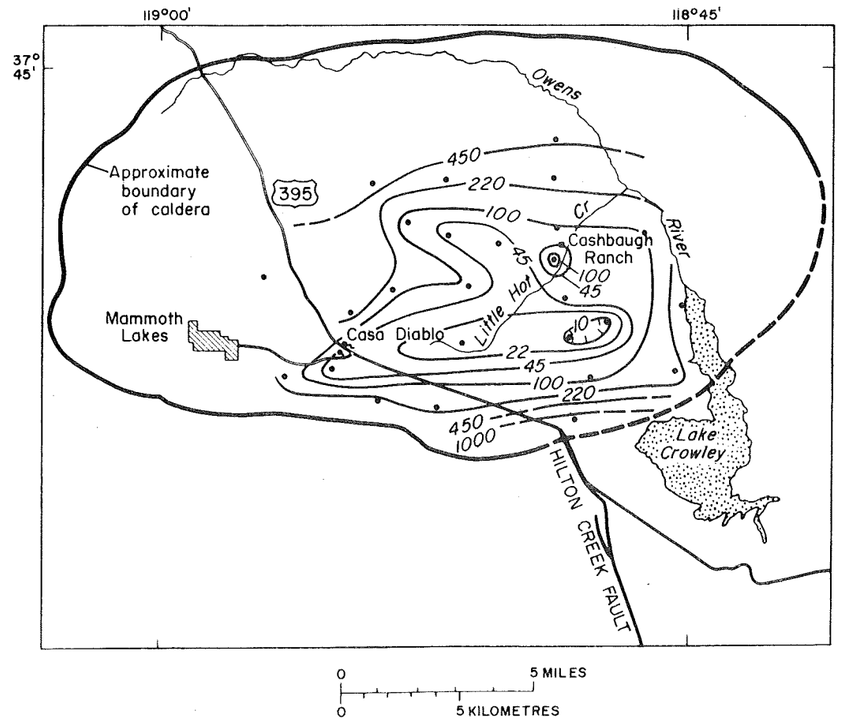

Fig. 7. The 26-Hz apparent resistivity map, Long Valley, California (electric line north-south). Values are in ohm meters; contours are dashed where they are approximate.

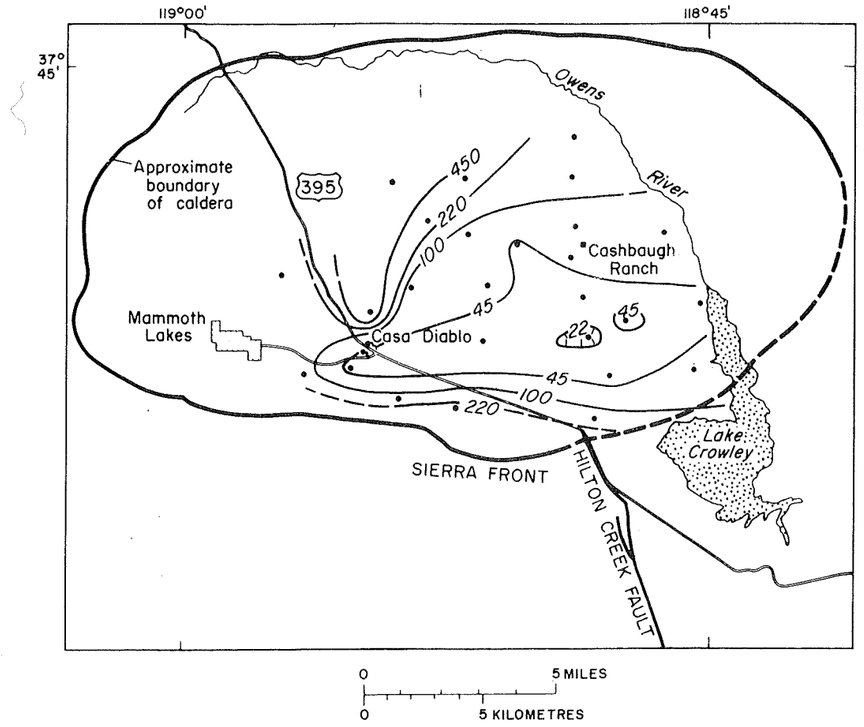

Fig. 8. The 7000-Hz apparent resistivity map, Long Valley, California. Values are in ohm meters; contours are dashed where they are approximate.

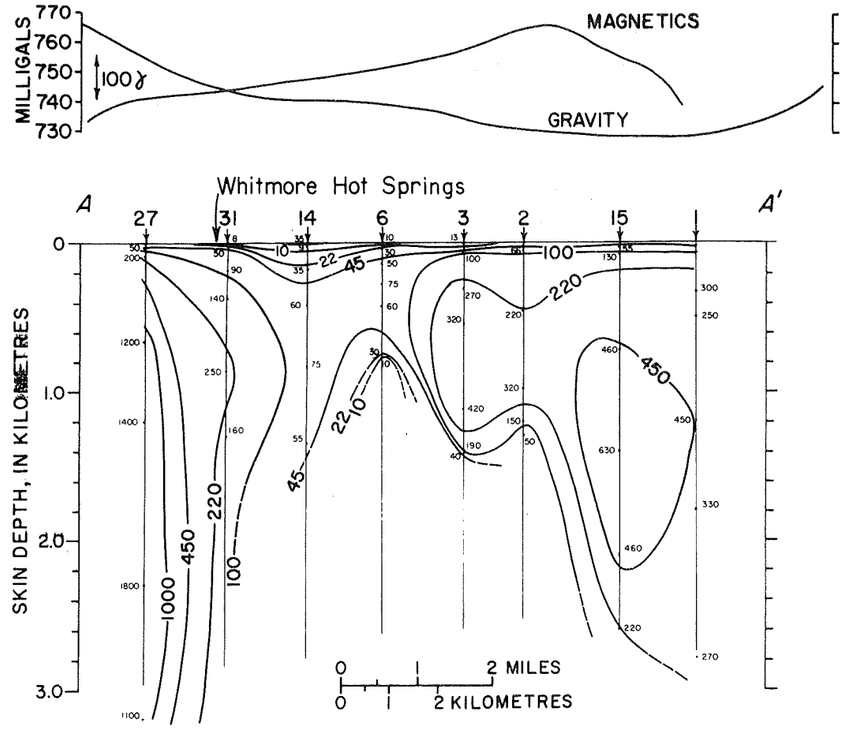

Fig. 9. Skin depth pseudosection along AA′ (electric line east-west), Long Valley, California. Line of section is shown in Figure 2. Values are in ohm meters.

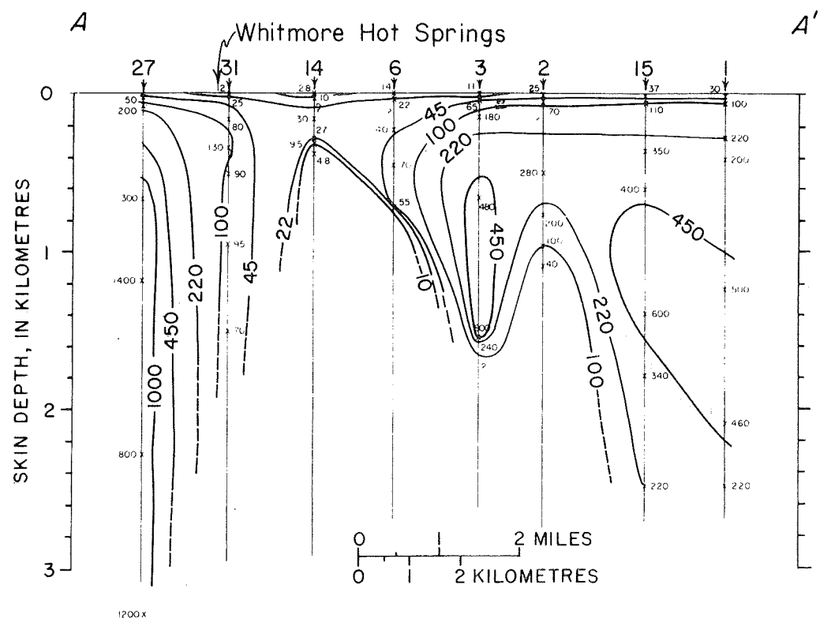

Fig. 10. Skin depth pseudosection along AA′ (electric line north-south), Long Valley, California. Line of section is shown in Figure 2. Values are in ohm meters.

AMT survey had been used to pinpoint an area for an intensive exploration program, the area selected would not have differed significantly from that identified by the more detailed surveys. The 2 man weeks of work involved in the field survey and the good correlation obtained with conventional techniques clearly demonstrate the effectiveness of AMT for reconnaissance exploration.

In terms of the geothermal potential of Long Valley the hot waters and associated alteration zones in near-surface materials appear from the geological and electrical data to be restricted to a V-shaped area extending from Casa Diablo, east to Whitmore Hot Springs, and then northwest to the head of Little Hot Creek. Within this region the thermal waters are concentrated along the fault zones, which act as channels along which hot water leaks from a poorly defined reservoir at depth. The AMT data thus imply that shallow exploration should be confined to faults within the V-shaped region encompassing the known hot springs.

REFERENCES

Bailey, R. A., G. B. Dalrymple, and M. A. Lanphere, Geology and geochronology of Long Valley caldera, Mono County, California, *J. Geophys. Res., 81,* this issue, 1976.

Bleil, D. F. (Ed.), *Natural Electromagnetic Phenomena Below 30 Kc/s,* pp. 205–260, Plenum, New York, 1964.

Cagniard, L., Basic theory of the magneto-telluric method of geophysical prospecting, *Geophysics, 18*(3), 605–635, 1953.

Frischknecht, F. C., Electromagnetic scale model study of geophysical methods using a plane wave source, Ph.D. thesis, Univ. of Colo., Boulder, 1973.

Keller, G. V., and F. C. Frischknecht, *Electrical Methods in Geophysical Prospecting,* pp. 90–196, Pergamon, New York, 1966.

Madden, T. R., and C. M. Swift, Magnetotelluric studies of the electrical conductivity structure of the crust and upper mantle, in *The Earth's Crust and Upper Mantle, Geophys. Monogr. Ser.,* vol. 13, edited by P. J. Hart, pp. 469–479, AGU, Washington, D. C., 1969.

Stanley, W. D., D. B. Jackson, and A. A. R. Zohdy, Deep electrical investigations in the Long Valley geothermal area, California, *J. Geophys. Res., 81,* this issue, 1976.

Strangway, D. W., and K. Vozoff, Mining exploration with natural electromagnetic fields, Mining and Ground Water Geophysics, 1967, *Econ. Geol. Rep. 26,* pp. 109–122, Can. Geol. Surv., Ottawa, Ontario, 1970.

Strangway, D. W., C. M. Swift, Jr., and R. C. Holmer, The application of audio-frequency magnetotelluric (AMT) to mineral exploration, *Geophysics, 38*(6), 1159–1175, 1973.

Vozoff, K., The magnetotelluric method in the exploration of sedimentary basins, *Geophysics, 37*(1), 98–141, 1972.

Ward, S. H., The electromagnetic method, in *Mining Geophysics,* vol. 2, *Theory,* pp. 224–372, Society of Exploration Geophysicists, Tulsa, Okla., 1967.

(Received January 23, 1975;
revised September 2, 1975;
accepted September 12, 1975.)

Deep Electrical Investigations in the Long Valley Geothermal Area, California

WILLIAM D. STANLEY, DALLAS B. JACKSON, AND ADEL A. R. ZOHDY

U.S. Geological Survey, Denver, Colorado 80225

Direct current resistivity and time domain electromagnetic techniques were used to study the electrical structure of the Long Valley geothermal area. A resistivity map was compiled from 375 total field resistivity measurements. Two significant zones of low resistivity were detected, one near Casa Diablo Hot Springs and one surrounding the Cashbaugh Ranch–Whitmore Hot Springs area. These anomalies and other parts of the caldera were investigated in detail with 49 Schlumberger dc soundings and 13 transient electromagnetic soundings. An extensive conductive zone of 1- to 10-Ωm resistivity was found to be the cause of the total field resistivity lows. Drill hole information indicates that the shallow parts of the conductive zone in the eastern part of the caldera contain water of only 73°C and consist of highly zeolitized tuffs and ashes in the places that were tested. A deeper zone near Whitmore Hot Springs is somewhat more promising in potential for hot water, but owing to the extensive alteration prevalent in the caldera the presence of hot water cannot be definitely assumed. The resistivity results indicate that most of the past hydrothermal activity, and probably most of the present activity, is controlled by fracture systems related to regional Sierran faulting.

INTRODUCTION

Geological, hydrological, geochemical, and geophysical studies have been completed in the Long Valley geothermal area and are reported in this special issue. This paper describes the results of electrical geophysical studies using dc resistivity and time domain electromagnetic methods. The goals for this electrical geophysical study were (1) to provide additional information on the geology and the structure of the Long Valley caldera, (2) to outline conductivity anomalies possibly caused by thermal effects, (3) to aid in test hole siting, and (4) to evaluate the overall hydrothermal potential of the caldera hot-water system.

Both dc and electromagnetic methods have been used extensively in geothermal areas [*Duprat,* 1970; *Meidav,* 1970; *Cheng,* 1970; *Zohdy et al.*, 1973; *Stanley et al.,* 1973; *Jackson,* 1973; *Risk et al.,* 1970]. Depending upon the geologic environment, rock resistivities in a hydrothermal system may be decreased by several orders of magnitude because of a combination of factors:

1. Increased temperature causes lowered resistivities because of increased ionic mobility.
2. Increased temperature generally causes more dissolved solids to occur in the rock fluids, lower resistivities resulting because of increased ionic concentrations.
3. Hydrothermal alteration, mainly the formation of clays and zeolites, provides higher ionic exchange capabilities.
4. Solution activity generally increases porosity and permeability in consolidated rocks, the rock resistivities thus being decreased. However, at the upper boundaries of a convecting system, precipitation of silicates and other dissolved solids may result in large thicknesses of an impermeable precipitate of high resistivity.

Steam phase zones or mixed phase zones may depart from the general rule of lowered resistivities in a hydrothermal system.

SURVEY METHODS

Total field resistivity measurements. In order to compile a resistivity map of the caldera representing rock resistivity down to 1–2 km, bipole-dipole mapping techniques [*Zohdy,* 1973] were used. In this application a long (3–5 km) grounded wire was used to transmit a square wave with frequencies from 0.035 to 0.14 Hz and amplitudes of up to 50 A at 600–800 V. The electric field was measured by using two quasi-orthogonal measurement dipoles at dipole stations surrounding the bipole, bipole center to dipole center separations of up to 16 km being used. The electric field E along one dipole is the potential difference divided by the dipole length. The bipole-dipole array used for these studies is illustrated in Figure 1. The current bipole is shown as AB, and the measurement dipoles as MN and MN'. In addition, measurement may be made along NN'. The total electric field E is resolved from the measured components as shown in the polar plot in the upper right portion of the figure. A measure of the accuracy of the total electric field determination is provided by the size of the triangle which is formed by the projection of the three components. The measurement of three components instead of two is particularly useful when one of the two normally measured components is very small or the sign and angle between the two components means that neither component is nearly as large as the total field, a situation conducive to large errors in computation.

The simple total field resistivity [*Zohdy,* 1973] is determined from the equation

$$\bar{\rho}_E = K_{e_0} |E|/I$$

where $|E|$ is the magnitude of the total electric field, I is the input current, and K_{e_0} is the geometric factor defined by

$$K_{e_0} = \frac{\rho_0 I}{E_0} = 2\pi\left[\left(\frac{Y}{AO^3} - \frac{Y}{BO^3}\right)^2 + \left(\frac{x+L}{AO^3} - \frac{x-L}{BO^3}\right)^2\right]^{-1/2}$$

where E_0 is the electric field magnitude which would be measured over a homogeneous half space of resistivity ρ_0 with an input current of I and x, y, L, AO, and BO are as indicated in Figure 1.

Direct current soundings. Direct current vertical electrical soundings (VES) were made by using the Schlumberger array [*Keller and Frischknecht,* 1966]. Apparent resistivities for the Schlumberger array $\bar{\rho}_s$ are computed from

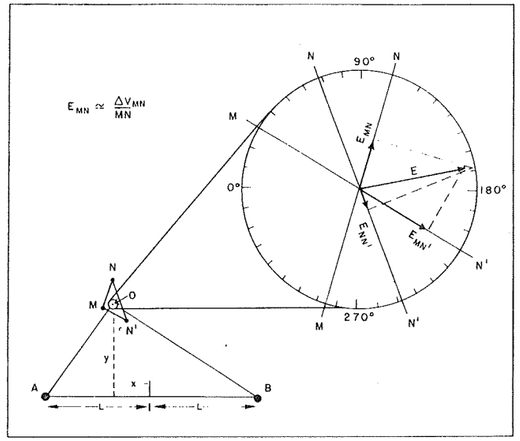

Fig. 1. Diagram of bipole-dipole array used in measuring simple total field resistivity. A and B are ground points for the bipole wire; M, N, and N' are the location of earth contact electrodes at the ends of the measurement dipoles. The polar plot in the upper right illustrates how the total field is resolved from the two or three measured components.

$$\bar{\rho}_s = \pi\left(\frac{(AB/2)^2}{MN} - \frac{MN}{4}\right)\frac{V_{MN}}{I}$$

where AB is the distance between current electrodes, MN is the distance between the potential electrodes, V_{MN} is the potential difference between the potential measuring electrodes, and I is the input current.

Time domain electromagnetic soundings. Time domain electromagnetic soundings [*Vanyan,* 1966; *Jacobson,* 1969] were made by measuring the derivative of the transient vertical magnetic field H_z caused by the current transition at the square wave input to the long grounded wire used for bipole-dipole mapping. This technique essentially measures the response of the earth to a step input. If a layered earth is assumed, information about layer thicknesses and resistivities can be obtained from the transient response. The vertical component of the transient magnetic field and the parallel component of the electric field are the most diagnostic measures of the layering parameters; however, because of induced polarization effects the electrical field measurement is less suitable than the magnetic field measurement for this type of sounding. Information about deep layers is contained mainly in the late time portion of the transient magnetic field, whereas information about the shallow layers is exhibited at early times. We denote the tran-

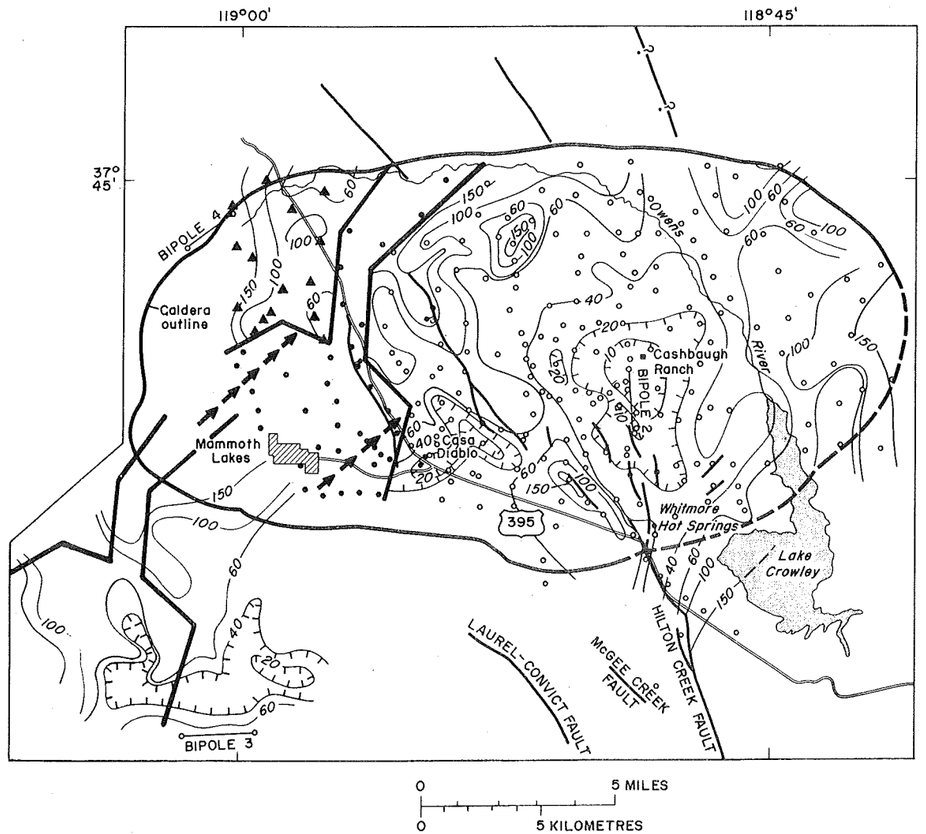

Fig. 2. Total field resistivity maps for bipole 2, 3, and 4 data. The contours for bipole 3 data have been displaced to the southwest for ease of presentation. The bold lines at the eastern margin of the bipole 4 map and at the western edge of the bipole 2 map (that define the area of the bipole 3 survey) have been reproduced on the displaced bipole 3 map to show its relationship to the other maps. Receiver stations for bipoles 2, 3, and 4 are denoted by open circles, solid circles, and solid triangles, respectively.

sient measurements described in this paper as transient magnetic soundings (TMS).

Instrumentation. The transmitter used for the bipole-dipole and TMS measurements is a square wave generator capable of an output of 80 A at 0.001–400 Hz. The square wave rise time for 3–5 km of #8 single conductor cable with a ground point resistance of 100 Ω is less than 1 ms, making it ideal for time domain electromagnetic soundings. A crystal oscillator controlling the transmitter can be synchronized with an identical oscillator in a receiver unit to provide a phase reference at the point of measurement. This phase reference was not used in synchronous detection as originally intended because a suitable detector had not been completed at the time of the survey. The phase reference was used, however, to determine the sign of the received wave form for electric field measurements and to determine time of switching for the TMS measurements.

All recording of electric fields for the bipole-dipole mapping and Schlumberger measurements was done by using strip chart recorders. Receiver dipoles were usually either 30 m or 150 m in length. The sensor for the TMS consisted of a 39-turn air core loop with an effective area of 256,000-m² turns; this loop was used to measure the derivative of the vertical component of the transient magnetic field. The voltages from the loop were amplified and recorded on a strip chart recorder after being passed through a notch filter for 60-Hz rejection.

Data Processing

Sounding data. The Schlumberger resistivity sounding data obtained in the field were adjusted to compensate for offsets caused by potential electrode spacing changes [*Kunetz*, 1966] and were smoothed to remove small cusps caused by near-surface lateral inhomogeneities [*Zohdy*, 1975]. The adjusted and smoothed curves were then digitized at six points per log cycle and processed by an automatic inversion program [*Zohdy*, 1974*c*, 1975]. The automatic program typically provides an interpretative solution of the field data consisting of seven to ten layers. Dar Zarrouk curves [*Zohdy*, 1974*a*] were then used to produce geoelectrically equivalent solutions that contained fewer layers and were correlated with nearby soundings. The final layering interpretations were checked by generating theoretical sounding curves [*Zohdy*, 1974*b*] for comparison with the field data.

Strip chart recordings of the TMS data were digitized, in terms of a time sequence of voltages, and an inverse filter was applied [*Brigham et al.*, 1968] to correct for recording system response. The resulting curves, plotted on log-log paper, were then compared with theoretical curves for a layered earth computed by using dipolar source programs developed by *Anderson* [1973] and also with curves for a finite source developed recently by W. L. Anderson (personal communication, 1974).

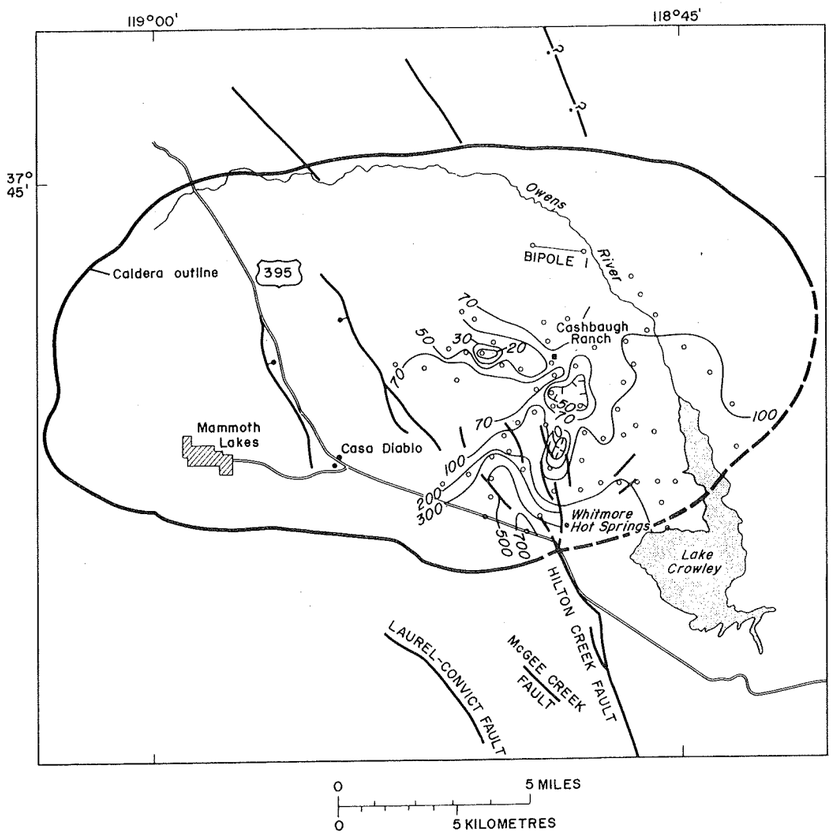

Fig. 3. Total field resistivity map for bipole 1 data. Receiver stations are denoted by open circles.

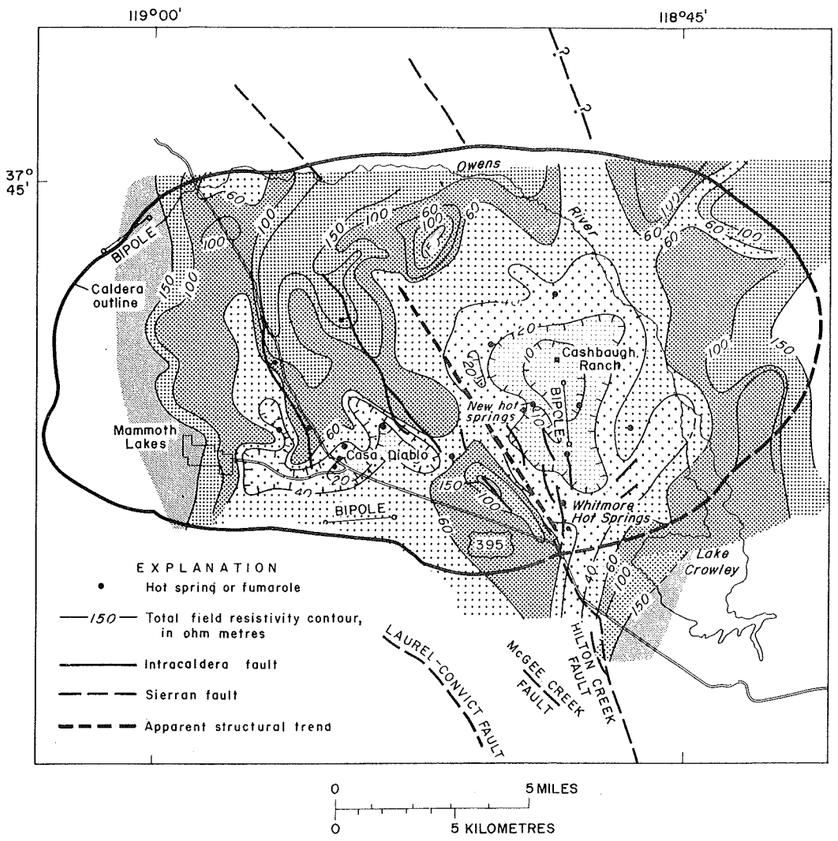

Fig. 4. Composite total field resistivity map for Long Valley caldera compiled by using data from bipoles 2, 3, and 4.

Bipole-dipole data. The total field resistivity data were processed in the field by using a programable calculator, further processing upon return from the field other than rechecking of values thus being unnecessary. The data obtained for each bipole installation were contoured for presentation in map form. Four separate apparent resistivity maps were compiled by using data from the four bipole installations. The maps for bipoles 2, 3, and 4 are shown in Figure 2, and the map for bipole 1 is shown in Figure 3. In order to compare the resistivity results with geology and other geophysical maps it was necessary to combine the four apparent resistivity maps into a single map. In considering the best method of doing this we were faced with the fact that the measured apparent resistivities about a given bipole source are a function not only of the resistivities of the geologic units in the area of the measurement but also of (1) the separation of dipole receiver and bipole transmitter, (2) the azimuth from bipole source to dipole receiver, and (3) the orientation of structures with respect to the source. Fortunately, in most geothermal areas, contrasts and physical dimensions are such that anomalies of interest are generally evident for a wide range of polarization directions and bipole-dipole separations (see, for instance, *Risk et al.* [1970] and *Stanley et al.* [1973]). This seemed to be true in Long Valley; for example, comparison of the maps for bipole 2 and bipole 3 reveals that the resistivity low near bipole 3 on that map shows up clearly on the bipole 2 map also. Comparison of the maps for bipole 1 (Figure 3) and bipole 2 (Figure 2), however (the bipole 1 stations are a subset of bipole 2 stations), indicates that the resistivity low near the bipole 2 site appears quite different on the two maps. This difference is caused by the fact that bipole 2 was inside the resistivity low, but bipole 1 was outside. Our electrical sounding interpretations show that the apparent resistivities from the bipole 2 source represent the true resistivities in the anomalous region more accurately. For this reason and because we covered most of the caldera using bipole 2, we elected to use only bipole 2, 3, and 4 data in compiling a composite map.

A synthesis of the three maps was achieved by using bipole 3 data in areas where data were not available from bipole 2 or bipole 4 and values from the latter bipoles in all other areas. The composite map (Figure 4) is the result of contouring the data values selected according to this scheme.

Interpretation of Geophysical Data

Total field resistivity map. The composite resistivity map shown in Figure 4 includes the locations of faults (modified from *Bailey et al.* [1976]) and thermal features in Long Valley, while Figure 5 provides an outcrop geology base [from *Bailey*

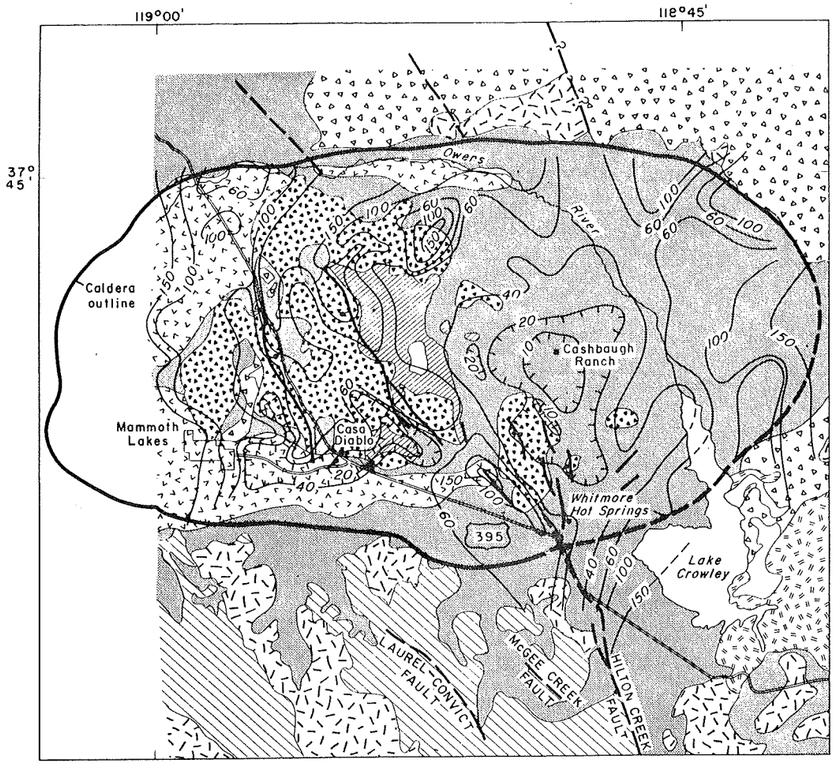

Fig. 5. Generalized geology of Long Valley caldera [after *Bailey et al.*, 1976]. Resistivity contours from this article are superimposed on the geology.

et al., 1976] for the resistivity map. The character of the total field map reveals the basic complexity of the volcanic units and hydrothermal alteration patterns within the caldera. The edge of the caldera appears to be well defined on the west, north, and east sides of the resistivity map, but on the south side the caldera boundary is not as well defined. This is probably caused by the fact that the south side of the caldera is bounded by a roof pendant of metasedimentary rocks, which are less resistive than the granodiorites that bound the structure on the other three sides.

The large volcanic centers in the resurgent dome [*Bailey et al.*, 1976] are outlined on the resistivity map by the complex of high resistivities north of Casa Diablo Hot Springs. The eastern half of the caldera is covered with unconsolidated sediments and is somewhat lower in resistivity than the western half. There are two major regions of low resistivities. The first of these is centered about the Cashbaugh Ranch area, and the second is in the region south of Casa Diablo Hot Springs.

The Cashbaugh Ranch anomaly is defined by the region with resistivities of less than 40 Ωm; however, apparent resistivities as low as 2 Ωm were measured. The anomalous region is bounded on the west by the indicated apparent structural

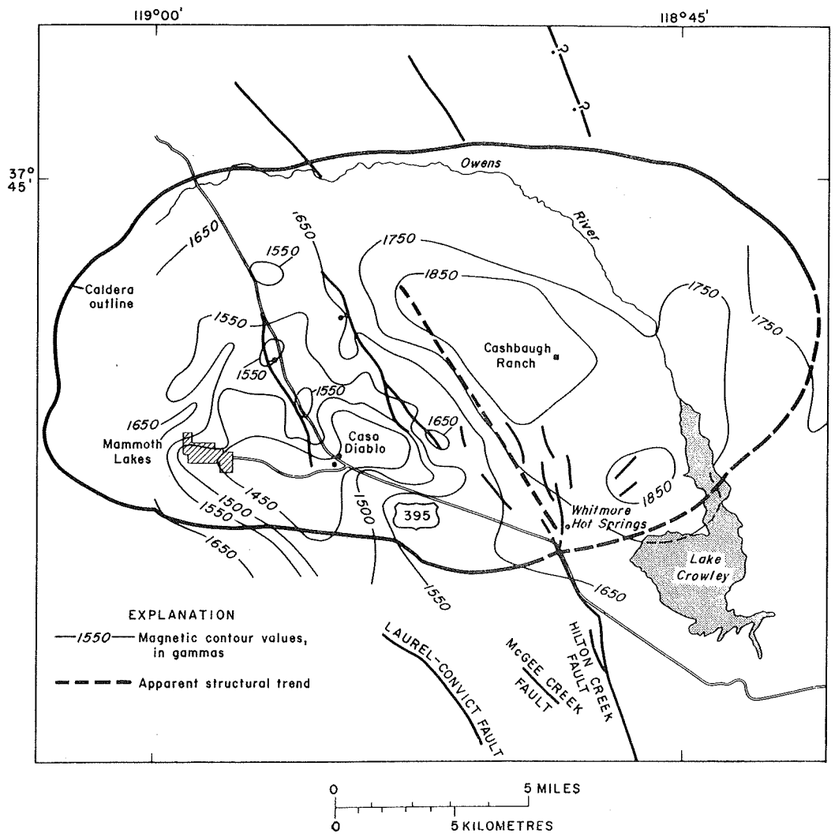

Fig. 6. Aeromagnetic map modified from *Pakiser et al.* [1964]. The map was compiled from data obtained at a flight elevation of 2.7 km.

trend, which is also evident on the aeromagnetic maps (Figures 6 and 7) and gravity map [*Kane et al.*, 1976]. On the north the resistivity anomaly appears to be truncated 2–3 km from the Cashbaugh Ranch. On the east the anomaly is truncated relatively sharply along a north-south line, and the extension of the anomaly southward into the Hilton Creek fault zone is evident. In addition to the main anomaly, there is a spur branching northeast from near the intersection of the Hilton Creek fault and the south caldera margin toward the north end of Lake Crowley. The lowest apparent resistivities were measured in a small graben southwest of Cashbaugh Ranch (small region of less than 10 Ωm aligned northwest-southeast). Several hot springs existed at the time of the survey in Hot Creek at the northwest end of this graben. Several new hot springs broke out at the northeast corner of the graben in August and October of 1973 after earthquakes occurred south and southeast of the caldera [*Bailey et al.*, 1976]. Thus the extremely low resistivities seem to indicate hot water in the highly fractured rocks of the small graben. Apparent resistivities of 2–4 Ωm were measured; therefore true resistivities are probably lower than this.

The second resistivity low is centered slightly south of Casa Diablo Hot Springs and is defined by the region with resistivities of less than 40 Ωm. The main part of the low trends in a roughly east-west direction but has a northwest-southeast pendant on the east end and an extension on the west following the keystone graben western boundary fault northward for several kilometers. These features of the anomaly shape may be representative of a ring fracture encircling the resurgent dome. The resistivity low is coincident with an aeromagnetic low of almost identical shape (Figure 6). The aeromagnetic low is superimposed upon a broader low which passes through the western part of the caldera from south to north (Figure 7). This throughgoing low is probably caused by nonmagnetic precaldera roof pendant rocks [*Kane et al.*, 1976]. The second aeromagnetic low corresponds to a total field resistivity low upon which the Casa Diablo resistivity low is superimposed. It has been estimated by using the aeromagnetic data that the roof pendant rocks are only 1 km beneath the surface in the western margin of the caldera (D. R. Mabey, personal communication, 1974), which agrees with indications from the total field maps and from sounding interpretations. The roof pendant rocks are probably more conductive than the Sierran granodiorites. However, it is possible that hot geothermal fluids in this zone could be contributing to the low resistivities. The central part of the Casa Diablo resistivity low is probably caused by extensive alteration in a tuff unit, hot geothermal fluids, or both. The central part of the Casa Diablo

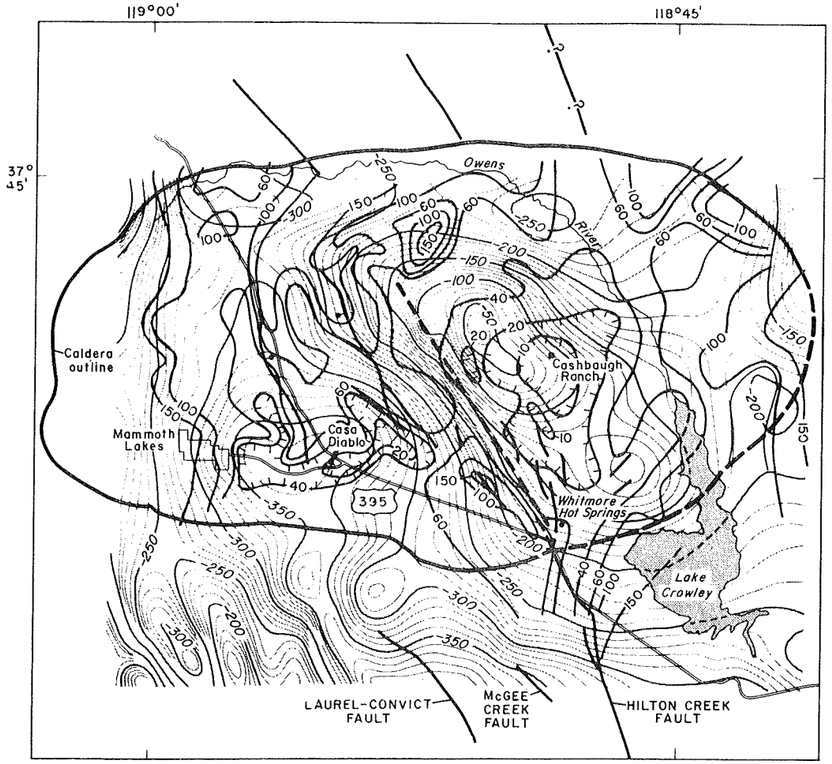

Fig 7. Aeromagnetic map from *Kane et al.* [1976] with resistivity contours from this article. The map was compiled from data obtained at a flight elevation of 4.5 km.

aeromagnetic low is probably due to hydrothermal destruction of magnetite, a phenomenon observed in hand samples from altered rhyolites around Casa Diablo Hot Springs.

Resistivity cross sections. The two main resistivity lows near Cashbaugh Ranch and Casa Diablo Hot Springs were investigated by electrical soundings to determine the probable causes of the map anomalies. Forty-nine Schlumberger VES were completed in the caldera by using maximum electrode spacings, $AB/2$, ranging from 1.22 to 3.66 km. Thirteen TMS were made by using bipoles 1 and 2.

Several resistivity cross sections were constructed from the VES and TMS interpretations, and the various electrical cross sections were used to construct a fence diagram through most of the area covered by the soundings. The locations of the fence segments, designated A–I in a clockwise direction, are shown in Figure 8 with all of the individual VES and TMS locations. In Figure 9 the fault patterns (modified from *Bailey et al.* [1976]), both regional and intracaldera, are superimposed on the fence diagram. The electrical layers may be classified as generally representing the following geologic units: (1) 1–10 Ωm, hydrothermally altered rhyolitic tuffs with both normal and high-temperature water, (2) 10- to 45-Ωm, clay-rich sediments or slightly altered rhyolitic volcanics, (3) 45- to 100-Ωm, unaltered water-saturated rhyolitic volcanics and coarse alluvium, and (4) 100- to 450-Ωm, unaltered basalt, dry volcanics, alluvial fan materials, and precaldera basement granodiorites.

A thick resistive layer at depths of 1–2 km (such as that at VES 26 on section CE) was detected on several of the soundings which are not shown on the fence diagram. This resistive layer (resistivities greater than 80–100 Ωm) is probably not precaldera basement rock but may represent the Bishop tuff, a unit which parametric VES data from outside the caldera indicate has a resistivity of about 80 Ωm. Seismic [*Hill et al.*, 1976] and gravity [*Kane et al.*, 1976] data indicate that batholith rocks are at a depth of about 3–4 km in the eastern part of the caldera.

We consider that the 1- to 10-Ωm layer generally represents rhyolitic rocks which have been extensively altered, contain large amounts of dissolved solids, and in some cases contain

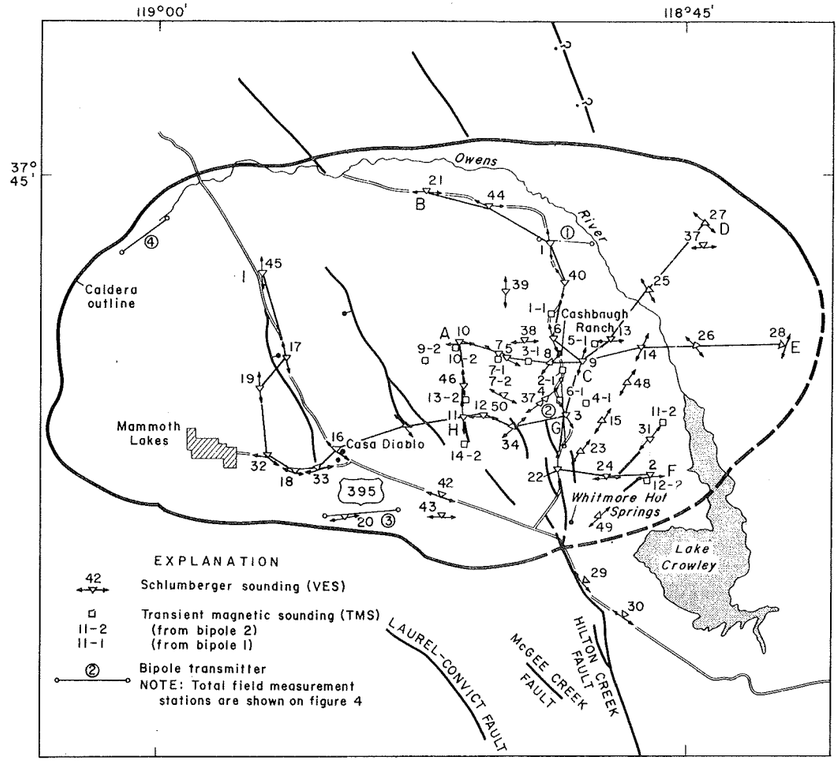

Fig. 8. Map showing location of VES and TMS and resistivity cross-section segments used in constructing the fence diagram of Figure 9. Fence segments are designated as A–I.

high-temperature water. Note that the Hilton Creek fault system has apparently been the major focus of activity along segments AC, AH, HG, CG, and GF of the fence diagram. The general attitudes and thicknesses of the conductive layer (1–10 Ωm) tend to suggest to us that the layer bears a close relationship to the occurrence of rhyolitic tuffs from sources around the resurgent dome (Figure 5). The thickening of the conductor layer along segment CGF is probably caused by a major active spur of the Hilton Creek fault passing about through points C and G. The total field resistivity low that extends from south of Whitmore Hot Springs to the north end of Lake Crowley is apparently caused by the deep conductor along segment GF.

How much of the 1- to 10-Ωm zone contains exploitable amounts of hot water is not known. It is known that wells at Casa Diablo Hot Springs have produced large amounts of hot water and steam and that considerable amounts of boiling water are issuing from the ground near the apex HGC. The only deep well data available in the eastern part of the caldera come from the U.S. Geological Survey test hole LV1, which was drilled to a depth of 300 m [*Lewis*, 1974]. The location of this test hole is shown in Figure 9, approximately midway between VES 7 and 8. The induction electrical log from LV1 was compared with pseudo-electric logs constructed from the interpretations of VES 7 and 8 (Figure 10). The VES interpretations and the interpretation of TMS 7-2, which was coincident with VES 7, were completed before the well was drilled; in fact, the well was sited to test the nature of the conductive layer. The temperature log from LV1 (Figure 10) shows a maximum temperature (at the bottom of the hole) of 73°C, certainly not indicative of a significant reservoir of hot water in this locality. Study of well cores by R. Lewis and R. Bailey (personal communication, 1974) of the U.S. Geological Survey reveals that the upper part of the hole, down to about 145 m, is in lake sediments and the remainder of the hole is in mainly rhyolitic tuffs and ashes that have been highly zeolitized by hydrothermal activity. Thus the extremely low resistivities for the conductive zone in the area of LV1 appear to have been caused by past alteration and not by the presence of hot water.

Interpretation of the true resistivity of the conductive layer was aided by the fact that TMS 7-2 was coincident with VES 7. The TMS data (Figure 11) indicated that the resistivity of the conductive layer was 1.5–3 Ωm, as the two TMS models illustrate. The model used to interpret the VES 7 data (Figure 12) agrees well with the TMS model C2 with regard to the conductive layer. The electromagnetic sounding is more sensitive to conductive layers and less sensitive to resistive layers than

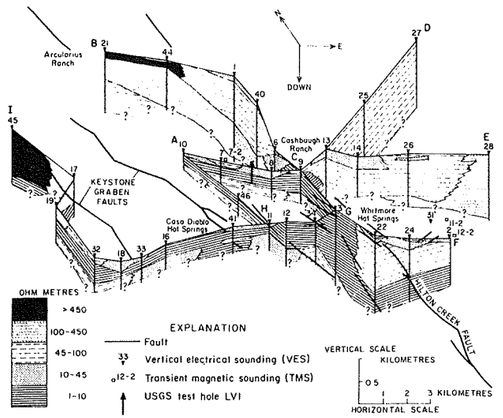

Fig. 9. Fence diagram constructed from sounding interpretations.

the VES. Therefore the models depart considerably in the shallow layers. We feel that when dc and electromagnetic sounding interpretations are combined in this way, a more accurate interpretation is obtained. This is supported by the fact that the induction log resistivities from LV1 had an average value of 2.5 Ωm for the conductive zone.

If the conductive zone (1–10 Ωm) shown in Figure 9 at Casa Diablo is due partly to highly zeolitized tuffs and partly to the presence of water up to 170°–180°C, as is indicated from the commercial wells at Casa Diablo, the effects cannot be separated. For a porous rock without clay minerals we would expect about a 250% decrease in resistivity for an increase in temperature from 73° to 180°C [*Meidav,* 1970]. However, with the high degree of alteration in the volcanics, such large resistivity differences might not be observed. The rocks in the Casa Diablo resistivity low may not be as highly altered as those near LV1, i.e., an effect from high-temperature fluids could be present but is undeterminable. Thus for all of the

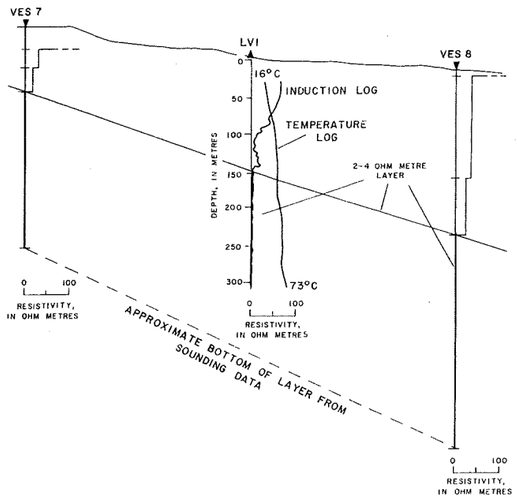

Fig. 10. Test hole LV1 temperature and induction logs with interpretations for VES 7 and VES 8.

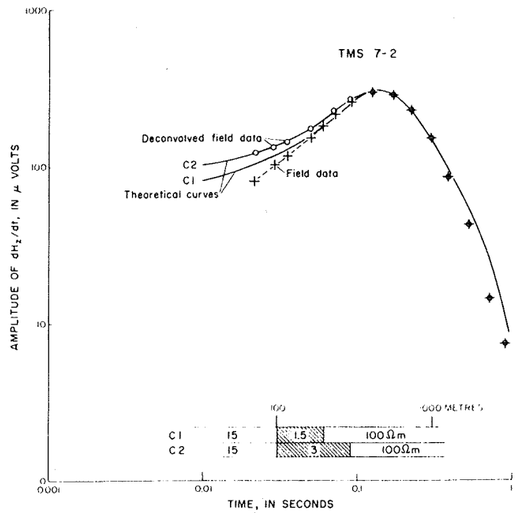

Fig. 11. Field data and interpretations for TMS 7-2. Models used for computing the theoretical curves C1 and C2 are plotted with depths along the horizontal logarithmic axis. The numbers in the model layers represent interpreted resistivity in ohm meters.

conductive zone (the 1- to 10-Ωm layer on the fence diagram) we cannot tell whether the resistivities are low owing to the presence of high-temperature fluids, alteration like that near LV1, or both.

A major question to be answered concerns the existence of deep conductors, such as the one shown on segment GF of Figure 9 at other locations in the caldera. We found no evidence in the total field data of any deep conductors except those shown on the fence diagram of the resistivity cross sections (Figure 9). Interpretation of the total field resistivity measurements as pseudo-soundings (by plotting the resistivities versus bipole-dipole center separation) were of no help in this respect because of the extreme lateral resistivity variations across the span of large bipole-dipole separations.

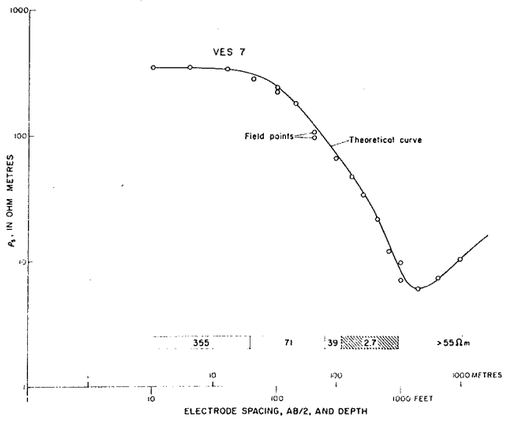

Fig. 12. Field data and interpretation for VES 7. Model used to calculate the theoretical curve is plotted with depth along the horizontal logarithmic axis, and the numbers in the model layers are interpreted resistivity in ohm meters.

Some constraints are placed upon the possibility of the existence of deep conductors, however, by the TMS data. To illustrate the effect that a conductor in the zone of 1–2 km would have upon the type of TMS data obtained in Long Valley, two model curves are presented in Figure 13. Curves A and B for models A and B show that the deep conductor has significant effect upon the TMS curve shape and the position of the asymptotic right branch. Model B in Figure 13 is modified from the model used for TMS 7-2 (Figure 11) by the addition of the deeper conductor.

From consideration of models such as those of Figure 13 we tend to rule out the possibility of extensive deep conductors in the eastern half of Long Valley (TMS data were not obtained in the western half). We do not see any evidence of major deep conductors in the TMS data other than the one on segment GF of Figure 9. From our TMS model studies we define a major conductor in Long Valley as one of at least 0.5-km thickness and less than 10-Ωm resistivity (greater than 50-mho conductance).

If major reservoirs with 150°–200°C or greater water exist in permeable rhyolitic volcanic rocks at depths less than 2 km, then we would expect them to approach our definition of major conductors (greater than 50-mho conductance) unless significant amounts of the reservoir fluids occur in a mixed phase system (steam and water). Under these assumptions a laterally extensive reservoir such as this was not detected in the electrical data in the upper 2 km.

Speculations and conclusions. The bipole-dipole resistivity, VES, and TMS data have provided a detailed picture of the electrical structure of the upper 2 km in Long Valley. These data reveal that hydrothermal activity observed at the surface and at depth by the electrical interpretations is largely controlled by fracture systems, especially those related to regional Sierran faulting. Most of the hydrothermal alteration patterns in the upper kilometer seem to be related to an ash and tuff unit flanking the resurgent dome. This conductive zone is known to contain water of only 73°C in one place (LV1) but water of up to 150°–180°C in another (Casa Diablo Hot Springs).

The only deep conductor detected which may represent a significant reservoir in the range 1–2 km is the conductive zone illustrated on segment GF of Figure 9. This zone may be representative of a reservoir in permeable volcanic rocks which is feeding the hot springs and shallow hot-water zones in this part of the caldera. The occurrence of hot water in this deep zone, if hot water is present, may be limited to the vicinity of the fractures related to the Hilton Creek fault system, as is suggested by the shape of the resistivity anomaly outlining this zone in Figure 4. This fracture system may be carrying hot water upward from depths even greater than 2 km, where the actual primary reservoir of 200°C water (suggested by geothermometric data) may occur in Long Valley. But then again the electrical anomaly may also be caused largely by extensive past hydrothermal alteration and not by the presence of high-temperature geothermal fluids. Zones in the upper 2 km of Long Valley which contain a mixed phase fluid may not have been delineated by the electrical data, although these zones may exist.

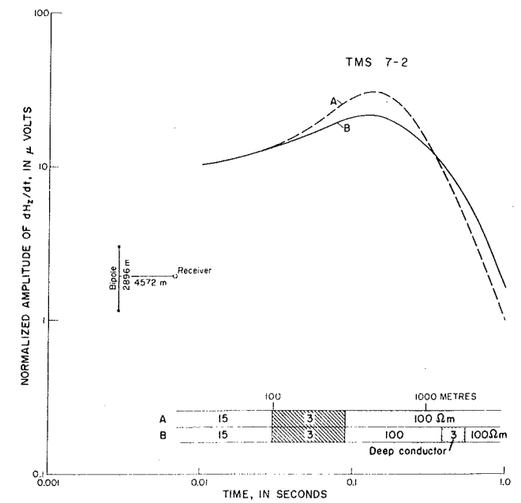

Fig. 13. Theoretical models and computed curves for TMS soundings. Model A is the model used for interpreting TMS 7-2. Model B has an additional deep conductor with a resistivity of 3 Ωm and a thickness of 500 m. Bipole length and bipole-receiver separation are shown in the lower left of the figure.

REFERENCES

Anderson, W. L., Fortran 4 programs for the determination of the transient tangential electric field and vertical magnetic field about a vertical magnetic dipole for an *m*-layer stratified earth by numerical integration and digital linear filtering, *Rep. PB2-21240,* 82 pp., Nat. Tech. Inform. Serv., Springfield, Va., 1973.

Bailey, R. A., G. B. Dalrymple, and M. A. Lanphere, Volcanism, structure, and geochronology of Long Valley caldera, Mono County, California, *J. Geophys. Res., 81*(2), this issue, 1976.

Brigham, O. E., H. W. Smith, F. X. Bostick, and W. D. Duesterhoeft, An iterative technique for determining inverse filters, *IEEE Trans. Geosci. Electron., 6*(2), 86, 1968.

Cheng, W . T., Geophysical exploration in the Tatun volcanic region, Taiwan, *Geothermics, Spec. Issue 2,* 262–274, 1970.

Duprat, A., Contribution de la géophysique à l'étude de la région géothermique de Denizle-Sararykay, Turquie, *Geothermics, Spec. Issue 2,* 275–286, 1970.

Hill, D. P., Structure of Long Valley caldera, California, from a seismic refraction experiment, *J. Geophys. Res., 81*(2), this issue, 1976.

Jaçobson, J. J., Deep electromagnetic sounding technique, Ph.D. thesis, Colo. Sch. of Mines, Golden, 1969.

Jackson, D. B., Map showing percent lateral effect of total field resistivity, Marysville area, Lewis and Clark Co., Montana, open file report, U.S. Geol. Surv., Menlo Park, Calif., 1973.

Kane, M. F., D. R. Mabey, and R.-L. Brace, A gravity and magnetic investigation of the Long Valley caldera, Mono County, California, *J. Geophys. Res., 81*(2), this issue, 1976.

Keller, G. V., and F. C. Frischknecht, *Electrical Methods in Geophysical Prospecting,* p. 95, Pergamon, New York, 1966.

Kunetz, G., *DC Resistivity Methods, Geoexploration Monogr.,* The Hague, Netherlands, 1966.

Lewis, R. E., Data on wells, springs, and thermal springs in Long Valley, Mono County, California, open file report, U.S. Geol. Surv., Menlo Park, Calif., 1974.

Meidav, T., Application of electrical resistivity and gravimetry in deep geothermal exploration, *Geothermics, Spec. Issue 2,* 303–310, 1970.

Pakiser, L. C., M. F. Kane, and W. H. Jackson. Structural geology and volcanism of Owens Valley regions, California—A geophysical study, *U.S. Geol. Surv. Prof. Pap. 438,* 1964.

Risk, G. F., W. J. P. MacDonald, and G. B. Dawson, D.C. resistivity surveys of the Broadlands geothermal region, New Zealand, *Geothermics, Spec. Issue 2,* 287–294, 1970.

Stanley, W. D., D. B. Jackson, and B. C. Hearn, Jr., Preliminary results of geothermal investigations near Clear Lake, Calif., open file report, U.S. Geol. Surv., Menlo Park, Calif., 1973.

Vanyan, L. L., *Electromagnetic Depth Soundings,* translated by G. V. Keller, Consultants Bureau, New York, 1966.

Zohdy, A. A. R., Total field resistivity mapping (abstract), *Geophysics, 38*(6), 1231, 1973.
Zohdy, A. A. R., The use of Dar Zarrouk curves in the interpretation of VES data, *U.S. Geol. Surv. Bull., 1313-D,* 1974*a*.
Zohdy, A. A. R., A computer program for the calculation of Schlumberger sounding curves by convolution, *Rep. PB-232056,* Nat. Tech. Inform. Serv., Springfield, Va., 1974*b*.
Zohdy, A. A. R., A computer program for the automatic interpretation of Schlumberger sounding curves over horizontally stratified media, *Rep. PB-232703,* Nat. Tech. Inform. Serv., Springfield, Va., 1974*c*.
Zohdy, A. A. R., Automatic interpretation of Schlumberger sounding curves using modified Dar Zarrouk functions, *U.S. Geol. Surv. Bull., 1313-E,* 1975.
Zohdy, A. A. R., L. A. Anderson, and L. J. P. Muffler, Resistivity self-potential, and induced polarization surveys of a vapor-dominated geothermal system, *Geophysics, 38*(6), 1130–1144, 1973.

(Received December 23, 1974;
revised September 12, 1975;
accepted September 15, 1975.)

VOL. 81, NO. 5 JOURNAL OF GEOPHYSICAL RESEARCH FEBRUARY 10, 1976

Seismic Noise Survey in Long Valley, California

H. M. IYER AND TIM HITCHCOCK

U.S. Geological Survey, Menlo Park, California 94025

In June 1973, seismic noise measurements were made in Long Valley, California, as part of the U.S. Geological Survey's geothermal investigations. Spatial variation of the average noise power shows high levels of noise extending over most of the eastern half of the Long Valley caldera. Since the noise high is almost similar in extent to the soft sedimentary Owens River basin, it is possible that ground amplification of seismic waves is at least partially responsible for the noise anomaly. Two lines of evidence indicate that geothermal noise may be present in Long Valley. (1) Relative amplification of teleseismic waves over soft ground, with respect to a reference station on hard rock, is about 12 dB. The noise anomaly, however, is at least 12 dB higher than this value. It is therefore difficult to explain the anomaly by postulating ground amplification of regional noise, thus indicating that a noise source may be present in the area of the anomaly. At wave frequencies below 2 Hz, river and cattle noise do not contribute much to the anomaly. (2) Group velocities of seismic noise, measured by using arrays, are in general quite low except at a few stations along the southern edge of the noise anomaly. The wave azimuths in the low-velocity areas show random propagation, whereas azimuths associated with the high-velocity waves point to the area where surface geothermal phenomena are found. The high-velocity waves also have frequencies below 2 Hz. If a noise source is present under the southern edge of the sedimentary basin, it could excite the basin much more than it does the hard ground directly above it and thus produce the observed noise anomaly.

INTRODUCTION

Even though there is considerable interest in using seismic noise in the frequency band of 1–10 Hz as a prospecting tool for geothermal energy, clear correlation between high noise levels and active hydrothermal reservoirs has been demonstrated only in very few regions [*Whiteford,* 1970; *Iyer and Hitchcock,* 1974]. The main problem is that cultural noise and noise generated by rivers and wind are in the same frequency band as geothermally generated seismic noise and often cause confusion in identifying the latter [*Douze and Sorrells*, 1972; *Iyer*, 1974]. As we shall show, ground conditions can cause amplification of background seismic noise; when this occurs in a geothermal area, it is difficult to interpret a seismic noise anomaly. Many case histories, such as the one on Long Valley to be discussed here, may eventually provide the material to evaluate the usefulness of seismic noise as a geothermal prospecting tool.

FIELD EXPERIMENT

The seismic noise survey in Long Valley during June 1973 follows the general procedure developed by the U.S. Geological Survey for noise studies in Imperial Valley, California, and Yellowstone National Park, Wyoming [*Iyer,* 1974; *Iyer and Hitchcock,* 1974]. EV-17 seismometers with slow-speed tape-recording systems (described by *Eaton et al.* [1970]) were used in the experiment. Profiles of 8 stations, with average spacing of about 2 km, were operated for 48 hours and then moved to a new location. One of two stations in a quiet area over hard ground was operated continuously during the entire period of the experiment. Nine stations had one vertical and two horizontal seismometers, 16 stations had three instruments arranged as an L array with 106-m instrument spacing, and the rest were single-component stations with vertical seismometers (Figure 1). Eight of the stations were reoccupied for 3 nights during November 1974. Noise measurements were also made for 1 night in Owens Valley near the town of Bishop, about 50 km south of Long Valley. The locations of stations and durations of their operations are given in Table 1.

DATA ANALYSIS

Analog tapes for the whole recording period were played back, and the records were carefully examined for instrumental malfunctions, cultural noise, transients, and earthquakes. In general, it is found that noise levels are much higher and more transients are present during the day than at night. Hence an hour-long data sample was selected from the quietest section of the night record for each profile and digitized at a rate of 50 samples per second. Samples at a permanent station were taken at approximately the same time as at the profile stations.

Two types of computations were performed on the digitized data. Spectral analysis of a typical noise sample of 40.96-s duration was done by using techniques developed for our Imperial Valley noise survey [*Iyer,* 1974]. Examination of several spectra shows that the predominant seismic noise energy in Long Valley is in the frequency band of 0.5–4 Hz. To study the spatial variation of noise energy in different frequency bands, the hour-long data sample is digitally filtered in frequency bands of 0–1, 1–2, 2–4, and 4–8 Hz, and average rms values are computed for successive 81.92-s data blocks. (The summation over the 0- to 1-Hz band representing low-frequency energy is uncorrected for seismometer response. Since the seismometer response drops off sharply below 1 Hz, there is very little contribution from seismic frequencies below about 0.25 Hz in this band.) The total unfiltered seismic energy is also calculated for each block. Out of the 43 values thus computed for each hour-long sample the quietest 30 were averaged to give a representative noise level in millimicrons per second of ground velocity.

Our noise survey at Long Valley lasted for 4 weeks. As mentioned earlier, the variation of noise level during this period was monitored by one of two reference stations, P2 and P3 (Figure 1), where noise levels are similar. The noise level in different frequency bands at these stations (Figure 2) varied somewhat during the period of the experiment. Because the profiles of stations in different areas were operated on different days, the observed noise levels have to be corrected for this regional variation. This correction is accomplished by computing relative noise levels (ratio of noise level at each station

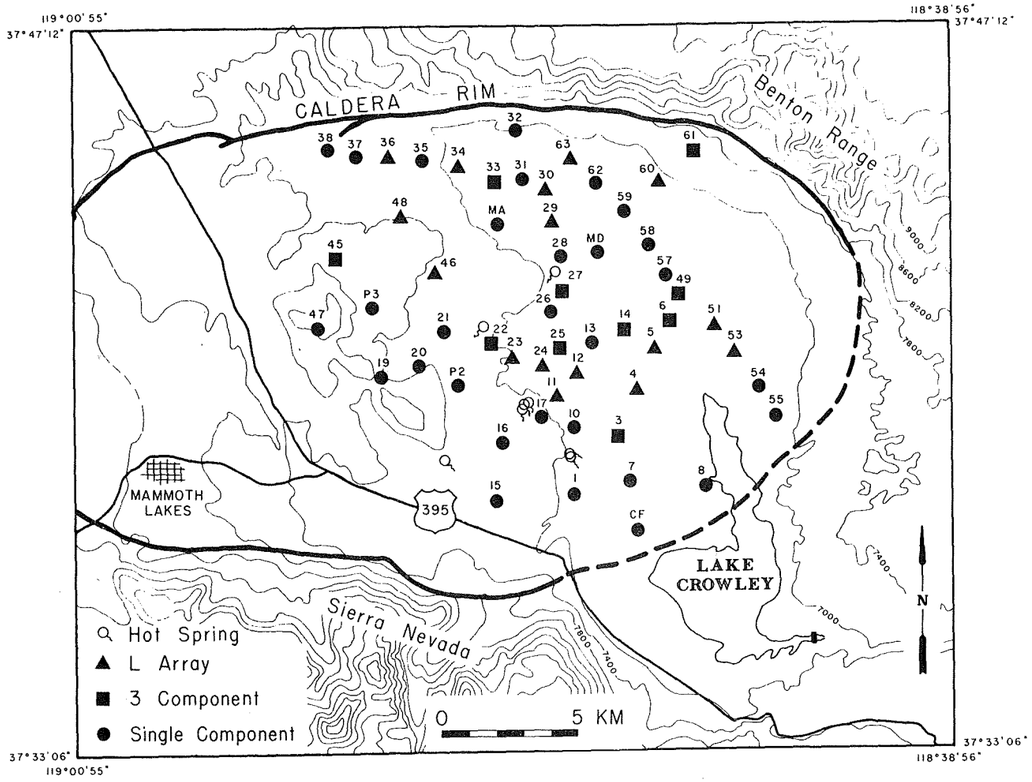

Fig. 1. Location of seismic stations in Long Valley. Numbers are station identifications; caldera boundary from geological evidence is shown by solid line where it is definite and by dashed line where it is indefinite.

to noise level at the reference station) and using them instead of actual noise levels in the plots. Samples at the reference stations were taken at the same time as the samples at the other stations in order to evaluate relative noise levels. The noise levels at the reference stations for the 11 nights shown in Figure 2 were sufficient to calculate relative noise levels at all the stations. In doing this correction it is assumed that the temporal variation of noise at the reference stations is representative of variation in the whole region and is not a local phenomenon associated with those stations. In any case, since the maximum spatial variation of noise levels is much higher than the maximum variation at the reference station during the experiment, the correction for temporal variation does not drastically change the shape of the noise anomalies discussed below.

The Noise Anomaly in Long Valley

Figures 3*a*–3*e* show the spatial variation of noise levels for four frequency bands and for unfiltered data. The units are in decibels with respect to P2 or P3. The most obvious feature of the noise level distribution is the energy high extending over most of the eastern half of the caldera. The anomaly has an amplitude of 12–18 dB in the 0- to 1-Hz band and 12–30 dB in the other frequency bands and unfiltered data. The peak of the anomaly is about 10 km long and 5 km wide. The gradients are very sharp east and west of this peak. However, there are two disturbing aspects to this anomaly. First, it is outside the area where the majority of hot springs in Long Valley are present (Figure 1), and second, it roughly coincides in extent to a soft sedimentary basin traversed by the Owens River and many small streams. The existence of about 500 m of sedimentary material of lower density than the underlying rock in this area is inferred from interpretation of a seismic refraction survey in Long Valley [*Hill*, 1976]. Sedimentary basins amplify ground motion associated with seismic waves. The amplification is usually caused by soft surficial layers of thickness comparable to the seismic wavelength. We shall show below that the group velocity of seismic noise waves in Long Valley is only of the order of 150 m/s at 2-Hz frequency. It was not possible to estimate phase velocity and hence wavelength. We believe, however, that the soft water-saturated river valley deposits in the region of the Owens River, which are probably only a few tens of meters thick and overlie the thicker sediments found by the refraction survey, are responsible for the noise anomaly. The alluvium can be excited by one or more of the following noise sources: (1) the regional background noise, which is about 40 mμ/s at P2, one of the quietest stations over hard ground; (2) river noise; (3) cattle (several hundred cattle were present on the pasture lands along the river during the experiment); and (4) the geothermal system.

Ground Amplification

Whatever may be the source of noise in Long Valley, the amplification of seismic waves by the Owens River basin is an

TABLE 1. Location of Noise Survey Stations and Their Time of Operation

Station	Latitude	Longitude	Day On	Time, UT	Day Off	Time, UT
P2	37°40′25″	118°51′25″	June 7, 1973	09h 39m	June 23, 1973	19h 23m
P2	37°40′25″	118°51′25″	Nov. 5, 1974	18h 55m	Nov. 9, 1974	19h 50m
P3	37°41′75″	118°53′36″	June 19, 1973	21h 52m	July 2, 1973	13h 45m
1	37°38′12″	118°48′32″	June 7. 1973	07h 52m	June 12, 1973	19h 30m
3	37°39′27″	118°47′25″	June 7, 1973	00h 49m	June 10, 1973	00h 37m
4	37°40′15″	118°46′75″	June 7, 1973	02h 40m	June 10, 1973	15h 50m
5	37°40′93″	118°46′28″	June 7, 1973	04h 20m	June 9, 1973	20h 15m
6	37°41′50″	118°45′89″	June 7, 1973	05h 52m	June 15, 1973	17h 45m
7	37°38′38″	118°46′90″	June 7, 1973	08h 20m	June 9, 1973	23h 07m
8	37°38′27″	118°45′05″	June 7, 1973	08h 44m	June 9, 1973	22h 26m
10	37°39′41″	118°48′35″	June 11, 1973	01h 30m	June 12, 1973	23h 18m
11	37°40′01″	118°48′78″	June 11, 1973	03h 08m	June 16, 1973	19h 20m
11	37°40′01″	118°48′78″	Nov. 7, 1974	00h 05m	Nov. 9, 1974	14h 52m
12	37°40′46″	118°48′25″	June 11, 1973	04h 08m	June 15, 1973	20h 15m
13	37°41′08″	118°47′87″	June 11, 1973	04h 45m	June 15, 1973	19h 32m
13	37°41′08″	118°47′87″	Nov. 7, 1974	00h 30m	Nov. 9, 1974	16h 58m
14	37°41′32″	118°47′02″	June 11, 1973	05h 10m	June 15, 1973	18h 55m
15	37°37′98″	118°50′26″	June 13, 1973	21h 42m	June 16, 1973	17h 26m
15	37°37′98″	118°50′26″	July 5, 1973	02h 35m	July 5, 1973	18h 45m
16	37°39′12″	118°50′14″	June 13, 1973	22h 39m	June 16, 1973	18h 05m
16	37°39′12″	118°50′14″	July 5, 1973	01h 34m	July 5, 1973	18h 10m
17	37°39′63″	118°49′18″	June 13, 1973	23h 34m	June 16, 1973	18h 45m
17	37°39′63″	118°49′18″	July 5, 1973	00h 34m	July 5, 1973	17h 40m
19	37°40′40″	118°53′17″	June 16, 1973	00h 20m	June 18, 1973	19h 31m
20	37°40′61″	118°52′20″	June 16, 1973	23h 06m	June 18, 1973	19h 50m
21	37°40′30″	118°51′57″	June 16, 1973	03h 05m	June 18, 1973	20h 05m
22	37°41′05″	118°50′39″	June 16, 1973	02h 01m	June 19, 1973	22h 46m
23	37°40′75″	118°49′88″	June 16, 1973	21h 55m	June 19, 1973	23h 02m
24	37°40′62″	118°49′12″	June 16, 1973	00h 41m	June 19, 1973	23h 52m
25	37°40′97″	118°48′67″	June 15, 1973	22h 35m	June 21, 1973	16h 47m
26	37°41′66″	118°48′88″	June 19, 1973	03h 56m	June 22, 1973	19h 20m
27	37°42′06″	118°48′60″	June 20, 1973	05h 30m	June 21, 1973	18h 45m
27	37°42′06″	118°48′60″	Nov. 6, 1974	20h 55m	Nov. 9, 1974	15h 22m
28	37°42′75″	118°48′63″	June 19, 1973	02h 35m	June 21, 1973	18h 15m
29	37°43′35″	118°48′85″	June 20, 1973	04h 45m	June 21, 1973	19h 14m
29	37°43′35″	118°48′85″	Nov. 6, 1974	23h 30m	Nov. 9, 1974	16h 20m
30	37°44′01″	118°49′03″	June 20, 1973	04h 05m	June 21, 1973	19h 54m
31	37°44′27″	118°49′57″	June 18, 1973	23h 43m	June 21, 1973	17h 47m
32	37°45′25″	118°49′67″	June 19, 1973	01h 37m	June 21, 1973	17h 15m
33	37°44′20″	118°50′34″	June 21, 1973	22h 35m	June 23, 1973	20h 12m
34	37°44′46″	118°51′26″	June 22, 1973	23h 21m	June 24, 1973	18h 32m
35	37°44′62″	118°52′09″	June 22, 1973	01h 52m	June 23, 1973	20h 34m
36	37°44′66″	118°52′97″	June 23, 1973	01h 11m	June 24, 1973	19h 38m
37	37°44′72″	118°53′75″	June 23, 1973	01h 58m	June 24, 1973	20h 28m
38	37°44′87″	118°54′46″	June 22, 1973	00h 20m	June 23, 1973	21h 10m
45	37°42′71″	118°54′30″	June 25, 1973	00h 42m	June 26, 1973	18h 40m
46	37°42′38″	118°51′80″	June 25, 1973	02h 10m	June 26, 1973	19h 22m
47	37°41′36″	118°54′73″	June 25, 1973	04h 53m	June 26, 1973	17h 18m
48	37°43′48″	118°52′66″	June 25, 1973	03h 36m	June 26, 1973	20h 25m
49	37°42′00″	118°45′67″	June 26, 1973	00h 28m	July 1, 1973	23h 07m
51	37°41′38″	118°44′80″	June 27, 1973	00h 44m	June 29, 1973	18h 30m
53	37°40′87″	118°44′29″	June 27, 1973	02h 20m	June 29, 1973	17h 57m
54	37°40′21″	118°43′66″	June 27, 1973	03h 01m	June 29, 1973	20h 22m
55	37°39′65″	118°43′26″	June 27, 1973	03h 57m	June 29, 1973	19h 55m
57	37°42′38″	118°46′01″	June 29, 1973	00h 10m	July 1, 1973	22h 40m
58	37°43′00″	118°46′41″	June 28, 1973	21h 17m	July 1, 1973	22h 04m
59	37°43′65″	118°47′04″	June 30, 1973	01h 52m	July 1, 1973	19h 16m
59	37°43′65″	118°47′04″	Nov. 7, 1974	01h 45m	Nov. 9, 1974	17h 45m
60	37°44′20″	118°46′23″	June 30, 1973	03h 14m	July 1, 1973	20h 50m
61	37°44′80″	118°45′33″	June 28, 1973	22h 40m	July 1, 1973	19h 55m
61	37°44′80″	118°45′33″	Nov. 7, 1974	02h 28m	Nov. 9, 1974	18h 40m
62	37°44′20″	118°47′77″	June 30, 1973	00h 35m	July 1, 1973	18h 44m
63	37°44′63″	118°48′41″	June 29, 1973	23h 25m	July 1, 1973	17h 42m
64	37°19′33″	118°17′64″	July 3, 1973	03h 19m	July 3, 1973	19h 00m
65	37°19′46″	118°18′20″	July 3, 1973	02h 48m	July 3, 1973	19h 00m
66	37°19′48″	118°19′00″	July 3, 1973	02h 05m	July 3, 1973	19h 00m
67	37°19′56″	118°19′57″	July 3, 1973	06h 25m	July 3, 1973	19h 00m
68	37°19′55″	118°20′05″	July 3, 1973	05h 52m	July 3, 1973	19h 00m
69	37°19′58″	118°20′58″	July 3, 1973	05h 20m	July 3, 1973	19h 00m
70	37°19′56″	118°21′10″	July 3, 1973	04h 52m	July 3, 1973	19h 00m
71	37°19′53″	118°21′67″	July 3, 1973	03h 55m	July 3, 1973	19h 00m
72	37°18′89″	118°20′62″	July 3, 1973	01h 23m	July 3, 1973	19h 00m
73	37°18′39″	118°20′46″	July 3, 1973	00h 44m	July 3, 1973	19h 00m
MA	37°43′89″	118°50′25″	July 1, 1973	02h 10m	July 4, 1973	03h 05m
MD	37°42′85″	118°47′71″	July 6, 1973	04h 10m	July 6, 1973	14h 52m
MD	37°42′85″	118°47′71″	Nov. 6, 1974	22h 30m	Nov. 9, 1974	15h 50m
CF	37°37′43″	118°46′73″	June 29, 1973	01h 40m	July 2, 1973	00h 00m

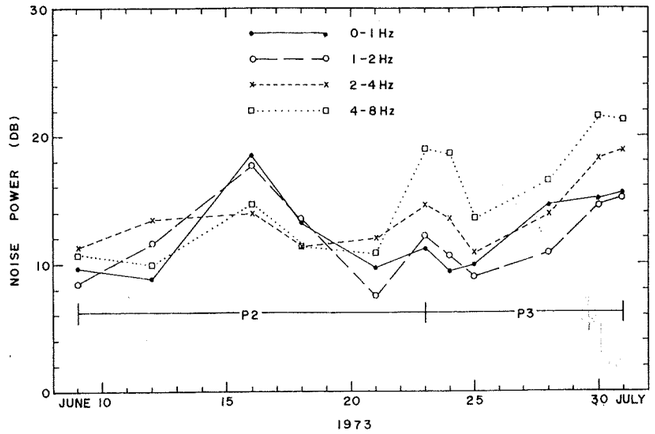

Fig. 2. Variation of noise levels in four frequency bands at reference stations P2 and P3 during the period of the experiment.

important parameter in understanding the noise anomaly. It is well known that seismic noise amplitudes are usually higher over alluvium and soft sedimentary basins. It is very difficult to make theoretical computations of noise amplification in such structures, even if the compressional and shear wave velocities are known, because of the complexity of wave types in seismic noise. Considerable work, however, has been done on theoretical and experimental computations of ground amplification of seismic waves from earthquakes with a view to understanding and overcoming earthquake damage. *Borcherdt* [1970] studied ground amplification in the San Francisco Bay area by comparing spectra of seismic waves from nuclear shots in Nevada, recorded by bedrock reference stations and at various locations over younger and older bay muds. He found (see Table 5 of his paper) that the ground amplification (ratio of seismic spectra at bay mud stations to the spectrum at the reference station on hard rock) of the horizontal and vertical components of ground motion was characterized by sharp peaks whose frequencies could be correlated with thickness of the bay muds. The ground motion was also much higher over

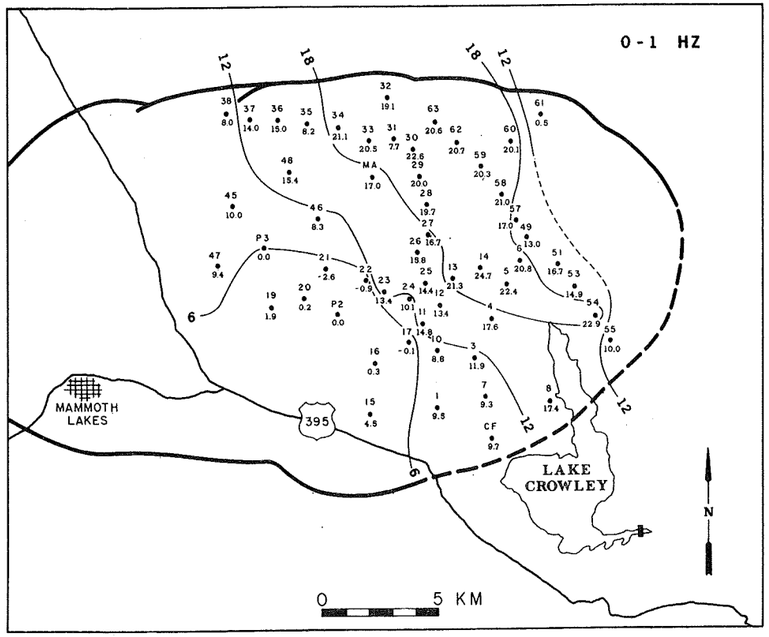

Fig. 3*a*. Spatial variation of noise level in the 0- to 1-Hz band. Dots are stations, station identification is shown by numbers above dots, relative noise levels, in decibels with respect to P2 or P3, are shown below dots, and the contour interval is 6 dB.

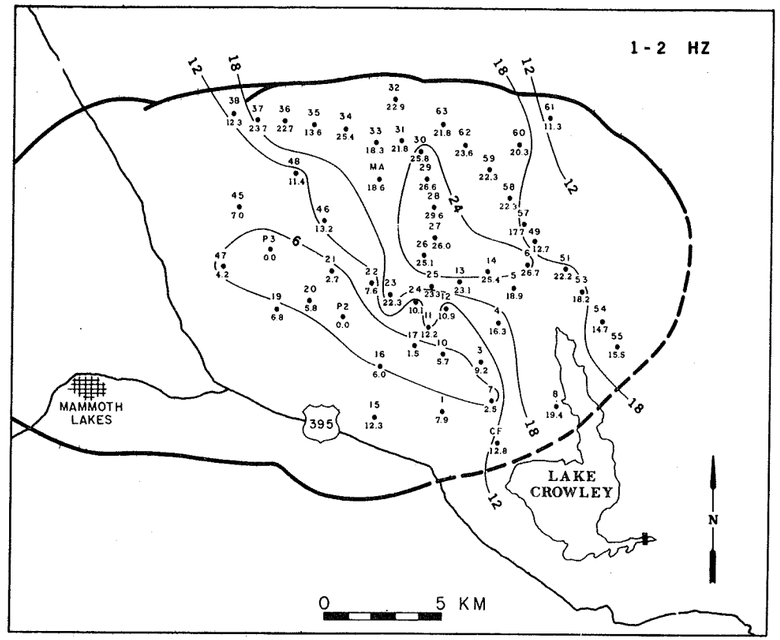

Fig. 3*b*. Spatial variation of noise level in the 1- to 2-Hz band. Dots are stations, station identification is shown by numbers above dots, relative noise levels, in decibels with respect to P2 or P3, are shown below dots, and the contour interval is 6 dB.

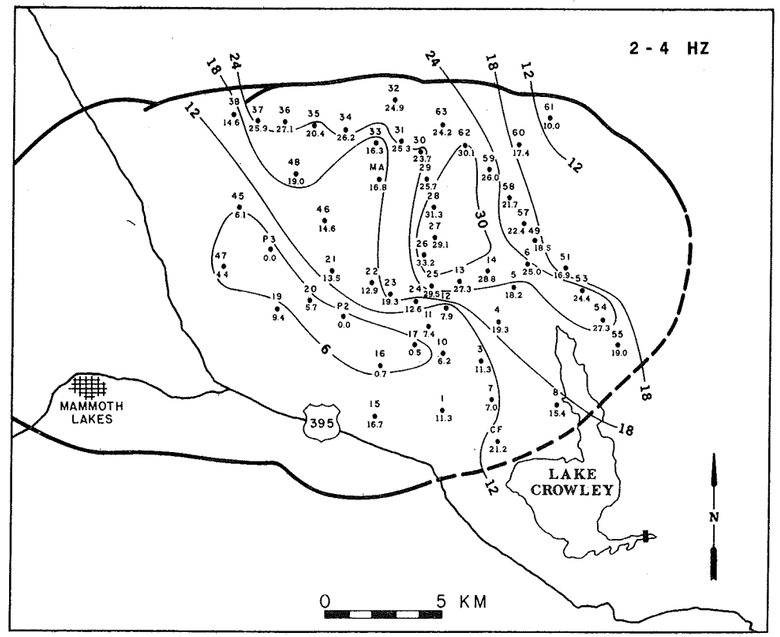

Fig. 3*c*. Spatial variation of noise level in the 2- to 4-Hz band. Dots are stations, station identification is shown by numbers above dots, relative noise levels, in decibels with respect to P2 or P3, are shown below dots, and the contour interval is 6 dB.

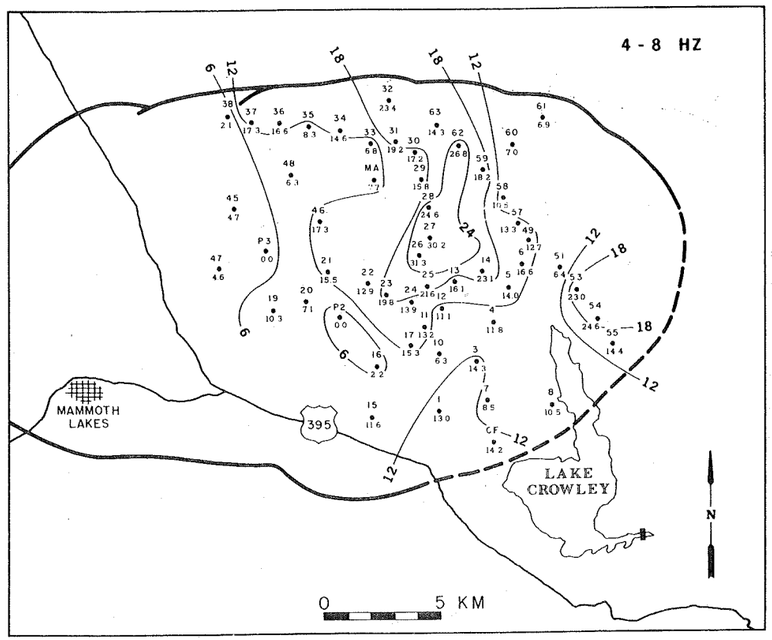

Fig. 3*d*. Spatial variation of noise level in the 4- to 8-Hz band. Dots are stations, station identification is shown by numbers above dots, relative noise levels, in decibels with respect to P2 or P3, are shown below dots, and the contour interval is 6 dB.

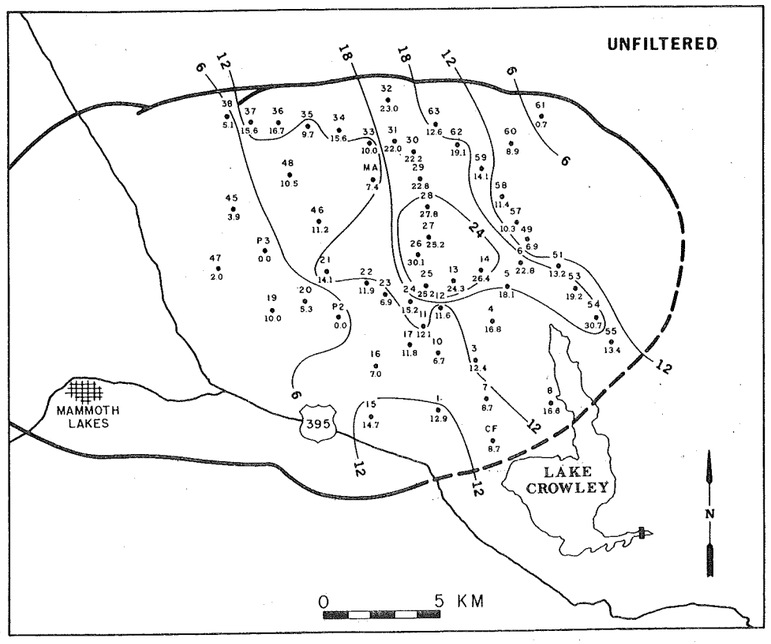

Fig. 3*e*. Spatial variation of noise level using unfiltered data. Dots are stations, station identification is shown by numbers above dots, relative noise levels, in decibels with respect to P2 or P3, are shown below dots, and the contour interval is 6 dB.

TABLE 2. Seismic Events Used in Ground Motion Study and Stations Recording Each Event

Date	Origin	Origin Time, UT	Latitude	Longitude	Magnitude	Depth, km	Recording Stations
June 9, 1973	Solomon Islands	08h 21m 27.3s	10.3°S	161.4°E	6.3	70	P2, 1, 3, 4, 5, 6, 7, 8
June 12, 1973	Southern Nevada	08h 15m 49.9s	37.2°N	116.3°W	4.8	5	P2, 10, 11, 12, 13, 14
June 16, 1973	Off Coast of Oregon	14h 43m 47.5s	45.0°N	125.8°W	5.6	33	P2, 15, 16, 17, 21, 22, 24
June 17, 1973	Hokkaido, Japan	03h 55m 02.9s	43.2°N	145.8°E	6.5	48	P2, 19, 20, 13
June 21, 1973	Unidentified	...	...	...	...	...	P2, 25, 26, 27, 28, 29, 30, 31, 32
June 28, 1973	Southern Nevada (NTS)	19h 15m 12.4s	37.1°N	116.1°W	4.9	0	P3, 51, 53, 54, 55
July 1, 1973	Off Coast of S. Alaska	13h 33m 34.6s	57.8°N	137.3°W	6.1	33	P3, 49, 57, 58, 59, 60, 62, 63, MA, CF
July 3, 1973	Southeastern Alaska	16h 59m 35.1s	58.0°N	138.0°W	6.0	33	64, 65, 66, 67, 68, 70, 71, 72, 73

bay muds than over hard rock. The average vertical ground velocity was about 4 times higher over younger bay muds from 7 to 23 m in thickness and about 2 times higher over older bay muds from 30 to 600 m in thickness. The maximum ground amplification occurred in the 1- to 2-Hz frequency band.

Ground amplification calculations in Long Valley using earthquake waves. Several teleseisms and blasts from Nevada Test Site (NTS) were recorded during our noise survey in Long Valley. Some of the events were sufficiently well recorded at the reference stations and the mobile stations so as to enable ground amplification calculations. Details of the seismic events used in the study and a list of stations recording them are given in Table 2. Spectra of the first 40 s of the seismic signal at each of the mobile stations are compared with the spectrum at the appropriate reference station. The ratio of the spectrum at the mobile station to the spectrum at the reference station gives the ground amplification spectrum. Both noise and event signals are amplified, but when the seismic wave amplitude from the event is much larger than the noise amplitude, the ground amplification measurement can be taken to be that associated with the seismic waves from the event. Noise spectra are computed for a sample just prior to the event, and only ground amplification values at frequencies where the event spectrum is at least 6 dB or more than noise spectrum are used. With this criterion the ground amplification values above 2 Hz are not meaningful except for one profile. In addition to a noise sample just prior to the event, the spectral ratio of a quiet noise sample at the mobile station to the reference stations is computed for comparison with the ground amplification spectrum.

Figure 4 shows typical analog seismograms along a profile

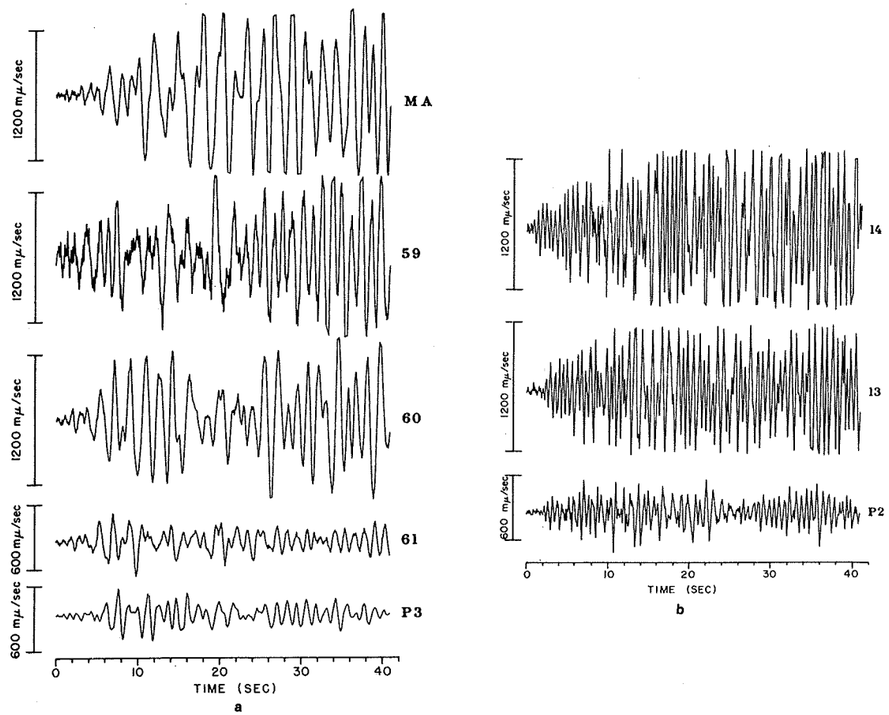

Fig. 4. Analog seismograms to show ground amplification at (left) stations P3 (reference), 59, MA, 60, and 61 for Alaskan event, and (right) P2 (reference), 13, and 14 for NTS event.

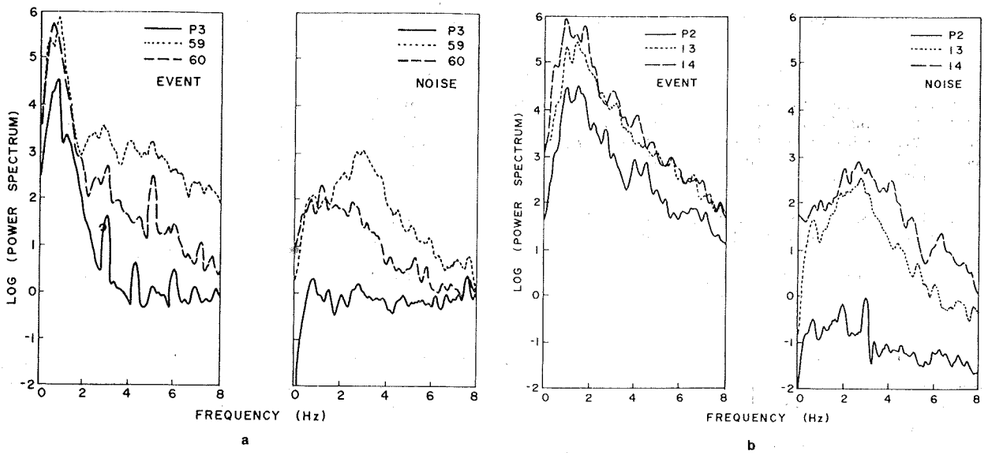

Fig. 5. Comparison of event spectra and noise spectra at (left) stations 59, 60, and P3 and (right) stations 13, 14 and P2.

from the northeast rim of the caldera toward the center of the sedimentary basin to illustrate the ground amplification problem in Long Valley. Note that the seismograms at P3 on hard ground and 61, also on hard ground at the caldera rim, have more or less the same amplitude. The signals increase in amplitude by a factor of 4 between 61 and MA as the thickness of the sediment increases (Figure 4*a*). Similarly, a comparison of seismic signals from a regional event from Nevada (NTS shot) shows large ground amplification at stations 13 and 14 over sediments near the center of the eastern half of the caldera (Figure 4*b*). The spectra shown in Figure 5 illustrate these results quantitatively. The earthquake signals are amplified by

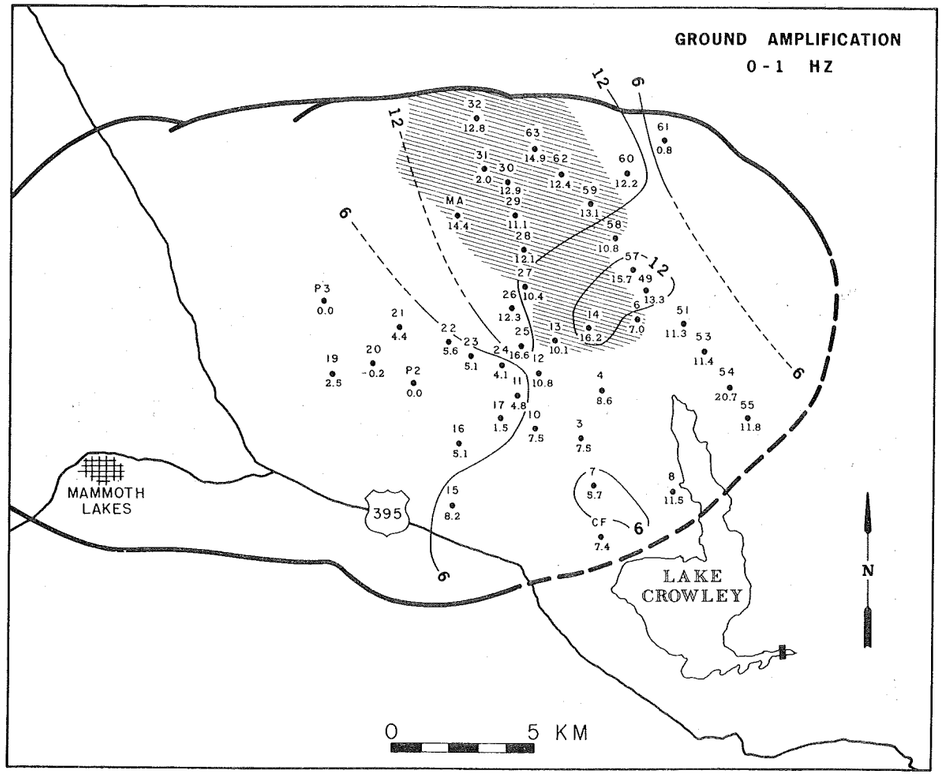

Fig. 6*a*. 0- to 1-Hz band.

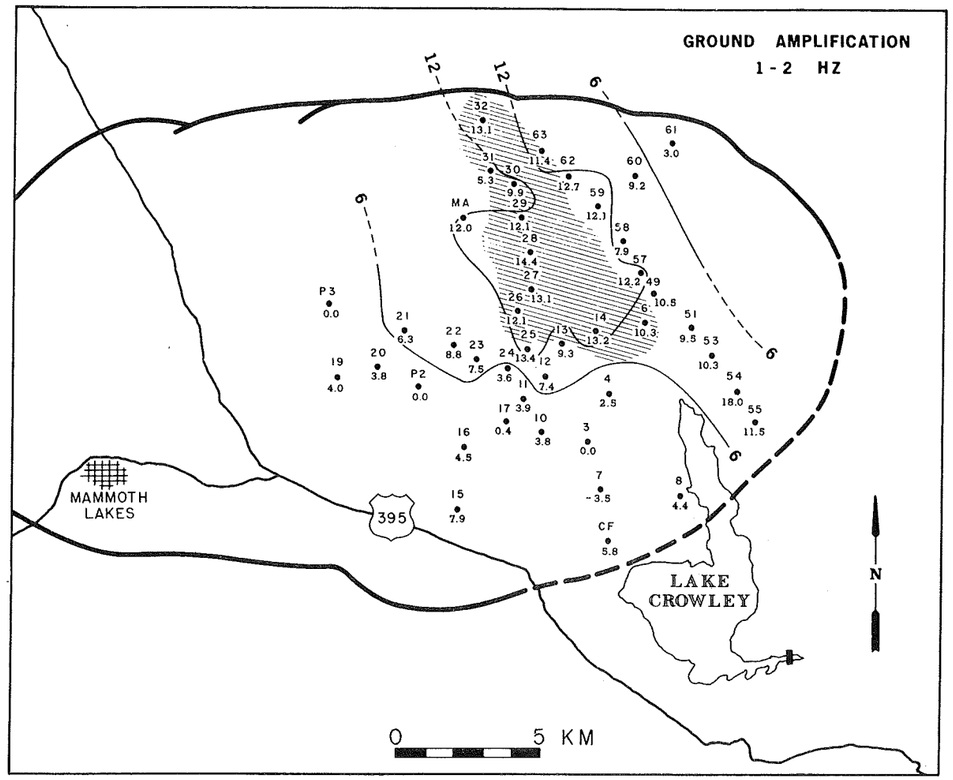

Fig. 6*b*. 1- to 2-Hz band.

Fig. 6. Ground amplification contours of earthquake waves. Dots are station locations, station identification is shown by numbers above dots, ground amplification, in decibels with respect to P2 or P3, is shown below dots, and the contour interval is 6 dB. Relative noise levels are above 18 dB in the hatched area.

about 12 dB at stations 59 and 60 relative to the reference station P3 in the frequency band of 0–2 Hz. The values at frequencies greater than 2 Hz are not relevant because at these frequencies the seismic noise is the dominating influence. The seismic noise spectra at these stations, using quiet night samples, are shown for comparison with event spectra. (These samples were not taken immediately prior to the event.) It is quite clear from the noise spectra at 59 and 60, in the 0- to 2-Hz band, that the seismic noise is at least 20 dB higher than that at P3 (Figure 5*a*). Spectra at stations P2, 13, and 14 using the NTS event and giving good signal to noise ratios across the whole spectral band show ground amplification at 13 and 14 to be about 10 dB. The ratio of noise at stations 13 and 14 to the ratio at P2, however, is over 30 dB.

Spectral peaks are found both in the event ratios (ratio of spectrum at any station to spectrum at reference station for seismic waves from a particular event; also called ground amplification) and in the noise ratios (ratio of spectrum at any station to spectrum at reference station using noise samples taken during the same time interval), but their frequencies and amplitudes are found to be different. The frequencies at which the peaks occur also vary somewhat from profile to profile owing to difference in location or because different seismic events are used. The average ground amplification in the 0- to 1- and 1- to 2-Hz bands seems to have a reasonably smooth spatial variation (Figures 6*a* and 6*b*); this indicates that we have not seriously erred in using several seismic events recorded at different locations to arrive at a composite picture of seismic ground amplification in Long Valley.

Comparison of the spatial distribution of ground amplification in the 0- to 1- and 1- to 2-Hz bands (Figures 6*a* and 6*b*) with the spatial distribution of noise ratios (Figures 3*a* and 3*b*) shows clearly that for each frequency band the two distributions are quite similar. However, in the anomalous region, the noise ratios are higher by 6–9 dB in the 0- to 1-Hz band and by 12–15 dB in the 1- to 2-Hz band.

Evidence for a Noise Source

Difference between ground amplification and noise ratio. Our main clue for proving that the noise anomaly is not caused by amplification of regional background noise, but by a local noise source in the vicinity of the anomaly, is derived from the observed difference between the ground amplification and noise ratio values. More examples of this phenomenon will now be presented. For the profile of stations 10–14, near the center of the eastern half of the caldera, there is a rapid increase in noise level, by about 12 dB in the 0- to 1- and 1- to 2-Hz bands. The gradient of noise level is very sharp within 2 km between stations 12 and 13 (Figure 3). The ground amplification and noise ratio spectra at stations 10–14 (Figure 7)

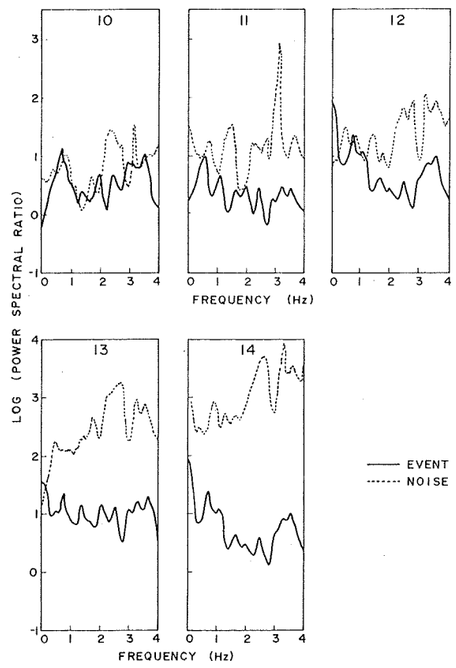

Fig. 7. Comparison of ground amplification spectra (solid line) and noise ratio spectra (dashed line) at stations 10, 11, 12, 13, and 14. P2 is the reference station.

show clearly that the two phenomena are not related in a predictable fashion. For example, at station 10 the two curves are similar except between 2 and 3 Hz where the noise is higher by about 10 dB. The peaks near 1 Hz are similar for noise and event ratio. At station 11 the two curves are distinctly different, the noise ratio being higher than the event ratio. Peaks can be seen in both the curves, but they occur at different frequencies and have different values. At station 12 the noise curve is significantly higher than the event curve above 1 Hz. The most spectacular difference between the ground amplification and the noise ratio, however, occurs at stations 13 and 14. It appears that either the mechanism by which the noise waves are amplified is entirely different from the amplification of seismic waves or a noise source that enhances the noise levels is present in the vicinity of station 13.

Another profile of stations across the noise anomaly from station 61 near the northeast edge of the caldera to station MA, near the center of the northern half of the caldera, shows that the noise ratios are definitely higher than the ground amplification (Figure 8). For this profile, unlike the previous profile where ground amplification values could be calculated throughout the spectra because of good signal to noise ratio, computations are valid only up to 2 Hz.

To compare theoretically the amplification of seismic noise in sedimentary basins with the amplification of earthquake waves, knowledge of the wave types involved in seismic noise is essential. More work is needed in this area and possibly also empirical studies in basins free from noise sources. In the present instance we could not find another water-saturated alluvial basin of the type found in Long Valley. However, some data are available from Owens Valley, about 50 km south of Long Valley, where we operated 10 stations for 1 night (Figure 9). The experiment was mainly intended to understand the generation and propagation of river-generated noise. One good teleseism was recorded during this period, and we were able to make some ground amplification calculations. The river noise is at frequencies above 6 Hz and cannot be detected beyond 1 km from the river. There was a clear spectral peak in the 2- to 4-Hz band, indicating what we infer to be an extraneous noise source associated with the town of Bishop, about 3 km northwest of the area where our stations were operated. All ground amplification values are with respect to station 64, on hard ground (Figure 10). The ground amplification and noise ratio spectra are in general within 6 dB of each other. The average values (indicated in Figure 10) in the 0- to 1- and 1- to 2-Hz bands are more or less alike for event and noise ratios. It is to be noted here that although our experimental area in Owens Valley has about 0.25 km of younger Cenozoic deposits and 0.75 km of older deposits overlying pre-Tertiary rocks (based on earlier seismic and gravity surveys [*Pakiser et al.*, 1964]), it is not like the water-saturated alluvium in Long Valley. The relative ground amplification and noise ratios in Owens Valley are similar to those at some of the stations in Long Valley (like station 10, Figure 7), which are outside the main peak of the noise anomaly. But ground amplification in Long Valley at stations within the noise anomaly (Figures 6*a* and 6*b*) is less than the noise ratios at these stations (Figures 3*a* and 3*b*) by at least 12 dB. The Owens Valley data, however, should not be taken as definite evidence that amplification of seismic waves produced by noise and events is about the same in sedimentary basins. They only indicate that such a situation is quite plausible, in which case, one possible explanation for a big difference between event and noise ratios is the presence of a noise source in the neighborhood of stations where such a difference was measured.

Possible noise sources. River and stream noise can be eliminated as a possible source of the noise anomaly in Long Valley because in Owens Valley the fast flowing river seems to be generating noise only at frequencies above 6 Hz, and even this high-frequency noise attenuates rapidly with distance. Comparison of spectra of seismic noise recorded at station 66, very near the Owens River, and at stations 67 and 68, 1 and 2 km

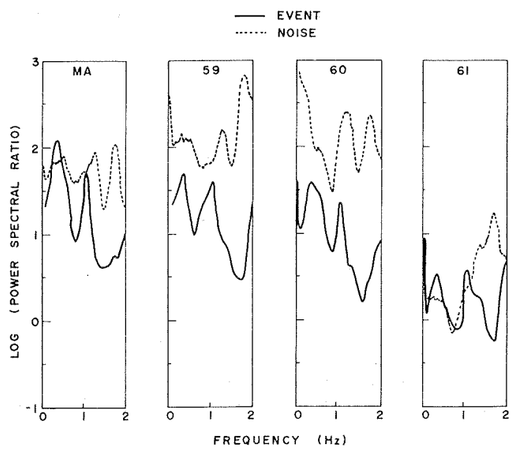

Fig. 8. Comparison of ground amplification spectra (solid line) and noise ratio spectra (dashed line) at stations MA, 59, 60, and 61. P3 is the reference station.

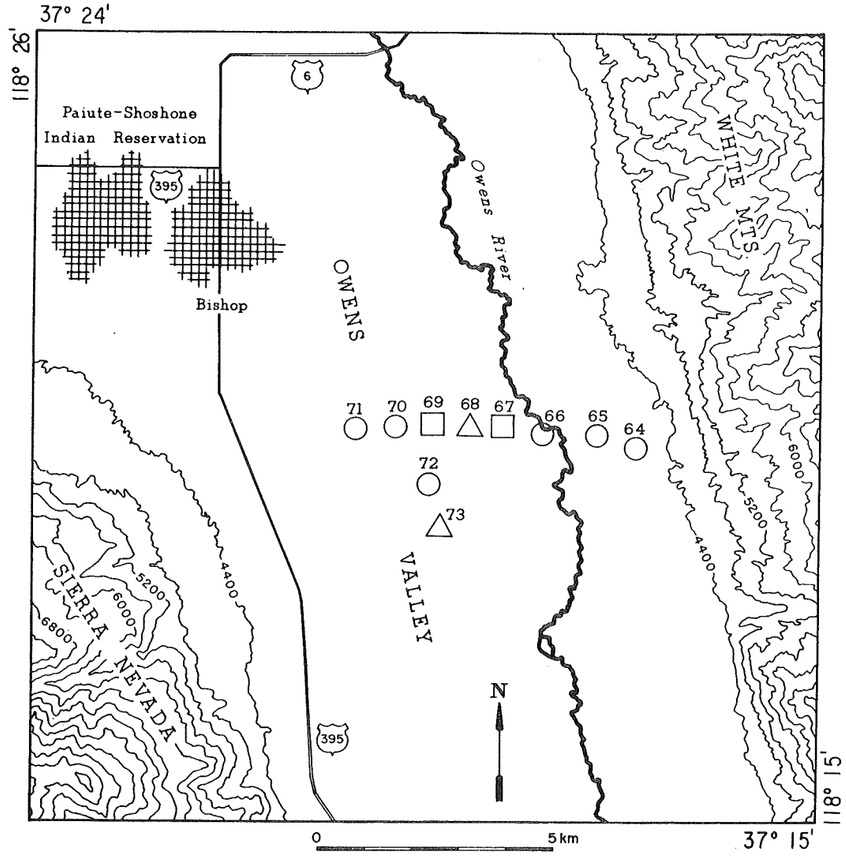

Fig. 9. Location of seismic stations in Owens Valley, near Bishop. Circles, squares, and triangles show single-component, three-component, and three-element array stations, respectively. Numerals are station identification.

from the river, shows that the high-frequency (above 6 Hz) noise drops by about 12 dB in 1 km (Figure 11). The rest of the spectra are not significantly different at these stations. At Long Valley the main Owens River and the associated streams are smaller and flow less rapidly than the river in Owens Valley. Hence we think it is highly improbable that a large noise anomaly like the one observed at frequencies below 4 Hz can be a result of river noise.

During our experiment, several hundred cattle were present along the grasslands by the river and near Lake Crowley in Long Valley. Because the noise anomaly is approximately located in this area, we thought that the cattle might be the possible source of seismic noise in Long Valley. We reoccupied eight of the stations for 3 nights during November 1974, when most of the cattle were gone and those remaining were mainly confined to one area near station 29 (Figure 12). In addition to the reference station P2 and the quiet station 61, six locations (11, 13, 27, 29, MD, and 59) that showed high noise levels in 1973 were reoccupied (Figure 12). The average noise levels (relative with respect to P2) in three frequency bands, based on 1-hour data recorded at night, and their comparison with the 1973 levels are also shown in Figure 12. In general, the noise levels are lower in November 1974 than in June 1973. The noise levels in the 0- to 1-Hz band are similar in 1973 and 1974. In the 1- to 2-Hz band the largest drop of about 7 dB occurs at station 27, the reduction at the other stations being about 3–6 dB. In the 2- to 4-Hz frequency band there is a general drop of about 6–12 dB in noise level. The only station that retains the 1973 level in this frequency band is 29. Since station 29 is very close to the area where 500 cattle were confined in November 1974, it is likely that the noise in this frequency band might be generated by cattle. If the noise in the lower-frequency bands is also due to cattle, it is difficult to understand how stations 13 and 59, about 5 km from the area of cattle concentration in 1974, can have similar noise levels to those at station 29 in the cattle zone. The levels at these stations have changed very little between 1973 and 1974. About 130 cattle were near station 13 during the first night recording in November 1974 but were removed before recording started on the second night. At this station there was virtually no change in noise levels except in the 2- to 4-Hz band. In this frequency band the noise level during the second night is less by about 4 dB than that during the first night, a phenomenon that can be attributed to removal of cattle from the area where the station is located. But the noise level decreased again by about 3 dB between the second and third nights.

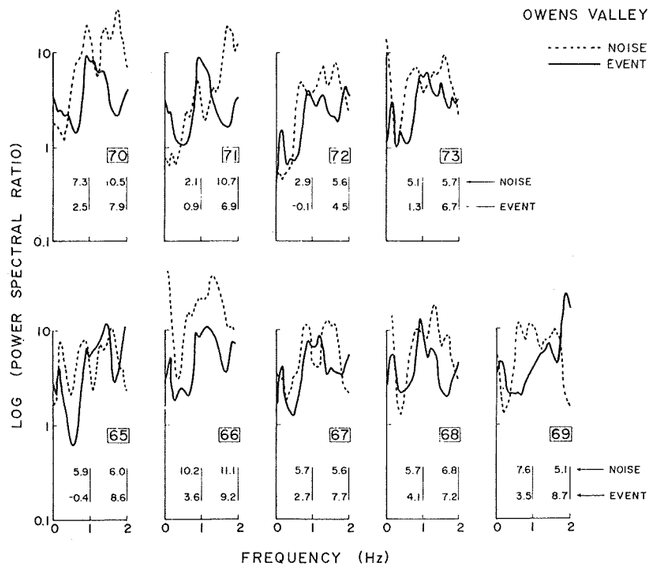

Fig. 10. Comparison of ground amplification spectra (solid line) and noise ratio spectra (dashed line) at stations 65–73 in Owens Valley. Station 64 is the reference station. The average values of noise ratio and ground amplification in the 0- to 1- and 1- to 2-Hz bands are shown below the graphs.

Comparison of some typical noise spectra in 1974 with spectra in 1973 shows clearly the decrease in noise level in 1974 (Figure 13). The most striking plots in this figure are the almost identical spectra at station 29 for the two periods. The reference station P2 shows a slight decrease in noise level in the frequencies from 1 to 3 Hz. Stations 13, 27, and MD show a large decrease in the 2- to 4-Hz band and somewhat less of a decrease in the 4- to 8-Hz band. Whatever the reason for this decrease in noise level may be, the important question is how it affects the interpretation of the noise anomaly. In order to make this evaluation it is helpful to compare the 1974 noise ratio curves and ground amplification spectra, as was done earlier (Figures 7 and 8). Such a comparison at stations 13, 27, and 29 is shown in Figure 14. It is seen that in the 0- to 2-Hz band the average noise ratio is still 10–15 dB higher than the ground amplification obtained by using earthquake waves. At higher frequencies, using results at station 13 where ground amplification values are available, there is very little difference between noise and event ratios.

The above observations show that the noise anomaly in the 2- to 4-Hz band (Figure 3*c*) could have been caused by non-geothermal noise sources such as cattle and regional noise amplified by the alluvium. The anomalies in the 0- to 1- and 1- to 2-Hz bands cannot be explained by these sources. The high apparent velocity waves seen in the 1- to 2-Hz band (see later section) provide evidence for the generation of geothermal seismic noise under the southern edge of the noise anomaly.

Velocity and Direction Studies

A seismic array can be used to identify a local noise source. As mentioned earlier, we operated several arrays in Long Valley in 1973. The arrays are L-shaped with three instruments, the length of each arm being 106.7 m (see Figure 1 for array locations). Selected samples of array data were played back and carefully examined for visual coherence between wave trains. Even though occasional short bursts of propagating wave trains could be identified, it was difficult to draw any inferences as to a constant source direction or wave velocity. The signals were filtered in 0- to 1-, 1- to 2-, and 2- to 4-Hz bands and examined. There is good coherence in the 0- to 1-Hz band, but the time shifts are quite small due to the short array arms. The data in the 1- to 2- and 2- to 4-Hz bands show occasional coherence, as in unfiltered data (Figure 15).

In an earlier study of direction of travel of seismic noise

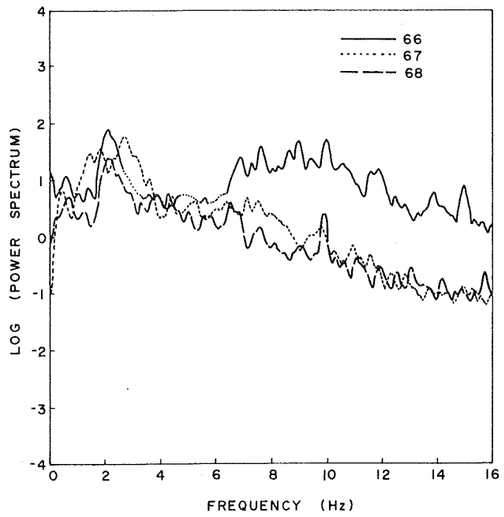

Fig. 11. Comparison of noise spectra at station 66, close to the Owens River, with spectra at stations 67 and 68, farther away from the river.

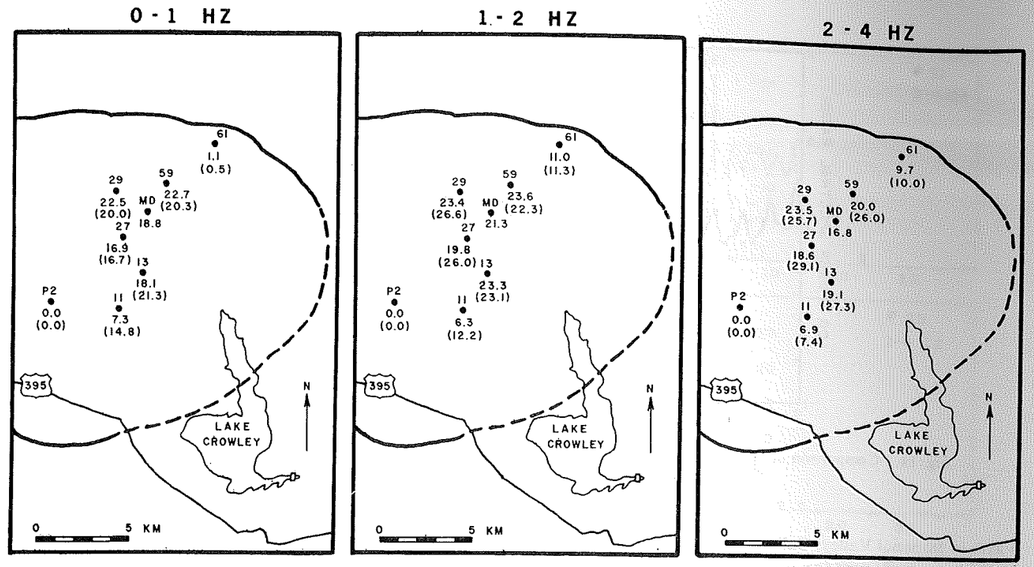

Fig. 12. Comparison between results of 1973 and 1974 surveys using filtered data in 0- to 1-, 1- to 2-, and 2- to 4-Hz bands. Dots are stations, station identification is shown by numbers above dots, 1974 noise levels, in decibels with respect to level at P2, are shown below the dots, and corresponding 1973 values are shown in parentheses.

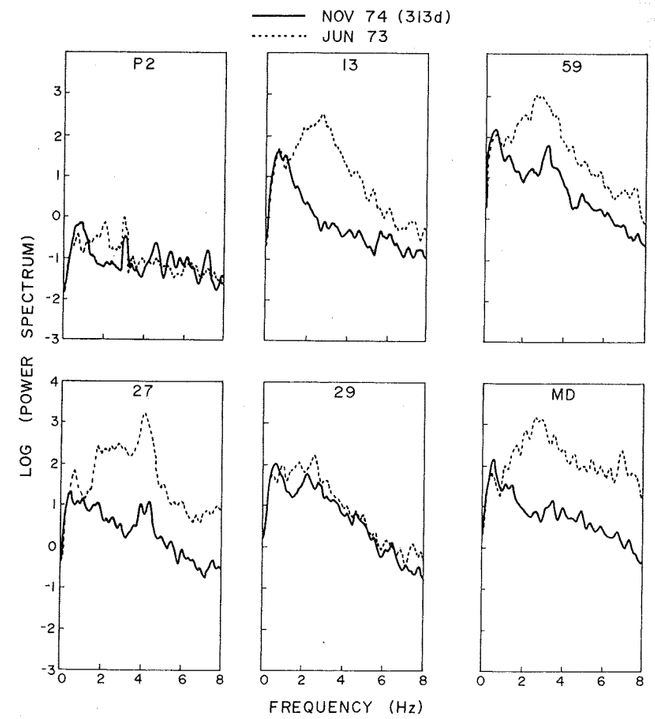

Fig. 13. Typical seismic noise spectra from 1974 data (solid line) and 1973 data (dashed line).

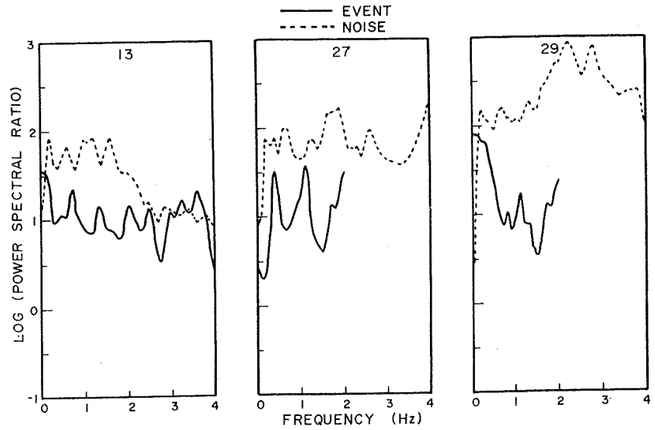

Fig. 14. Comparison of ground amplification spectra (solid line) and noise ratio spectra (dashed line) at stations 13, 27, and 29 using 1974 data. P2 is the reference station.

waves in Imperial Valley, California [*Iyer*, 1974], a cross-spectral technique was used to compute coherence and phase difference between records from an array at several frequencies. Such a technique was tried by using the Long Valley data, but the picture that emerged was extremely confusing. Two prerequisites for the success of the cross-spectral technique are that (1) the spacing between array elements should be much less than half the wavelength of the seismic signal being processed, so that the phase differences can be determined uniquely, and (2) the records should be 'stationary,' meaning that the phase difference between channels does not change within the sample being analyzed. In Long Valley the average group velocity of seismic noise waves is about 140 m/s (see below). Phase velocity and wavelength estimates were not possible. Hence we are not sure if condition (1) is met for the array spacing of 106.7 m. Visual examination of records showed that the phase differences between wave trains in the array changed even within short samples. Hence condition (2) is not satisfied. Because of these factors a different technique of direction and velocity estimation using array data was tried in Long Valley. Short sections (3 s) of data from pairs of array channels are correlated for varying lags. The lag at which maximum correlation occurs is a measure of the phase difference between wave trains and hence is an estimate of the time taken by the wave train to travel between the two elements of the array. Two values of phase difference can thus be obtained by correlating records from the central element of the array with records from the first and third elements, and by using these values, velocity and azimuth of wave travel can be computed by simple trigonometry. The method has the advantage that correlation is done over a whole train of waves in addition to individual peaks and troughs. After experimenting with different time windows, we decided to use 3-s segments of data for correlation. The time window was moved in steps of 1 s so that successive segments overlapped to ensure that no well-formed whole wave train was missed. The analysis was carried out for filtered data in frequency bands of 0–1, 1–2, and 2–4 Hz.

Results using a few seconds of data at several stations show that although velocity measurements are very stable, the azimuths are widely scattered. To build up sufficient statistics, we analyzed 10 min of data for a selected number of arrays in and around the noise anomaly. At each station, 540 velocity and azimuth values are computed for each frequency band. The surprising result is the persistence of the low group velocity,

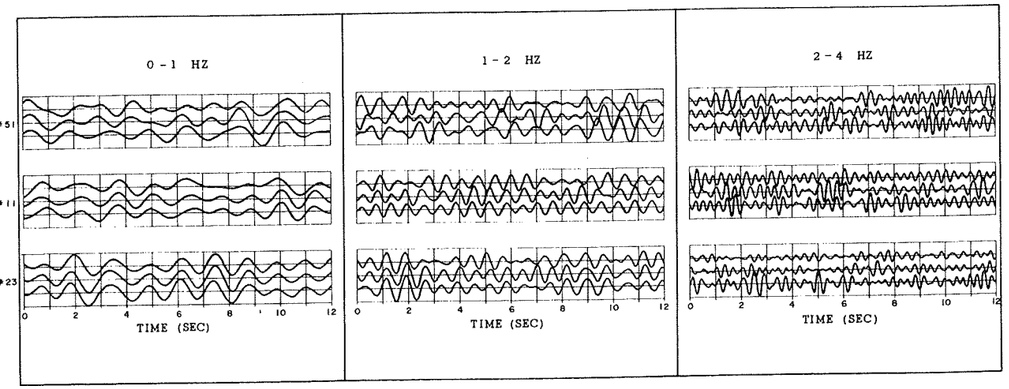

Fig. 15. Typical filtered noise samples at array stations 11, 23, and 51.

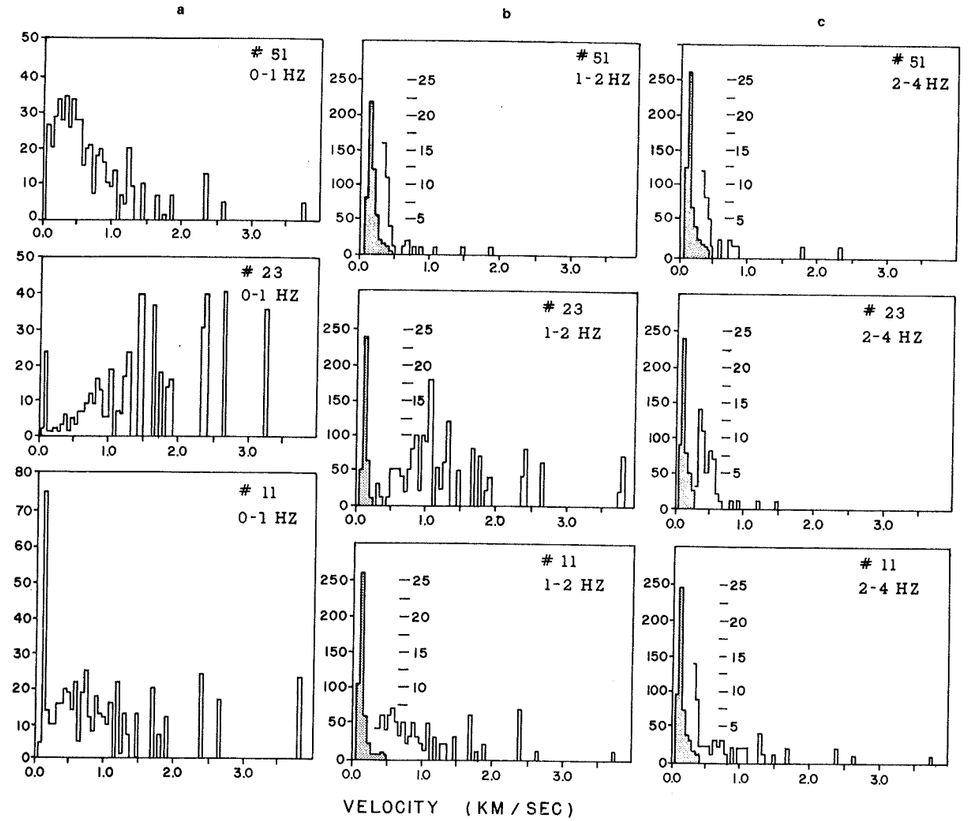

Fig. 16. Frequency distribution of velocities at stations 51, 23, and 11 for (left) 0- to 1-Hz band, (middle) 1- to 2-Hz band, and (right) 2- to 4-Hz band. Dotted area outlines histograms with normal scale shown to the left. Open area outlines histograms for the higher velocities with magnified scale shown to the right.

around 0.14 km/s, in the 1- to 2- and 2- to 4-Hz bands and the velocity of about 0.45 km/s in the 0- to 1-Hz band at all the stations. At the group of stations along the southern edge of the noise anomaly, however, there are many velocity values that are substantially higher than the average values of 0.14, particularly in the 1- to 2-Hz band. Typical velocity distributions using data in the three frequency bands are shown in Figure 16.

In the 0- to 1-Hz band the velocity distributions at eight of the 11 stations are similar to those (shown in Figure 16*a*) at station 51. The exceptions are stations 11 and 24, where the values are distributed over a wide velocity range, and station 23, where the distribution peaks near 1.5 km/s (Figure 16*a*). In the 1- to 2-Hz band the largest concentration of velocity values occurs between 0.1 and 0.15 km/s at all stations, as shown by the examples in Figure 16*b*. At stations 11, 12, 23, and 24, however, secondary peaks indicate the presence of higher-velocity waves (as shown for station 11 and 23 in Figure 16*b*). In the 2- to 4-Hz band (Figure 16*c*) the low-velocity parts of the distributions are identical to the velocity distributions in the 1- to 2-Hz band. The evidence for higher-velocity arrivals, however, is not clear. We believe that the consistent low velocity of around 0.15 km/s seen very clearly in the 1- to 2- and 2- to 4-Hz band and to some extent in the 0- to 1-Hz band (note sharp peaks in the 0.1- to 0.15-km/s range in the velocity distribution of Figure 16) is associated with the fundamental mode of excitation of the soft sedimentary layer. Since our measurements are based on correlating whole wave trains rather than peaks and troughs of individual waves, the resultant estimates give group velocities rather than phase velocities. The excitation probably corresponds to the Airy phase associated with a stationary value of group velocity of surface wave propagation in layered media [*Ewing et al.*, 1957, chap. 4]. Surface wave trains with similar velocities have been observed in explosion seismograms in Long Valley [*Hill*, 1976]. Even though it is difficult to make an exact estimate of the thickness of the sedimentary layer that is responsible for these waves, it is possible to infer that the material is only a few tens of meters thick. The characteristic velocity peak around 0.5 km/s in the 0- to 1-Hz band found at most of the stations is probably due to these waves (which have longer wavelengths than those at higher frequencies) 'seeing' a thicker layer overlying the soft upper layer.

At stations 11, 12, 23, and 24, southeast of the noise maximum in Figure 3*b*, seismic waves with velocities in the range of 0.9–1.5 km/s are found in addition to the low-velocity waves described earlier. If these high velocities are due to higher modes of propagation, they should have been seen at all

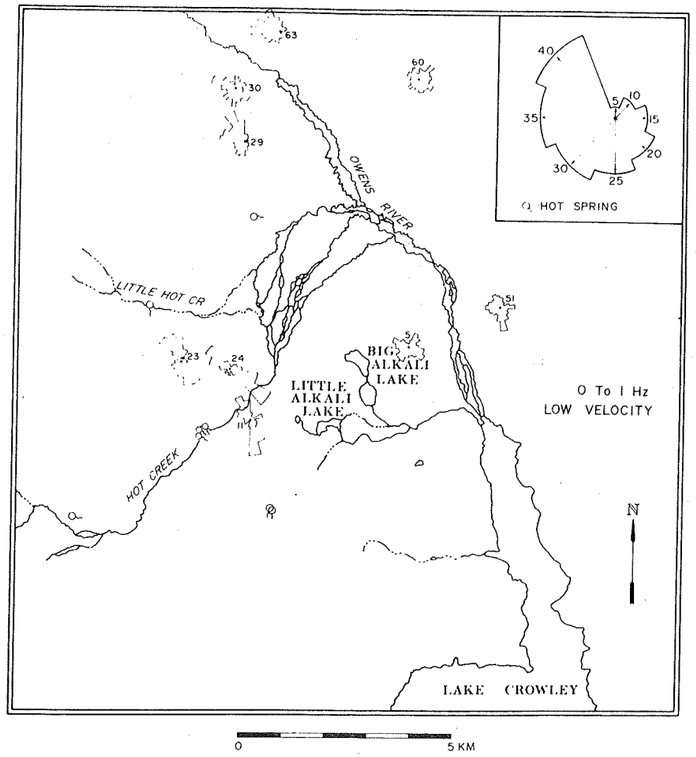

Fig. 17*a*. Spatial display of frequency distribution of azimuths of low-velocity noise in the frequency band 0–1 Hz.

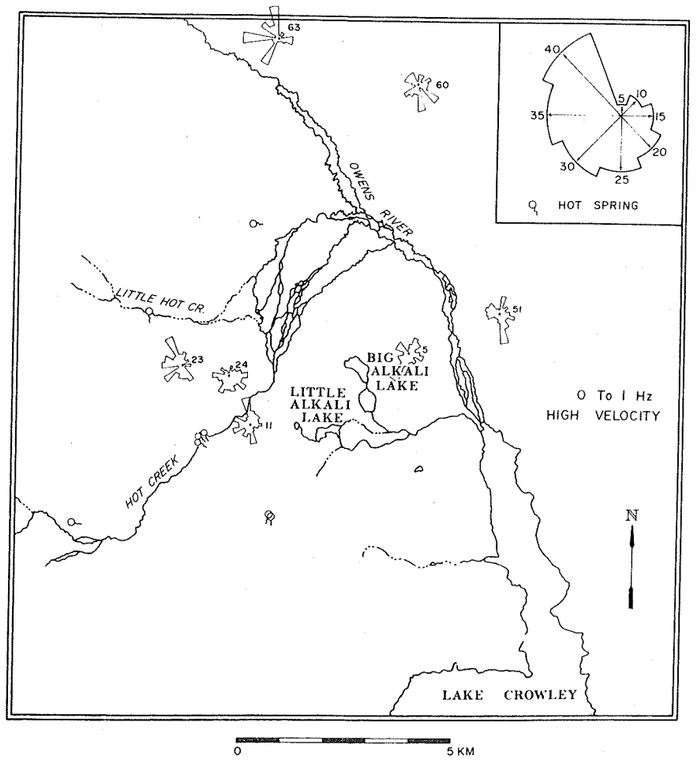

Fig. 17*b*. Spatial display of frequency distribution of azimuths of high-velocity noise in the frequency band 0–1 Hz.

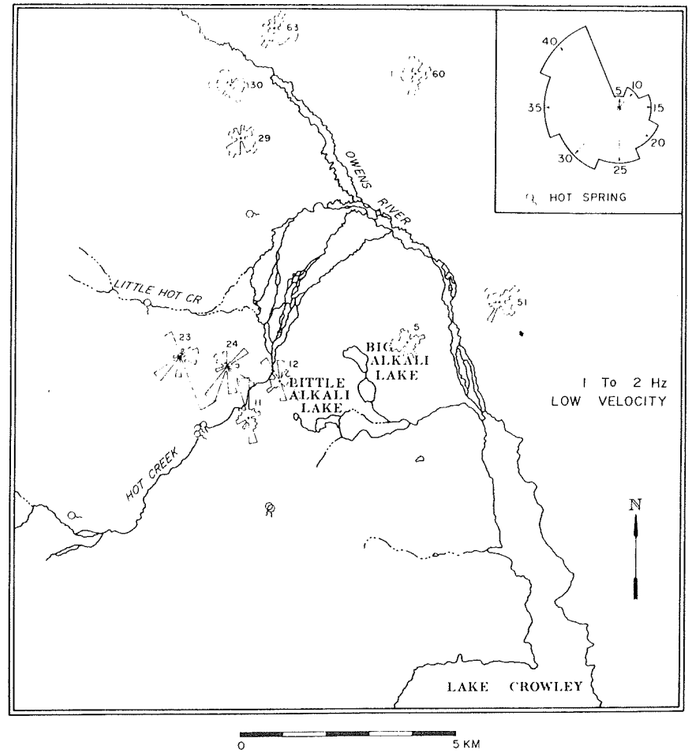

Fig. 18*a*. Spatial display of frequency distribution of azimuths of low-velocity noise in the frequency band 1–2 Hz.

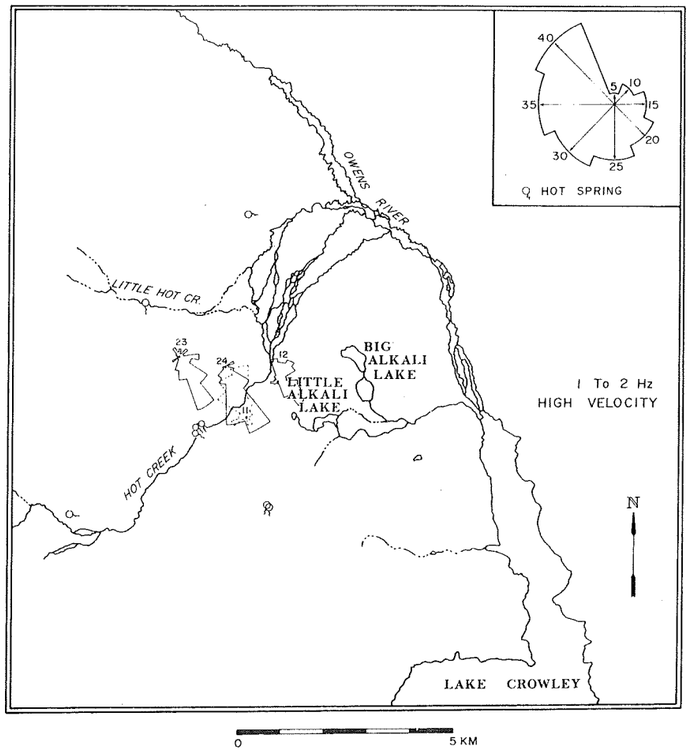

Fig. 18*b*. Spatial display of frequency distribution of azimuths of high-velocity noise in the frequency band 1–2 Hz.

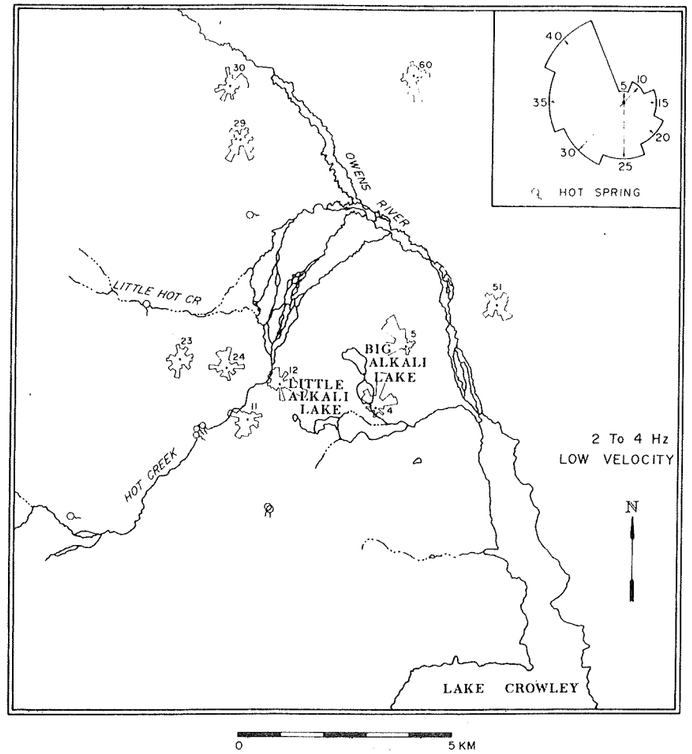

Fig. 19*a*. Spatial display of frequency distribution of azimuths of low-velocity noise in the frequency band 2–4 Hz.

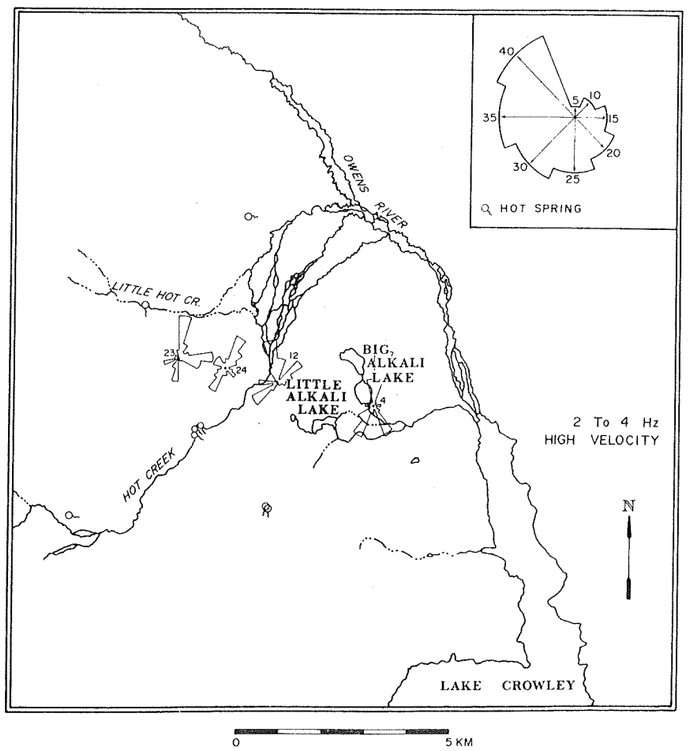

Fig. 19*b*. Spatial display of frequency distribution of azimuths of high-velocity noise in the frequency band 2–4 Hz.

stations over the sedimentary basin. Note that these four stations are in the part of Long Valley with many surface expressions of geothermal phenomena. We think that a geothermal source under these stations could generate seismic waves that in a soft sedimentary basin would travel directly to the stations at a higher apparent velocity than the horizontally propagating surface waves excited by the same source. It is interesting to note that the high-velocity values are close to the *P* wave velocities of 1.5–2.0 km/s in the upper layers of the east part of the caldera [*Hill*, 1976].

Direction studies. We have plotted histograms of distribution of azimuths for low-velocity (less than 1 km/s for 0- to 1-Hz band, less than 0.3 km/s for 1- to 2- and 2- to 4-Hz bands) and high-velocity data (where at least 50 values are available) at the array locations in Figures 17, 18, and 19.

0- to 1-Hz band (Figures 17a and 17b). Stations 29, 30, and 63, located near the north central part of the caldera, indicate the presence of a broad source of low-velocity seismic noise in this band toward northwest. Stations 11, 23, and 24, in the south central part of the caldera, point to sources in the northwest and southeast directions. The northwestern source of noise may be associated with ocean waves along the coast, the cause of persistent seismic noise (microseisms) with predominant frequencies around 0.13 Hz [*Haubrich*, 1967]. No doubt there are various other sources of noise in the area as shown by the low-velocity distribution at stations 60, 5, and 51 and the high-velocity distributions shown in Figure 17*b*.

1- to 2-Hz band (Figures 18a and 18b). Azimuthal distributions of low-velocity arrivals show a multiplicity of sources with no clear evidence of a concentrated noise source under the noise level peak indicated by the anomaly. The high-velocity noise observed at stations 11, 23, and 24, however, indicates the presence of a noise source between 11 and 24. Station 12 shows a wide source toward the east where the peak of the noise anomaly is present. If the high velocities are interpreted as a result of noise sources beneath the stations, the evidence shown here can be taken to indicate that geothermal noise sources are present in the vicinity of this cluster of stations.

2- to 4-Hz band (Figures 19a and 19b). The low-velocity distributions indicate the presence of many sources. High velocities were clearly seen in this frequency band only at station 12. At stations 4, 23, and 24 the evidence for high velocities was not clear, although we have shown the results from these stations in the figure. The velocity distributions point to sources to the northeast (toward the peak of the noise anomaly) and the southwest. As we showed earlier, the noise in this frequency band is probably most susceptible for contamination by nongeothermal local sources, and we are not sure that velocity distributions can be given any meaningful interpretation.

Discussion and Conclusions

The evidence presented shows the following:

1. A noise anomaly exists over most of the east half of the Long Valley caldera.
2. The anomaly is over an area of soft sedimentary material that can amplify seismic ground motion from regional and teleseismic sources by almost 12 dB.
3. The noise anomaly is about 12–18 dB higher than can be explained by postulating amplification of regional background noise by the sedimentary basin by the same factor as in the case of the amplification of earthquake waves.
4. A few measurements taken 18 months later, in November 1974, showed that the noise levels had decreased by about 6 dB in the 1- to 2-Hz band and 12 dB in the 2- to 4-Hz band. This change in noise level reduces the margin between the noise anomaly and ground amplification. In spite of this difficulty the difference between the noise and event amplification can be explained by the presence of a noise source generating seismic waves of about 2 Hz or less in frequency. This might very well be a geothermal noise source. The higher frequency waves could be generated by cultural sources or cattle.

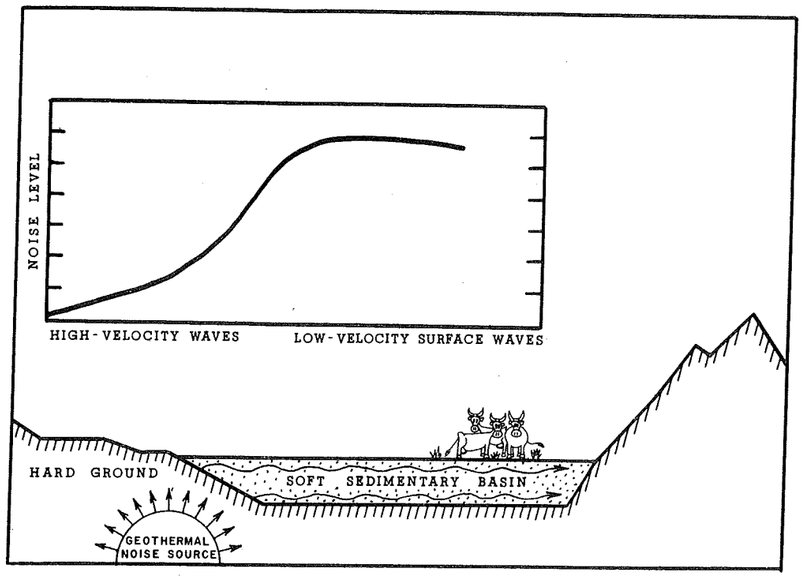

Fig. 20. A schematic model to illustrate how a geothermal noise source under hard ground can create high seismic amplitudes over an adjacent sedimentary basin. Arrows around noise source show seismic waves radiating from it. They are trapped by the sedimentary basin and propagate horizontally as surface waves as shown by the wavy lines. The top curve shows spatial variation of noise level at the surface.

5. Wave direction and group velocity measurements suggest that the seismic noise consists predominantly of surface waves generated by the excitation of a thin layer of sedimentary material by one or more sources. However, some high-velocity waves seem to originate from localized sources beneath the area where most of the hot spring activity is found.

The above evidence is inadequate to make a convincing case for the presence of a geothermal noise source in Long Valley. Another detailed noise survey in fall or winter, experimental and theoretical work on measuring amplification of seismic noise by soft ground, and velocity measurements using a closely spaced high-resolution array around the hot springs in Long Valley are required to resolve the problem. If there is a geothermal source under the region of high seismic velocities, it is not very difficult to reconcile the offset of the noise anomaly to the north. Since the high-velocity area is over relatively harder ground than the area where the anomaly exists, it is excited much less even though the noise source is closer to it. This possibility is schematically shown in Figure 20. However, this is purely a hypothesis that cannot be asserted with any great certainty because of the presence of extraneous cultural noise sources such as cattle in Long Valley during our noise survey. In spite of this difficulty, on the basis of the high velocities observed at some stations and the plausible geothermal noise model of Figure 20, a likely spot for experimental or exploratory drilling in Long Valley would be in the region of stations 11, 12, 23, and 24.

Acknowledgments. The authors are indebted to John Coakley for the field work, Jeanne Taylor for playing back the tapes and digitizing data, and D. P. Hill and L. J. P. Muffler for critically reviewing the manuscript.

REFERENCES

Borcherdt, R. D., Effects of local geology on ground motion near San Francisco Bay, *Bull. Seismol. Soc. Amer., 60,* 29–61, 1970.

Douze, E. J., and G. G. Sorrells, Geothermal ground-noise surveys, *Geophysics, 37,* 813–824, 1972.

Eaton, J. P., M. E. O'Neill, and J. N. Murdock, Aftershocks of the 1966 Parkfield-Cholame, California earthquake, a detailed study, *Bull. Seismol. Soc. Amer., 60,* 1151–1198, 1970.

Ewing, W. M., W. S. Jardetzky, and F. Press, *Elastic Waves in Layered Media,* pp. 145–149, McGraw-Hill, New York, 1957.

Haubrich, R. A., Microseisms, in *International Dictionary of Geophysics,* vol. 2, pp. 975–977, Pergamon, New York, 1967.

Hill, D. P., Structure of Long Valley caldera, California, from a seismic refraction experiment, *J. Geophys. Res., 81,* this issue, 1976.

Iyer, H. M., Search for geothermal seismic noise in the East Mesa area, Imperial Valley, California, *Open File Rep. 74-96,* 52 pp., U.S. Geol. Surv., Washington, D. C., 1974.

Iyer, H. M., and T. Hitchcock, Seismic noise measurements in Yellowstone National Park, *Geophysics, 39,* 389–400, 1974.

Pakiser, L. C., M. F. Kane, and W. H. Jackson, Structural geology and volcanism of Owens Valley region, California—A geophysical study, *U.S. Geol. Surv. Prof. Pap. 438,* 68 pp., 1964.

Whiteford, P. C., Ground movements in the Waiotapu geothermal region, New Zealand, *Geothermics, 2,* part 2, 478–486, 1970.

(Received January 28, 1975;
revised August 5, 1975;
accepted August 5, 1975.)

Microearthquakes in and Near Long Valley, California

DON W. STEEPLES[1] AND A. M. PITT

U.S. Geological Survey, Menlo Park, California 94025

Sixteen portable seismograph stations were deployed in the vicinity of the Long Valley geothermal area, California, from April 27 to June 2, 1973. Only minor microearthquake activity was detected in the Long Valley caldera, but a high level of activity was detected to the south and east of the caldera. The abrupt spatial seismicity decrease at the southern boundary of the caldera suggests that the caldera is either structurally less competent than the surrounding crust or is at a junction of different regional tectonic deformation trends. No significant attenuation or delays occurred for either local *P* or *S* waves that traversed the caldera.

INTRODUCTION

Sixteen portable seismograph stations were deployed in the area of Long Valley, California, from April 27 to June 2, 1973, as part of a U.S. Geological Survey (USGS) multidisciplinary investigation for possible geothermal resources in the Long Valley caldera. The principal objective of this study was to detect and locate microearthquakes in the Long Valley caldera, an area of present-day hydrothermal activity.

Facca and Tonani [1964] suggested that the delineation of specific faults would be a valuable tool in the search for permeable fracture zones in geothermal areas. *Ward* [1972] suggested that microearthquakes might be used to locate active faults that may channel hot fluids toward the surface.

Brune and Allen [1967] and *Thatcher and Brune* [1971] have reported microearthquake activity associated with geothermal areas in the Imperial Valley south of the Salton Sea. *Ward and Bjornsson* [1971] located over 2100 earthquakes in Iceland, and they noted a difference between the continuous microearthquake activity in the geothermal areas and the larger shocks followed by aftershock sequences in other parts of the island. *Lange and Westphal* [1969] detected microearthquake activity near The Geysers, California, during a recording period of 5 days. In several other geothermal areas of the western United States they detected such activity in recording periods of similar duration. *Hamilton and Muffler* [1972] located 53 microearthquakes within 10 km of the then producing area at The Geysers, California, in a 3-week period.

Microearthquakes may have other uses in geothermal exploration. *Hamilton and Muffler* [1972] suggested that the maximum focal depths of microearthquakes may be a temperature indicator. *Brace and Byerlee* [1970] showed that high temperature may prevent stick slip (i.e., earthquakes) and induce stable sliding.

The Long Valley caldera is an elliptical depression 19 by 29 km (Figure 1). Rhyolitic extrusion has occurred in the last 1500 yr, and hot spring activity persists to the present time. *Bailey et al.* [1976] have noted a difference in the character of faulting inside and outside the caldera, and they suggest that the material inside the caldera was decoupled for a time from the uplift of the Sierras to the south and west.

Gumper and Scholz [1971] and *Ryall et al.* [1972] located microearthquakes in Chalfant Valley and in a zone trending northwestward from Bishop toward Mammoth. Their networks suffered from azimuthal control and distance with respect to Long Valley, and events smaller than magnitude 1.5 in Long Valley could not be detected. *Pitt and Steeples* [1975] detected only two microearthquakes in the Long Valley caldera while they confirmed the seismicity pattern established by the earlier investigators south and east of Long Valley. There has been considerable historic seismicity in the region, including the great 1872 earthquake in Owens Valley, about 100 km southeast of the Long Valley caldera. *Pitt and Steeples* [1975] interpreted microearthquake focal mechanisms just outside the southeastern edge of the caldera in terms of right lateral strike slip. Those microearthquakes were located near the epicenters of two magnitude 6.0 earthquakes that occurred within the last 50 yr [*California Department of Water Resources,* 1964].

THE NETWORK

The instruments used for this study were the USGS portable seismograph systems that have been described in detail by *Eaton et al.* [1970]. Sixteen of these systems were operated at 20 different locations during the recording period. The array was centered on the eastern half of the caldera, and six locations from a previous study by *Pitt and Steeples* [1975] were reoccupied (Table 1).

CRUSTAL MODEL

A shallow crustal model for the immediate Long Valley area was described by *Hill* [1976]. The microearthquakes recorded (discussed later) were mostly outside the caldera, so the local Hill model was bypassed in favor of a regional model derived from the reversed refraction profile between Mono Lake and China Lake, California, described by *Eaton* [1966]. This profile passes near the center of the seismic array of the present study. The model consists of the following sequence of horizontal constant velocity layers, where velocity is in kilometers per second and depth is in kilometers:

P Wave Velocity	Depth to Top of Layer
3.0	0.0
6.0	1.7
6.4	15.0
6.9	28.0
7.9	54.0

Using this model, well-recorded blasts within the network were located to within 1 km horizontally and 2 km vertically. It is assumed that well-recorded earthquakes that occurred within the network were located to this same order of accuracy and that earthquake locations outside the network may be in

[1] Now at Kansas Geological Survey, University of Kansas, Lawrence, Kansas 66044.

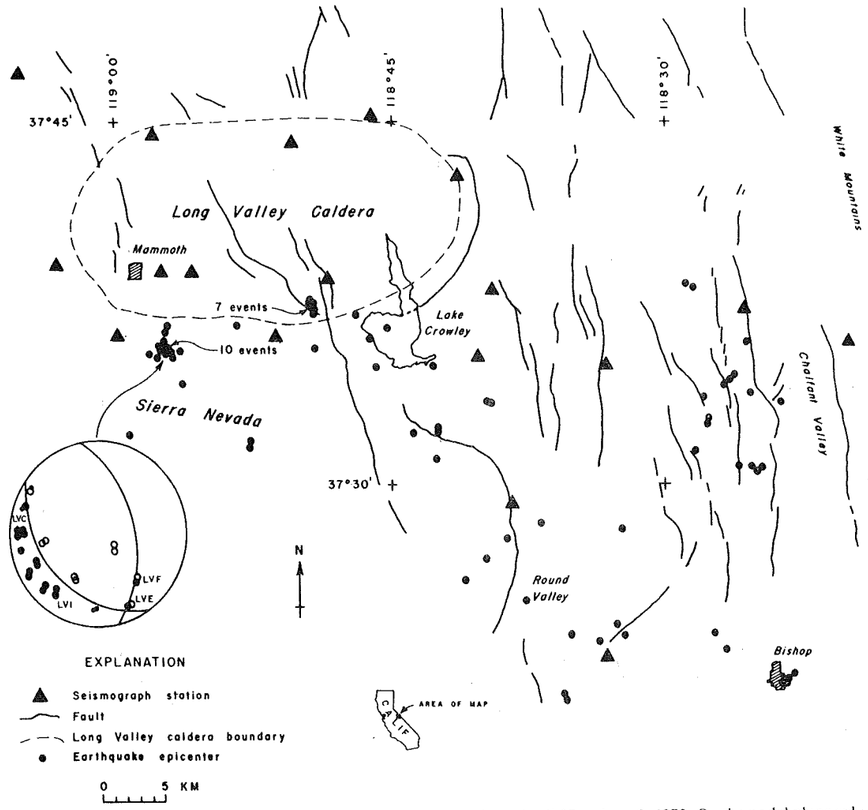

Fig. 1. Microearthquakes in the vicinity of Long Valley caldera from April 27 to June 2, 1973. On the nodal plane solution, solid circles represent initial compression, and open circles initial dilatation; smaller circles indicate less reliable first motions. Stations mentioned in Figure 2 are designated by three letters on the nodal plane solution.

error by 2 km or more. Relative locations of closely spaced events within the network may be accurate to a few hundred meters. No elevation or station corrections were used.

Selection of Data Set

All local events that appeared at three or more stations were analyzed. *P* arrivals were picked and timed to 0.01 s by using station WWVB or internal chronometer corrected to WWVB. *S* arrivals were timed on the five three-component stations and where possible on the 11 one-component stations. Reading errors (as distinguished from picking errors) are no more than ±0.02 s.

S arrivals were only used to locate events when the *P*-only solution produced *S* residuals suggesting poor quality locations. A Wadati diagram was used to establish the proper *Vp/Vs* ratio for the region (1.70). The uncertainties in picking the *S* arrivals may be ½ s or more, but balanced *S* residuals (i.e., some positive, some negative) are considered to indicate stable (good quality) hypocenter solutions. Events with fewer than five *P* arrivals picked to better than 0.25 s were dropped from the data set unless the location was within 5 km of the edge of the Long Valley caldera, in which case all events with three or more stations were kept.

Hypocenters and magnitudes from the signal duration [*Lee et al.*, 1972] were determined by Geiger's method using the computer program HYPO71 [*Lee and Lahr*, 1972] (Table 2). The magnitudes determined here may differ from the classical Richter local magnitudes by as much as one third of a magnitude unit and should therefore be regarded as local magnitude approximations.

Microearthquake Distribution

The events listed in Table 2 are plotted in Figure 1 (except for two events outside the map area). The activity is concentrated in a WNW trending band extending from near Bishop almost to Mammoth. Focal depths range from 1 to 15 km with no systematic pattern to the depth distribution. The seismicity pattern is very similar to that found by *Gumper and Scholz* [1971] and *Ryall et al.* [1972]. It is also similar to the pattern found by *Pitt and Steeples* [1975], except that the swarm near 37°36'N, 118°57'W (Figure 1) is in an area in which only two events were detected in a 20-day recording period in 1970.

The 1973 data alone (Figure 1) are insufficient to present the trends that emerge when all our data are plotted together. In Figure 3 all of the microearthquake data from 1970 and 1973 are displayed, along with station locations from 1973. Approximately 50 of these events (of over 200 plotted) had fewer than five readings, and perhaps a half dozen (shallow events within 15 km of the D in Sierra Nevada (Figure 3)) of the 50 could be

TABLE 1. Seismograph Station Data

Location	Station	North Latitude	West Longitude	Elevation, m	Instruments
1	LVA	37°36.16′	118°59.68′	2768	USGS Portable
2	LVB	37°36.13′	118°51.15′	2310	USGS Portable
3	LVC	37°34.97′	118°33.17′	2231	USGS Portable
4	LVD	37°45.14′	118°46.03′	2195	USGS Portable
5	LVE	37°46.82′	119°04.96′	2365	USGS Portable
6	LVF	37°39.03′	119°03.01′	2755	USGS Portable
7	LVG	37°44.41′	118°57.81′	2292	USGS Portable
8	LVH	37°38.83′	118°57.33′	2365	USGS Portable
9	LVI	37°44.20′	118°50.36′	2121	USGS Portable
10	LVJ	37°38.50′	118°48.37′	2140	USGS Portable
11	LVK	37°42.73′	118°41.28′	2249	USGS Portable
12	LVL	37°38.05′	118°39.38′	2316	USGS Portable
13	LVM	37°35.22′	118°40.42′	2170	USGS Portable
14	LVN	37°35.87′	118°20.25′	1792	USGS Portable
15	LVO	37°29.21′	118°38.19′	1719	USGS Portable
16	LVP	37°23.03′	118°33.14′	1451	USGS Portable
17	LVR	37°38.82′	118°55.67′	2341	USGS Portable
18	LVS	37°35.47′	118°50.07′	2426	USGS Portable
19	LVT	37°55.86′	118°56.30′	2077	USGS Portable
20	LVU	37°36.71′	118°23.92′	1378	USGS Portable
21	DFOD	37°33.18′	117°45.16′	2173	USGS Telemetered NCER
22	TIN	37°03.30′	118°13.70′	1195	Cal Tech

explosions. The hypocenters of these poorly located events could be in error by more than 5 km horizontally and 10 km vertically. The good events from 1970 are plotted in the work by *Pitt and Steeples* [1975].

A north-south trend is apparent in Chalfant Valley. A larger and more extensive trend from northern Owens Valley toward Long Valley caldera reinforces the trend suggested in Figure 1, including the abrupt decrease in activity at the edge of Long Valley caldera. It is particularly noteworthy that few events were detected within the Long Valley caldera. This is discussed in detail later.

Nodal Plane Solution

The directions of first motion of *P* arrivals were noted when sufficiently strong and classified on three quality levels: (1) certainly correct because of the amplitude and character of the arrival; (2) probably correct because of the character of the arrival but of lower amplitude than events in the first class; and (3) less certain than classes (1) and (2) but still worth using in order to increase the density of coverage on the focal sphere. Computer program HYPO71 provides an equal-area projection of first motions on the lower hemisphere.

Figure 1 shows a nodal plane solution with an arrow pointing to the epicenter on the map. The solution, a composite of two nearly identical events, has nodal planes that can be drawn by using arrivals from both events but using only two fortuitously located stations. The two events used had hypocenters within a few hundred meters of each other. At 13 stations (of 15 operating) the seismograms could almost be traced one event upon the other. Figure 2*a* shows typical examples of this similarity. The remaining two stations (LVE and LVF) possessed nodal character (much smaller amplitude) for the *P* arrival and showed a reversal of sense of first motion from one event to the other (Figure 2*b*). It is known [e.g., *Helmberger*, 1974] that *P* nodes and *S* nodes coincide at only two diametrically opposite points on a focal sphere and also that the *P* nodal planes are mutually perpendicular, intersecting along a straight line connecting the two points. This can be visualized by imagining a perfect vertical strip-slip focal sphere viewed from above. The north pole of the sphere is a point of intersection of the two *P* nodal planes. The north pole is also a point of intersecting *S* nodes. The south pole of the focal sphere is the only other point where both *P* nodes and *S* nodes coincide. This special case of perfect vertical strike slip can be generalized to the present (or any other) case simply by rotating the focal sphere.

Figure 2*c* shows that station LVE was at or very near a point of coincidence of *P* node and *S* node, so that the diametrically opposed nodal points are both known to within a very few degrees. In addition, station LVF showed *P* nodal character, so that three *P* nodal points are known and thus one *P* nodal plane is uniquely determined. The second *P* nodal plane is also uniquely determined, since it must pass through the two diametrically opposed *P* and *S* node coincidence points and at the same time be perpendicular to the *P* nodal plane previously determined.

The nodal planes drawn by this method are in total agreement with the first motions for both events at the other 13 stations as shown in Figure 1. In this case the data agree well with the double-couple mechanism theory.

This particular pair of events shows how important radiation pattern can be in determining the amplitude of *S* waves. When this severe attenuation of *S* waves was first observed by the authors, the tendency was to think it might be related to attenuation by magma as in studies by *Kubota and Berg* [1967] and *Matumoto* [1971] at Mt. Katmai, Alaska, and *Pitt* [1974] at Yellowstone. This is an example that indicates that the radiation pattern can drastically affect amplitudes but that near total attentuation is limited to small areas of the focal sphere.

As originally conceived, part of this investigation was to include attenuation data from local earthquakes that sent energy through the Long Valley caldera in a study similar to that at Yellowstone by *Pitt* [1974]. This study produced negative results, as the ray paths involved did not penetrate to sufficient depth in the caldera to encounter significant low-velocity material, other than that in the upper 3 or 4 km described in the refraction study of *Hill* [1976]. The ray paths in the caldera were too shallow to detect the low-velocity material described by *Steeples and Iyer* [1976] and *Steeples* [1975].

TABLE 2. Microearthquakes in the Long Valley Vicinity From April 27 to May 30, 1973

Date	Origin	Epicenter North Latitude	Epicenter West Longitude	Depth of Focus, km	M	N	Gap, deg	D_{min}, km	rms, s	ERH, km	ERZ, km	Q
April 27	13h 05m 09.13s	37°37.01′	118°46.90′	5.00	1.29	3	187	6.5	0.00			AD
April 30	23h 05m 04.48s	37°27.72′	118°38.63′	5.36	1.79	7	163	2.8	0.08	1.1	1.4	BC
April 30	07h 28m 43.08s	37°33.35′	118°39.68′	7.99	1.34	5	143	3.6	0.06	1.0	2.0	BD
May 1	05h 58m 15.53s	37°36.56′	118°57.06′	8.35	2.07	23	172	4.2	0.14	0.5	0.8	AC
May 1	07h 35m 29.05s	37°30.49′	118°25.09′	9.87	2.44	16	269	18.2	0.15	1.6	3.0	BD
May 1	07h 40m 38.65s	37°30.61′	118°24.91′	13.01	2.59	10	270	18.5	0.12	3.4	3.7	CD
May 1	08h 59m 58.56s	37°28.37′	118°36.80′	5.00	1.59	3	163	2.6	0.03			AD
May 1	10h 37m 34.68s	37°35.40′	118°57.43′	8.06	1.89	11	187	6.3	0.10	0.8	1.3	AD
May 1	11h 27m 25.07s	37°35.41′	118°57.43′	7.70	1.42	10	197	6.3	0.12	1.2	1.9	BD
May 1	19h 14m 18.85s	37°35.17′	118°57.65′	5.00	1.44	6	201	10.6	0.13	2.1	12.0	CD
May 1	22h 43m 24.89s	37°35.22′	118°56.84′	5.00	1.66	7	181	4.5	0.11	1.3	2.6	BD
May 2	03h 14m 21.92s	37°30.71′	118°26.14′	9.53	1.67	10	264	13.0	0.12	2.7	2.7	CD
May 2	09h 40m 58.78s	37°33.34′	118°39.62′	9.56	1.07	8	115	7.9	0.23	2.1	4.6	BB
May 2	10h 37m 08.42s	37°35.75′	118°25.63′	7.88	2.08	12	265	11.2	0.15	3.3	2.9	CD
May 2	11h 58m 33.73s	37°36.26′	118°57.14′	7.40	1.15	16	152	3.7	0.13	0.7	0.9	AC
May 2	14h 21m 17.69s	37°34.09′	118°56.27′	5.00	1.18	4	234	6.3	0.04			AD
May 2	17h 06m 59.16s	37°35.47′	118°56.36′	2.00	1.35	4	193	5.1	0.08			AD
May 2	17h 53m 44.03s	37°35.88′	118°46.14′	9.61	1.51	8	135	8.5	0.14	1.4	4.3	BC
May 3	09h 11m 58.34s	37°33.30′	118°23.73′	12.62	1.21	6	285	14.2	0.13	5.5	3.9	DD
May 3	14h 36m 53.39s	37°32.07′	118°43.74′	13.69	0.95	14	217	7.6	0.37	2.3	2.7	CD
May 3	15h 03m 24.08s	37°26.88′	118°39.77′	7.20	1.23	4	174	4.9	0.00			AD
May 5	09h 21m 51.38s	37°25.99′	118°40.95′	6.49	1.01	9	189	7.2	0.05	0.5	0.9	AD
May 5	09h 40m 06.85s	37°30.66′	118°25.34′	9.57	1.71	13	181	12.2	0.14	1.4	3.0	BD
May 8	09h 09m 04.61s	37°35.59′	118°56.85′	4.89	0.86	7	171	4.3	0.04	0.6	1.4	AC
May 8	09h 10m 28.41s	37°35.86′	118°57.19′	6.86	1.10	9	165	3.7	0.06	0.5	0.8	AC
May 9	06h 41m 14.48s	37°23.13′	118°26.74′	9.04	1.78	25	247	9.4	0.24	1.3	1.6	BD
May 9	08h 06m 43.82s	37°23.78′	118°27.43′	9.09	1.36	15	235	8.5	0.17	1.1	1.3	BD
May 9	08h 58m 44.41s	37°36.57′	118°53.31′	2.96	0.83	7	161	3.3	0.04	0.4	1.2	AC
May 9	16h 04m 56.41s	37°31.83′	118°52.54′	5.54	1.02	9	204	8.2	0.08	0.8	2.1	BD
May 9	16h 47m 59.12s	37°31.57′	118°52.63′	3.33	1.28	12	208	8.7	0.07	0.6	3.8	BD
May 9	19h 17m 23.33s	37°35.70′	118°57.57′	9.08	2.49	17	162	3.2	0.09	0.5	0.6	AC
May 9	20h 32m 59.19s	37°35.46′	118°57.22′	6.25	1.74	11	177	3.8	0.09	0.8	1.2	AC
May 9	21h 23m 59.54s	37°35.47′	118°56.97′	6.85	1.34	10	175	4.2	0.08	0.8	1.2	AC
May 9	22h 28m 40.76s	37°20.91′	118°35.43′	12.42	2.52	14	235	5.2	0.09	1.0	0.6	AD
May 10	05h 28m 28.62s	37°21.16′	118°35.53′	11.83	1.78	15	235	4.9	0.11	0.9	0.6	AD
May 10	16h 48m 24.17s	37°34.79′	118°45.82′	6.34	1.37	13	138	7.8	0.08	0.4	1.1	AC
May 10	21h 08m 17.75s	37°35.57′	118°56.94′	6.56	1.34	9	172	4.2	0.08	0.9	1.3	AC
May 11	08h 14m 03.58s	37°35.54′	118°56.85′	5.00	1.05	6	203	4.3	0.06	1.0	1.8	BD
May 12	04h 48m 10.85s	37°35.56′	118°49.10′	5.81	1.02	9	148	3.2	0.09	0.8	1.2	AC
May 12	12h 23m 44.34s	37°34.05′	118°26.87′	0.92	1.74	12	144	9.4	0.17	1.5	142.1	CC
May 12	12h 28m 26.15s	37°34.24′	118°26.58′	4.03	1.80	11	146	9.8	0.15	1.7	6.0	CC
May 13	02h 31m 50.50s	37°35.35′	118°58.01′	9.27	2.56	19	164	2.9	0.15	0.8	0.8	BC
May 13	04h 35m 36.23s	37°36.50′	118°45.24′	10.35	0.85	10	157	5.9	0.11	1.3	2.1	BC
May 13	05h 42m 36.22s	37°35.90′	118°57.25′	7.73	1.63	12	164	3.6	0.08	0.7	1.0	AC
May 13	09h 50m 34.42s	37°35.36′	118°56.99′	6.41	0.97	8	199	4.2	0.06	0.8	1.1	AD
May 13	17h 48m 45.60s	37°31.30′	118°28.44′	9.43	1.29	8	149	9.7	0.15	1.7	3.3	BC
May 14	10h 22m 56.58s	37°32.65′	118°27.72′	5.76	2.00	16	143	9.1	0.13	0.8	2.5	BC
May 17	08h 12m 14.19s	37°22.27′	118°23.02′	6.49	1.71	14	266	15.0	0.12	2.6	4.5	CD
May 17	08h 43m 34.11s	37°21.99′	118°23.36′	9.27	2.97	20	120	14.6	0.16	0.8	1.4	BB
May 17	17h 44m 19.26s	37°21.77′	118°23.73′	5.00	1.22	6	309	14.1	0.13	5.5	5.1	DD
May 18	14h 54m 39.74s	37°34.45′	118°26.31′	2.40	1.08	5	167	9.3	0.06	1.4	21.9	CD
May 19	11h 53m 09.82s	37°32.20′	118°42.43′	12.85	0.99	22	145	6.3	0.13	0.5	0.7	AC
May 19	11h 53m 40.73s	37°32.20′	118°42.45′	12.22	1.12	23	145	6.3	0.11	0.4	0.6	AC
May 20	15h 18m 15.67s	37°23.55′	118°33.78′	11.93	1.55	24	225	21.1	0.39	3.3	6.5	CD
May 20	15h 24m 05.75s	37°37.41′	118°49.46′	9.09	1.28	13	119	2.6	0.09	0.6	0.9	AB
May 20	16h 14m 36.17s	37°37.55′	118°49.50′	9.26	1.03	11	115	2.4	0.09	0.7	1.2	AB
May 20	21h 03m 54.33s	37°37.52′	118°49.28′	10.73	1.11	7	126	2.3	0.07	0.8	1.1	AB
May 21	06h 29m 28.56s	37°37.47′	118°49.42′	11.26	0.44	5	140	2.5	0.04	2.3	1.6	BD
May 21	08h 21m 20.18s	37°37.35′	118°49.36′	12.40	0.37	7	144	2.6	0.04	0.6	1.0	AC
May 21	11h 12m 41.04s	37°37.58′	118°49.39′	11.51	0.57	11	116	2.3	0.11	0.9	1.9	AB
May 21	11h 13m 39.21s	37°37.05′	118°49.20′	10.86	0.44	10	134	2.9	0.12	1.0	2.1	BB
May 21	13h 03m 09.61s	37°57.88′	118°42.58′	14.50	1.29	17	273	20.4	0.14	1.1	1.8	BD
May 21	20h 36m 56.25s	37°31.03′	118°42.52′	0.32	2.87	18	221	8.4	0.21	1.2	0.9	BD
May 21	22h 58m 15.89s	37°32.48′	118°27.76′	9.73	1.81	8	218	9.2	0.17	3.6	3.8	CD
May 22	06h 21m 16.33s	37°38.17′	118°28.96′	11.30	1.55	14	159	7.9	0.14	1.4	2.2	BC
May 22	10h 11m 22.46s	37°32.09	118°59.20′	1.93	0.85	5	267	7.6	0.08	2.3	20.8	CD
May 23	06h 04m 14.24s	37°33.48′	118°27.95′	7.94	1.23	6	207	8.2	0.11	4.4	3.3	CD
May 23	07h 05m 48.23s	37°24.23′	118°32.69′	5.00	1.61	13	259	19.9	0.14	2.9	14.6	CD
May 23	09h 00m 57.80s	37°37.10′	118°26.06′	2.27	1.98	15	197	34.1	0.08	0.8	94.7	CD
May 23	17h 22m 35.34s	37°23.72′	118°32.28′	5.00	1.93	8	261	20.8	0.12	3.4	19.6	CD
May 25	07h 48m 36.20s	37°34.83′	118°42.68′	8.17	0.55	5	310	3.4	0.03	1.0	0.4	AD

TABLE 2. (continued)

Date	Origin	Epicenter North Latitude	Epicenter West Longitude	Depth of Focus, km	M	N	Gap, deg	D_{min}, km	rms, s	ERH, km	ERZ, km	Q
May 28	08h 13m 31.43s	37°23.78′	118°35.20′	9.71	1.58	9	268	20.9	0.07	3.2	6.3	CD
May 28	14h 43m 16.81s	37°28.09′	118°32.47′	8.58	2.00	13	239	12.8	0.21	3.0	5.2	CD
May 28	15h 24m 19.72s	37°25.13′	118°37.55′	8.84	1.52	9	282	19.1	0.08	2.8	4.5	CD
May 29	13h 04m 33.77s	37°38.04′	118°28.48′	8.20	1.99	14	171	7.1	0.16	1.6	2.9	BC
May 30	12h 25m 19.55s	37°33.65′	118°25.40′	7.09	2.81	16	184	6.1	0.15	1.4	1.7	BD

M is the magnitude of the earthquake; N is the number of stations used in locating the earthquake; the gap is the largest azimuthal separation between stations; D_{min} is the epicentral distance to the nearest station; rms is the root mean square error of the time residuals (rms = $\Sigma_i R_i^2/N$, where R_i is the observed seismic wave arrival time less the computed time at the ith station); ERH is the standard error of the epicenter ($ERH = SDX^2 + SDY^2$, where SDX and SDY are the standard errors in latitude and longitude, respectively, of the epicenter); ERZ is the standard error of the depth (left blank if it is ≥10).

Q is the solution quality of the hypocenter (given as two letters) based on both the statistical measure of the solution and the nature of the station distribution with respect to the earthquake. Each of these two factors is rated independently according to the following scheme. For the statistical measure (first letter), for A, rms < 0.15, $ERH \leq 1.0$, and $ERZ \leq 2.0$. For B, rms < 0.30, $ERH \leq 2.5$, and $ERZ \leq 5.0$. For C, rms < 0.50, and $ERH \leq 5.0$. For D, the values are other than those given above. For the station distribution (second letter), for A, $N \geq 6$, the gap ≤ 90, and $D_{min} \leq$ depth or 5. For B, $N \geq 6$, the gap ≤ 135, and $D_{min} \leq 2$ times depth or 10. For C, $N \geq 6$, the gap ≤ 180, and $D_{min} \leq 50$. For D, the values are other than those given above.

DISCUSSION

Pitt and Steeples [1975] noted the similarity between their 1970 seismicity and the historic seismicity from 1934 to 1970, as well as the similarity of their seismicity to patterns determined by *Gumper and Scholz* [1971] and *Ryall et al.* [1972]. The pattern of seismicity in Figure 3 is very similar to the historic seismicity. It is probably not valid to try to correlate this short sample of epicenters to specific faults in the Long Valley vicinity. There are faults both inside and outside the

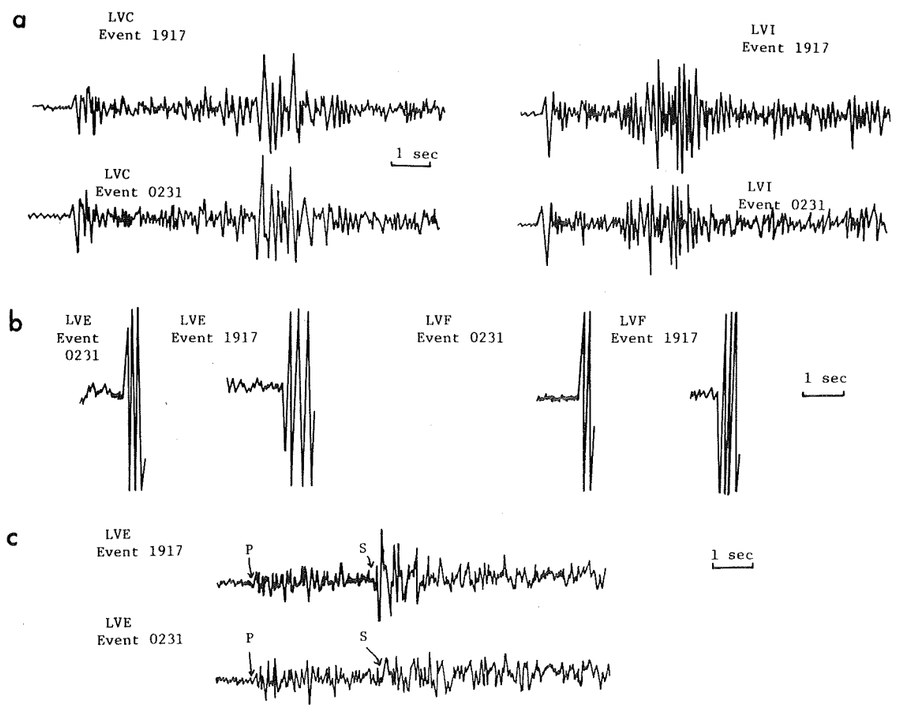

Fig. 2. Seismograms used to construct nodal plane solution near Mammoth in Figure 1. (*a*) Low-gain trace seismograms from station LVC (left) and LVI (right) showing similarity, which was typical at all but two stations between events. (*b*) High-gain trace seismograms from stations LVE (left) and LVF (right) showing reversal of first motion from one event to the other. The low-gain P arrivals were emergent at these two stations relative to the low-gain arrivals at the other 13 stations. Compare low-gain arrivals in (*a*) with low-gain P arrivals in (*c*). (*c*) The low-gain trace seismograms from station LVE showing a weak P arrival for both events (compare with (*b*)). Note almost total disappearance of S arrival for the 0231 event at station LVE.

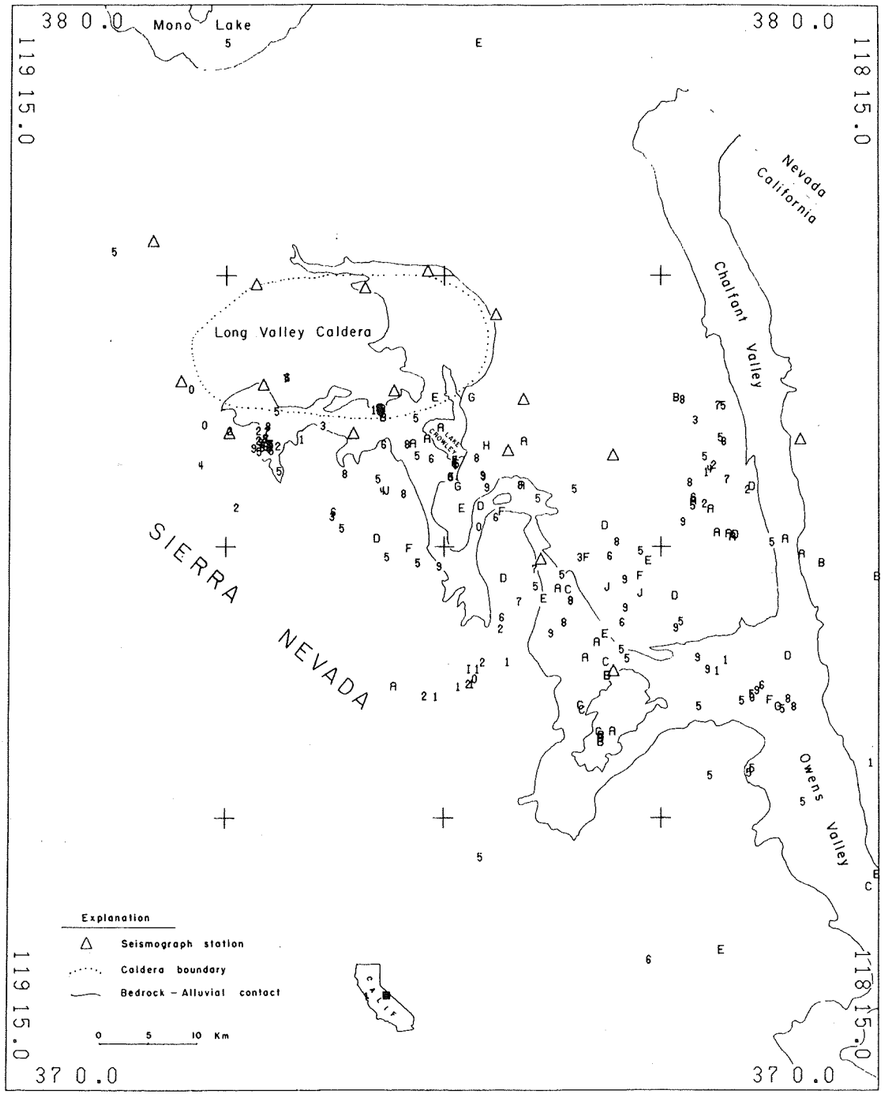

Fig. 3. All microearthquakes from both studies (1970 and 1973). Triangles show 1973 station locations; 1970 stations are not plotted but are shown in the work by *Pitt and Steeples* [1975]. Note the low level of activity in the Long Valley caldera. Focal depths of microearthquakes in kilometers are indicated by numbers and letters (A = 10 km, B = 11 km, etc.). Note the north-south trend from Chalfant Valley to Owens Valley and the northwest-southeast trend from Long Valley caldera to Owens Valley.

caldera that show recent displacements [see *Bailey et al.,* 1976].

Several nodal plane solutions presented in the work by *Pitt and Steeples* [1975] indicate a relative tension axis oriented within a few degrees of east-west. The normal dip-slip solution shown in Figure 1 also has a tension axis oriented roughly east-west, a pressure axis that is roughly vertical. The east-west extension in the Basin and Range province is well known, so the relative tension axis is in agreement with tectonic deformation to the east of the Sierra Nevada.

Ward [1972] has pointed out that microearthquakes occur in most major geothermal areas. He also stated,

> The observation that large numbers of microearthquakes are often found within but not outside of geothermal areas during short periods of field recording suggests that seismic activity within the geothermal areas may be a far more continuous process than seismic activity in most other areas, even though all the seismic activity may be along the same fault system and in response to the same regional stresses.

The data presented here from Long Valley are opposite to the above observation; i.e., there are many microearthquakes just outside the Long Valley caldera but few within the caldera where geothermal prospects are thought to be best. There are several possible explanations:

1. Either Long Valley is not a major geothermal area, or it is an exception to *Ward*'s [1972] observation.
2. The recording period coincided with an aseismic period in Long Valley. *Pitt and Steeples* [1975] located two microearthquakes in west central Long Valley from a 20-day recording period in 1970, and activity outside the caldera was comparable to the present study.
3. The microearthquakes in Long Valley were too small to be detected by our network. The network was capable of detecting events down to about magnitude zero or perhaps −0.5.
4. Some part of the upper crust in Long Valley is not strong enough to support the stresses required for detectable earthquakes. This might be true if magma or partial melt were present in the upper 15 km of the crust. Such a soft zone could effectively isolate the upper 15 km from regional stresses that are obviously present as shown by microearthquake activity near the Long Valley caldera.
5. High temperatures could produce stable sliding instead of brittle fracture [*Brace and Byerlee,* 1970] in the upper crust in the caldera.
6. *Gumper and Scholz* [1971] noted a similar lack of activity in the vicinity of the Long Valley caldera and northern Chalfant Valley. As shown in Figure 3, seismic activity virtually ceases along an east-west line projected along the southern edge of the caldera. This may have some tectonic significance that is not yet understood but is not thought to be a result of inadequate station coverage. *Gumper and Scholz* [1971] suggested that the Owens Valley is a spreading ridge. This would explain the presence of volcanic activity in the Long Valley vicinity but might not explain the petrology of the more silicic igneous rocks.

Whatever the explanation, the only microearthquakes recorded within the caldera are at the extreme southeastern edge of the caldera, and they are about 10 km deep. These may be on the Hylton Creek fault (the only fault in Figure 1 that crosses the southern caldera boundary), and they are probably associated with regional deformation. It is impossible to tell from this small cluster of events if a zone facilitating upward movement of hot water or steam is present. The termination of seismic activity at the southern edge of the caldera may suggest permeable zones (or at least fractured material) close to that edge.

Although microearthquakes have been of some use in locating apparent fracture zones at some of the earlier mentioned geothermal localities, the method is far from proven in the more general sense of geothermal exploration. The difficulty of locating fracture zones with microearthquakes is exemplified by the San Andreas fault. One merely has to look at a National Center for Earthquake Research seismicity report for central California [e.g., *Wesson et al.,* 1974] to see that the seismicity is typically placed a kilometer or two off the fault trace. If one is interested in drilling for a geothermal resource, the exploration technique should be capable of locating fracture zones to better than of the order of a couple of kilometers. Another limitation of microearthquakes is that their absence does not imply the absence of active faults. Some parts of the San Andreas fault have broken the surface in historic time but yet have little or no microearthquake activity at the present time, as can be seen in the previously mentioned report of Wesson et al.

Acknowledgments. The field work for this investigation was performed by John Coakley and Tim Hitchcock. Tapes were played back and records prepared by Jeanne Taylor. Publication was authorized by the Director, U.S. Geological Survey.

REFERENCES

Bailey, R. A., G. B. Dalrymple, and M. A. Lanphere, Volcanism, structure, and geochronology of Long Valley caldera, Mono County, California, *J. Geophys. Res., 81,* this issue, 1976.

Brace, W. F., and J. D. Byerlee, California earthquakes: Why only shallow focus?, *Science, 168,* 1573, 1970.

Brune, J. N., and C. R. Allen, A microearthquake survey of the San Andreas fault system in southern California, *Bull. Seismol. Soc. Amer., 57,* 277, 1967.

California Department of Water Resources, Crustal strain and fault movement investigation—faults and earthquake epicenters in California, *Calif. Div. Mines Geol. Bull., 116-2,* 1964.

Eaton, J. P., Crustal structure in northern and central California from seismic evidence, *Calif. Div. Mines Geol. Bull., 190,* 419–426, 1966.

Eaton, J. P., M. E. O'Neill, and J. N. Murdock, Aftershocks of the 1966 Parkfield-Cholame, California earthquake: A detailed study, *Bull. Seismol. Soc. Amer., 60,* 1151–1198, 1970.

Facca, G., and F. Tonani, Theory and technology of a geothermal field, *Bull. Volcanol., 27*(2), 143–189, 1964.

Gumper, F. J., and C. H. Scholz, Microseismicity and tectonics of the Nevada seismic zone, *Bull. Seismol. Soc. Amer., 61,* 1413–1432, 1971.

Hamilton, R. M., and L. J. P. Muffler, Microearthquakes at The Geysers geothermal area, California, *J. Geophys. Res., 77,* 2081–2086, 1972.

Helmberger, D. V., Generalized ray theory for shear dislocations, *Bull. Seismol. Soc. Amer., 64,* 45–64, 1974.

Hill, D. P., Structure of Long Valley caldera, California, from a seismic refraction experiment, *J. Geophys. Res., 81,* this issue, 1976.

Kubota, S., and E. Berg, Evidence for magma in the Katmai volcanic range, *Bull. Volcanol., 31,* 175–214, 1967.

Lange, A. L., and W. H. Westphal, Microearthquakes near The Geysers, Sonoma County, California, *J. Geophys. Res., 74,* 4377, 1969.

Lee, W. H. K., and J. C. Lahr, HYPO71: A computer program for determining hypocenter, magnitude, and first motion pattern of local earthquakes, open file report, 100 pp., U.S. Geol. Surv., Menlo Park, Calif., 1972.

Lee, W. H., R. E. Bennett, and K. L. Meagher, A method of estimating magnitude of local earthquakes from signal duration, open file report, 28 pp., U.S. Geol. Surv., Menlo Park, Calif., 1972.

Matumoto, T., Seismic body waves observed in the vicinity of Mount Katmai, Alaska, and evidence for the existence of molten chambers, *Geol. Soc. Amer. Bull., 82,* 2905–2920, 1971.

Pitt, A. M., Evidence from local earthquakes for the existence of a region of seismic body wave attenuation in the upper crust under the Yellowstone caldera (abstract), *Eos Trans. AGU, 55,* 1191, 1974.

Pitt, A. M., and D. W. Steeples, Microearthquakes in the Mono Lake-northern Owens Valley region from September 28 to October 18, 1970, *Bull. Seismol. Soc. Amer., 65,* 835–844, 1975.

Ryall, A. S., W. U. Savage, and D. B. Slemmons, Seismic potential in the western Basin and Range/eastern Sierra Nevada region, Nevada and California (abstract), *EOS Trans. AGU, 53,* 442, 1972.

Steeples, D. W., Teleseismic *P*-delays in geothermal exploration with application to Long Valley, California, Ph.D. thesis, Stanford Univ., Stanford, Calif., 1975.

Steeples, D. W., and H. M. Iyer, Low-velocity zone under Long Valley as determined from teleseismic events, *J. Geophys. Res., 81,* this issue, 1976.

Thatcher, W., and J. N. Brune, Seismic study of an oceanic ridge earthquake swarm in the Gulf of California, *Geophys. J. Roy. Astron. Soc., 22,* 473, 1971.

Ward, P. L., Microearthquakes: Prospecting tool and possible hazard in the development of geothermal resources, *Geothermics,* 1, 3–12, 1972.

Ward, P. L., and S. Bjornsson, Microearthquakes, swarms, and the geothermal areas of Iceland, *J. Geophys. Res., 76,* 3953–3982, 1971.

Wesson, R. L., F. W. Lester, and K. L. Meagher, Catalog of earthquakes along the San Andreas fault system in central California, January–March 1973, open file report, 47 pp., U.S. Geol. Surv., Menlo Park, Calif., 1974.

(Received December 26, 1974;
revised July 22, 1975;
accepted July 24, 1975.)

Low-Velocity Zone Under Long Valley as Determined From Teleseismic Events

DON W. STEEPLES[1] AND H. M. IYER

U.S. Geological Survey, Menlo Park, California 94025

A temporary seismograph station network was used to estimate teleseismic *P* wave residuals in the vicinity of Long Valley geothermal area, California. Relative *P* wave delays of 0.3 s persist at stations in the west central part of the Long Valley caldera after regional and near-surface effects have been removed. Ray tracing indicates that low-velocity material exists beneath the caldera at depths greater than 7 km and less than 40 km, probably less than 25 km. The velocity contrast with normal crust must be at least 5% to satisfy the data and is probably in the range 10–15%. We believe that the low velocity indicates anomalously hot rock at depth and that relative teleseismic *P* residuals may be useful for investigation of sources of geothermal energy.

INTRODUCTION

This paper reports on the results of a study using teleseismic *P* wave arrival time residuals at temporary seismograph networks centered on the Long Valley caldera, California. The method allowed the exploration of the crustal velocity structure to a depth of about 40 km in the caldera. The recording of distant earthquakes is a commonly used method of extracting velocity information about the crust and upper mantle. For example, such studies have been made using the large aperture seismic array (Lasa) in Montana [*Iyer and Healy,* 1972; *Chinnery and Toksoz,* 1967], the Tonto Forest Seismic Observatory in Arizona [*Niazi and Anderson,* 1965], and the U.S. Geological Survey (USGS) seismic network in Yellowstone [*Iyer et al.*, 1974; *Iyer,* 1975]. The investigation at Yellowstone is the first such study in a known geothermal area, and indeed the Yellowstone network was installed for the purpose of investigating passive seismic techniques in such areas. Relative teleseismic *P* delays at Yellowstone were interpreted in terms of an anomalous hot zone extending downward to at least 250-km depth (possibly to 400 km), well into the upper mantle.

Press and Biehler [1964] used correlations between *P* wave delays and gravity anomalies to infer higher than normal temperatures in the lower crust beneath the Sierra Nevada batholith. An alternate interpretation of their data may be possible in view of later work involving azimuthal variation in teleseismic *P* residuals. *Bolt and Nuttli* [1966] and *Nuttli and Bolt* [1969] investigated relative teleseismic *P* residuals in northern California. They found azimuthal variations of up to 2.4 s between Shasta and Berkeley for relative residuals, smaller effects being observed at other stations. They suggested that the azimuthal effects were due to changes in depth and/or thickness of the low-velocity layer in the upper mantle. *Koizumi et al.* [1973] interpreted early teleseismic arrivals at some stations in Nevada as being due to a dipping lithospheric plate in the upper mantle (i.e., a fossil subduction zone). Regional effects such as these are not present at Long Valley (as will be discussed later).

The following information is needed to calculate relative teleseismic *P* residuals: (1) hypocenter location and origin time T_0 of the earthquake and (2) location and arrival time TA_i at the *i*th station. Expected travel times TE_i from each hypocenter to each station are read (by computer in the present work) from the *Herrin* [1968] tables. The absolute *P* residual RA_i for the *i*th station is calculated by subtraction:

$$RA_i = (TA_i - T_0) - TE_i$$

Absolute residuals are of little use in local crustal studies because they are a measure of inaccuracies in the computed hypocenter, source-station effects, and how much the true earth *P* wave velocity differs from the *Herrin* [1968] earth *P* wave velocity model along path lengths of thousands of kilometers in the mantle. Hence for local crustal studies, relative *P* residuals RR_i are calculated by subtracting the absolute *P* residual at some reference station *RAR* from the absolute *P* residuals at the *i*th station:

$$RR_i = RA_i - RAR$$

If RR_i is positive, a delay must have occurred somewhere along the ray path from the earthquake hypocenter to the *i*th station relative to the ray path to the reference station. Since a teleseismic focus represents essentially a point source at its origin, the rays to different stations of a small array follow very similar ray paths until they are far from the focus. Since the lower mantle is thought to be homogeneous on the scale of a few kilometers, it is reasonable to assume that most of the contribution to relative residuals of a local network comes from crustal or upper mantle velocity differences beneath the stations. The ramifications of this assumption are discussed in detail later.

The reference station should be situated such that ray paths to the station represent some average or 'normal' path that does not penetrate the volume of rock under investigation. This requires the reference station to be outside the suspected anomalous area under investigation but at the same time close to the area to keep any regional effects to a minimum. The technique is identical to that used by others [*Utsu,* 1973; *Wyss and Holcomb,* 1973; *Cramer and Kovach,* 1974] searching for temporal variation in *P* residuals caused by physical changes in the vicinity of impending earthquake hypocenters. The only difference is that the present emphasis is on spatial rather than temporal variations.

Signals from distant earthquakes are particularly useful as a supplement to refraction or reflection surveys for local crustal studies because the ray paths are nearly vertical when they reach the surface. Estimated angles of incidence [*Richter,*

[1] Now at Kansas Geological Survey, University of Kansas, Lawrence, Kansas 66044.

TABLE 1. Station Locations

Station	North Latitude deg	North Latitude min	West Longitude deg	West Longitude min
ML01	37	45.63	119	06.52
ML04	37	57.49	119	09.03
ML05	37	49.86	118	25.98
ML06	37	45.13	118	46.03
ML07	37	38.06	118	39.33
ML08	37	36.22	118	59.60
ML09	37	35.85	118	20.23
ML10	37	34.98	118	33.15
ML11	37	32.92	118	48.82
ML12	37	29.22	118	38.19
ML13	37	28.60	118	28.65
ML14	37	22.69	118	33.60
ML16	37	23.04	118	40.49
ML17	37	21.00	118	16.97
ML18	37	13.57	118	36.24
LVA	37	36.16	118	59.68
LVB	27	36.13	118	51.15
LVC	37	34.97	118	33.17
LVD	37	45.14	118	46.03
LVE	37	46.82	119	04.96
LVF	37	39.03	119	03.01
LVG	37	44.41	118	57.81
LVI	37	44.20	118	50.36
LVJ	37	38.50	118	48.37
LVK	37	42.73	118	41.28
LVL	37	38.05	118	39.38
LVM	37	35.22	118	40.42
LVN	37	35.87	118	20.25
LVO	37	29.21	118	38.19
LVP	37	23.03	118	33.14
LVR	37	38.82	118	55.67
LVS	37	35.47	118	50.07
LVP1	37	39.53	118	46.29
LVP2	37	40.25	118	51.25
LVP3	37	41.75	118	53.36
LVP4	37	42.29	118	58.14
LVCF	37	37.43	118	46.73
LVMA	37	43.39	118	50.25
LV01	37	38.12	118	48.32
LV02	37	38.64	118	47.80
LV03	37	39.27	118	47.25
LV04	37	40.15	118	46.75
LV05	37	40.93	118	46.28
LV06	37	41.50	118	45.89
LV07	37	38.38	118	46.90
LV08	37	38.27	118	45.05
LV11	37	40.01	118	48.78
LV12	37	40.46	118	48.25
LV16	37	39.12	118	50.14
LV17	37	39.63	118	49.18
LV18	37	40.02	118	54.31
LV19	37	40.40	118	53.17
LV20	37	40.61	118	52.20
LV21	37	40.30	118	51.57
LV22	37	41.05	118	50.39
LV23	37	40.75	118	49.88
LV24	37	40.62	118	49.12
LV25	37	40.97	118	48.67
LV34	37	44.46	118	51.26
LV35	37	44.62	118	52.09
LV36	37	44.66	118	52.97
LV37	37	44.72	118	53.75
LV38	37	44.87	118	54.46
LV39	37	45.01	118	55.87
LV40	37	44.88	118	56.65
LV41	37	43.25	118	59.82
LV42	37	42.83	118	55.66
LV43	37	40.82	118	59.67
LV44	37	40.83	118	57.02
LV46	37	42.38	118	51.80
LV47	37	41.36	118	54.73
LV48	37	43.48	118	52.66
LV49	37	42.00	118	45.67
LV57	37	42.38	118	46.01
LV58	37	43.00	118	46.41
LV59	37	43.65	118	47.04
LV60	37	44.20	118	46.23
LV63	37	44.63	118	48.41

Seventy-eight different station locations were used. ML stations operated for 20 days in 1970 (except 1, 4, and 10, which only operated for about 10 days). LV stations with three-letter names operated during the whole month of May 1973, except B, O, P, and S, which were moved the last week of May. LV stations A, C, D, and E operated through the month of June also. LV stations with four-character designations operated for a few hours to a few days each. A complete schedule of operation is given by *Iyer and Hitchcock* [1976].

1958] for typical teleseisms used in this study ranged from about 28° from vertical for events in Alaska (Δ (great circle distance) approximately 40°) to about 19° from vertical for events from Japan (Δ approximately 75°). Local refraction surveys provide velocity information only for the upper few kilometers of the crust. The information supplied by local refraction or reflection surveys is essential to the interpretation of teleseismic *P* residuals because it enables us to remove near-surface effects and concentrate on deeper effects.

DATA

It should be pointed out that the data used in the preparation of this paper were gathered from seismic arrays designed to perform entirely different functions than a study of teleseismic *P* delays. For that reason this study should by no means be construed to place limits on the accuracy or precision with which the low-velocity anomaly described herein may eventually be delineated. It should also be pointed out that the western United States is in an ideal position geographically to use the *P* delay method, since many teleseisms arrive along northwest-southeast azimuths approximately 180° apart as shown in Table 2. From theoretical wave propagation limits the *P* delay method is incapable of detecting a 'root' or pipe extending down into the upper mantle if such a pipe is less than perhaps a few kilometers in diameter.

Sixteen portable seismograph stations were deployed for approximately 9 weeks in the Long Valley vicinity to record microearthquakes [*Steeples and Pitt*, 1976, this issue] and monitor seismic noise [*Iyer and Hitchcock*, 1976, this issue]. All well-recorded teleseisms that occurred during these two studies were analyzed. The station locations and teleseismic events used are given in Tables 1 and 2, respectively.

The portable seismograph system is described in detail by *Eaton et al.* [1970]. Since the system was designed primarily to record microearthquakes, picking first arrivals of small teleseisms recorded by the equipment is difficult and uncertain at best. Large teleseisms occur infrequently, and the data set is limited by short periods of recording, so the problem becomes serious when small teleseisms must be used to increase the size of the data set.

Some of the uncertainties of emergent first arrivals can be eliminated by timing the first peak or first trough. When this

TABLE 2. Teleseisms Used

No.	Locality	Date	Origin	Latitude* deg	Latitude* min	Longitude* deg	Longitude* min	Depth, km	Epicenter Azimuth From LVC, deg	Epicenter Distance From LVC, deg
				1970 Data						
1	Kamchatka	Oct. 8	04:53:21.8	+53	48.0	−160	24.0	59	315	56
2	Andreanof	Oct. 8	13:02:05.0	+50	24.0	+176	12.0	38	307	42
3	Russia-China	Oct. 12	09:33:37.0	+42	48.0	−131	00.0	555	315	78
4	Novaya Zemlya	Oct. 14	05:59:57.1	+73	18.0	−55	06.0	1	2	69
5	Fiji	Oct. 14	10:40:58.0	−18	06.0	+178	30.0	609	237	79
6	Honshu	Oct. 16	05:26:13.0	+39	18.0	−140	42.0	24	308	74
				1973 Data						
7	Fiji	April 30	08:39:07.7	−17	30.0	−179	36.0	613	239	80
8	Fiji	May 3	13:26:31.0	−17	54.0	+178	24.0	600	237	79
9	Russia	May 6	14:39:28.1	+43	30.0	−132	18.0	497	315	77
10	Fiji	May 8	04:44:56.4	−17	36.0	+178	54.0	543	238	79
11	Chile	May 10	07:55:07.6	−25	36.0	+70	24.0	44	136	77
12	Fiji	May 14	17:11:13.8	−16	36.0	−175	54.0	54	242	82
13	Fiji	May 14	21:15:47.9	−22	00.0	+179	06.0	501	235	82
14	Honshu	May 17	15:44:19.5	+33	06.0	−140	42.0	62	303	78
15	Fiji	May 27	06:38:13.4	−21	18.0	+177	54.0	422	234	81
16	Rat Island	May 29	01:46:44.9	+51	42.0	−176	12.0	46	309	47
17	Peru	May 30	12:39:54.3	−14	06.0	+72	48.0	90	131	67
18	Gulf of California	May 30	17:33:51.0	+26	18.0	+110	42.0	33	147	13
19	Guatemala	May 31	05:39:18.8	+13	54.0	+90	54.0	99	126	34
20	Unimac	May 29	06:14:22.3	+54	00.0	+163	48.0	30	312	35
21	Ecuador	May 30	04:38:01.8	−02	18.0	+78	30.0	111	128	54
22	Guatemala	June 7	18:32:42.9	+14	18.0	+92	00.0	78	127	33
23	Guatemala	June 7	18:34:46.3	+14	12.0	+91	54.0	70	127	33
24	Solomon	June 9	08:21:27.3	−10	18.0	−161	24.0	70	255	88
25	Andreanof	June 15	13:38:23.1	+51	18.0	+179	24.0	50	308	44
26	Fiji	June 15	23:04:58.6	−25	54.0	+177	24.0	94	231	84
27	Hokkaido	June 17	03:55:02.9	+43	12.0	−145	48.0	48	309	69
28	Hokkaido	June 17	20:37:57.3	+42	42.0	−146	00.0	50	308	69
29	Southern Alaska	June 18	10:17:26.3	+52	12.0	+164	54.0	15	310	35
30	Hokkaido	June 18	17:45:43.7	+42	30.0	−146	00.0	29	308	69
31	Bolivia	June 19	04:46:01.5	−20	48.0	+68	48.0	118	132	75
32	Kermadec	June 20	12:01:56.7	−28	30.0	+176	48.0	41	229	85
33	Andreanof	June 23	05:26:49.0	+51	54.0	+176	54.0	62	309	43
34	Kuril	June 24	02:43:25.5	+43	18.0	−146	24.0	50	309	69
35	Kuril	June 24	03:04:18.6	+43	12.0	−146	48.0	55	308	68
36	Kuril	June 24	03:28:38.5	+43	18.0	−146	48.0	47	309	68
37	Kuril	June 24	05:07:46.8	+43	06.0	−146	36.0	44	308	69
38	South Pacific	June 25	15:03:18.7	−35	54.0	+103	54.0	33	168	74
39	Sitka	July 1	13:33:34.6	+57	48.0	+137	18.0	33	335	24

*Positive denotes north and west; negative denotes south and east.

method was first used to time the teleseisms, the results showed considerable scatter but suggested that the data might contain significant new information about deep crustal velocity beneath Long Valley caldera.

Instead of using the peak and trough method, we tried timing the zero crossing (i.e., the end of the first cycle) (Figure 1). Somewhat to our surprise the scatter in the relative residuals decreased significantly when this technique was used. The standard deviations of relative residuals for a given azimuth decreased by approximately a factor of 2 at most of the stations.

Other investigators at the U.S. Geological Survey have subsequently adopted the zero crossings as timing points (C. Cramer and J. Evans, oral communication, 1975). They have statistically compared the technique to the peak-trough method and the first-break method. Both agree that the zero-crossing method is much superior to first breaks and is slightly better than the peak-trough method, particularly since the zero crossings are more objective picks.

There are several important advantages to the zero-crossing technique:

1. The second zero crossing often crosses the zero-amplitude line at a very steep angle, thus effectively filtering high-frequency noise and reducing the picking uncertainty. It is usually possible to attain a reading accuracy of ±0.02 s.

2. The uncertainty due to changes in wave shape is small because of the very small aperture (Δ = 1/2°) of the seismic array used in this experiment. For the best events both the first arrivals and second zero crossings were timed, and the standard deviations of the period of the first cycle for a particular event were generally in the range 0.04–0.06 s. This provides assurance that the travel time anomalies observed in the caldera are not caused by changes in wave shape or the picking technique. Most events recorded had first-cycle periods of very nearly 1 s, and the wave shape of the first pulse was stable across the array. *Mack* [1969] noted changes in signal shape across the Lasa in Montana, but a look at his published data shows that the first cycle was relatively uniform across the array.

3. For weakly recorded teleseisms resulting from small event magnitudes or low station sensitivity, the first peak or trough, the first zero crossing, and the first break are often ob-

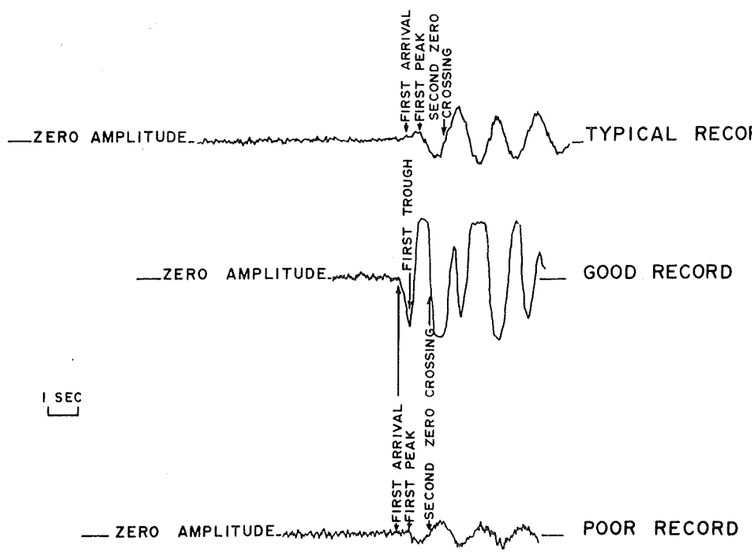

Fig. 1. Tracings of seismograms illustrating various picking points.

scured by noise or attenuated in such a way that the second zero crossing is the first and only reliable pick (Figure 1). Readings beyond the second zero crossing introduce intolerable levels of uncertainty into the data as a result of reflections, scattering, diffraction, and other common wave deformation phenomena [see *Mack,* 1969]. Since the present investigation deals with relative residuals, it is most important to pick the same phase of the signal at all stations.

The data set was recorded in an analog fashion on magnetic tape and played back with an ink-squirting strip chart recorder at a paper speed of 1 cm/s. Two radio station WWVB timing traces were played back parallel to the signal trace. Zero crossings are read to 0.01 s, and picking errors vary from 0.02 s for the best seismograms to about ±0.05 s for signals that do not cross zero at a very steep angle. The uncertainty due to previously mentioned changes in wave shape is of the order of 0.04–0.06 s. Hence the maximum likely uncertainty for a given reading is normally about ±0.11 s for the lower-quality teleseisms used. These error estimates are somewhat subjective but reasonable, and they are based on experience and discussions with other USGS investigators.

The criterion for playback of a teleseism was that it be well recorded at Casa Diablo Mountain (LVC), the reference station (Figure 2). The uncertainty of the timing at LVC is ±0.02 s for picking error and ±0.06 s for wave shape change, since all events except one at the reference station had excellent second zero crossings. Since we are dealing with relative residuals, the usual maximum uncertainty in a relative residual value is the sum of the uncertainties at the reference station and the station of interest, in this case about 0.19 s for the poor events and about 0.16 s for the good events.

At many stations three or more readings from the same azimuth are available. Residuals at these stations were averaged for each approach azimuth, and standard deviations of the data were generally in the range 0.04–0.11 s. We conclude that the likely uncertainty of average relative residual of three or more events from a particular azimuth at a given station is about 0.1 s.

The interpretation of *P* delay data in some cases requires removal of regional azimuthal variations [see *Press and Biehler,* 1964; *Bolt and Nuttli,* 1966]. As is shown below, such a correction was not needed at Long Valley, partly because of the local nature of the array.

Figure 2 shows relative residuals with respect to LVC for stations outside the Long Valley caldera. Some of these readings (six events) come from a network that operated for 20 days in 1970 to record microearthquakes in the northern Owens Valley–Mono Lake region [*Pitt and Steeples,* 1975]. The data in Figure 2 indicate that regional effects for events from the northwest and southeast azimuths are less than 0.05 s, even though two stations have values of +0.16 and −0.18 for events from the southeast. The limited data from southwest events suggest a possibility of relative arrivals southwest and northwest of the Long Valley caldera 0.2 s earlier than those at stations near Bishop, which is about 50 km southeast of Long Valley. Elevation corrections were not used but would add 0.01–0.03 s to residuals in the caldera, since the elevation of the reference station (LVC) is 50–200 m greater than the elevation at stations in the caldera.

Figure 3*a* shows stations in and near the Long Valley caldera that recorded at least one event from the northwest. Relative delays (positive residuals) are about 0.2 s near the northwest corner of the caldera, increasing to about 0.5 s toward the center of the caldera.

Figure 3*b* shows stations that recorded at least one event from the southeast. For this azimuth, delays of the order of 0.5 s are present in the northwest section of the caldera. Thus the largest delays are for stations on the opposite side of the caldera from the approach direction. As is shown below, this change in the spatial pattern for delays for opposite azimuths can be caused only by material deep under the center of the caldera.

Interpretation of the delays requires the removal of near-surface effects. Three different techniques were used to estimate the surface effects:

1. A crustal refraction survey by *Hill* [1976, this issue] was centered on the caldera. Ray tracing and travel time calculations show that the effect of the upper 6 km of the crust should produce only delays of the order of 0.15–0.2 s in most of the caldera including the area where 0.5-s delays were found. The travel times are highly dependent on the thickness of shallow sediment near the surface (velocity 1.5–1.7 km/s) along the Owens River in the northeast section of the caldera. Delays approaching 0.4 s may occur in this region, but it is east of the deep anomalous zone.
2. Teleseismic rays that are recorded near the edge of the caldera but that do not pass up through the center of the caldera show relative delays of 0.2 s, whereas some of the same stations show 0.5-s delays for ray paths that traverse the center of the caldera (Figure 4*c*). This indicates that the near-surface effects are of the order of 0.2 s and that deep effects are 0.3 s beneath the center of the caldera.
3. Some of the larger local microearthquakes south and east of the Long Valley caldera [*Steeples and Pitt,* 1976] could be well located without the use of arrival times from stations within the caldera (LVG, LVI, LVJ). The local earthquake residuals thus obtained at these three caldera stations are a measure of near-surface velocity anomalies in the caldera. Stations LVG and LVJ had local residuals suggesting near-surface delays of 0.2 s. Station LVI, which is near Owens River, has local residuals indicating near-surface delays of 0.30–0.35 s.

Figures 4*a* and 4*b* show residuals from northwest and southeast at stations in the caldera and vicinity after estimated surface effects have been removed. Surface effects were taken at 0.35 s near Owens River Valley (in the hachured area of Figure 4*c*) and 0.2 s elsewhere. Only stations in the caldera that had readings from both northwest and southeast are shown in Figure 4*c*. The estimated near-surface effects have been removed at the five stations shown. Note the azimuthally dependent differences of $\frac{1}{4}$ to $\frac{1}{8}$ s as mentioned in the second technique above. Figures 4*a* and 4*b* show all the available data from the two different azimuths.

An attempt was also made to use regional events from the San Andreas Fault and explosions from the Nevada Test Site in the hope of further constraining the low-velocity volume in the caldera. That effort was a failure because the Long Valley caldera was at or near the critical distance from both sources and it was impossible to distinguish *Pn, P**, and *Pg*.

Discussion

Figures 5*a* and 5*b* show two sectional views of the caldera using readings in a zone 2 km wide centered along AA′ of Figure 4*c* with typical distant ray paths drawn from northwest and southeast teleseisms to the surface. Unfortunately, few large events were recorded from the southeast azimuth because of the relatively short period of recording. Thus there is a scarcity of ray paths from the southeast in a critical part of our

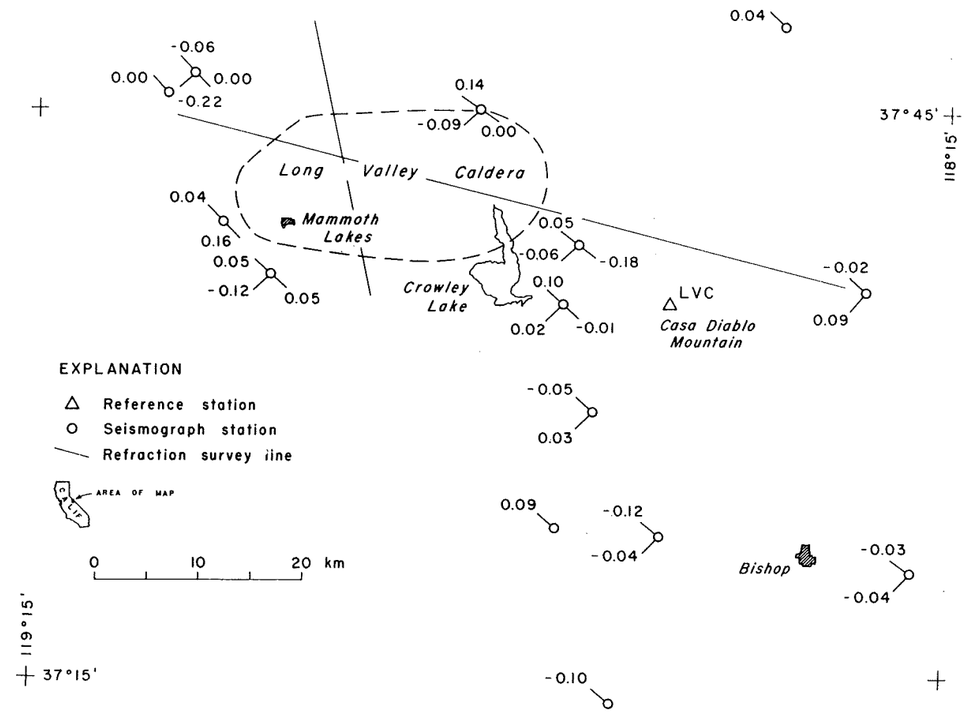

Fig. 2. Teleseismic *P* wave residuals relative to Casa Diablo Mountain (LVC) at stations surrounding the Long Valley caldera. The lines from the stations show the three primary azimuths used. Each number is an average of three or more residuals from the azimuths indicated by the lines. Refraction survey lines are from *Hill* [1976].

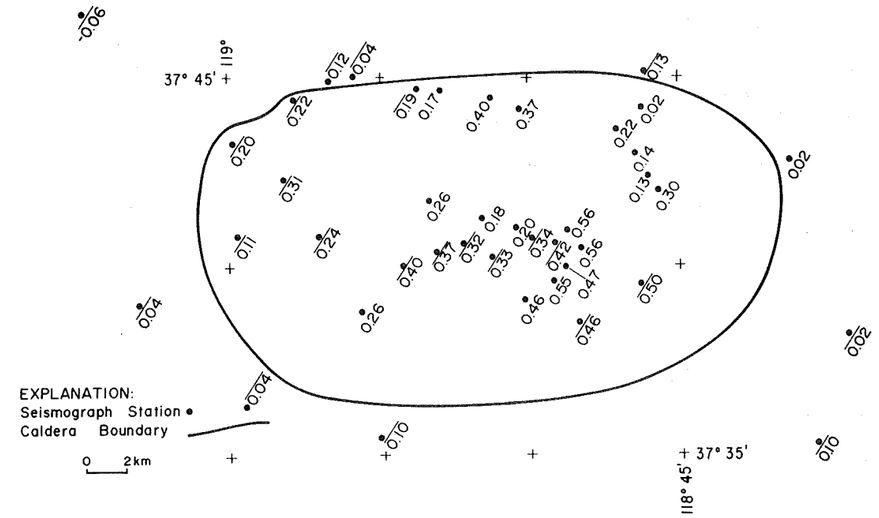

Fig. 3*a*. Teleseismic *P* wave residuals for events from the northwest relative to LVC (not shown). Residual values with bars are averages of three or more events and values without bars are averages of only one or two events. Uncertainty expected is ±0.1 s for barred values and ±0.16 s for unbarred values.

model. It is assumed that somewhere along these ray paths in the crust below 7-km depth (the vertical extent of the refraction survey [*Hill*, 1976, this issue]) a velocity anomaly exists. We consider velocity anomaly models with decreases of 5, 10, and 15% in the *P* wave velocity, and the path lengths required to produce the observed delays. The equation governing path length required is

$$L_P = (\Delta t)\,(V_1)\,(V_2)/(V_1 - V_2)$$

where L_P is path length, Δt is amount of time delay, V_1 is normal crustal velocity (taken as 6.0 km/s), and V_2 is the anomalous low velocity.

When this equation is used, a 5% velocity decrease requires 34.2 km of anomalous ray path to produce 0.3-s delay. Ray

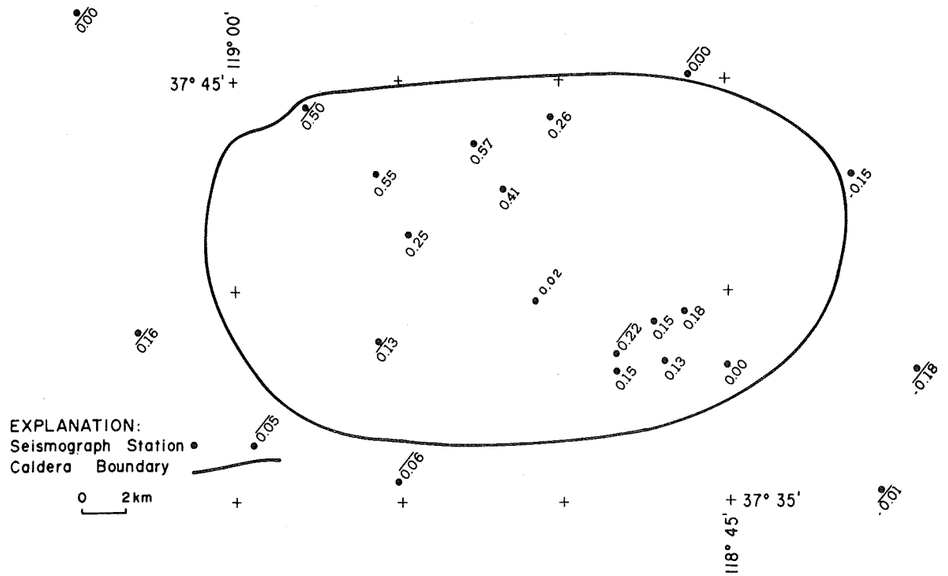

Fig. 3*b*. Teleseismic *P* wave residuals for events from the southeast relative to LVC (not shown). Otherwise the same as Figure 3*a*.

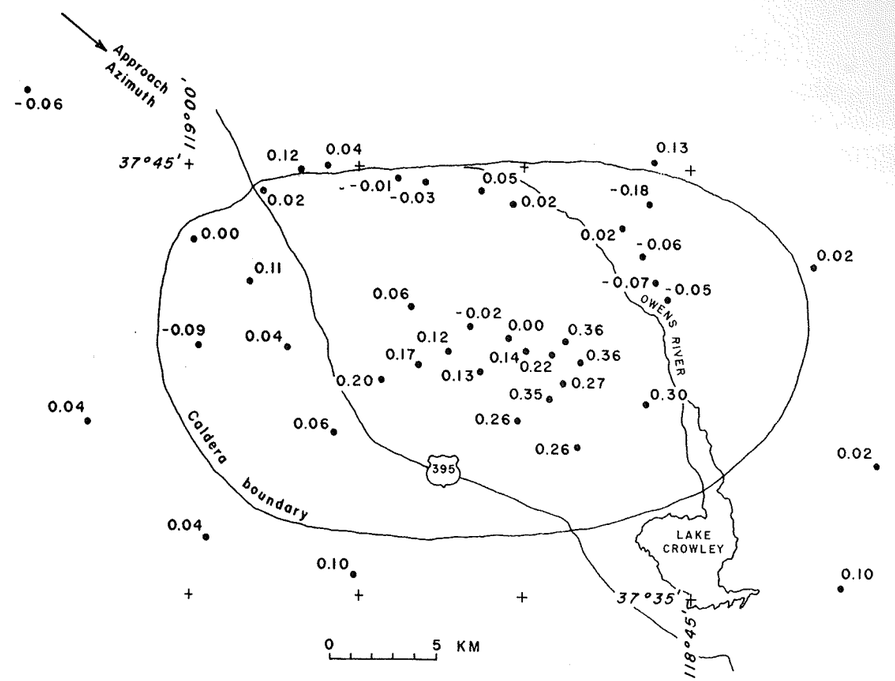

Fig. 4*a*. All data in Long Valley vicinity from northwest azimuth after near-surface effects have been removed as in Figure 4*c*. Station locations depicted by dots.

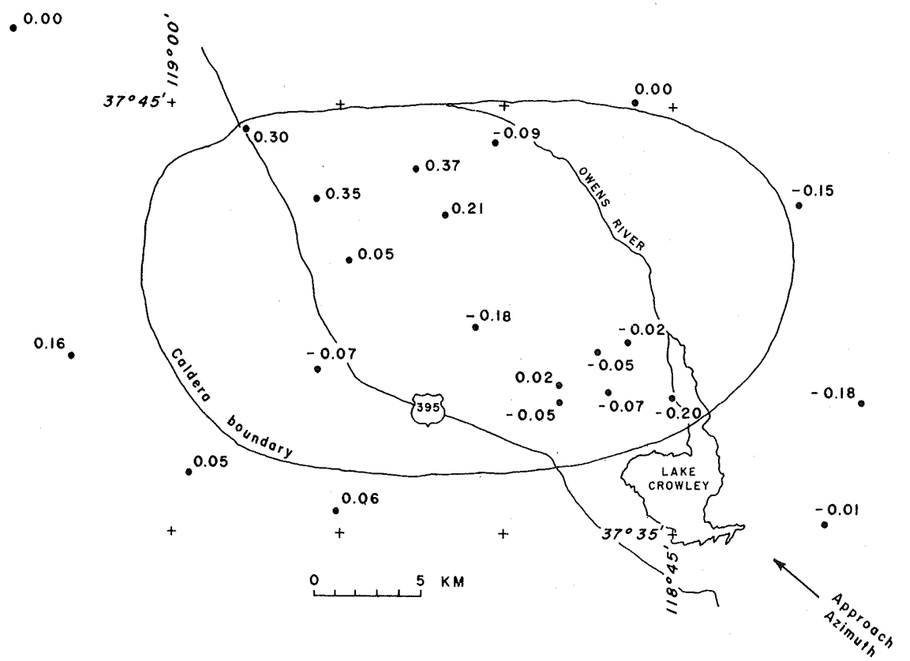

Fig. 4*b*. All data in Long Valley vicinity from southeast azimuth after near-surface effects have been removed as in Figure 4*c*. Station locations shown by dots.

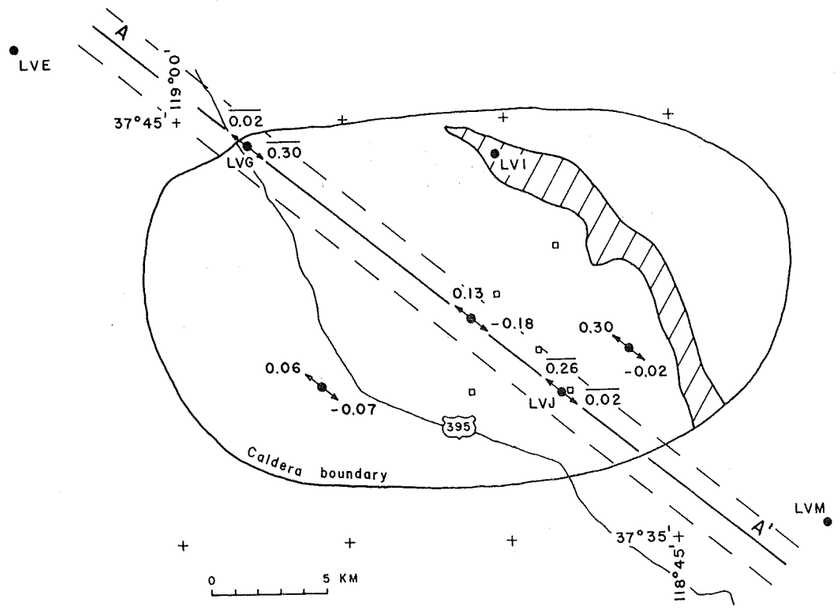

Fig. 4*c*. Teleseismic *P* wave relative residuals at stations within the caldera that recorded events from both northwest and southeast with estimated near-surface effects removed. Cross-hatched area shows where near-surface effects are estimated to be 0.35 s; elsewhere in the caldera, 0.2 s. Note remaining corrected relative residuals of 0.3 s for ray paths that have penetrated up through the center of the caldera. Stations mentioned in text are identified by three-letter names. Stations within dashed lines are projected onto section AA′ in Figures 5*a* and 5*b*. Small squares represent hot springs in the caldera.

paths outside the stippled zone in Figure 5*a* do not detect the velocity anomaly, so the low-velocity material must be above the depth where they intersect (approximately 40 km). It is impossible to fit all the required 34.2-km-long ray paths inside the stippled zone, so we conclude that the velocity decrease in the anomalous zone must be greater than 5%.

A 10% velocity decrease requires anomalous ray paths only 16.2 km long. Figure 5*a* shows a hypothetical model of an anomalous zone with a 10% decrease in velocity. The heavy parts of the ray paths are proportional in length to the delay seen by the ray paths. It is assumed that the material is isotropic with respect to *P* wave velocity. The heavy parts of the intersecting ray paths must then form an internally consistent body, putting constraints on the volume that may be occupied by the anomalous zone. The models are drawn as a first approximation to fit the data and do not take into account the refraction that would occur if such an anomalous body were present. This was taken into account (and shown not to be of first-order importance) by computer ray tracing [*Steeples*, 1975].

Figure 5*b* shows a 15% velocity decrease model. One event from the southeast occurred at an epicentral distance of 1450 km ($\Delta = 13°$). Events from this distance have angles of incidence determined by the upper mantle velocity and the granitic crustal velocity from Snell's law. A mantle velocity of 7.9 km/s yields an angle of incidence of 49° from vertical when a normal crustal velocity of 6.0 km/s is assumed. If one chooses to believe data from this single event, an additional constraint is placed on the depth of the low-velocity material, since station LVE shows a delay of 0.1 s for the event. If that ray path to LVE and the 10% velocity decrease model were used, the delay at station LVE would be 0.3 s instead of 0.1 s for this event. On the other hand, the 15% velocity decrease model requires a delay of only 0.1 s at LVE and is thus preferred over the 10% velocity decrease model. This particular ray path arrived from a slightly different azimuth, however, and may not have passed through the heart of the anomalous volume.

Additional models with greater velocity contrasts could undoubtedly be constructed without developing inconsistencies in the data. At some point the wave shape of the first pulse would begin to show changes as diffraction around the low-velocity body occurred. While we cannot now put a maximum limit on the decrease in velocity, it does not seem reasonable to expect a decrease of more than 20–30% in the *P* wave velocity for this material, even if it is fully molten. *Murase and McBirney* [1973] observed velocity decreases of up to 40% in rock melts at low pressures. A similar 40% velocity drop occurs at the core-mantle boundary, but some of that drop is due to compositional change [*Bullen*, 1965]. *Mizutani and Kanamori* [1964] observed a *P* velocity drop of only 20% in a metal alloy upon melting. On the basis of these limited observations, *P* velocity drops of 40% are too high for most rock melts at pressures of a few kilobars.

One may speculate upon the cause of such low-velocity material. Earthquakes of magnitude 6.0 have occurred near Long Valley caldera in the not too distant past (1927, 1941), so the idea of a low-velocity volume signaling an impending moderate earthquake cannot totally be ruled out. A more attractive (and more likely) hypothesis is that the low velocity is

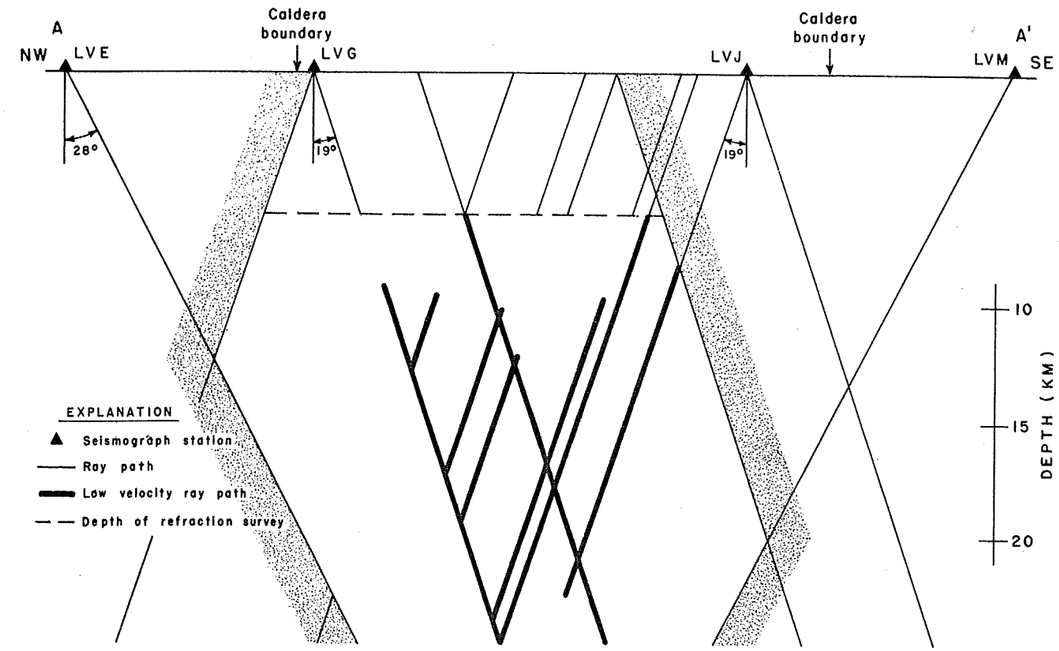

Fig. 5*a*. Sectional view of Long Valley caldera along AA′ of Figure 4*c*. Stations within 1 km of section line AA′ have been projected to the section. Model represents velocity contrast of 10% along heavy ray paths. Heavy lines on ray paths are proportional in length to delays detected along respective ray paths. Velocities outside the stippled zone are normal (6.0 km/s), and the effects of the upper 6 km of material (depth penetrated by refraction survey) have been removed.

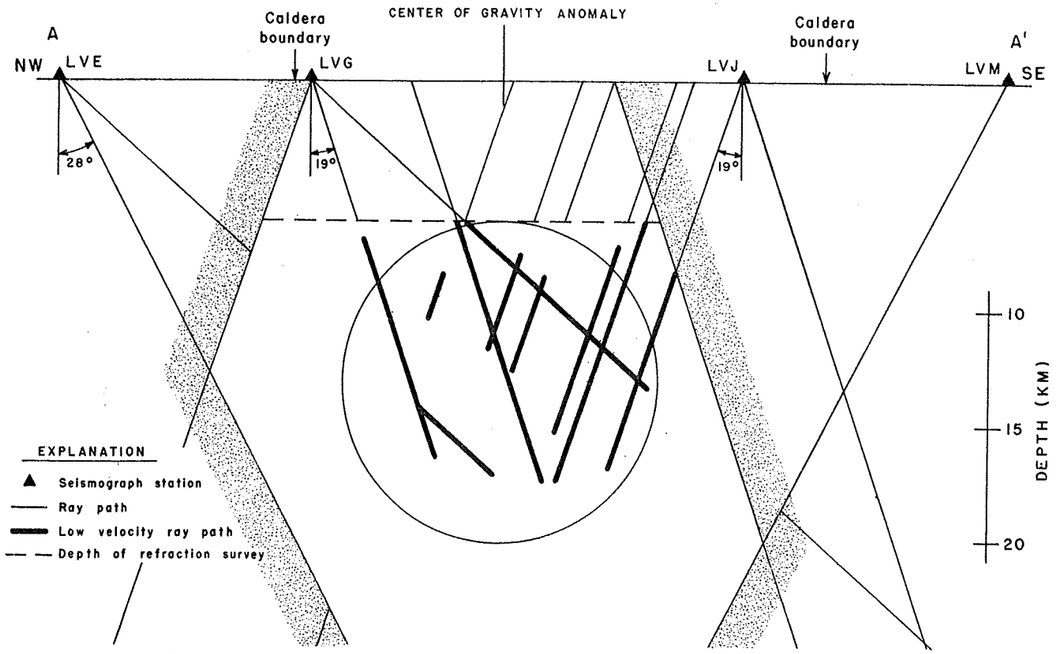

Fig. 5*b*. This model depicts a 15% velocity decrease along the heavy ray paths. The circle is a sectional view of a sphere 14 km in diameter. A density contrast of 0.18 g cm^{-3} would produce a 10-mGal gravity anomaly at the surface directly above the center of the sphere. Otherwise the same as Figure 5*a*.

associated with the intrusive body or bodies that fed the extrusions from the caldera vicinity in the past 700,000 years. It is interesting to note that rhyolitic extrusion has occurred in the Long Valley caldera vicinity within the past 1500 years [*Bailey et al.*, 1976, this issue]. The resurgent part of the caldera is where the low velocity is most pronounced.

Compressional velocity in rock decreases with increase in temperature [e.g., *Murase and McBirney*, 1973]. If this hypothesis is true, eventually it may become possible to make a reliable heat anomaly estimate for Long Valley using the hot rock hypothesis. Such reliable estimates, however, await the collection of velocity data at 10 kbar and 1000°C. A 15% decrease in velocity could represent at least partial melt, but the degree of melt could be highly dependent upon the amount of water present [*Spencer*, 1975].

If a large volume of magma were present under the caldera, teleseismic *S* waves would not be transmitted up through the caldera (analogous to *S* wave attenuation at the earth's liquid core). The seismic equipment used for this experiment was not designed to record teleseismic *S* waves, but four stations near and in the caldera (including LVG and LVJ) had 1-s horizontal seismometers. Stations both inside and outside the caldera recorded teleseismic *S* waves, but the quality was very poor because most of the shear energy occurred at lower frequencies. It was shown, however, that the low-velocity material beneath the caldera transmits some *S* wave energy (assuming that the angles of *P* and *S* incidence are equal, which may not be strictly true). This indicates that if true magma is present along the ray paths in question, it is in small pockets (probably less than 4 km thick, the approximate wavelength of the *S* waves recorded), or it has sufficient viscosity to transmit *S* waves. Local earthquake *S* waves did not penetrate deep enough to pass through the heart of the anomalous body in the caldera [*Steeples and Pitt*, 1976, this issue].

The question arises whether a few thousand meters of sediment or other low-velocity material at the surface caused the observed velocity anomalies. We believe not for three reasons that have already been discussed, but we mentioned them again for emphasis because the point is critical to our study:

1. Teleseismic ray paths reaching the earth's surface are very nearly vertical, so that the amount of low-velocity material traversed near the surface is relatively independent of approach azimuth. Four stations in the caldera showed azimuthally dependent differences of 0.3 s, which would require highly unlikely lateral heterogeneity to be explained by near-surface material.

2. The refraction survey does not show near-surface material that could cause the delays except near the Owens River valley away from most of the stations which show delays of ½ s or more.

3. Microearthquake residuals in the caldera are out of character with the residuals normally seen in the region when *Eaton*'s [1966] model is used. The arrivals suggest that the near-surface effects are correctly calculated by the methods in points 1 and 2 above.

Bailey et al. [1976] and *Lachenbruch et al.* [1976] believe that any residual magma from mid-Pleistocene intrusion must be at a depth of 10 km or greater in the caldera. The seismic data in this paper do not conflict with that conclusion, although *Hill* [1976] detected arrivals on some of his refraction records that are compatible with a low-velocity volume beginning at 7–8 km depth. Those arrivals could, however, be multiple reflections from some shallower interface. From Figures 5*a* and 5*b* it is evident that much of the low-velocity material probably lies in a depth range of 10–15 km.

While the vertical and linear horizontal extent of the low-velocity material has been somewhat constrained, nothing has yet been stated about the areal extent of the velocity anomaly. Only limited data are available to make such an approximation, but an attempt is depicted in Figure 6. In addition to data already presented, a Russian nuclear explosion and events from the southwest Pacific are plotted.

In an effort to estimate the maximum horizontal extent of the velocity anomaly, rays were projected along straight paths back toward the epicenters to a depth of 12 km, a technique similar to that used by *Iyer and Healey* [1972] at Lasa. A velocity contrast of 15% is assumed so that the diameter of the dots plotted in the caldera are thickness estimates. Figure 6 shows all the rays available for projection from the teleseismic *P* delay study at Long Valley.

A surprisingly consistent trend emerges as almost all the anomalous points plot in the west-central part of the caldera with only minor anomalous points plotted outside the caldera. The northern boundary is quite well constrained, but the eastern boundary is poorly constrained because of a lack of data points. The western and southern boundaries appear to be constrained to within about ±3 km horizontally.

It is interesting to note that the western two thirds of the caldera appears to be more anomalous than the eastern third. *Lachenbruch et al.* [1976] indicated that heat flow evidence suggests that the eastern half of the caldera may have been extinct for some time. Heat flow data show a positive anomaly in the western half of the caldera. This supports our hypothesis that the western half of the caldera may have low velocity at depth due to hot rock. However, it should be remembered that heat flow data involve a time lag of the order of thousands of years for conduction from depths as shallow as 10 km. The heat flow data therefore may not show any indication of intrusions occurring in the last thousand years or so.

A negative complete Bouguer gravity anomaly with 30-mGal closure is centered on the Long Valley caldera [*Pakiser et al.*, 1964]. *Kane et al.* [1976, this issue] have interpreted most of this gravity low in terms of up to 3 km of sedimentary or brecciated fill. They also pointed out the existence of gravity gradients outside the caldera that suggest a deep-seated mass deficiency beneath the caldera.

If a volume of hot rock or partial melt were present at depth in the caldera, a gravity low would result, since rock decreases in density with increase in temperature. Igneous rocks generally decrease in density from 6 to 10% upon melting [*Harris et al.*, 1970; *Murase and McBirney*, 1973].

A simple theoretical deep gravity model was constructed to fit our teleseismic *P* delay data. The anomaly in and around the caldera can be explained in part by a buried spherical mass with its center 13 km deep centered on section AA′ as shown in Figure 5*b*. The calculation was done by using the gravitational field equation for a sphere given by *Dobrin* [1960, pp. 172–177] and the gravity map of *Pakiser et al.* [1964]. The spherical model used in the calculation had a radius of 7 km, resulting in a required density contrast of 0.018 g cm^{-3} mG^{-1}. If one chooses to attribute a 10-mGal anomaly to this hypothetical sphere, a density contrast of 0.18 g cm^{-3} is required. The observed gravity gradients outside the caldera do not allow a spherical mass much larger, deeper, or less dense than the model just discussed. Density of rock decreases with increase in temperature because of thermal expansion, so up to 10 mGal in excess of the observed 30 mGal gravity anomaly in the caldera could be due to hot rock and/or partial melt. It should be pointed out that rock density decreases only about 1% for each 400°C change in temperature [*Skinner*, 1966]. That in turn implies that the density change of hot rock without partial melt could produce no more than about 3 mGal of gravity anomaly for the model just discussed. This indicates that if the deep gravity model is accurate and compositional change is not a factor, then some degree of partial melt is needed to explain the rest of the gravity anomaly.

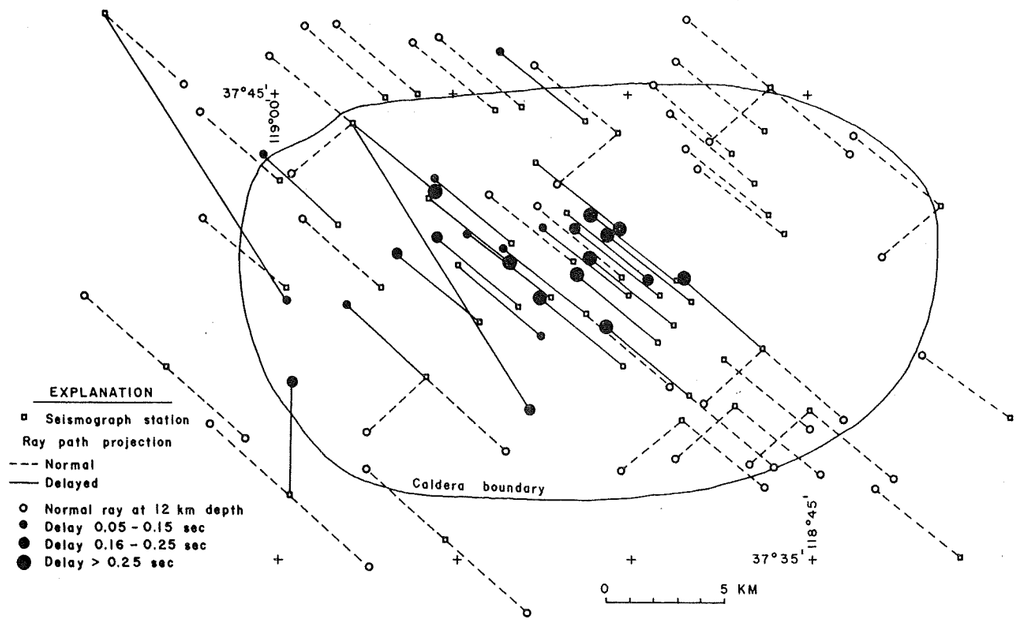

Fig. 6. Rays are projected back toward the epicenters to a depth of 12 km, nonrefractive paths being assumed. Note that almost all anomalous points form an internally consistent body in the west-central part of the caldera.

Conclusions

The low *P* velocity observed beneath Long Valley is probably caused by anomalously high temperature. The anomalous zone is more than 7 km but definitely less than 40 km deep, probably less than 25 km deep. The velocity contrast with the surrounding material is more than 5% and is probably in the range 10–15%. The areal extent of the low-velocity material is poorly constrained but is probably confined to the caldera, possibly to the west half of the caldera. A possible deep-seated gravity low lends circumstantial support to our hot rock/partial melt hypothesis.

The teleseismic *P* delay technique may become a viable method of exploring the sources of geothermal energy. It should not be used without a thorough knowledge of the upper crustal velocity structure such as that normally obtained from seismic reflection or refraction surveys. In addition to vertical instruments, it is desirable to use horizontal seismometers capable of recording teleseismic *S* waves so that *S* delays and possible *S* attenuation can be investigated in conjunction with *P* wave studies.

Timing the first or second zero crossing may be one way of attaining better relative accuracy in measuring arrival times, particularly for marginal quality events. The technique is probably most useful on small aperture arrays. One can determine the applicability of the zero crossing timing method by timing both first arrival and zero crossings for high quality events and comparing the two methods. In our case, the two timing methods produce the same results, but the zero crossing method allows the use of about 50% more data while it decreases the scatter in the data.

The estimation of heat anomalies by the teleseismic *P* delay method awaits the laboratory measurement of rock velocities at pressures approaching 10 kbar and temperatures of 1000°C.

Acknowledgments. The field data for this study were obtained by John Coakley, and records were prepared by Jeanne Taylor. Extensive and fruitful discussions with Dave Boore, Dave Hill, and George Thompson were appreciated. The manuscript was critically reviewed by Dave Boore, Dave Hill, and Bob Engdahl. Publication authorized by the Director of the U.S. Geological Survey.

References

Bailey, R. A., G. B. Dalrymple, and M. A. Lanphere, Volcanism, structure, and geochronology of Long Valley caldera, Mono County, California, *J. Geophys. Res., 81*, this issue, 1976.

Bolt, B. A., and O. W. Nuttli, *P* wave residuals as a function of azimuth, 1, Observations, *J. Geophys. Res., 71*, 5977–5986, 1966.

Bullen, K. E., *An Introduction to the Theory of Seismology*, 3rd ed., pp. 217–249, Cambridge University Press, London, 1965.

Chinnery, M. A., and M. N. Toksoz, *P*-wave velocities in the mantle, 1, Below 700 km, *Bull. Seismol. Soc. Amer., 57*, 199–226, 1967.

Cramer, C. H., and R. L. Kovach, A search for teleseismic travel-time anomalies along the San Andreas Fault zone, *Geophys. Res. Lett., 1*, 90, 1974.

Dobrin, M. B., *Introduction to Geophysical Prospecting*, 2nd ed., pp. 172–177, McGraw-Hill, New York, 1960.

Eaton, J. P., Crustal structure in northern and central California from seismic evidence, *Calif. Div. Mines Geol. Bull., 190,* 419–426, 1966.
Eaton, J. P., M. E. O'Neill, and J. N. Murdock, Aftershocks of the 1966 Parkfield-Cholame, California earthquake: A detailed study, *Bull. Seismol. Soc. Amer., 60,* 1151–1198, 1970.
Harris, P. G., W. Q. Kennedy, and C. M. Scarfe, Volcanism versus plutonism—The effect of chemical composition, in Mechanism of Intrusion, edited by Geoffrey Newall and Nicholas Rast, *Geol. J. Spec. Issue 2,* 187–200, 1970.
Herrin, E., Introduction to '1968 seismological tables for P phases,' *Bull. Seismol. Soc. Amer., 58,* 1193, 1968.
Hill, D. P., Structure of Long Valley caldera from a seismic refraction experiment, *J. Geophys. Res., 81,* this issue, 1976.
Iyer, H. M., Anomalous delays of teleseismic *P*-waves in Yellowstone National Park, *Nature, 253,* 425–427, 1975.
Iyer, H. M., and J. H. Healy, Teleseismic residuals at the Lasa-USGS extended array and their interpretation in terms of crust and upper mantle structure, *J. Geophys. Res., 77,* 1503, 1972.
Iyer, H. M., and T. Hitchcock, Seismic noise survey in Long Valley, California, *J. Geophys. Res., 81,* this issue, 1976.
Iyer, H. M., J. R. Evans, and J. Coakley, Teleseismic evidence for the existence of low-velocity material deep into the upper mantle under the Yellowstone caldera (abstract), *Eos Trans. AGU, 55,* 1191, 1974.
Kane, M. F., D. R. Mabey, and R. Brace, A gravity and magnetic investigation of the Long Valley caldera, Mono County, California, *J. Geophys. Res., 81,* this issue, 1976.
Koizumi, C. J., A. Ryall, and K. F. Priestley, Evidence for a high-velocity lithospheric plate under northern Nevada, *Bull. Seismol. Soc. Amer., 63,* 2135–2144, 1973.
Lachenbruch, A. H., M. L. Sorey, R. E. Lewis, and J. H. Sass, The near-surface hydrothermal regime of Long Valley caldera, *J. Geophys. Res., 81,* this issue, 1976.
Mack, H., Nature of short-period *P* wave signal variations at Lasa, *J. Geophys. Res., 74,* 3161–3170, 1969.
Mizutani, H., and H. Kanamori, Variation of elastic wave velocity and attenuative property near the melting temperature, *J. Phys. Earth, 12*(2), 43–49, 1964.
Murase, T., and A. R. McBirney, Properties of some common igneous rocks and their melts at high temperatures, *Geol. Soc. Amer. Bull., 84,* 3563–3592, 1973.
Niazi, M., and D. L. Anderson, Upper mantle structure of western North America from apparent velocities of *P* waves, *J. Geophys. Res., 72,* 4633, 1965.
Nuttli, O. W., and B. A. Bolt, *P* wave residuals as a function of azimuth, 2, Undulations of the mantle low-velocity layer as an explanation, *J. Geophys. Res., 74,* 6594–6602, 1969.
Pakiser, L. C., M. F. Kane, and W. H. Jackson, Structural geology and volcanism of Owens Valley region, California—A geophysical study, *U.S. Geol. Surv. Prof. Paper 438,* 68 pp., 1964.
Pitt, A. M., and D. W. Steeples, Microearthquakes in the Mono Lake—Northern Owens Valley region from September 28 to October 18, 1970, *Bull. Seismol. Soc. Amer., 65,* 835–844, 1975.
Press, F., and S. Biehler, Inferences on crustal velocities and densities from *P* wave delays and gravity anomalies, *J. Geophys. Res., 69,* 2979, 1964.
Richter, C. F., *Elementary Seismology,* pp. 664–666, W. H. Freeman, San Francisco, 1958.
Skinner, B. J., Thermal expansion, in Handbook of Physical Constants, rev. ed., edited by S. P. Clark, Jr., *Geol. Soc. Amer. Mem. 97,* 75–96, 1966.
Spencer, J. W., Jr., Ultrasonic velocities in rocks under crustal conditions, Ph.D. thesis, Stanford University, Stanford, Calif., 1975.
Steeples, D. W., Teleseismic *P*-delays in geothermal exploration with application to Long Valley, California, Ph.D. thesis, Stanford University, Stanford, Calif., 1975.
Steeples, D. W., and A. M. Pitt, Microearthquakes in and near Long Valley, California, *J. Geophys. Res., 81,* this issue, 1976.
Utsu, T., Temporal variations in traveltime residuals of *P*-waves from Nevada sources, *J. Phys. Earth, 21,* 475–480, 1973.
Wyss, M., and D. J. Holcomb, Earthquake prediction based on station residuals, *Nature, 249,* 139, 1973.

(Received December 26, 1974;
revised July 31, 1975;
accepted July 31, 1975.)

VOL. 81, NO. 8 JOURNAL OF GEOPHYSICAL RESEARCH MARCH 10, 1976

Application of the Self-Potential Method to Geothermal Exploration in Long Valley, California

LENNART A. ANDERSON AND GORDON R. JOHNSON

U.S. Geological Survey, Denver, Colorado 80225

A self-potential survey made in the Long Valley caldera produced an anomaly derived from a dipolar source superimposed on potentials negative in polarity in relation to the area outside the caldera. The dipolar anomaly, consisting of negative and positive components differing amplitude by approximately 1 V, is centered over a resurgent dome in the west central part of the caldera. The exact nature of the potential source is unknown; however, electrofiltration processes caused by movement of heated groundwater that gives rise to streaming potentials are thought to be the principal cause of the dipolar anomaly. Diffusion potentials resulting from concentration differences between rising volcanic water and descending meteoric water may be responsible for the negative potentials measured within the caldera. Potential increases as high as 1100 mV were observed across the perimeter of the caldera.

INTRODUCTION

The mapping of natural electrical potentials within the Long Valley caldera, located in the east central part of California (Figure 1), constitutes an attempt to utilize the self-potential method in the detection and delineation of thermal sources within a known geothermal area. The use of the self-potential method in geothermal exploration was most unorthodox in that an absolute correlation between anomalous surface potentials and thermal sources at depth had not been established. However, higher than normal background potentials in geothermal areas have been reported by *White et al.* [1964] and *Corwin* [1973], and a single profile obtained across the Mud Volcano area in Yellowstone National Park produced a positive anomaly of about 40–50 mV which was unmistakably caused by phenomena related to thermal activity [*Zohdy et al.*, 1973]. On the basis of the possible utility of the self-potential method in geothermal exploration as suggested in these reports it was considered of practical interest to carry out a self-potential survey in Long Valley, where other geophysical data were available for interpretational support.

FIELD PROCEDURE

Self-potential measurements were made with copper–copper sulfate nonpolarizing electrodes spaced 300 ft (91.5 m) apart and a high-impedance millivoltmeter. Because of the large area to be surveyed, potential gradients were measured along a traverse, and individual readings added successively to construct a profile of potentials relative to a base station established at the junction of old U.S. Highway 395 and Mammoth Lakes Road (Figure 1). All self-potential data were subjected to a low-pass filtering process to remove short-wavelength potential variations generated by near-surface effects. Figure 2 shows an example of profile data in the three forms of measured, compiled, and filtered data obtained along traverse A-A′ (Figure 1).

Data initially were collected on a long closed loop traverse; where it was possible, subsequent traverses were tied to the original traverse at two points. Closure offsets were distributed linearly along the profile to compensate for accumulative errors. Errors in individual readings were minimized by selecting electrodes which produced less than 1 mV in a side-by-side arrangement and by reversing the relative position of the electrodes for alternate readings in order to counteract electrode potential imbalance if it should occur during the course of the day. Assuring contact with the moist overburden was a particular problem in Long Valley because of the insulating properties of the large quantities of pumice within the surface material. The contact problem was overcome by watering the area of electrode emplacement, but this procedure often produced potentials in the vicinity of the electrodes because of salinity gradients and the downward filtration of the introduced water. In time an equilibrium level was reached; however, in many instances fluctuations of the self-potential field decreased the accuracy of the measurement, and thus a probable source of much of the profile closure error was produced.

Typically, traverses completed on the same day or on successive days closed with very little error. For example, the initial loop, a 26-mi (42 km) traverse starting south of Casa Diablo Hot Springs and circling to the east and south, was completed within 3 days and closed with an error of 55 mV.

SURVEY RESULTS

The contoured self-potential data shown in Figure 3 produced some unexpected and rather spectacular results. The most obvious and impressive features on the map are the positive and negative anomalies overlying the south and north parts of the Cenozoic volcanic rock, respectively. Each anomaly exceeds 400 mV, so that there is a minimum net potential difference approaching 900 mV across a distance of about 5 km. The nearly equal amplitude of each anomaly suggests that a common source was responsible for generating the anomalies, and on the basis of the gradient between peak values it may be inferred that the source is deeply buried.

In the part of the caldera west of U.S. Highway 395, self-potentials continue to decrease. Profile data, insufficient to permit contouring, indicate that the potentials fall to at least −800 mV. The potential field in the southern part of the caldera is rather uniform, but to the north and northwest the self-potentials increase as the caldera perimeter is approached.

SOURCE MECHANISMS

In designating the negative and positive anomalies located over the volcanic rock as the most significant features on the map it is assumed that the anomalies are produced by effects associated with thermal activity at depth. Thus far no follow-up studies have been done using borehole investigations to confirm the results of the self-potential survey; therefore very

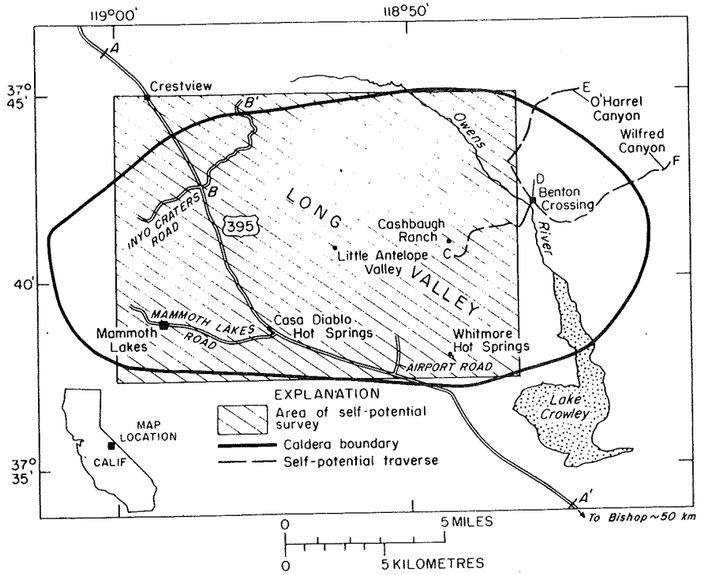

Fig. 1. Index map showing survey locations, Long Valley, Mono County, California.

little information exists from which a source mechanism can be positively identified. However, extensive previous work on self-potential phenomena provides enough information to permit speculation on possible processes involved in generating self-potential anomalies in geothermal fields. A paper by *Nourbehecht* [1963] is of particular interest in that it sets forth those internal conditions necessary to produce electrical signals at the earth's surface. The stated conditions are not repeated herein.

Many mechanisms may conceivably generate natural electromotive forces and thereby contribute to the total observed anomaly. However, the fact that the negative and positive anomalies have similar amplitudes and occur in a relatively uniform geologic environment suggests a singular predominating mechanism. It is thought that this mechanism is related to the heat-triggered movement of water in a convective cell. The potentials are believed to be generated by electrofiltration processes, the result being an effect called 'streaming potential.'

The electromotive force generated by streaming potentials is primarily controlled by fluid pressure for a given set of rock conditions. According to *Dakhnov* [1962], streaming potentials are caused by the preferential adsorption of one ion species on the grain surfaces comprising the pore walls. Be-

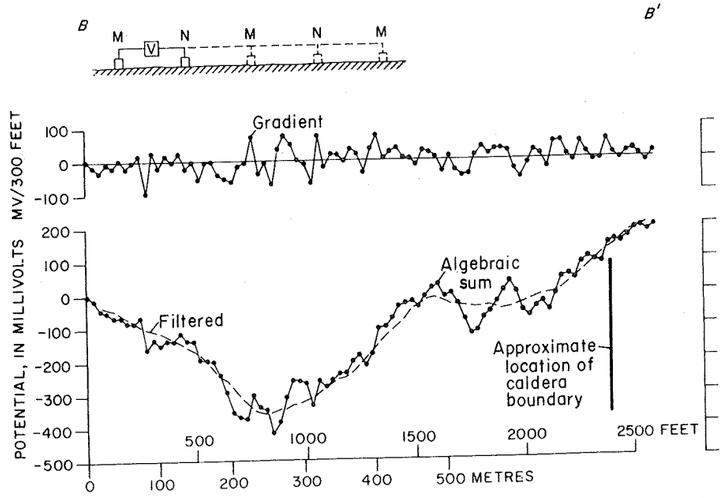

Fig. 2. Self-potential profile A-A′ data as measured, compiled, and filtered prior to contouring.

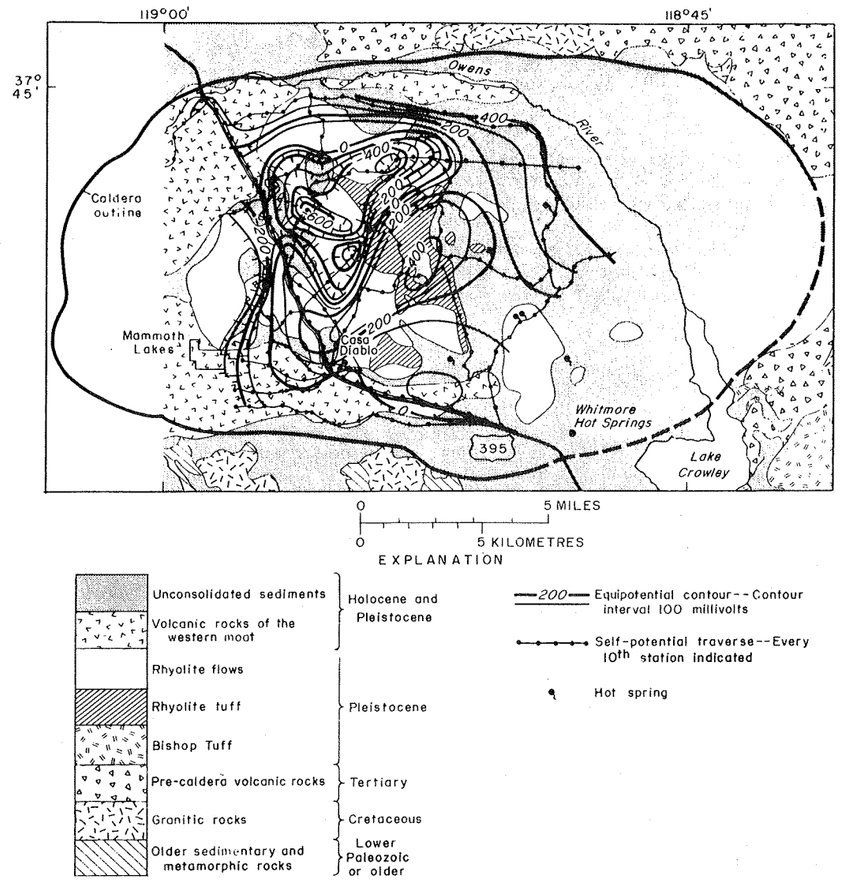

Fig. 3. Self-potential and generalized geologic map of the west central part of Long Valley, Mono County, California. Geology generalized from *Bailey et al.* [1976].

cause the adsorbed ions are all of the same polarity, the free liquid in the center of the pore spaces is enriched in ions of opposite charge. In the presence of a differential pressure across the rock formation the pore waters will move so as to produce a net charge separation along the line of water movement. In most rock systems, anions are adsorbed; therefore the pore waters carry a surplus of cations, and a positive potential is set up in the direction of flow. Some clays and carbonate rocks in basic solutions will produce the opposite effect.

Streaming potentials are dependent upon factors best described by the equation

$$E_s = \epsilon\zeta\Delta P/\xi[\sigma + \sigma_s(2/r)] \qquad (1)$$

where ΔP is the pressure difference across the rock formation, r is the crack width or pore radius of the rock, σ_s is the surface conductance of the diffuse layer within the pore spaces, and ϵ, ζ, σ, and ξ are the dielectric constant, zeta potential, conductivity, and viscosity of the pore water, respec-

potential is that which exists across the fixed charges at the pore walls and those charges within the mobile layers of liquid. The properties ϵ, ξ, and σ are always positive; therefore the polarity of a surface anomaly arising from streaming potentials will be dependent upon the direction of water flow and the zeta potential.

Typically, (1) is expressed as a ratio of $E_s/\Delta P$, which is an equilibrium statement implying that the charge separation caused by fluid movement will be counteracted by electrostatic forces so as to reach an asymptotic value for a given set of rock conditions. As the pressure increases, the streaming potential will increase proportionately.

Phenomenologically, one can envision a deeply buried thermal source heating the groundwater so as to cause an upward migration of the water. Upward-moving water generally produces positive potentials at the surface; therefore we may attribute the positive anomaly over the Quaternary rhyolite to ascending groundwaters. In the event that the movement of water is impeded by a cap rock of low permeability, the heated water either travels through fracture systems to the surface, where it forms hot springs, or following some loss of heat, cycles downward if no escape is possible. Descending waters will generate a negative potential at the surface, and this mechanism may be responsible for the negative anomaly over the northern part of the Quaternary rhyolite. A similar negative counterpart is not developed south of the positive anom-

aly because, as is shown in Figure 3, the heated waters have found escape routes to the surface through the hot springs along the east and south flanks of the rhyolite; the relatively high potentials observed south and southeast of the positive anomaly are thereby sustained. The escaping water must certainly be replenished if the hot water convection cell is to be maintained. Groundwater recharge areas conceivably exist at several locations within the caldera; however, surficial evidence suggests that the principal source of fresh water is from surface flow off the Sierra highlands into the western part of the caldera. The downward percolation of meteoric water through rocks which are primarily basalt may be responsible for generating the high negative potentials observed in the western part of the survey areas.

Electrochemical effects may be responsible, at least in part, for the anomalies over the volcanic rock. On the basis of data provided by *Lewis* [1974] we know that springwaters north of the anomalous area are low in dissolved solids. If this fresh water can find access to a permeable layer within the volcanic sequence and thus come in contact with the saline thermal waters, then mechanisms for generating significant surface potentials will be activated. The first of these mechanisms involves processes by which diffusion potentials are produced. Diffusion potentials are developed across a liquid junction when two solutions of differing salinities are in direct contact. Ions from the more concentrated solution migrate into the dilute solution at a rate dependent upon the mobility of the ions involved. The more mobile ions are typically of one polarity; therefore a separation of charge will develop across the solution boundary, the result being a net current flow. Temperature differences between solutions will increase ion mobility, the effect being thereby enhanced, and the presence of clays within the rock may do the same.

The second of these mechanisms that take place at the interfacing of unlike solutions produces oxidation-reduction potentials if certain conditions are met. According to *Sato and Mooney* [1960] a difference in the Eh or redox potential of the solutions in contact must exist in order to provide the driving source for the transfer of electrons from one solution to the other. The electron transfer also requires the presence of a conductive body across the solution boundary and an electron mobility rate which exceeds the mobility of the upward-moving positive ions in the surrounding solution. To attribute the observed Long Valley anomalies to an oxidation-reduction process, the fresh water must contain free oxygen to create an oxidizing environment, and in like manner, the thermal waters must provide a reducing environment. Data from *Lewis* [1974] show that there may be sufficient dissolved iron in the thermal waters to satisfy the latter condition; however, the vehicle for electron transfer is still lacking. A paper by *Willey et al.* [1974] indicates that dissolved sulfides exist in relative abundance within the groundwaters of Long Valley. If these sulfides are deposited in disseminated form in the zone of groundwater mixing, then a mechanism for electron flow will exist [*Sato and Mooney,* 1960]. In the Mud Volcano area in Yellowstone National Park, core samples extracted from a borehole indicated the presence of disseminated pyrite deposited by thermal waters in the near-surface layer. Pyrite was found at a depth of 50 ft (15.2 m), and it increased in abundance down to the bottom of the hole at 347 ft (105.8 m) [*Zohdy et al.,* 1973].

Pyrite deposition is not uncommon in areas of thermal activity, nor are reducing agents uncommon in thermal waters. The main concern, however, is whether sufficient free oxygen can be maintained within the infiltrating groundwaters to provide an oxidizing environment at the necessary redox potential to generate the observed surface potentials. Free oxygen is generally depleted rapidly, particularly in the presence of dissolved organic materials.

Nourbehecht [1963] in his study of diffusion and electrokinetic source mechanisms calculated the upper limit of potential amplitude measurable at the surface for each effect. Maximum surface potential for the diffusion process is given as 100 mV; the streaming potential mechanism has a calculated capability of producing anomalies of 'several hundred millivolts.' *Sato and Mooney* [1960] indicated that half-cell potentials relating to oxidation-reduction effects usually range in amplitude from 400 to 500 mV, although much higher potentials have been observed in the field.

A number of other naturally occurring phenomena may conceivably act to produce measurable self-potentials at the surface. However, for the known possible processes there are so many variables involved that all necessary conditions will rarely be met.

PROFILE DATA

Because individual traverses did not normally extend beyond the caldera boundaries, the contoured data do not adequately define the self-potential gradients observed in the vicinity of the caldera walls. Contours in the northern part of Figure 3 indicate an increase in potential as the edge of the caldera is approached; this effect, however, can better be seen in profile form.

Profile data obtained along traverse A-A′ (Figure 1), as shown in Figure 4, were relatively smooth and therefore were not filtered in the usual manner. Instead, every 10th data point was plotted, a somewhat angular appearance to the profile thus being imparted. The traverse extended beyond the physical limits of the caldera as inferred from gravity data [*Pakiser et al.,* 1964]. The character of the profile indicates that the self-potentials within the caldera are substantially lower than or negative with respect to those potentials generated outside the caldera. On approaching the northern wall of the caldera the

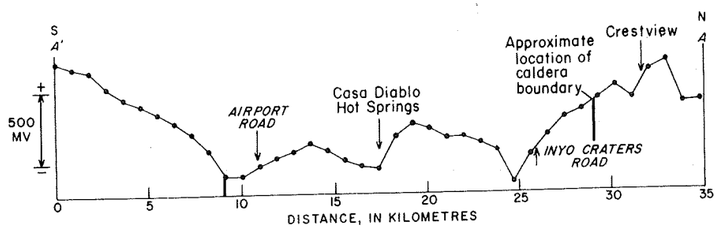

Fig. 4. Self-potential profile obtained along a north-south trending traverse following U.S. Highway 395.

potentials increase, but beyond the wall the potentials show signs of decreasing. The fact that self-potentials do decrease outside the caldera suggests that the high potentials are caused by effects localized near the caldera edge. A decrease in self-potential was not observed south of the caldera boundary; however, unlike the other caldera walls the southern wall is not physically apparent. Indeed, the gravity data obtained in the southern part of the caldera have a lower gradient than data from elsewhere along the caldera perimeter. This fact suggests that the southern caldera wall may consist of a series of fault blocks rather than a single offset, a structural characteristic which would tend to broaden those effects that may be attributed to a source near the edge of the caldera.

Profiles (C-D, D-E, D-F) obtained in the eastern part of the caldera (Figure 5) (see Figure 1 for location) show a gradual and virtually uninterrupted increase in potentials from their starting point to the wall of the caldera, where the potentials level off and eventually begin to decrease outside the caldera. The potential rise on each profile is substantial; the potential increased by more than 1100 mV along the traverse leading through Wilfred Canyon and nearly 1000 mV on the O'Harrel Canyon traverse.

The cause of the potential increase near the caldera boundary is unknown, but possibly, a combination of the mechanisms previously discussed may be responsible for the observed effect. It was first thought that the potential gain could be attributed to outward-flowing current that increased in density within the surface layer as a result of a lateral increase in resistivity encountered at the caldera edge. To test this supposition, a two-dimensional model was formulated with the use of a buried current source and a vertical contact separating media of differing resistivities.

Image theory was used to derive equations for calculating potentials on each side of the contact. For a current source buried within the medium of resistivity ρ_1 the equations are

$$V_1 = \frac{\rho_1 I}{2\pi}\left\{\frac{1}{[(k-a)^2+d^2]^{1/2}} + \frac{k}{[(x-a)^2+d^2]^{1/2}}\right\} \quad (2)$$

$$V_2 = \frac{\rho_1 I}{2\pi}(1+k)\left\{\frac{1}{[(x-a)^2+d^2]^{1/2}}\right\} \quad (3)$$

where V_1 and V_2 are potentials measured over ρ_1 and ρ_2 material, respectively; d, the depth of burial to a point current source; a, the distance from the source to the vertical contact; I, the current strength; and k, the reflection coefficient equal to $(\rho_2 - \rho_1)/(\rho_2 + \rho_1)$. By using these equations, profiles of potential field distribution can be compiled from any number of randomly positioned current sources of either polarity.

To simulate the potential effects observed at the edge of the caldera, it was necessary to provide for a horizontal offset in the relative locations of current sources. Figure 6 shows profiles calculated for the indicated dipolar current source arrangement by using first a medium of uniform resistivity and second a resistivity contrast, where ρ_2 is 10 times larger than ρ_1. From the shape of the curves it is seen that no lateral resistivity changes are required in order to produce the observed edge effects. However, a resistivity increase representing the caldera walls will serve to enhance the relative increase in potential as measured from a point within the caldera. These calculations suggest that a source mechanism that produces potentials positive in polarity exists near the perimeter of the caldera.

The nature of the various mechanisms which may possibly combine to create the anomalous potentials associated with the caldera perimeter is, of course, speculative. Perhaps the

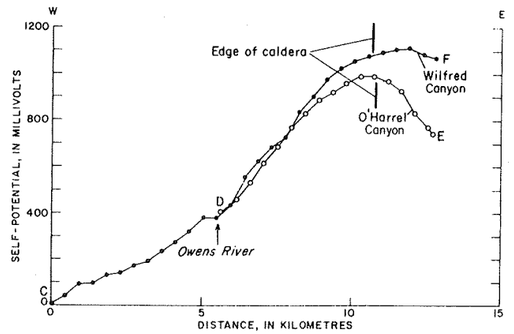

Fig. 5. Self-potential profiles along the eastern caldera traverses, Long Valley, Mono County, California.

surface potentials within the caldera are relatively low as a result of diffusion and oxidation-reduction processes occurring at the junction of meteoric and thermal waters. These electrochemical effects would most often result in a negative potential at the surface. In addition, it may be supposed that thermal waters flow upward along a relatively permeable path created around the perimeter of the caldera during the time of subsidence. The upward-migrating waters would generate streaming potentials positive in polarity, the observed edge effect thus being produced. To our knowledge there are no hot springs along the borders of the caldera; therefore if the streaming potential concept is valid, the thermal waters are either returned to the depths nearer the center of the caldera, the relatively low inner-surface potentials thereby being enhanced, or they simply merge with meteoric groundwaters within the alluvium.

SUMMARY AND CONCLUSIONS

Field observation and theory both indicate that anomalous self-potentials may be expected in geothermal areas. Previous reported attempts to utilize the self-potential method in geothermal exploration produced ambiguous results, probably because these earlier surveys were generally limited to areas of

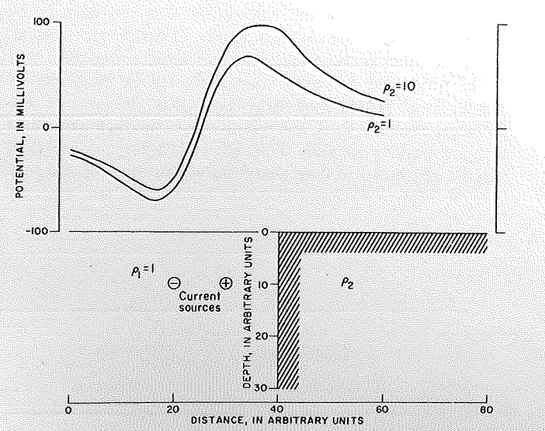

Fig. 6. Theoretical profiles calculated for a buried dipolar source in homogeneous media and for a source near a vertical contact dividing media of differing resistivities.

hot spring activity. In Long Valley we chose to extend our survey to cover a major part of the caldera and, by data filtering, to remove the effects of near-surface potentials from those potentials emanating from sources at depth. We acknowledge, however, that potentials from near-surface effects, particularly in hot spring areas, can be substantial and can thereby evoke undeserved attention.

The Long Valley self-potential survey yielded a number of interesting results. As an example, potentials associated with the perimeter of the caldera are very much higher than those associated with the central area of the caldera. Whether this phenomenon is unique to Long Valley or whether it can be observed in other calderas is a question yet to be answered. However, the effect was found to be generally symmetrical about the mapped edge of the caldera, and the possibility that an external source mechanism causes the perimeter potentials was thereby precluded.

The dipolar anomaly overlying the Quaternary volcanic rock in the west central part of the caldera is the most significant feature of this self-potential survey in terms of thermal potential. The positive anomaly covers the southern part of a resurgent dome and is ringed to the south and southeast by hot springs. No similar surface manifestation is affiliated with the negative anomaly to the north. Although several source mechanisms may combine to produce the dipolar anomaly, we believe that electrokinetic phenomena, primarily in the form of streaming potentials, principally cause the observed surface potentials. The resistivity of the pore waters within the thermal zone is typically very low; however, low-resistivity pore water moving through a thick section of rock over a very broad area may be magnified into potentials of considerable magnitude.

The depth to the current source is unknown primarily because the manner in which surface potentials are produced is very complex [*Nourbehecht,* 1963]. However, it is believed that the large-scale anomalies are caused by sources at depth. The deep lobes of the negative anomaly, particularly the westernmost one and its associated positive anomaly immediately south, may indicate the presence of a secondary hot water convection cell within the major water system or an unidentified source mechanism at an intermediate depth.

The results of other geophysical surveys do not correlate well with the findings of the self-potential survey. Perhaps the thermal zone beneath the volcanic rock is too deep to be detected by controlled source methods, or perhaps the emphases of the other surveys were on other aspects or areas.

The total field resistivity map presented in the paper by *Stanley et al.* [1976] does show the area of the positive self-potential anomaly to be less resistive than the rock associated with the negative anomaly. This resistivity difference, however, may be attributed to clay alteration within the volcanic rock caused by the upward migration of thermal waters rather than to effects of the hot water convection cell itself.

We are reasonably confident that the self-potential method will find application to geothermal exploration, although the fundamental relationship between them has yet to be completely understood. Despite the fact that source mechanisms have not been specifically defined, there is sufficient theoretical evidence to support the notion that high-amplitude potentials can be systematically mapped at the surface. In Long Valley we have demonstrated that anomalies covering many square miles can be defined and separated from short-wavelength potentials originating from shallow sources. Although field procedures may need to be refined in order to make measurements with greater reliability, the self-potential method as a reconnaissance technique is relatively simple to apply and may prove to have the advantage of sensing the dynamic aspects of a thermal system at depths greater than those possible with most controlled source methods.

REFERENCES

Bailey, R. A., G. B. Dalrymple, and M. A. Lanphere, Volcanism, structure, and geochronology of Long Valley caldera, Mono County, California, *J. Geophys. Res., 81,* 725–744, 1976.

Corwin, R. F., Offshore application of self-potential prospecting, Ph.D. thesis, Univ. of Calif., Berkeley, 1973.

Dakhnov, V. N., Geophysical well-logging—The application of geophysical methods; electrical well-loggings, *Colo. Sch. Mines Quart.,* Engl. Transl., *57*(2), 445 pp., 1962.

Lewis, R. E., Data on wells, springs, and thermal springs in Long Valley, Mono County, California, open file report, 52 pp., U.S. Geol. Surv., Menlo Park, Calif., 1974.

Nourbehecht, B., Irreversible thermodynamics in homogeneous media and its application to certain geoelectric problems, Ph.D. thesis, Mass. Inst. of Technol., Cambridge, 1963.

Pakiser, L. C., M. F. Kane, and W. H. Jackson, Structural geology and volcanism of Owens Valley region, California—A geophysical study, *U.S. Geol. Surv. Prof. Pap. 438,* 68 pp., 1964.

Sato, M., and H. M. Mooney, The electrochemical mechanism of sulfide self-potentials, *Geophysics, 25*(1), 226–249, 1960.

Stanley, W. D., D. B. Jackson, and A. A. R. Zohdy, Deep electrical studies in the Long Valley caldera, Mono and Inyo Counties, California, *J. Geophys. Res., 81,* 810–820, 1976.

White, D. E., G. A. Thompson, and C. H. Sandberg, Rocks, structure, and geologic history of Steamboat Springs thermal area, Washoe County, Nevada, *U.S. Geol. Surv. Prof. Pap. 458-B,* B1–B63, 1964.

Willey, L. M., J. R. O'Neil, and J. B. Rapp, Chemistry of thermal waters in Long Valley, Mono County, California, open file report, 19 pp., U. S. Geol. Surv., Menlo Park, Calif., 1974.

Zohdy, A. A. R., L. A. Anderson, and L. J. P. Muffler, Resistivity, self-potential, and induced-polarization surveys of a vapor-dominated geothermal system, *Geophysics, 38*(6), 1130–1144, 1973.

(Received January 27, 1975;
revised December 4, 1975;
accepted December 15, 1975.)